



University  
of Glasgow

Irthiea, Ihsan Khalaf (2014) *Process analysis and design in micro deep drawing utilizing a flexible die*. PhD thesis.

<http://theses.gla.ac.uk/4807/>

Copyright and moral rights for this thesis are retained by the author

A copy can be downloaded for personal non-commercial research or study, without prior permission or charge

This thesis cannot be reproduced or quoted extensively from without first obtaining permission in writing from the Author

The content must not be changed in any way or sold commercially in any format or medium without the formal permission of the Author

When referring to this work, full bibliographic details including the author, title, awarding institution and date of the thesis must be given

# **Process Analysis and Design in Micro Deep Drawing Utilizing a Flexible Die**

## **THESIS**

**Submitted in Partial Fulfilment of the Requirements  
for the Degree of Doctor of Philosophy in  
the School of Engineering at the  
University of Glasgow**

**By**

**Ihsan Khalaf Irthiea**

**\*\*\*\*\***

**University of Glasgow**

**2013**

## **Acknowledgements**

---

First and foremost I would like to thank the almighty God (ALLAH) for giving me the knowledge, strength and patience to complete this work. May His blessings continue to shower on Prophet Mohammad (peace be upon him). I pray that He continues the same the rest of my life.

I wish to express my sincere thanks to Dr. Graham Green, my study advisor, for his generosity in spending a lot of time with me and precise guidance throughout the research project, upon which this dissertation is based. Moreover, I am grateful for his unique suggestions on my mental attitude towards both research works and people around me. His knowledgeable insights, outstanding perception and friendly personality showed me not only how to be an engineer, but how to be an active member in my community. This work would not have been possible without his continuous support and enthusiasm for applied research. My special thanks go to Dr. Safa Hashim for his helping to complete this work.

My special gratitude goes to my sponsor the Embassy of republic of Iraq in London and the Ministry of Higher Education and Scientific Research of Iraq for giving me the opportunity and the scholarship for my studies. I would also like to acknowledge the funding provided by the School of Engineering, University of Glasgow, in support of my attendance in the 14<sup>th</sup> international conference on Advances in Materials and Processing Technologies (AMPT 2011).

I wish to thank the wonderful people in the workshop in the James Watt South building/University of Glasgow for their technical support, assistance and kindness in manufacturing all the parts that I needed in this work. Special thanks for Mr. Kearns and Mr. Robb for their great help, support and friendly personality.

Thanks to everyone who helped me in completing this work especially my friends Dr. Abdulbast Kriama and Dr. Muayad Al-Sharad.

I sincerely thank big family for their unending support and patience for more than four years living abroad.

Finally, I am immensely grateful for my wife, Safa and I wish to express my unlimited appreciations for her patience, her encouragement her unconditional love! She always makes me strong, happy, hopeful and optimistic even with the most difficult circumstances.

## **Abstract**

---

As a result of the remarkable demands on electronic and other portable compact devices, the need to produce various miniaturized parts, particularly those made from metallic sheet is growing. In other words, in order for manufacturing companies to stay in competition, they are required to develop new and innovative fabricating processes to produce micro components with more complex features and a high standard of quality and functionality. Microforming is a micro fabrication process that can be employed efficiently for mass production with the advantages of greatly minimizing material waste and producing highly accurate product geometry. However, since the clearance between the rigid tools, i.e. punch and die, utilized in microforming techniques is relatively very small, there is a high risk of damaging the tools during the forming operations. Therefore, the use of forming tools made of flexible materials in sheet metal forming processes at micro scale has powerful potential advantages. The main advantages include a reduction in the production cost, eliminating the alignment and mismatch difficulties, and also the creation of parts with different geometrical shapes using the same flexible tool. As the workpiece is in contact with a flexible surface, this process can significantly improve the quality of the obtained products. Despite these clear advantages, micro flexible forming techniques are currently only utilized in very limited industrial applications. One reason for this is that the deformation behaviour and failure mode of sheet metals formed at micro scale are not yet well understood. Additionally, the experience-based knowledge of the micro-forming process parameters is not sufficient, particularly when flexible tools are used. Hence, to advance this technology and to improve the production quality of formed micro parts, more investigation of the key process parameters related to the material deformation are needed.

The main contribution of this work is the development of a novel technique for achieving micro deep drawing of stainless steel 304 sheets using a flexible die and where an initial gap (positive or negative) is adopted between the blank holder plate and an adjustment ring utilized in the size-scaled forming systems developed for this purpose. The interesting point here is that this study presents the first attempt of employing flexible material as a forming die tool in the micro deep drawing technology to produce micro metallic cups at different scaling levels. Polyurethane rubber materials are employed in this study for the forming flexible die with various Shore A hardness. Also, the stainless steel 304 sheets utilized for the workpieces have different initial thicknesses. Various parameters that have a significant influence on the

sheet formability at micro scale are carefully considered, these include initial gap value, rubber material properties, initial blank thickness, initial blank diameter, friction coefficients at various contact interfaces, diameter and height of the rubber die and process scaling factor. The size effect category of process dimension was also taken into account using similarity theory. Three size-scaled micro deep drawing systems were developed correspondingly to three different scaling factors. In each case, finite element simulations for the intended micro drawing systems are performed with the aim of identifying optimum conditions for the novel forming methodology presented in this thesis. The numerical models are built using the known commercial code Abaqus/Standard. To verify the microforming methodology adopted for the proposal technique as well as to validate the predictions obtained from simulations, an appropriate number of micro deep drawing experiments are conducted. This is achieved using a special experimental set up, designed and manufactured to fulfil the various requirements of the micro-forming process design procedure. The new knowledge provided by this work provides, for the first time, a predictive capability for micro deep drawing using flexible tools that in turn could lead to a commercially viable production scale process.

# **Process Analysis and Design in Micro Deep Drawing Utilizing a Flexible Die**

## **Declaration**

---

I declare that this thesis is a record of the original work carries out by myself under the supervision of Dr. Graham Green in the School of Engineering at the University of Glasgow, United Kingdom. The copyright of this thesis therefore belongs to the author under the terms of the United Kingdom Copyright acts. Due acknowledgment must always be made of the use of any material contained in, or derived from, this thesis. The thesis contains no material previously published or written by another person, except where due reference is made in the text of the thesis. The thesis has not been presented elsewhere in consideration for a higher degree.

Signature: .....

Date: .....

Printed name: Mr. Ihsan Khalaf Irthiea

Signature: .....

Date: .....

Printed name: Dr. Graham Green

## **List of Contents**

---

<b>Acknowledgements</b>	II
<b>Abstract</b>	III
<b>Declaration</b>	V
<b>List of Contents</b>	VI
<b>List of Figures</b>	X
<b>List of Tables</b>	XIX
<b>List of Acronyms</b>	XX
<b>CHAPTER ONE: INTRODUCTION</b>	
1.1 INTRODUCTION	1
1.2 OVERVIEW OF METAL FORMING TECHNOLOGY	1
1.3 SHEET METAL FORMING PROCESSES	3
1.4 DEEP DRAWING PROCESS	4
1.5 FLEXIBLE TOOLING IN SHEET METAL FORMING	5
1.6 MOTIVATIONS	7
1.7 OBJECTIVES AND RESEARCH HYPOTHESES	8
<b>CHAPTER TWO: ASPECTS OF DEEP DRAWING AND MICROSCALE TECHNOLOGY</b>	
2.1 DEFINITION OF DEEP DRAWING	11
2.2 MECHANICS OF DEEP DRAWING	12
2.3 ANALYSIS OF DEEP DRAWING	14
2.3.1 LIMITING DRAWING RATIO	18
2.3.2 EFFECT OF SHEET ANISOTROPY	20
2.3.3 EFFECT OF STRAIN HARDENING	21
2.3.4 PERCENTAGE REDUCTION IN DEEP DRAWING	22
2.4 DEEP DRAWING-ASSOCIATED DEFECTS	23
2.5 EARING	25
2.6 FORMABILITY	26
2.6.1 TENSILE TEST	26
2.6.2 CUPPING TEST	26
2.7 FORMING LIMIT DIAGRAM	27
2.8 IRONING	28
2.9 MICROSCALE MANUFACTURING	29
2.10 MICROFORMING PROCESSES	31
2.11 SIZE EFFECTS IN MICROFORMING PROCESSES	33
<b>CHAPTER THREE: LITERATURE REVIEW</b>	
3.1 INTRODUCTION	36
3.2 CONVENTIONAL DEEP DRAWING	36
3.2.1 BLANK HOLDING FORCE (BHF)	36

3.2.2	TOOL GEOMETRY	39
3.2.3	LUBRICANT STATUS	42
3.2.4	TOOL HEATING CONDITIONS	44
3.3	HYDRAULIC PRESSURE-ASSISTED DEEP DRAWING	47
3.3.1	HYDRO-MECHANICAL DEEP DRAWING	48
3.3.2	HYDROFORMING DEEP DRAWING	49
3.3.3	DEEP DRAWING AGAINST HYDRAULIC COUNTER PRESSURE	50
3.3.4	HYDRAULIC PRESSURE-AUGMENTED DEEP DRAWING	51
3.4	FLEXIBLE SHEET METAL FORMING TECHNOLOGY	52
3.5	SIZE EFFECT ON MICRO FORMING	56
3.6	MICRO DEEP DRAWING TECHNOLOGY	61
3.6.1	BLANK AND TOOL GEOMETRY	62
3.6.2	CONTACT SURFACE CONDITIONS	70
3.6.3	CHARACTERISTICS OF BLANK MATERIALS	79
3.7	FLEXIBLE TOOL-ASSISTED MICRO SHEET METAL FORMING	82

#### **CHAPTER FOUR: PROPOSED TECHNIQUES**

4.1	INTRODUCTION	92
4.2	PROPOSED TECHNIQUE	94
4.2.1	MICRO DEEP DRAWING WITH INITIAL POSITIVE GAP	95
4.2.2	MICRO DEEP DRAWING WITH INITIAL NEGATIVE GAP	97
4.2.3	MULTI SUBSTROKES-MICRO DEEP DRAWING WITH INITIAL POSITIVE GAP	98

#### **CHAPTER FIVE: CHARACTERIZATION OF MATERIAL BEHAVIOURS**

5.1	INTRODUCTION	102
5.2	TENSILE TEST OF SS 304 SHEET METALS	102
5.2.1	PREPARING THE TESTING SPECIMENS	102
5.2.2	TESTING PROCEDURE AND RESULTS	104
5.3	CALCULATING THE ANISOTROPY FACTORS	107
5.4	CHARACTERIZATION OF POLYURETHANE RUBBER PROPERTIES	111
5.5	UNIAXIAL COMPRESSION TEST OF URETHANE RUBBER MATERIALS	111
5.6	VOLUMETRIC COMPRESSION TEST OF URETHANE RUBBER MATERIALS	115
5.7	CALCULATING THE RUBBER MATERIAL PARAMETERS	118

#### **CHAPTER SIX: FE INVESTIGATIONS OF MICRO FLEXIBLE DEEP DRAWING**

6.1	INTRODUCTION	123
6.2	BASIC CONCEPTS OF FINITE ELEMENT METHOD	123
6.2.1	HISTORICAL BACKGROUND	124
6.2.2	OBTAINING THE STIFFNESS MATRIX	125



6.2.3	FORMULATING THE SHAPE FUNCTION	126
6.2.4	TRANSFORMING THE LOCAL SYSTEM TO THE GLOBAL SYSTEM	127
6.3	PROCESS SIMULATION BY ABAQUS SOFTWARE	130
6.3.1	INTRODUCTION TO ABAQUS SOFTWARE	130
6.3.2	ABAQUS BASICS	130
6.3.3	IMPLICIT AND EXPLICIT NUMERICAL SIMULATION APPROACHES	131
6.3.4	MODELLING THE MICRO DEEP DRAWING SYSTEM	132
6.3.4.1	FE MODELS FOR PART MATERIALS	134
6.4	SIMULATION RESULTS AND DISCUSSION	136
6.4.1	INITIAL GAP	139
6.4.2	RUBBER DIE MATERIAL	147
6.4.2.1	RUBBER TYPE	147
6.4.2.2	RUBBER HARDNESS	151
6.4.2.3	RUBBER COMPRESSIBILITY	156
6.4.3	RUBBER DIE DIMENSIONS	160
6.4.3.1	RUBBER DIE DIAMETER	160
6.4.3.2	RUBBER DIE HEIGHT	167
6.4.4	FRICTION COEFFICIENTS	169
6.4.4.1	FRICTION COEFFICIENT AT BLANK-HOLDER INTERFACE	170
6.4.4.2	FRICTION COEFFICIENT AT BLANK-RUBBER INTERFACE	173
6.4.4.3	FRICTION COEFFICIENT AT BLANK-PUNCH INTERFACE	175
6.4.5	BLANK DIMENSIONS	177
6.4.5.1	INITIAL BLANK DIAMETER	177
6.4.5.2	INITIAL BLANK THICKNESS	181
6.4.6	PUNCH TRAVEL	184
6.4.7	SCALING FACTOR	186
6.4.8	ANALYSIS OF THE INTERACTIONS OF PROCESS PARAMETERS	192

## **CHAPTER SEVEN: EXPERIMENTAL VALIDATIONS FOR FE SIMULATIONS**

7.1	INTRODUCTION	198
7.2	PREPARATION OF DRAWING WORKPIECES	198
7.3	DEVELOPMENT OF EXPERIMENTAL SETUP	201
7.4	DRAWING TOOLS	205
7.4.1	RIGID PUNCHES	205
7.4.2	BLANK HOLDERES	206
7.4.3	RUBBER DIES AND CONTAINERES	207
7.5	EXPERIMENTAL PROCEDURE	208
7.6	PREPARATION OF PRODUCED CUPS FOR MEASUREMENT	210
7.7	EXPERIMENTAL RESULTS AND COMPARISON	212
7.7.1	INITIAL GAP	214
7.7.1.1	THICKNESS DISTRIBUTION	214
7.7.1.2	PUNCH LOAD-TRAVEL RELATIONSHIPS	219
7.7.2	RUBBER TYPE	220
7.7.2.1	THICKNESS DISTRIBUTION	220
7.7.2.2	PUNCH LOAD-TRAVEL RELATIONSHIPS	224
7.7.3	BLANK DIAMETER	225

7.7.3.1 THICKNESS DISTRIBUTION	225
7.7.3.2 PUNCH LOAD-TRAVEL RELATIONSHIPS	229
7.7.4 BLANK THICKNESS	230
7.7.4.1 THICKNESS DISTRIBUTION	230
7.7.4.2 PUNCH LOAD-TRAVEL RELATIONSHIPS	234
7.7.5 PUNCH TRAVEL	235
7.7.5.1 THICKNESS DISTRIBUTION	235
7.7.5.2 PUNCH LOAD-TRAVEL RELATIONSHIPS	239
<b>CHAPTER EIGHT: CONCLUSION AND FUTURE WORK</b>	
8.1 CONCLUSION	243
8.2 RECOMMENDATIONS FOR FUTURE WORK	247
8.3 FUTURE WORK	248
<b>References</b>	249
<b>Appendix A</b>	257
<b>Publications</b>	268

## List of Figures

---

Figure	Title	Page
Figure 1-1	Classification of metal forming processes	2
Figure 1-2	Automotive parts produced by sheet metal forming	3
Figure 1-3	Schematic illustration of deep drawing process	5
Figure 2-1	Deep drawn products	11
Figure 2-2	Scheme of Deep Drawing Process	12
Figure 2-3	Steps of Deep Drawing Process	13
Figure 2-4	Deformation modes of elements in the flange and sidewall of deep drawn cup	14
Figure 2-5	Scheme showing the coordinate system on a partially drawn cup	16
Figure 2-6	Tensile test specimen cut from sheet metal along rolling direction	19
Figure 2-7	(a) Drawing force-stroke relationships with different (n) values (b) Limiting drawing ration values with different strain-hardening exponents	21
Figure 2-8	Deep drawing process in which the cross section area of the edge $A_0$ is reduced to $A_1$	22
Figure 2-9	Stress status on the flange portion of a formed cup	23
Figure 2-10	Failure modes in deep drawing process	24
Figure 2-11	Earing in a deep drawn cup	25
Figure 2-12	(a) Grid pattern (b) Samples used in cupping test	27
Figure 2-13	(a) Forming limit diagram for various sheet metals (b) the definition of positive and negative minor strains	28
Figure 2-14	Schematic view of ironing process	29
Figure 2-15	Examples on micro components	30
Figure 2-16	Typical devices produced through micro forming technology	32
Figure 2-17	Micro sheet metal products	33
Figure 2-18	Effect of geometric factor on flow stresses	34
Figure 2-19	Microstructure of a specimen in both macro and micro scale	35
Figure 3-1	Schematic of construction and movement of tapered blank holder	39
Figure 3-2	Four typical hydraulic pressure-assisted deep drawing methods	47
Figure 3-3	Hydroforming process using multiple membranes	50
Figure 3-4	Flow curves of CuNi18Zn20 obtained through tensile test for different thicknesses	58

Figure 3-5	Schematic representation of the three main groups of size effects, F force, $F_A$ adhesion force, $F_F$ friction force, $F_G$ gravity	59
Figure 3-6	Variation of (a) maximum load and yield point load with grain size and (b) tension and bending yield strength with thickness to grain size ratio.	60
Figure 3-7	Effect of N (thickness to grain size ratio) on material flow stress	60
Figure 3-8	Effect of (a) specimen/grain size (N) and (b) feature/specimen size (M) on material flow stress	61
Figure 3-9	Micro deep drawing results for 0.1mm blank thickness, $\beta$ =Limit drawing ratio	63
Figure 3-10	Punch force versus normalised drawing depth	66
Figure 3-11	Friction function of micro deep drawing process with a punch diameter of 1mm	68
Figure 3-12	Drawn parts out of (a) non-optimized and (b) optimized blank shapes for Al99.5	68
Figure 3-13	Lubricant pocket theory for the coefficient of friction	71
Figure 3-14	Example of surface roughness model (under surface of blank)	73
Figure 3-15	Surface roughness of the micro cups drawn through (a) first-stage (b) second-stage	74
Figure 3-16	Comparison of micro and macro deep drawing cups	75
Figure 3-17	Variation of friction $\mu$ for punch diameter 8 mm	76
Figure 3-18	Frictions in deep drawing	77
Figure 3-19	Sheet thickness of various measurement points	78
Figure 3-20	Cups drawn of different Al-Zr foils with different drawing ratios	80
Figure 3-21	The plot of the average cup heights of all cases	82
Figure 3-22	The average cup height increase percentage for all cases	82
Figure 3-23	Rigid lower dies	83
Figure 3-24	Defects of formed cups by SR dies	84
Figure 3-25	Micro/meso sheet forming process to manufacture micro-groove features	85
Figure 3-26	(a) Process amendment to eliminate the wrinkle at the corner (b) rigid die	86
Figure 3-27	Schematic of Maslennikov's process	87
Figure 3-28	(a) velocity distributions of the polyurethane ring and the blank (b) Variations of radial stress distributions	88
Figure 3-29	Sketch of rubber pad forming: (a) concave deformation style and (b) convex deformation style	89
Figure 3-30	Photograph of the forming equipment for the experiment	89
Figure 3-31	(a) front of the bipolar plate and (b) back of the bipolar plate	90
Figure 3-32	Die inserts: 1-channel, 3-channel, and 6-channel dies	91

Figure 4-1	(a) Concave die and (b) convex die drawing strategies	93
Figure 4-2	The basic schematic configuration of the proposed technique	94
Figure 4-3	The first strategy of micro deep drawing adopted with positive gap	95
Figure 4-4	The second strategy of micro deep drawing adopted with negative gap	97
Figure 4-5	The third strategy of micro deep drawing with multi stages	100
Figure 5-1	Tensile test specimen	103
Figure 5-2	3D micro computerized cutting machine	103
Figure 5-3	Tensile test specimens	104
Figure 5-4	(a) Instron 5969 machine (b) Tested specimens (c) Broken specimen on the machine	105
Figure 5-5	Stress-strain relationship for SS 304 sheet of 60 $\mu$ m in thickness at three different directions	106
Figure 5-6	Stress-strain relationship for SS 304 sheet of 100 $\mu$ m in thickness at three different directions	106
Figure 5-7	Stress-strain relationship for SS 304 sheet of 150 $\mu$ m in thickness at three different directions	106
Figure 5-8	Measuring the rubber hardness using Durometer Shore A	111
Figure 5-9	Instron 3956 machine used for the uniaxial compression test	112
Figure 5-10	(a) Rubber specimens (b) Rubber 40A specimen under compression load	113
Figure 5-11	Uniaxial compression load-displacement relationships of 40 Shore A rubber hardness	114
Figure 5-12	Uniaxial compression load-displacement relationships of 63 Shore A rubber hardness	114
Figure 5-13	Uniaxial compression load-displacement relationships of 75 Shore A rubber hardness	114
Figure 5-14	Uniaxial compression load-displacement relationships of rubber materials with different hardness	115
Figure 5-15	Experimental device for the volumetric testing	116
Figure 5-16	Volumetric testing load-displacement relationships of 40 Shore A rubber hardness	116
Figure 5-17	Volumetric testing load-displacement relationships of 63 Shore A rubber hardness	117
Figure 5-18	Volumetric testing load-displacement relationships of 75 Shore A rubber hardness	117
Figure 5-19	Volumetric compression load-displacement relationships	117
Figure 5-20	Pressure versus volume ratio relationship for rubber 40 Shore A	120
Figure 5-21	Pressure versus volume ratio relationship for rubber 63 Shore A	120
Figure 5-22	Pressure versus volume ratio relationship for rubber 75 Shore A	121

Figure 6-1	Relation of nodes, elements and mesh	124
Figure 6-2	Basic element structure	125
Figure 6-3	A simple element with local coordinate system	127
Figure 6-4	(a) Global coordinate system (b) Local coordinate system	128
Figure 6-5	Transformation of local coordinate system	128
Figure 6-6	The main stages of analysis procedure in Abaqus	130
Figure 6-7	Scheme of the micro deep drawing system	133
Figure 6-8	FE meshing of the deep drawing components	135
Figure 6-9	Models of drawn cups obtained from FE simulations (a) Von-Mises stress distribution (b) thickness distribution	136
Figure 6-10	Thickness distributions at rolling diagonal and transverse directions for a drawn cup	137
Figure 6-11	Tensile strain distributions at rolling, diagonal and transverse directions for a drawn cup	138
Figure 6-12	Flange region profile	139
Figure 6-13	The profiles of the final cups drawn with different initial gaps	140
Figure 6-14	Thickness distribution along the rolling direction for cups drawn with different gaps	140
Figure 6-15	Thickness distribution along the diagonal direction for cups drawn with different gaps	141
Figure 6-16	Thickness distribution along the transverse direction for cups drawn with different gaps	141
Figure 6-17	The maximum reduction in thickness at the transverse direction using different initial gaps	142
Figure 6-18	Strain distribution along the rolling direction for cups drawn with different gaps	144
Figure 6-19	Strain distribution along the transverse direction for cups drawn with different gaps	144
Figure 6-20	Strain distribution along the diagonal direction for cups drawn with different gaps	144
Figure 6-21	Punch load-travel relationship for different initial gaps	145
Figure 6-22	Maximum punch load values obtained from simulations using different initial gaps	146
Figure 6-23	Profiles of the final cups produced through simulations using different rubber die materials	148
Figure 6-24	Stress distribution obtained from simulation for different rubber materials	148
Figure 6-25	Thickness distribution along the rolling direction using different rubber materials	149
Figure 6-26	Thickness distribution along the diagonal direction using different rubber materials	149
Figure 6-27	Thickness distribution along the transverse direction using different rubber materials	150

Figure 6-28	Punch load-travels relationships obtained of using different rubber materials and initial gaps	151
Figure 6-29	Punch load-travels relationships obtained of using different rubber materials with no initial gap	151
Figure 6-30	Cups Obtained from numerical simulations with different rubber hardness	152
Figure 6-31	Final profiles of cups obtained from simulations	153
Figure 6-32	Thickness distribution along the rolling direction with using different rubber hardness values	154
Figure 6-33	Thickness distribution along the diagonal direction with using different rubber hardness values	154
Figure 6-34	Thickness distribution along the transverse direction with using different rubber hardness values	155
Figure 6-35	Punch load-travel relations with using different rubber hardness	156
Figure 6-36	Cups Obtained from numerical simulations with different rubber Poisson's ratios (a) 0.499399 (b) 0.499715 (c) 0.499874	157
Figure 6-37	Thickness distribution along the rolling direction with using different rubber Poisson's ratios	158
Figure 6-38	Thickness distribution along the diagonal direction with using different rubber Poisson's ratios	158
Figure 6-39	Thickness distribution along the transverse direction with using different rubber Poisson's ratios	158
Figure 6-40	Punch load-travel relations with using different rubber Poisson's ratios hardness	160
Figure 6-41	Profiles of the final cups obtained with different rubber die diameters	161
Figure 6-42	The specified initial gaps required to be used with different rubber die diameter	161
Figure 6-43	Von-Mises stress distributions obtained by using different rubber-die diameters ( $D_R$ )	162
Figure 6-44	Thickness distributions obtained by using different rubber-die diameters with no gaps	163
Figure 6-45	Maximum reduction in thickness obtained by using different rubber -die diameters with no gaps	163
Figure 6-46	Thickness distributions obtained by using different rubber-die diameters with specified gaps	164
Figure 6-47	Maximum reduction in thickness obtained using different identified gaps	164
Figure 6-48	Punch load-travel relationships obtained by using different rubber-die diameters with no gap	165
Figure 6-49	Maximum punch load obtained by using different rubber-die diameters with no gaps	165
Figure 6-50	Punch load-travel relationships obtained with different rubber-die diameters and identified gaps	166
Figure 6-51	Maximum punch load obtained by using different rubber-die diameters with identified gaps	166
Figure 6-52	Cups obtained from simulations with different rubber-die heights ( $h_R$ ) with no gaps	167
Figure 6-53	Thickness distribution along the transverse direction with identified gaps	168

Figure 6-54	Punch load-travel relationships obtained by using different rubber-die heights with identified gaps	169
Figure 6-55	Stress distribution along the transverse direction obtained by using different $\mu_{BH}$ values	170
Figure 6-56	Thickness distribution along the transverse direction obtained by using different $\mu_{BH}$ values	171
Figure 6-57	Maximum reduction in thickness obtained by using different $\mu_{BH}$ values	172
Figure 6-58	Punch load-travel relationships obtained by using different $\mu_{BH}$ values	172
Figure 6-59	Maximum punch load obtained by using different $\mu_{BH}$ values	173
Figure 6-60	Thickness distribution along the transverse direction obtained by using different $\mu_{BR}$ values	174
Figure 6-61	Punch load-travel relationships obtained by using different $\mu_{BH}$ values	175
Figure 6-62	Thickness distribution along the transverse direction obtained by using different $\mu_{BP}$ values	176
Figure 6-63	Maximum reduction in thickness obtained by using different $\mu_{BP}$ values	176
Figure 6-64	Punch load-travel relationships obtained by using different $\mu_{BP}$ values	177
Figure 6-65	Cups obtained from simulation with different initial blank diameters ( $D_b$ )	178
Figure 6-66	Thickness distributions along the rolling direction of cups drawn with different blank diameters	179
Figure 6-67	Thickness distributions along the diagonal direction of cups drawn with different blank diameters	179
Figure 6-68	Thickness distributions along the transverse direction of cups drawn with different blank diameters	179
Figure 6-69	Maximum reductions in thickness for cups formed from different blank diameters	180
Figure 6-70	Punch load-travel relationships obtained using different blank diameters	180
Figure 6-71	Cups obtained from simulation using different initial blank thickness	181
Figure 6-72	Thickness distribution obtained using blank of 60 $\mu$ m initial thickness	182
Figure 6-73	Thickness distribution obtained using blank of 100 $\mu$ m initial thickness	182
Figure 6-74	Thickness distribution obtained using blank of 150 $\mu$ m initial thickness	182
Figure 6-75	Maximum reduction in thickness using different initial blank thicknesses	183
Figure 6-76	Punch load-travel relationships obtained by using different initial blank thicknesses	184
Figure 6-77	(a) stress and (b) thickness distributions for cups obtained from FE simulations with different drawing strokes	185
Figure 6-78	Thickness distribution along transverse direction for different punch strokes	186
Figure 6-79	Profiles of cups produced with different scaling factors	187
Figure 6-80	Thickness distribution along rolling direction obtained for different scaling factors	188



Figure 6-81	Thickness distribution along diagonal direction obtained for different scaling factors	188
Figure 6-82	Thickness distribution along transverse direction obtained for different scaling factors	189
Figure 6-83	Punch load-travel obtained with different scaling factors	189
Figure 6-84	Maximum reductions in thickness obtained for different friction coefficient $\mu_{BH}$	190
Figure 6-85	Stress and thickness contour distributions obtained with aspect ratio of 1.48 and $\lambda=1$	191
Figure 6-86	Maximum reductions in thickness obtained with different scaling factors for aspect ratio of approximately 1.5	192
Figure 6-87	Initial gap via friction coefficient relationship for blank diameter of 9mm	193
Figure 6-88	Initial gap via friction coefficient relationship for blank diameter of 10mm	193
Figure 6-89	Initial gap via friction coefficient relationship for blank diameter of 11mm	193
Figure 6-90	Initial gap via friction coefficient relationship for blank thickness of 60 $\mu$ m	194
Figure 6-91	Initial gap via friction coefficient relationship for blank thickness of 100 $\mu$ m	195
Figure 6-92	Initial gap via friction coefficient relationship for blank thickness of 150 $\mu$ m	195
Figure 6-93	Initial gaps adopted at different scaling factors	196
Figure 6-94	Maximum reductions in thickness obtained at different scaling factors	197
Figure 6-95	Maximum punch loads obtained at different scaling factors	197
Figure 7-1	Applications of micro stainless steel cups	199
Figure 7-2	Stainless steel 304 blanks of different thicknesses ( $t_b$ ) (a) failed cutting process with obvious burrs	200
Figure 7-3	Blanking tools, punch of head diameter $D_p=10$ mm and dies of opening diameters of (a) 10.012mm (b) 10.02mm and (c) 10.03mm	200
Figure 7-4	(a) Blanking punch-die sets tools (b) SS 304 blanks of 100 $\mu$ m in thickness with different diameters	201
Figure 7-5	Experimental set up	202
Figure 7-6	Components of the experimental set up (a) upper component set and (b) lower component set	203
Figure 7-7	Drawing tools	204
Figure 7-8	Assembly of the drawing tools	204
Figure 7-9	Rigid punches of different head diameters ( $D_p$ ) corresponding to different scaling factors	205
Figure 7-10	Blank holders of corresponding to different scaling factors ( $\lambda$ )	206
Figure 7-11	Rubber containers used at different scaling factors ( $\lambda$ )	207
Figure 7-12	Rubber Pisces that are used for the flexible forming dies	208
Figure 7-13	The experimental; apparatus is set on the Instron machine	209

Figure 7-14	Tubular-shaped positioning components for different blank diameters ( $D_b$ )	210
Figure 7-15	The high precise cut-off saw machine used for cutting the produced cups	211
Figure 7-16	Cutting section of the metallic cup and epoxy black	212
Figure 7-17	(a) Physical cups (b) Comparison between physical and simulated cups in terms of final profiles	213
Figure 7-18	Surtronic 3P Taylor-Hobson roughness tester	214
Figure 7-19	Physical parts formed with different initial gaps	215
Figure 7-20	Physical cups drawn with different initial gaps and cut along the rolling and transverse directions	216
Figure 7-21	Experimental and numerical thickness distributions with initial gap of 100 $\mu$ m	217
Figure 7-22	Experimental and numerical thickness distributions with no initial gap	217
Figure 7-23	Experimental and numerical thickness distributions with initial gap of -100 $\mu$ m	217
Figure 7-24	Maximum reductions in thickness with different initial gaps	218
Figure 7-25	Comparison between punch load-travel relationships with different initial gaps	219
Figure 7-26	Comparison between maximum punch loads obtained from experiments and simulations	220
Figure 7-27	Physical cups formed using different rubber materials with different initial gaps	221
Figure 7-28	Physical cups drawn under conditions of different rubber materials	222
Figure 7-29	Experimental and numerical thickness distributions obtained using rubber 40 Shore A hardness	223
Figure 7-30	Experimental and numerical thickness distributions obtained using rubber 63 Shore A hardness	223
Figure 7-31	Experimental and numerical thickness distributions obtained using rubber 75 Shore A hardness	223
Figure 7-32	Maximum reductions in thickness with different rubber materials	224
Figure 7-33	Comparison between punch load-travel relationships obtained using different rubber materials	224
Figure 7-34	Comparison between maximum punch loads obtained with using different rubber materials	225
Figure 7-35	Physical cups formed using blanks of different initial diameters ( $D_b$ )	226
Figure 7-36	Experimental and numerical thickness distributions obtained using a blank of 9mm in diameter	227
Figure 7-37	Experimental and numerical thickness distributions obtained using a blank of 10mm in diameter	227
Figure 7-38	Experimental and numerical thickness distributions obtained using a blank of 11mm in diameter	227
Figure 7-39	Maximum reductions in thickness with different blank diameters	228
Figure 7-40	Comparison between punch load-travel relationships obtained using different blank diameters	229

Figure 7-41	Comparison between maximum punch loads obtained with using different blank diameters	230
Figure 7-42	Cups formed from different sheet metal thicknesses with no initial gap	230
Figure 7-43	Physical cups formed using blanks of different initial thickness ( $t_b$ )	231
Figure 7-44	Physical cups drawn from blanks of 150 $\mu$ m and 60 $\mu$ m in thickness	231
Figure 7-45	Experimental and numerical thickness distributions obtained using a blank of 60 $\mu$ m in thickness	232
Figure 7-46	Experimental and numerical thickness distributions obtained using a blank of 100 $\mu$ m in thickness	232
Figure 7-47	Experimental and numerical thickness distributions obtained using a blank of 150 $\mu$ m in thickness	233
Figure 7-48	Maximum reductions in thickness with different blank thicknesses	233
Figure 7-49	Comparison between punch load-travel relationships obtained using different blank thicknesses	234
Figure 7-50	Comparison between maximum punch loads obtained with using different blank thicknesses	235
Figure 7-51	Comparison between the numerical and experimental cups with different depths	236
Figure 7-52	Experimental and numerical thickness distributions obtained for aspect ratio of 0.75	237
Figure 7-53	Experimental and numerical thickness distributions obtained for aspect ratio of 1	237
Figure 7-54	Experimental and numerical thickness distributions obtained for aspect ratio of 1.25	237
Figure 7-55	Maximum reductions in thickness with different aspect ratios	238
Figure 7-56	Comparison between punch load-travel relationships obtained for different aspect ratios	239
Figure 7-57	Comparison between maximum punch loads obtained with different aspect ratios	240
Figure 7-58	Comparison between the physical and simulated cups using the multi sub-strokes-drawing technique	241
Figure 7-59	Physical cups drawn at the scaling factors $\lambda=0.5$ and $\lambda=1$	241
Figure 7-60	Physical cups drawn at different scaling factors for different aspect ratios	242

## **List of Tables**

---

<b>Table</b>	<b>Title</b>	<b>Page</b>
Table 3-1	Cases investigated in the experimental work	62
Table 3-2	Tool data table: geometry parameters of tool sets	65
Table 3-3	Description of the process dimensions used in this study	69
Table 3-4	Tool data table	76
Table 3-5	The die diameters and shoulder radii of the three experimental dies	81
Table 4-1	Geometrical parameters for the micro deep drawing of cylindrical parts	101
Table 5-1	Chemical composition of SS304 sheets	103
Table 5-2	Mechanical properties of SS 304 sheets	107
Table 5-3	The r-values and anisotropic stress yield ratios of SS 304 sheets	110
Table 5-4	Mechanical properties of different Polyurethane rubber materials	122
Table 6-1	Process parameters for micro deep drawing simulations using different rubber materials	147
Table 6-2	Process parameters for micro deep drawing simulations under different friction conditions	169
Table 6-3	Geometrical parameters of the micro deep drawing process	187

## Abbreviations

---

LDR	Limiting Drawing Ratio
$n$	Strain Hardening Exponent
$\varepsilon_z$	Strain in thickness direction
$\eta$	Deformation Efficiency
R	Plastic Strain Ratio or Normal Anisotropy
$R_0$	Plastic Strain Ratio at Rolling Direction
$R_{45}$	Plastic Strain Ratio at 45° Diagonal Direction
$R_{90}$	Plastic Strain Ratio at Transverse Direction
$\bar{R}$	Average plastic strain ratio
$\Delta R$	Planar Anisotropy
$\sigma_f$	Flow Stress
FLD	Forming Limit Diagram
MOES	Micro-Optical Electronics Systems
MEMS	Micro-Electro-Mechanical Systems
MOEMS	Micro-Optical-Electro-Mechanical Systems
LIGA	Lithography, Electroforming, and Moulding
$\lambda$	Scale Factor
BHF	Blank Holding Force
BHP	Blank Holding Pressure
CAD	Computer-Aided Design
CAM	Computer-Aided Manufacturing
DLC	Diamond Like Carbon Film
PE	Polyethylene Film
PET	polytetrafluoroethylene film
$D_p$	Punch Diameter
$R_p$	Punch Corner Radius
$D_b$	Blank Diameter
$D_r$	Rubber Diameter
$h_r$	Rubber Height
$\sigma_o$	Yield Strength
$\sigma_{ult}$	Tensile Strength
$\nu$	Poisson's ratio
K	Strength Coefficient
$\varepsilon_L$	Length Strain
$\varepsilon_W$	Width Strain
$\theta$	Angle to Rolling Direction
$C_{01}, C_{10}$	Rubber Hyperelastic Behaviour Factors (Mooney-Rivlin Coefficients)
$D_1$	Rubber Compressibility Factor
$J_{el}$	Elastic Volume Ratio
$K_o$	Bulk Modulus
$\mu_o$	Initial Shear Modulus
$\mu_{BH}$	Friction Coefficient at Blank/Holder Interface
$\mu_{BR}$	Friction Coefficient at Blank/Rubber Interface
$\mu_{BP}$	Friction Coefficient at Blank/Punch Interface

# **CHAPTER ONE**

## **INTRODUCTION**

\*\*\*\*\*

### **1.1 INTRODUCTION**

The current research study investigates the capability of achieving deep drawing processes on stainless steel 304 sheets of different thicknesses at micro scale via employing flexible forming tool. This work proposes a novel technique for conducting micro deep drawing processes through a adopting an initial gap (positive or negative) between the blank holder plate and the adjustment ring utilised in the forming system developed for this purpose. In accordance with this proposed system, the blank holder is allowed to move against spring forces under the effect of hydrostatic pressure excited in the rubber material during the drawing operation. The interesting point here is that this study presents the first attempt of employing flexible material (Polyurethane rubber) as a forming die tool in micro deep drawing technology to produce micro metallic cups at different scaling levels. The main target is to advance the micro deep drawing technology owing to reduce the overall production cost and to improve the final quality of the formed parts. Therefore, it is of high importance to present a background on metal forming processes, particularly sheet metal forming, to explain what the various techniques used in this field and the industrial applications in which this technology can be efficiently utilized. Also, in order to provide a clear vision on the subject of this research, it is essential to understand how flexible materials can be utilized in sheet metal forming and what the contributions of this technique. Therefore, an overview on using flexible tools in sheet metal forming processes is briefly introduced in this chapter.

### **1.2 OVERVIEW OF METAL FORMING TECHNOLOGY**

In the various industrial fields 85% of all metal is processed through so called casting operation to obtain products in simple forms like ingots and slabs, and these products are then used for further deformation operations [1]. In manufacturing the deformation processes can be divided into groups depending on temperature, shape and size of the used workpieces and operation type. For example, there are three categories of processes based on temperature as a criterion, which are cold, warm and hot working. In dependence on the type of the deformation operation, the processes can be also classified as primary and secondary working. Primary working operations include taking pieces of metallic products that are generally in a cast state, and then they can be formed into other shaped parts such as slabs, plates and

billets. Additional processing can be performed on some of those products through secondary working to produce the final shape of desired components such as bolts, sheet metal parts and wire [2].

Metal forming includes a wide range of manufacturing processes in which metal workpiece is experienced a plastic (permanent) change in the shape via applying external forces by means of various forming tools called dies. However, metal forming processes preserve both the mass and the cohesion [1-3]. It is very important to distinguish between the terms “forming” and “deforming”. In the case of controlled plastic straining to gain a specific shape for the product, the term forming should be used, whereas the term deforming should be used with uncontrolled plastic strain [4].

In metal forming processes that use forming tools, usually called dies, stresses exceeding the yield strength of the metal are generated in the processed workpiece. The metal hence deforms and the desired part is produced with a shape taken from the geometry of the used die. The success of the metal forming process indicates that the plastic deformation of the workpiece occurs without material failure. However, flowing of the metal into the forming die is not easy because the deformation occurs in the solid state. Therefore, it is necessary in designing metal working processes to take into account not only the laws of material behaviour but also the ductility of material and pressure, forces and power requirements. In addition, the interactions between material properties and process conditions play the major crucial role in success of the metal forming processes [1]. All of the shaping processes such as solidification processes, formation processes and material removal, are generally classified under the title of metal forming technology [2].

In accordance with the size and shape of the workpiece, it is possible to classify the metal forming processes into two main categories: Bulk deformation processes and sheet metal processes. As shown in **Figure 2-1** each of these two categories can be divided to various types of shaping operations [3].

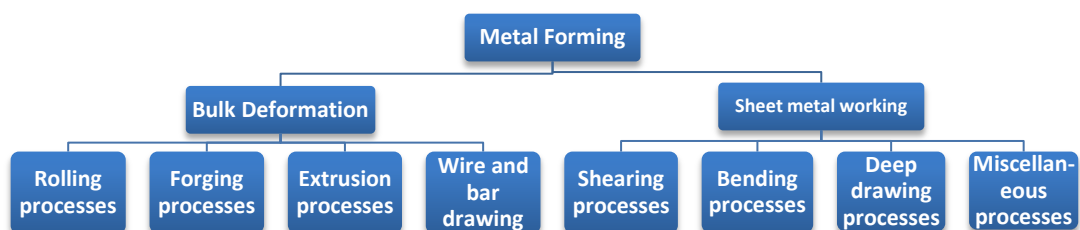


**Figure 2-1. Classification of metal forming processes [3]**



Bulk deformation can be defined as the forming process that changes extensively the size and/or shape of the cross section of the workpiece [5]. In this process, the distinctive characteristic of the workpiece is the small ratio of surface area to volume (or surface area to thickness), and the term “bulk” describes this small ratio. Moreover, bulk deformation can be categorised in general into four major shaping operations which are rolling, wire and bar drawing, forging and extrusion as seen in **Figure 2-1** [1, 3].

### 1.3 SHEET METAL FORMING PROCESSES

Sheet metal working can be generally identified by cutting and forming operations performed on metallic sheets [3]. In order to distinguish between the terms “sheet” and “plate”, it is important to realize that the range of sheet thickness is typically from 0.4mm to 6mm, while the term plate usually refers to the product of thickness greater than 6mm. The work metal used in sheet metal forming, whether sheet or plate is produced by rolling, hence the significant importance of sheet metal forming outlines the importance of the rolling process. Traditionally sheet is available as coils if it is thin; otherwise it is supplied as flat sheet or plate. Sheet metal parts are utilized in different industrial applications such as automobile and truck bodies, aircraft, railway cars, farm and construction equipment, beverage cans, kitchen utensils, etc. [2] (see **Figure 2-2**).



**Figure 2-2. Automotive parts produced by sheet metal forming [6]**

Unlike the bulk forming processes, the major characteristic of sheet metal forming is the use of a workpiece with high ratio of surface area to thickness. In sheet metal forming, tensile forces are mainly utilized in the plane of the sheet to achieve the process, whereas compressive forces that are generated in the transverse direction as a result of the tension may result in folding or wrinkling of the sheet. As a result, any reduction in the thickness is due

to tensile stress induced in the sheet itself. Therefore, the most important concern in all sheet metal forming processes is to avoid excessive decreasing in thickness, which can lead to necking and fracture [2, 7]. Usually most of the sheets forming processes are carried out at room temperature (cold processing conditions) excepting if the workpiece is thick; the sheet metal is brittle or the deformation is massive. Almost with these cases warm conditions are adopted through the forming operation. As shown in **Figure 2-1** sheet metal forming processes are generally divided into three major categories that are cutting, bending and drawing [3].

#### 1.4 DEEP DRAWING PROCESS

One of the most common and industrial applicable processes in sheet metal forming is deep drawing. It can fabricate a variety of objects with cylindrical, square or even complex shapes by using this technique [8]. Deep drawing is defined as a manufacturing process through which a sheet metal work piece is subjected to tensile and compressive stresses by mechanical punch to press the blank into a die cavity as seen in **Figure 2-3**. The condition of the product to be deep drawn is that the final depth is greater than a half of the drawing punch diameter; otherwise the product is classified as a shallow part. In order to prevent the material blank from flowing freely into the die cavity through the process, a third forming tool, which is named blank holder, is employed to hold down the blank [9]. This technique can be widely applied to manufacture metal products with an aspect ratio larger than unity. Currently, the deep drawing process has an extensive role in aerospace and automobile industries to manufacture structural components, and in computer and communication industries to produce covers and thin-walled part of devices, like laptop, cameras, and CD and DVD drivers. In addition, it is used in fabricating aluminium cans, canisters, sinks, baking pans, oil filters, home décor, etc. [10].

In the deep drawing technique, the flat piece obtained from a large sheet metal is named blank which is usually clamped on the top surface of the forming die by means of a rigid tool conventionally called blank-holder. In order to obtain a symmetric shape for a defects-free product, the centre point of the blank should coincide exactly with the centre of the die opening. In general, two main resources contribute in providing the force needed to form the sheet metal blank completely. The first force is that used to hold the sheet in contact with the upper surface of the die. This force is known as the blank holding force because it is applied through the blank holder to catch the blank. The other one is provided by the punch.

The function of the punch force is to form the blank into the die cavity. Therefore, consequently the main tools required in deep drawing process are a male punch, a female die and a blank holder plate [11]. Usually between the sides of the drawing punch and die, a particular clearance is embraced and the value of this clearance is about 10% greater than the original blank thickness [3].

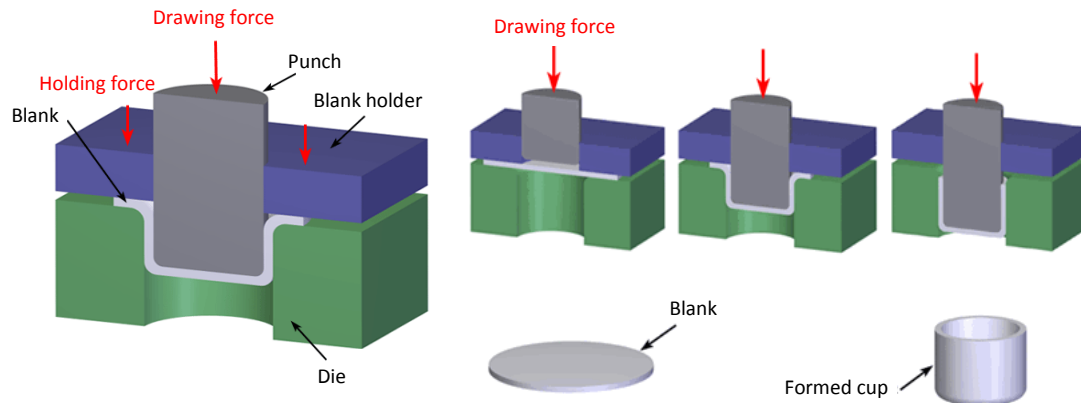


Figure 2-3. Schematic illustration of deep drawing process. [12]

It is obvious now that sheet metal forming by deep drawing techniques has a remarkable role in many manufacturing fields in the world. Several deep drawing techniques have been proposed in the last 50 years to improve the performance of this technology. Actually, developing the deep drawing technique does not mean only how it can overcome the problems corresponding the process, but the main object is what are the possible procedures to increase the drawing ratio, minimize the thickness variation of the drawn cups, and reduce the tooling cost especially for products with complex features [13]. Therefore, to increase the productivity and efficiency of the drawing operation and to get satisfactory-quality drawn cups, many special techniques have been embraced to achieve deeper products.

## 1.5 FLEXIBLE TOOLING IN SHEET METAL FORMING

Of the key parameters in sheet metal forming processes that have crucial influence on the quality of the final formed products are the punch and die radii, the punch to die clearance, the heat treatment of tooling, the lubrication, the press force and the blank-holding pressure. Therefore, an inappropriate tooling design actually results in unsuccessful forming operation, failed products and even excessive tooling wear, and this in turn leads to increase in manufacturing time and cost of the tools used. It have been found that one of the best

solutions which can greatly reduce the tooling cost is replacing the rigid punch/or die by others made from flexible materials. Therefore, it is important to present here an overview on contribution of flexible tools in sheet metal forming technology [14].

In the preceding section, it can be noticed that the forming processes are performed using tools (both punch and die) made from solid materials. In fact there are special operations defying this usual role by adopting unconventional forming tools. During the last 50 years. Many innovative techniques were experienced in metal forming, which can be classified in different categories depending on the nature of the tools used. The unconventional operations are in fact assisted by hydraulic pressure and flexible materials (elastomers) in forming workpieces. Flexible tools-assisted forming processes employ different types of rubber such as natural rubber, polyurethane rubber, silicon rubber and polyamide rubber [14].

Since 1960 when polyurethane is introduced into industry fields with a wide range of hardnesses. Using flexible tools in metal forming processes became more interesting. Polyurethane rubber has a significant potential in different applications, where it is employed as wear pad, springs and male and female dies. Because the polyurethane is provided in high level of hardnesses, even much higher than that of the natural rubber, it has greater resistance to wear and corrosion of oil and other chemicals [15]. Furthermore, polyurethane rubber is able to endure loading of up to 50000 cycles and temperature of up to 150°C [14].

In competition with conventional forming processes, adopting flexible tools in metal forming provides several advantages, such as no accurate assembly between the male and female dies is required because just one rigid former is utilized in this process thus the cost and time of tool manufacturing can be significantly reduced. Moreover, different shapes for formed parts can be produced using the same flexible pad and however just changing the rigid forming die. Also, because the blank is in direct contact with soft surface of the flexible material, then products with high surface quality can be obtained. Usually in flexible forming processes, there is no need for using lubricants especially at the interface between rubber tool and blank. Furthermore, as the contact surface between the rubber pad and the rigid die is flexible, the formability of the blank material therefore can be remarkably improved [14, 15].

On the other hand, the disadvantages of this process involve higher press capacity is needed over the conventional forming operations using rigid tools. That is because as the rigid punch advances, the rubber pad acts as a cushion generating somewhat like hydraulic pressure on the blank surface to support it against the punch. Also, the number of the forming strokes is

limited for each flexible pad and then it need to be replaced with a new one. The main techniques in which flexible tool commonly employed are Guerin process, Marforming Process and Verson-Wheelon. As well as many forming operations including bending, embossing, drawing, roll forming, blanking and piercing, free forming and tube bulging, using flexible tooling can be performed depending on the principles of those techniques [14, 15].

## **1.6 MOTIVATIONS**

As well known, the technology has become the main source of the various facilities that are mainly needed in our life, therefore progressive development is widely noticed nowadays in different modern industries. Also, a significant orientation to miniaturization, integration and compaction in devices used in different industrial fields, such as electronics, medical equipment, telecommunication components, automotive industry, etc., can be increasingly observed. The increasing demand on mini and compact devices through the last decade has resulted in growing rate in producing competitive miniaturized parts. As a result, consumers are looking now for more modern styles of these devices, including integrated functions. Hence, currently portability and miniaturization represent the most imperative requirements for markets as well as the most important goal for manufacturers.

The tiny parts, such as micro screws, micro springs and connector pins, are usually utilized and extremely required in mass production, in some electronics equipment such as CD players, DVD players, microprocessors and IC units that can be classified into micro-electromechanical systems (MEMS). As a result of all what mentioned above, it is essential to provide appropriate fabrication processes in order to produce micro metallic components and parts which can be used in of such mini devices. Although, high dimensional accuracy and product quality can be obtained by the micromachining and lithographic technologies, especially LIGA – processes, the tool costs are comparatively high and the types of material which can be processed are limited. Moreover, another challenge still facing the micro electro mechanical system technology (MEMS) is the difficulty in fabricating 3D components accurately. So, it has been investigated that the best alternative technology, especially for micro sheet metal products, is micro forming because of its simplicity, high production rate, excellent mechanical properties, minimized material waste and close tolerance. However, it can be realized that there is no clear revelation on the principles of micro forming technology enabling one to predict anything related to process directly. When a forming process is scaled

down from macro to micro size, the challenges is not only coming from the peculiarity of the process itself, but other problems related to tools, machine and also material behaviour are associated strongly with the miniaturization.

On the other hand, in order to keep up the technological advances and to stay competitive, manufacturing companies are required to develop innovative techniques to improve the characteristics of their products in terms of quality, production rate and cost as well. Due to the several interesting advantages of utilizing flexible tools in sheet metal forming processes, which are related to the issues aforementioned just above, it seems one of the most attractive technologies for producing micro sheet formed parts. Although that, this technology however has not yet received proper attention of manufacturers and even researchers particularly at micro scale, where just scanty information are available on it. There are various parameters related to using flexible materials as forming tools especially in sheet metal forming are not explored clearly. In addition to the attitude of the technique itself, many essential process parameters, related to the properties of the flexible tool material such as hardness and compressibility, rigid former, blank material behaviour, and also the interactions between the characteristics of the flexible tool-blank and flexible tool-rigid former used in the operation, need more investigations. Regarding to using flexible tooling in deep drawing process at micro scale, there is no satisfactory acknowledgment with which it can be identified what conditions are the optimums. As well as, no sufficient accumulated research experience can help to address parameter valued for a successful drawing operation. Furthermore, as a result of the size effects it is very difficult to predict the quality of the cup produced by micro deep drawing technology. Understanding the deformation behaviour of blank material through drawing operation at micro scale plays an important role in understanding the blank drawability. It is essential to create proper simulation models for process that provide ability for predicting the influence of other operation parameters.

## **1.7 OBJECTIVES AND RESEARCH HYPOTHESES**

The long term aim of the area of this research is to contribute in developing the modern technologies utilized in our life essentials in which mini devices with dimensions of few millimetres containing various miniaturised parts are used. As well as to advance the current status of micro forming processes, particularly micro sheet metal forming, in order to produce qualitatively effective miniaturized components required extremely in mass production. The

main focus of this study is to reveal what the potential of using rubber tool in sheet metal forming at micro scale is, and to provide obvious information on the interactions of flexible tool with micro sheet characteristics on a side and process parameters on the other side. Moreover, in this research innovative concepts are adopted for understanding clearly how the proposed technique can provide appropriate and predictive approaches for the industrial applications related to micro sheet metal forming area. Therefore, it is hoped this study would help in eliminating the consumption of the manufacturing time and this in turn is expected to reduce the total cost of the entire process and improve the product quality.

In the proposed technique, a deep drawing process is carried out to produce tiny cups using thin stainless steel 304 foils with a flexible rubber forming die. In order to improve the aspect ratio of the products a particular initial gap is adopted between blank holder, which is initially in direct contact with the workpiece, and an adjustment ring. The following aspects were considered for achieving this work:

1. Investigating the characterization of micro deep drawing processes using flexible die made of polyurethane rubber with different initial gaps. The interactions of the initial gap values with some particular forming parameters, such as rubber types used for the drawing die, aspect ratio targeted for the final products, blank dimensions, friction coefficients at contact interfaces and rubber dimensions are revealed. For this purpose, positive and negative gaps are adopted in this research in dependence on the process conditions taken into account for a particular case.
2. Due to the forming operation needs special tooling requirements to be accomplished successfully, a specified set up for deep drawing of metallic foil blanks at micro scale was manufactured and effectively developed for characterizing the drawing technique proposed in this project. High precisions and tight tolerances were intended in the design of this set up as such small scale requires. Moreover, the design of this set up was executed in a way so that its capabilities are sufficient to accommodate various values for the initial gap, blank diameter and even the initial compression applied on the spring supporting the blank holder over its journey through the initial gap.
3. Studying the effects of key process parameters on the production quality of the submillimeter deep drawn cups made from thin stainless steel 304 foils in efforts to identify the optimum conditions for each case of micro deep drawing carried out in this research. In the light of this issue, three types of polyurethane rubber in terms of

hardness were used for the flexible forming die, as well as in order to reveal the possibility of adopting rubber tool as the process is scaled down six different diameters were embraced for the drawing workpiece. On the way, the rigid punch which its shapes is imparted to produced cups was used with three diameters, this turn in results in producing cups of three different sizes.

4. Various investigations related with the key process parameters of microscale deep drawing are undertaken in this work, and thus owing to save the experimental work, the numerical analysis method “finite element method FEM” was utilized. For this purpose, the commercial finite element analysis code Abaqus/Standard was used for simulating the micro deep drawing operations through several FEA models. The results obtained from these simulation models were partially validated by the drawing experiments, and therefore additional cases under different process conditions were simulated as well using this numerical technique.



**CHAPTER TWO**

**ASPECTS OF DEEP DRAWING AND MICROSCALE  
TECHNOLOGY**

\*\*\*\*\*

## 2.1 DEFINITION OF DEEP DRAWING

Drawing is defined as that sheet metal forming process in which a flat workpiece of sheet metal, named “blank”, is placed over a die cavity, and then is formed into a cup-shape, box-shape or other complex hollow-shaped products by means of a punch. The drawing operation mainly involves pushing the blank gradually into the cavity of the forming die by the punch to be formed into the required shape. Another tool named blankholder is usually used to hold the flange portion of the blank down against die shoulder [2].

In 1700s the deep drawing technology was first developed, since then many relevant studies have been achieved, thereby it has become one of the most important forming processes in various industrial applications. The parts that are produced through drawing operations can be classified, depending on the final depth, into shallow and deep drawn parts. As mentioned before, the deep drawing process can be distinguished as long as the product is deeper than one-half its diameter. Typical examples of these products are cartridge cases, flashlights, beverage cans, automobile panels and steel pressure vessels [16] (see **Figure 2-1**).



Figure 2-1. Deep drawn products [17]

**Figure 2-2** shows simple deep drawing operation of a cylindrical cup with the basic parameters. A rigid punch with a diameter ( $D_p$ ) and nose radius ( $R_p$ ) applies a drawing force ( $F$ ) on a circular blank with initial diameter ( $D_b$ ) and thickness ( $t_b$ ). Usually the blank is pressed into a die cavity with a corner radius ( $R_d$ ) and is held down at the flange portion by the blankholder force ( $F_h$ ). It can be observed that if the corners of the forming punch are sharp ( $R_p$  and  $R_d = 0$ )

then a cutting operation would be performed rather than a drawing operation. Also, it is essential to adopt a clearance between the sidewalls of the punch and the die cavity. This clearance is usually about 10% greater than the initial thickness of the blank used [3].

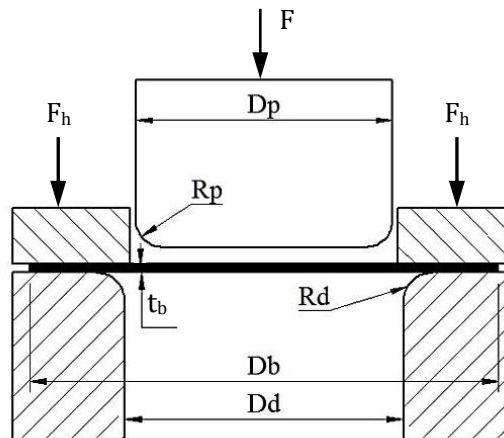


Figure 2-2. Scheme of Deep Drawing Process

In conventional deep drawing processes, the essential independent parameters are:

1. Properties of the blank material
2. The thickness of the blank
3. The ratio of the blank diameter to the punch diameter
4. The clearance between the punch and the die
5. The corner radii of the punch and die
6. The holding force
7. Friction conditions at the blank/tool interfaces

## 2.2 MECHANICS OF DEEP DRAWING

The drawing operation begins when the punch moves down, pushing the blank into the die cavity. Through the operation, the blank experiences a complex sequence of stresses and strains continuously as it is formed into the required shape. The drawing process involves different forming stages, shown in **Figure 2-3**. At the beginning, the forming force is transmitted to the blank through the punch, resulting in a bending action in the metal over the punch and die corners. In this stage the metal is drawn slightly towards the opening of the forming die to produce an initial shallow cup as shown in **Figure 2-3b**. As the punch is kept moving downwards, the metal bent previously just over the around corner of the die is drawn into the clearance between the punch and the die, where it must be straightened to form the side wall of the

final cup. At the same time, the bottom of the initial cup and the metal that was bent over the punch corner move downwards correspondingly with the punch. In order to keep the metal at the die corner not stretched excessively at this stage more metal must be sent from the flange portion. Consequently, the outer portion of the blank is drawn continuously towards the die cavity to compensate the metal being used in forming the side wall, resulting in reducing perimeter diameter of the blank [2, 3].

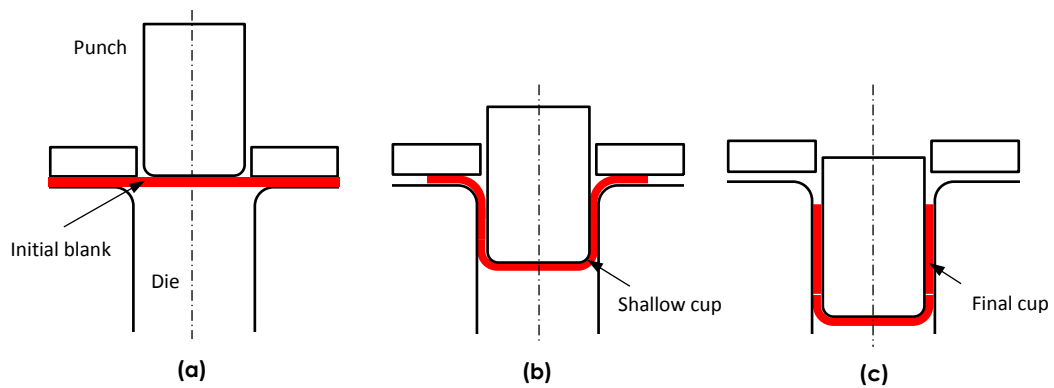
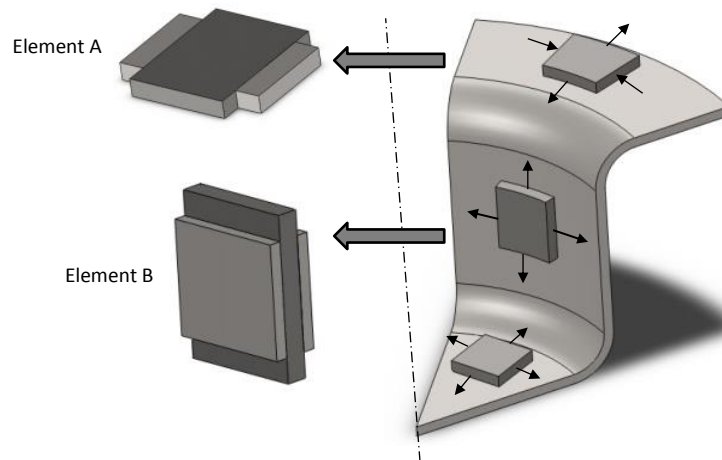


Figure 2-3. Steps of Deep Drawing Process

It is clear now that the flange region and the side wall of the cup significantly experience the great portion of the deformation through drawing processes. In the flange region, the friction forces play a crucial role in the success of the drawing operation. Once the drawing force is applied to the flange portion conquers the friction between the blank and the surfaces of the blankholder and the die, and then the material starts moving towards the forming cavity. As a result of this drawing aspect, this region of the sheet metal usually experiences a state of tensile stresses. Stress state of an element at the flange portion of the cup being drawn is shown in **Figure 2-4**. It can be seen that this element is subjected to tensile radial stresses and compressive circumferential stresses, as well as compression force normal on the sheet plane. The tensile action is created as the sheet metal is pulled towards the die opening, and also due to the friction force which obstructs the material flow. In addition to this aspect and also because of the principle of volume constancy of the blank material, the sheet metal at the flange is squeezed in the circumferential direction creating the hoop compressive stresses. Thereby wrinkling might occur in the remaining material of this region especially when the holding force is not sufficient and/or the friction coefficients are too small. That means that the tension in the radial direction is actually the main source of these hoop compressive stresses [18].

Element B in **Figure 2-4** illustrates the stresses state on the sidewall of the cup being formed. It can be observed that biaxial tensile stress conditions affect the material at this portion. It is axiomatically understood that the axial (longitudinal) tensile stresses are due to the drawing force transmitted through the sidewall to the flange part. Another important explanation is when the metal that was bent over the die corner is properly stretched through the clearance to form the sidewall, it will be tightly held on the punch, this turn in causes the tensile stresses in the hoop direction shown in the figure [1, 3].



**Figure 2-4. Deformation modes of elements in the flange and sidewall of deep drawn cup**

It can be concluded now that the blankholder force is a determining factor in the success of the drawing operation. In general, wrinkling may occur, especially at the flange region, if the holding force is low. Otherwise, too high holding force prevents the metal from flowing properly into the die cavity, thence excessive stretching takes place at the sidewall resulting in necking and possibly failure by tearing. Another important issue is that keeping the punch moving downwards progressively leads to more material flowing into the die opening, causing thinning in the cup thickness especially at the sidewall. This indicates that thinning is normal aspect in the deep drawing process; however successful operation can involve thinning limited by not greater than 25% of the initial thickness of the blank formed [3].

### 2.3 ANALYSIS OF DEEP DRAWING

In order to get the analysis of deep drawing easily understood, it is useful to divide the flat blank into three regions. The outer annular region called flange in which the sheet metal is usually in direct contact with the die shoulder and blank holder. The other one is the inner

annular area which is initially free where it lies through the space between the around corners of the punch and the die. The last region is the circular disc which is in contact with the flat bottom of the drawing punch. One of the important aspects that should be realized in analysing any deep drawing process is to understand the engineering processes prevailing on the regions mentioned above. In general, the main processes that take place during the different stages of deep drawing are [16]:

1. Radial drawing between the die and blankholder
2. Bending and sliding over the die corner
3. Stretching between the die wall and punch
4. Bending and sliding over the punch corner
5. Stretching and sliding over the punch nose [19].

Practically, drawing process can be carried out with or without using a blankholder. Drawing without blankholder is often adopted when the sheet blank has sufficient stiffness in order to avoid any possible wrinkling. This technique is always characterized by shallow products with blank diameter to punch diameter ratio (drawing ratio)  $<1.2$ . However, higher ratio can be obtained using a thick blank relative to its initial diameter [1]. As an approximation, drawing operations without blank holder are in general restricted as  $D_o - D_p < 5t_o$ , where  $D_o$  is the initial blank diameter,  $D_p$  is the punch diameter and  $t_o$  is the initial blank thickness [2]. Otherwise, in order for a relatively thin sheet to form and drawing ratio  $>1.2$  to be achieved, the drawing process should involve a blankholder with appropriate holding force. As approximation, to produce successful deep drawn cup the holding pressure may be taken as 1.5% of the yield strength of the sheet material [1].

The other essential aspect in this treatment of deep drawing is to realize that the flange and side wall of the cup being formed are the most important regions to be considered. The significant part of deformation usually occurs at the flange, whilst the forming force required to draw the flange portion into the die cavity is sufficiently transmitted through the sidewall. If the initial diameter of the blank too large compared to the punch diameter, the flange portion will be larger as well, this means, therefore, that the drawing force supplied by the sidewall will be excessive. This situation will cause the cup to fail by tearing or necking at its wall. In such case, the drawing ratio, which is the ratio of the initial diameter of the blank to the punch diameter, refers to the formability [2, 16]. In order to simplify the analysis of the deep drawing process, the following assumptions will be taken into account:

1. The entire external load applied through the punch is to deform the material at in the flange region. Therefore, the work expended against the friction forces at the interfaces between the blank and tools, and the work to bend and un-bend the sheet over the corners of the punch and the die are neglected initially, and will be accounted for later by use an efficient factor.
2. No change in the sheet thickness and therefore plan strain conditions ( $\epsilon_z=0$ ) characterize the flow state in the flange region.
3. No strain hardening occurs in the sheet material, thus an ideally plastic deformation will be considered with ( $n=0$ ).

As assumption as plane strain condition ( $\epsilon_z=0$ ) is applied in the flange region, which indicates that the total surface area remains constant.

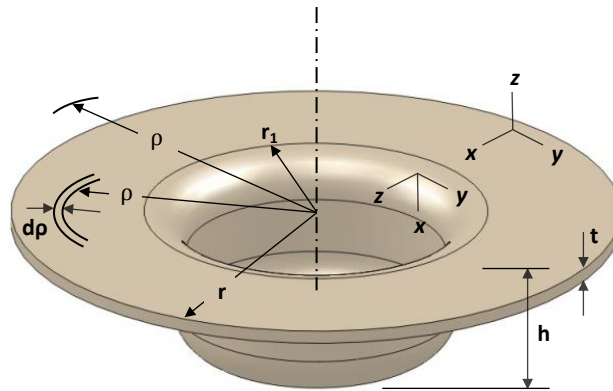


Figure 2-5. Scheme showing the coordinate system on a partially drawn cup

Therefore, if an element is taken originally at radial position ( $\rho_0$ ) and currently at ( $\rho$ ) as shown in **Figure 2-5**, it can say:

$$\pi\rho_0^2 = \pi\rho^2 + 2\pi r_1 h = \text{constant} \quad 2-1$$

deriving this equation results in:

$$2\pi\rho d\rho + 2\pi r_1 dh = 0 \quad 2-2$$

$$d\rho = -r \frac{dh}{\rho} \quad 2-3$$

the circumferential strain on the considered element is:

$$d\epsilon_y = \frac{2\pi(\rho+d\rho) - 2\pi\rho}{2\pi\rho} = \frac{d\rho}{\rho} \quad 2-4$$

due to the plane strain condition ( $\varepsilon_z=0$ ), one can obtain:

$$d\varepsilon_x = -d\varepsilon_y = -\frac{d\rho}{\rho} = \frac{r_1 dh}{\rho^2} \quad 2-5$$

where (dh) is the incremental movement of the drawing punch. The work done on this element located between the radii  $\rho$  and  $\rho+d\rho$  can be expressed by the incremental work per volume ( $\sigma_x d\varepsilon_x + \sigma_y d\varepsilon_y + \sigma_z d\varepsilon_z$ ) times the volume of the element itself ( $2\pi r_1 \rho d\rho$ ). Since the plan strain condition is applied, and then the work per volume is reduced to  $(\sigma_x - \sigma_y) d\varepsilon_x$ , so the total work on the element is:

$$dW = (2\pi r_1 \rho d\rho) (\sigma_x - \sigma_y) \frac{r_1}{\rho^2} dh \quad 2-6$$

despite the values of  $(\sigma_x)$  and  $(\sigma_y)$  vary through the drawing operation, the term  $(\sigma_x - \sigma_y)$  however should be constant and is designated by  $(\sigma_f)$  (the flow strength of the flange material when  $(d\varepsilon_z=0)$ ). The total work done for all such element per increment of punch travel with assumption of ideal plastic material is:

$$\frac{dW}{dh} = \int_{r_1}^r \frac{2\pi r_1 t \sigma_f d\rho}{\rho} = 2\pi r_1 t \sigma_f \ln\left(\frac{r}{r_1}\right) \quad 2-7$$

the drawing force ( $F_d$ ) equals  $(dW/dh)$ , however the largest value required to draw the flange into the die cavity can be estimated when  $r=r_o$ , so:

$$F_{d(\max)} = 2\pi r_1 t \sigma_f \ln\left(\frac{d_o}{d_1}\right) \quad 2-8$$

where  $(d_o)$  and  $(d_1)$  are the diameters of the blank and cup respectively. The tensile stress that the sidewall must carry is:

$$\sigma_x = \frac{\text{Maximum drawing force}}{\text{Cross section area of the sidewall}} \quad 2-9$$

$$\sigma_x = \frac{F_{d(\max)}}{2\pi r_1 t} = \sigma_f \ln\left(\frac{d_o}{d_1}\right) \quad 2-10$$

the maximum axial stress allowed is that at which the wall will begin to neck, which equals the yield strength of the wall ( $\sigma_w$ ):

$$\sigma_w = \sigma_f \ln\left(\frac{d_o}{d_1}\right) \quad 2-11$$



In order for the work done against the friction and that to cause bending can be taken into account, it should be realised that the axial stress calculated as well as the drawing force in equation (2-10) should be modified by the term  $(1/\eta)$ , where  $(\eta)$  is known as deformation efficiency.

$$\sigma_w = \frac{1}{\eta} \sigma_f \ln \left( \frac{d_o}{d_1} \right) \quad 2-12$$

$$F_{d(\max)} = \frac{1}{\eta} \pi d_1 t \sigma_f \ln \left( \frac{d_o}{d_1} \right) \quad 2-13$$

It can be obviously indicated that when the drawing force applied through the punch exceeds that force that the sidewall can support, the formed cup then fails by fracture. Thus, it is important to provide estimation of the limits to the attainable drawing. That can be accomplished over some simple measures that can be easily done for given operation conditions. The following process aspects can provide an evident guide for the successful drawing process.

### 2.3.1 LIMITING DRAWING RATIO

Drawing drawability can be defined as the capability of the sheet metal to be drawn successfully from the flange into die cavity using a punch with a particular diameter. Thus, higher drawability term implies that the blank of larger diameter can be formed. The ratio of the maximum diameter of the circular blank to the diameter of the used punch, which can be attained without failure, is expressed as the Limiting Drawing Ratio (LDR). This ratio therefore represents a measure of the drawability of the blank material. During a deep drawing process, when the material flows into the die cavity, it can be observed that the blank will experience a reduction in width as its diameter decreases progressively through drawing stroke. Therefore, the width strain can be correlated with the strain in thickness in the expression:

$$R = \frac{\epsilon_w}{\epsilon_t} = \frac{\ln \frac{w_o}{w_f}}{\ln \frac{t_o}{t_f}} \quad 2-14$$

the term  $(R)$  is called as the normal anisotropy or the plastic strain anisotropy of the sheet metals. The subscripts  $(O)$  and  $(f)$  refer to the initial and final status respectively. When  $(R=1)$  then the sheet metal is characterised as isotropic which means that the width and thickness

strains equal each other. Usually the thickness of the sheet is small in comparison with the other dimensions, thus measuring thickness strain possibly involves some errors. Therefore, the normal anisotropy can be written in the form:

$$R = \frac{\ln \frac{W_0}{W_f}}{\ln \frac{W_f l_f}{W_0 l_0}} \quad 2-15$$

here ( $l$ ) is the gage length of the test specimen. The final length and width are taken at elongation of 15% or 20%, and for low ductile materials at the elongation that is just below the necking point [2]. It is known that most of sheet metals are produced by rolling process, and they generally have planar anisotropy which implies that the value of ( $R$ ) depends on the orientation which is measured with respect to the rolling direction (see **Figure 2-6**).

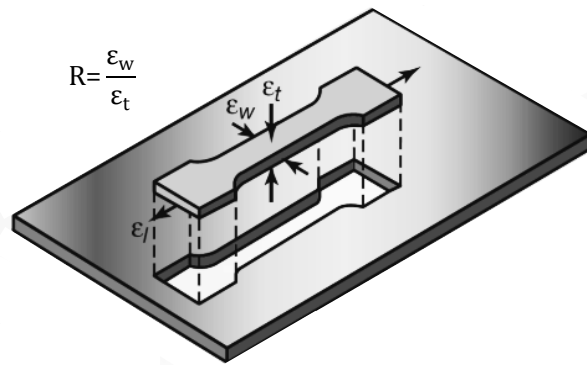


**Figure 2-6.** Tensile test specimen cut from sheet metal along rolling direction [20]

Thus the average value  $\bar{R}$  of  $R$  calculated below in equation 2.16 is adopted:

$$\bar{R} = \frac{R_0 + 2R_{45} + R_{90}}{4} \quad 2-16$$

where 0, 45° and 90° indicate the directions at which the test specimens cut with respect to the rolling direction. It can be concluded readily that the materials that have an isotropic behaviour can be characterised by unity value for  $\bar{R}$  as they have  $R=1$  at all directions mentioned above. The directional values  $R_0$ ,  $R_{45}$  and  $R_{90}$  can also be used properly to define the planar anisotropy  $\Delta R$  as following [2]:

$$\Delta R = \frac{R_0 - 2R_{45} + R_{90}}{2} \quad 2-17$$

### 2.3.2 EFFECT OF SHEET ANISOTROPY

It has been found that as the  $(\bar{R})$  value increases, the limiting drawing ratio increases as well. Due to the  $(\bar{R})$  value is a function of the directional values of R, thus it can say that the limiting drawing ratio increases with R values. This means that a high R value leads to low resistance to the deformation in the flange and high resistance to the reduction in thickness occurred commonly in the sidewall [21]. The material at the sidewall region is usually constrained by the punch in the circumferential direction, so the deformation there can be prevailed by plain strain conditions so that  $\varepsilon_y=0$ . As a result, the limiting drawing ratio can be expressed in terms of the two plane-strain flow strengths,  $(\sigma_w)$  at the side wall and  $(\sigma_f)$  at the flange as below:

$$\ln(\text{LDR}) = \frac{\sigma_w (\varepsilon_y=0)}{\sigma_f (\varepsilon_z=0)} = \beta \quad 2-18$$

For anisotropic material:

$$\ln(\text{LDR}) = \eta\beta \quad 2-19$$

Various process parameters such as holding force, blank thickness, die geometry and lubrication affect the value of the efficiency ( $\eta$ ). For isotropic materials with  $\beta=1$ , the (LDR) values range between 2.1 to 2.2, which can be adopted for ( $\eta$ ) to be estimated from 0.74 to 0.79. On the other side, for planar anisotropic materials, and according to Hill's 1948 criterion [22], the value of the factor  $\beta$  would be given as:

$$\beta = \sqrt{\frac{(R+1)}{2}} \quad 2-20$$

this results in:

$$\ln(\text{LDR}) = \eta \sqrt{\frac{(R+1)}{2}} \approx \eta \sqrt{\frac{(\bar{R}+1)}{2}} \quad 2-21$$

Where R=the radially symmetric plastic strain ratio

$\bar{R}$ =the average plastic strain ratio [16, 23].

### 2.3.3 EFFECT OF STRAIN HARDENING

Despite the blank radius decreasing during drawing process, the flow stress required to draw the flange region inwards still increases and this due to the strain hardening aspect. As well as, the strain hardening causes the flow stress to be non-uniform distributed across the flange. Therefore, it can be understood from the mentioned above that there are two aspects relating the drawing flow stress. The first one is the increasing in the flow stress as the blank material became strain hardened, and the other is the reducing in the stress due to the reduction in the surface area of the flange region as the blank radius becomes smaller. The general description of the stress in drawing process is to increase initially until reaching a maximum point and then decreases [7]. The constitutive equation known the Ludwik-Hollomon power law,  $\sigma = k \epsilon^n$ , can be used in the previous analysis in order to reveal the influence of strain hardening. **Figure 2-7a** illustrates the relationship between the drawing force ( $F_d$ ) normalized by the wall strength ( $F_{w(max)}$ ) and the punch stroke ( $h$ ) normalized by the entire targeted stroke ( $h_{max}$ ) with different values for the strain hardening exponent ( $n$ ) and constant deformation efficiency ( $\eta=1$ ). It can be seen obviously that as the  $n$  increases the time for the drawing force to reach the maximum value increases as well [16].

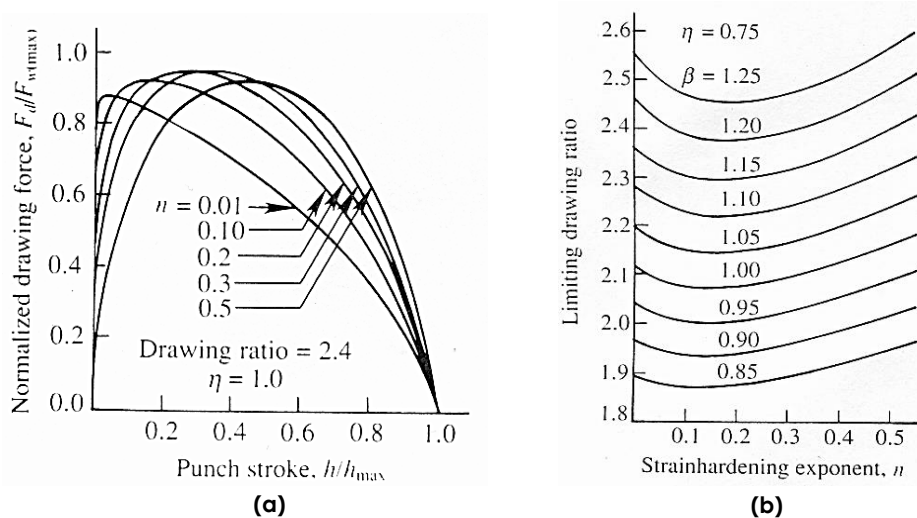


**Figure 2-7. (a) Drawing force-stroke relationships with different ( $n$ ) values (b) Limiting drawing ration values with different strain-hardening exponents [16]**

**Figure 2-7b** shows the influence of both the strain hardening exponent  $n$  and the plan-strain flow strength ratio ( $\beta$ ) on the LDR at constant efficiency of 0.75. It is clear that the (LDR) increases in general with increasing ( $\beta$ ). However, the important observation here is that the dependence of the (LDR) on the ( $n$ ) value is even insignificant in the range  $0.1 \leq n \leq 0.3$  [16, 21].

### 2.3.4 PERCENTAGE REDUCTION IN DEEP DRAWING

Beside the limiting drawing ratio, the drawability of sheet metal can be properly represented in another way by adopting the percentage reduction in area. Also, the deep drawing process can be characterized either by the limiting drawing ratio or the equivalent percentage reduction in area. It has become understood that the average anisotropic plastic strain ratio ( $\bar{R}$ ) plays an important role in assessing the amount of the material that can be drawn successfully, and refers therefore to the drawability grade and fracture resistance. In fact, the material is regarded as a resistant to thinning and has good drawability, if  $\bar{R} > 1$ . Likewise, the material yields thinning easily and has poor drawability, if  $\bar{R} < 1$  [3, 16].

The cross section area of blank is based here in calculating the percentage reduction in deep drawing. In **Figure 2-8**, ( $A_0$ ) and ( $A_1$ ) are the cross section areas of the outer edge and the inner sector edge of the flange respectively, and ( $S_0$ ) and ( $S_1$ ) are the length of the arcs of the outer and inner section. ( $S_0$ ) and ( $S_1$ ) can be given as:

$$S_0 = 2r_0 \alpha = D_0 \alpha \quad 2-22$$

$$S_1 = D_1 \alpha \quad 2-23$$

where ( $\alpha$ ) is the apex half-angle of the sector in radians. As assumption, as  $t$  remains constant, ( $A_0 = \alpha D_0 t$ ) and ( $A_1 = \alpha D_1 t$ ) which result in the percentage reduction in area is:

$$\%R = \frac{(\alpha D_0 t - \alpha D_1 t) * 100}{\alpha D_0 t} = \left( \frac{D_0 - D_1}{D_0} \right) * 100 \quad 2-24$$

which is actually the percentage reduction in diameter rather than in area [16].

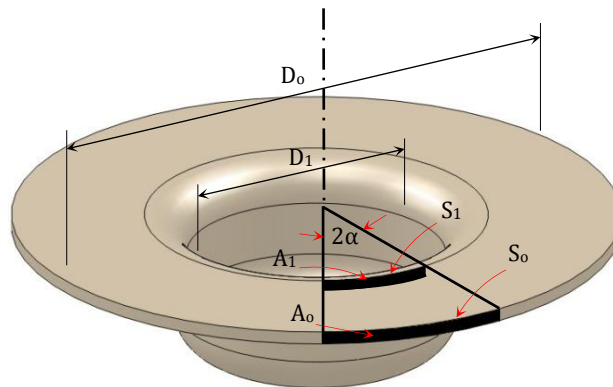


**Figure 2-8.** Deep drawing process in which the cross section area of the edge  $A_0$  is reduced to  $A_1$

## 2.4 DEEP DRAWING-ASSOCIATED DEFECTS

In the deep drawing technique, the flat piece obtained from a large sheet metal is named blank. The blank holder clamps the blank on the top surface of the die to produce the demanded cup. In order to obtain symmetric shape for a free defects-product, the centre point of the blank should be coincided exactly with the centre of the die opening. In general, two main resources contribute in providing the force needed to form the sheet metal blank completely. The first force is that used to hold the sheet in contact with the upper surface of the die. This force is known as the blank holding force because it is applied through the blank holder to catch the blank. The other one is provided by the punch. The punch force is functioned to form the blank into the die cavity. Therefore, consequently the main tools required in deep drawing process are a male punch, a female die and a blank holder plate [24].

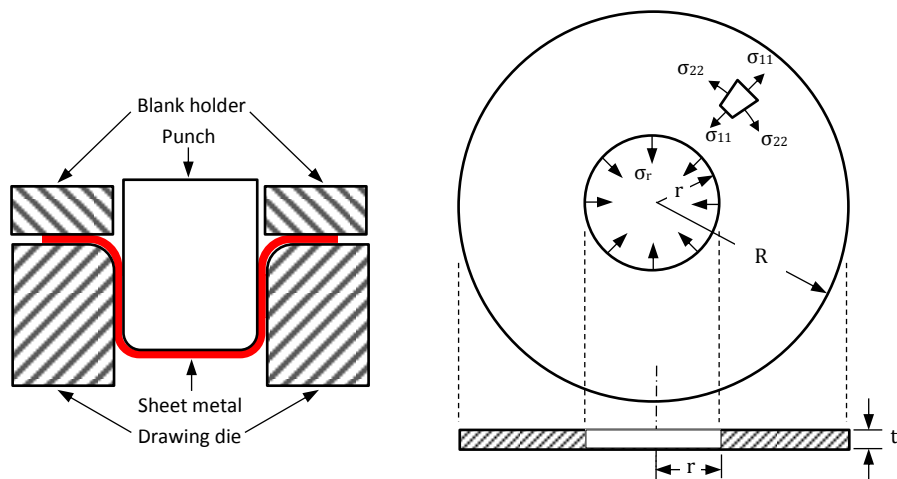
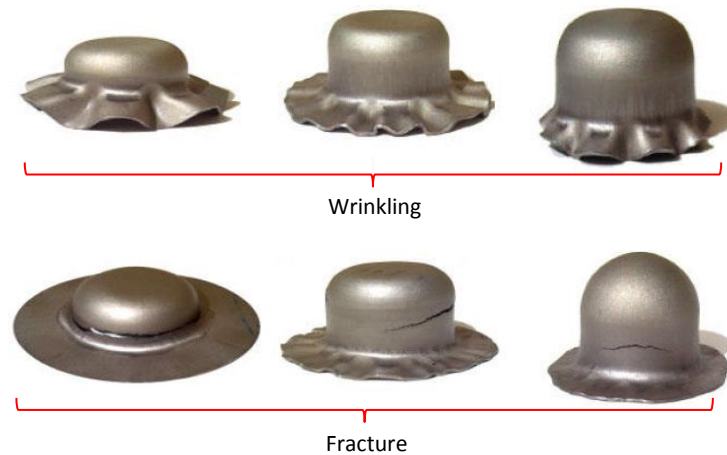


Figure 2-9. Stress status on the flange portion of a formed cup

The movement of the blank part positioned between the tools is controlled by an appropriate clearance to prevent the cup being drawn from wrinkling. Therefore, the punch and die have to be designed with sufficient radii to obtain free defects-metal product. In the deep drawing technique, the failure which may be probably occurred during the operation have two major forms wrinkling or/and necking [25]. As the punch force takes the blank down into the die cavity, the material would be subjected to tensile and compressive stresses, which may be excessive at some critical regions as shown in **Figure 2-9**. Thus, radial tensile and circumferential stresses are generated on the flange portion as a result of the tension at the cup sidewall [26]. Through the deep drawing process, if the ratio of original blank diameter to punch diameter, is too large, or if the cup height-to-diameter ratio is large then excessive

circumferential compressive stress would be generated at the flange part. As result, these compressive stresses may cause wrinkling at this critical region as illustrated in **Figure 2-10**. As it can be seen from what mentioned above that the current state of stresses and local geometry developed on the blank material at the flange portion during the process are responsible of the wrinkling occurrence at this region in deep drawing technique [26].



**Figure 2-10. Failure modes in deep drawing process [27]**

On the other hand, a larger drawing ratio means larger flange area, and then higher drawing force supplied by the punch is required to complete forming the blank. Indeed this case will result in higher tensile stress on the sidewall of the cup being drawn through the operation. In addition, the cup sidewall-induced tensile stresses are the responsible of providing bending and unbending over the die radius. Moreover, these stresses have to overcome the friction resistance between the tools and the blank to produce successful parts [28]. Unfortunately, increasing the drawing punch force may cause necking and tearing whether at profile punch radius or at sidewall of the cup [26]. Briefly, the causes of the common problems that may take place through deep drawing processes can be summarized as follows:

- Metal fracture during the process:
  - Deep drawing radii too small.
  - Clearance between punch and die is too little.
  - Blank holder pressure is too great.
  - Lubricant is inadequate or unsuitable.
  - Punch nose radius is too small.
- Wrinkles on top edge or flange:
  - Blank holder pressure is too tight

- Draw radius is too large
  - Punch nose radius is too large
  - Wrinkling on the cup side or flange caused by an unbalanced blank holder pressure
  - Clearance between punch & Die is too large
  - Blank thickness wrong or out of tolerance
- Excess material at top of drawn cup:
- Material thickness too great or punch die clearance too small or uneven
  - Punch nose radius larger than cup bottom radius
  - Draw radius too large, causing wrinkles to start that enlarge during redraw of cup [29].

## 2.5 EARRING

The drawn part usually has a non-uniform side wall in terms of height. The top edges of the cup perimeters consist of peaks and valleys, and therefore it looks like wavy, as shown in **Figure 2-11**. These features along the top edges are called ears, and the phenomenon is known as earring. The number of ears may be two, four, six or even eight, but the most common are four ears. Planar anisotropic behaviour of the blank material is the main cause of earring.



**Figure 2-11. Earring in a deep drawn cup [30]**

Moreover, the height and the angular position of the ears depend significantly on the parameter  $\Delta R$  shown in equation 2-17. In general,  $\Delta R=0$  means no ears form,  $\Delta R>0$  implies the ears at  $0^\circ$  and  $90^\circ$  to the rolling direction of the sheet metal, and  $\Delta R<0$  implies the ears at  $\pm 45^\circ$  [21]. Increasing  $\Delta R$  value results in increase of the height of the formed ears. This can be often interpreted that when the R-values are relatively small, more thickening occurs especially at the flange portion. That results in the height of the cup wall to be lower at all [16].



## **2.6 FORMABILITY**

The formability of sheet metal has a great importance in various sides related to technologies and economy; therefore it has been one of the most interesting aspects of sheet forming. Sheet metal formability is defined as the ability of a sheet to undergo a specific forming process through which its original shape is changed to the desired shape without failure. Actually this definition refers to three main elements that are material, process and shape. As the interactions of these elements in any forming process essential, it is emphasized to consider them simultaneously in investigations of formability. The main factors which have a significant influence on sheet formability are (a) properties of sheet metal (b) lubrication conditions at contact interfaces (c) characteristics of tooling used in forming the sheet. There are several testing techniques adopted to estimate the formability which are tension tests, cupping tests and forming limit diagrams [2].

### **2.6.1 TENSILE TEST**

As a result of its simplicity, the tension test is basically the most common technique used in order to determine formability. The mechanical properties of the sheet metal, which can be provided through this test, are the most important in evaluating the formability of sheet metal. Of these properties the elongation at fracture, the module of elasticity, the yield point, the ultimate tensile strength, the strain hardening exponent, the planar anisotropy and also the normal anisotropy [2].

### **2.6.2 CUPPING TEST**

Another test, but even earlier, can be adopted to evaluate the formability of sheet metal is known as cupping test. This type of testing depends on the base of that sheet forming is a biaxial stretching process. There are two main procedures to perform this test, which are known as the Erichsen and Olsen tests (stretching) and the Swift and Fukui test (drawing). The tools required in the Erichsen test are circular flat die, steel ball and holder. The test begins by clamping the sheet metal specimen by the holder over the flat die with a load of 1000kg. Then the steel ball with diameter 20mm pushes the specimen into the die until the formed part just starts cracking. The distance which the steel ball moves down is called the Erichsen number. Higher Erichsen number indicates that the sheet formability is better. Although cupping tests

are relatively simple and provide a good prediction on the formability, however the axisymmetric stretching state prevailing the material under the ball do not represent the exact conditions of the actual forming operation [2].

## 2.7 FORMING LIMIT DIAGRAM (FLD)

When evaluating formability of sheet metals, it is essential to create forming limit diagram. This can be executed through stretching test in which a grid pattern of circles is intended on the sheet blank using chemical-etching or photoprinting technologies. The typical range of the diameter of the pattern circles is 2.5 to 5mm. The sheet specimen is usually constrained by means of beads, which overcome flow the material into the die (see **Figure 2-12a**). The forming force is then applied through rigid punch until the sheet to fail in forms of necking and tearing. At this instance the deformation of the pattern circles is measures just where the failure occurs. As the circle diameters are small as well as the grid lines is narrow as possible, the accuracy of the deformation measurement will be improved [2].

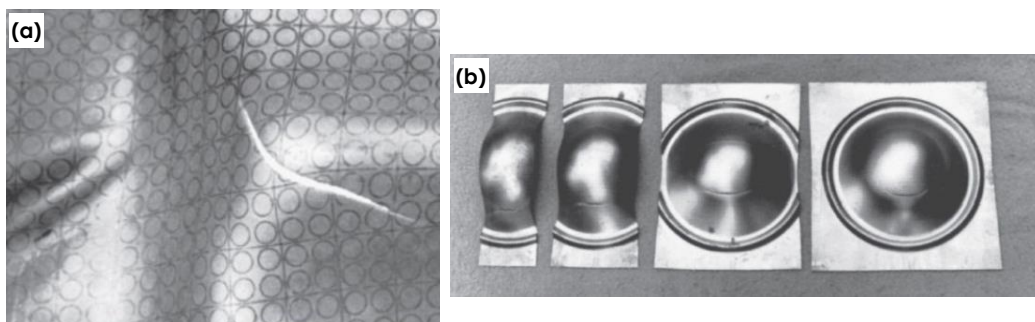


**Figure 2-12. (a) Grid pattern (b) Samples used in cupping test [2]**

**Figure 2-12b** shows tested specimens, and it is obvious that they are initially prepared with different width in order to provide various strain paths. The specimen with small width undergoes a uniaxial stretching, while a state of equal (balanced) biaxial stretching prevail the central portion of the square specimen. The forming limit diagram shown in **Figure 2-13** is constructed after a series of these tests which are achieved on a particular type of sheet metal. The boundaries of the safe and failure region on the forming limit diagram are patently presented. The different strain paths illustrated in **Figure 2-13** are (1) the equal biaxial strain path is represented by the line at  $45^\circ$  on the right (2) the plane strain path is represented by the vertical line at the centre, and the vertical strain means that the minor strain is zero which is exactly what the plane strain considers (3) the line on the left with 2:1 slop refers to the

simple tension (uniaxial stretching) state, and this slope means that the Poisson's ratio for these conditions is 0.5 (4) finally the line with slope of  $45^\circ$  on the left refers to the pure shear.

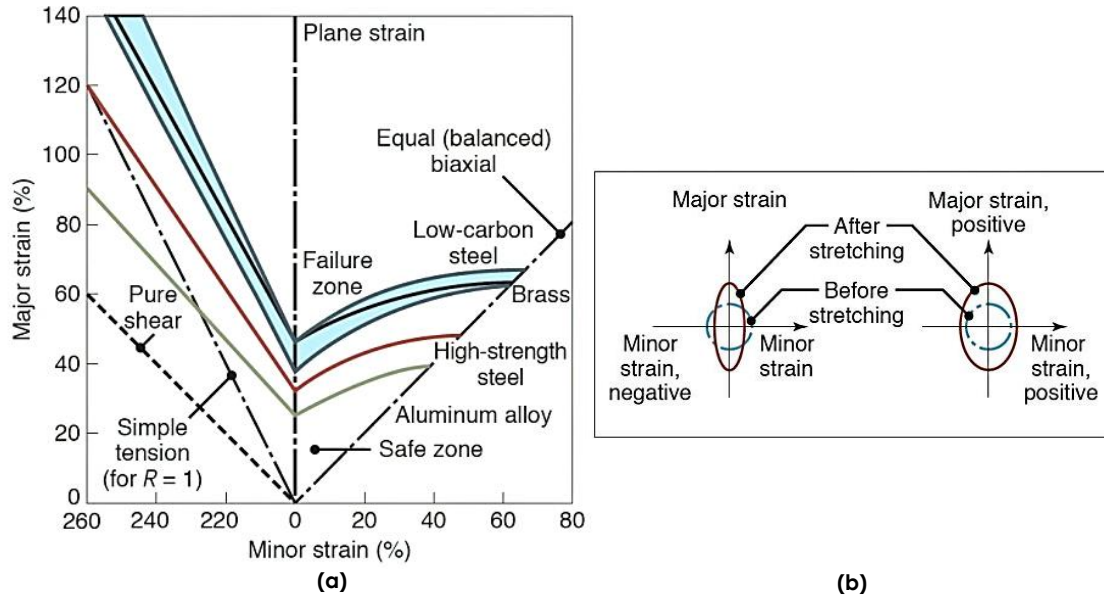


Figure 2-13. (a) Forming limit diagram (b) the definition of positive and negative minor strains [2]

In order to know how the major strains and minor strains presented in the figure are obtained, the following procedure should be well understood. First of all, it is important to realize that the grid pattern is deformed exactly how the sheet metal itself deforms. When the test finish the original shape of the pattern circles will be changed into ellipse shape. The maximum diameter of this ellipse indicates the direction and magnitude of the maximum stretching resulting in the major strain. Likewise, the direction and magnitude of the minor strain are referred by the minimum diameter of the ellipse. Moreover, the major strain is always positive as it is created due to stretching that usually prevails the sheet forming processes (if not in two directions, then at least in one direction). On the other hand, the minor strain may be positive (stretching) or negative (shrinking) [2].

## 2.8 IRONING

Ironing can be defined as a forming process which involves reducing the wall thickness of a drawn cup, and consequently yields increase in the height as shown in **Figure 2-14**. There are two ways for the ironing to occur; the first one is during the initial drawing in the top region of the wall. This ironing is known as simultaneous drawing and ironing and takes place when the clearance between the punch and the die is smaller than the range 130% to 150% of

the blank thickness, then a forced reduction in thickness of the drawn cup is resulted. The other way is by performing the ironing through a separated process after the deep drawing operation, and this time it is called conventional ironing. In general, for a tight range of ironing reduction, the limiting drawing ratio can be increased; however, it may be reduced if this clearance is less than 85% of the blank thickness. Also, the ironing reduction should be restricted by a limiting range for each pass, because high reduction causes an excessive stretching in the wall leading probably to failure by necking and tearing [16, 21].

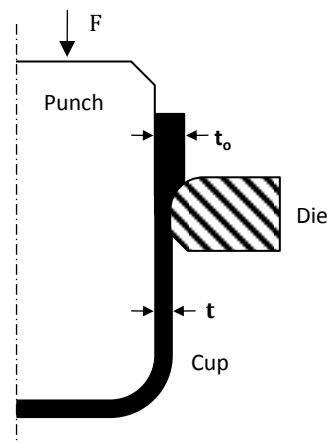


Figure 2-14. Schematic view of ironing process

Both of the two ways make the formed cups more uniform in wall thickness; however that produced through the conventional ironing are better in terms of thickness distribution [16, 31]. Usually the top region of the wall is required to be ironed. In order to attain that the clearance between the punch and die lip should be designated so that no ironing occurs until the outer portion of the flange, which is thickened previously through drawing process, flows on the die lip. The maximum ironing reduction per pass, termed as  $[(t_o - t_1)/t_o]_{max}$ , correlates well with the strain hardening exponent ( $n$ ) and slightly with the average plastic anisotropy strain ratio ( $\bar{R}$ ). It is found that increasing the ( $n$ ) value causes remarkable decreasing in the thickness reduction in ironing. Moreover, high  $R$ -values implies that the thickening in the cup wall produced through the initial drawing operation is less, therefore the reduction required to be achieved through the ironing will be smaller [16].

## 2.9 MICROSCALE MANUFACTURING

Not only the increasing demands on whether conventional products or new ones has influenced the manufacturing technologies, but also there are other factors relating social,

economic and even political issues have played an important role in establishing the manufacturing plan. In order to improve the life quality, health condition and also the working efficiency, innovative techniques are needed to be developed and then adopted in producing new models of modern devices and components such as computers, mobile phone, CD and MP3 players, medical instruments, etc. As a result of the huge development in the global economy through the last 15 years, the big challenge became how to organize the manufacturing instead of how to manufacture the product itself. As well as the other major issue is how to keep reasonable balance between the product quality and its total cost. In order to stay competitive, manufacturing industries need to adopt new innovations which can contribute in improving the quality of their products with low cost. Therefore, the major purposes of the developed industries are reducing the cost, developing the technologies, providing sophisticated quality and efficient products [32].

The increasing demand on mini and compact devices during the last decade has significantly resulted in growing progress in producing such miniaturized products/systems and components such as MEMS (micro-electro-mechanical systems), micro reactors, micro medical components, micro mechanical devices, fuel cells which are usually used in telecommunication and IT facilities, aircrafts, medical devices, home appliances [33] (see **Figure 2-15**).

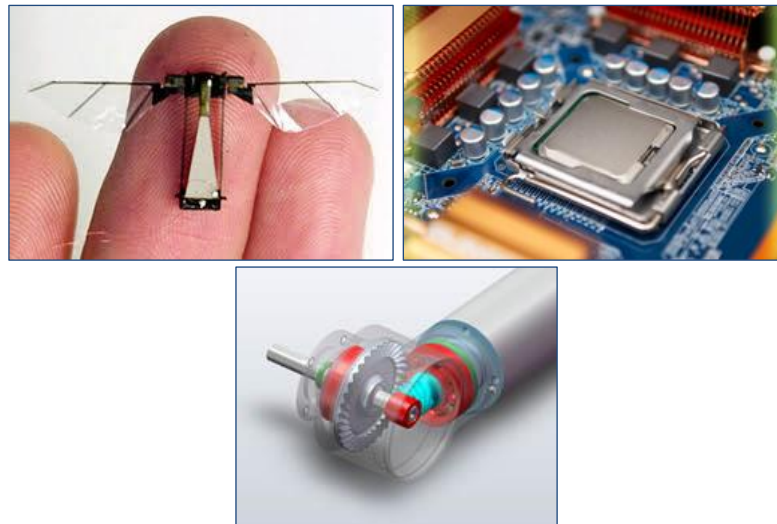


**Figure 2-15. Examples on micro components [34, 35]**

There is a wide variety of micro products/systems, and the major types however usually involve micro-electronic products, micro-optical electronics systems (MOES), micro-electro-mechanical systems (MEMS) and micro-optical-electro-mechanical systems (MOEMS). Actually these micro systems depend in general on the functionalities of the products and the working

principles [32]. However, depending on the nature of the manufacturing process itself, the micro manufacturing techniques can be divided into MEMS manufacturing and non-MEMS manufacturing. The techniques enrolled under the title of MEMS manufacturing include photolithography, chemical etching, plating, LIGA, etc. While the non-MEMS manufacturing refers to the techniques such as micro-mechanical cutting, laser cutting, laser drilling, micro-injection moulding, micro-forming etc. Unlike who work in MEMS-based manufacturing, the people involved in non-MEMS-based manufacturing feel somehow that the term micro manufacturing is new, and they regard it as an emerging field recently. The reason behind this issue is because the manufacturing can be applied for a wide range of materials, with which the MEMS-based manufacturing cannot deal, and also scaling the process and tooling down from macro dimensions to that required for the desired features is a new issue and extremely challenging [32]. Therefore, micro manufacturing can now be defined as the miniaturization of existing conventional process-techniques to manufacture products/features at micro scale. The two major categories of the micro manufacturing processes are micro machining and micro forming. Micro machining processes involve controlled material removal of a piece of raw material to produce the desired final shape and size. While the micro forming process is defined as the technique by which the material deforms from an initial geometry to that required for the final product, and the micro forming processes include micro bulking forming and micro-thin sheet forming [33].

## **2.10 MICROFORMING PROCESSES**

MicroElectroMechanical systems (MEMS) technology has wide applications in different industrial fields, such as communications, medicine, and biotechnology. During the last decade, the MEMS technology has attracted many researchers to fabricate micro devices with various features. However, the increasing demand on these devices has caused this technology to experience huge challenges of promotion in industry. For example, using semiconductor material in manufacturing MEMS parts represents one factor enrolled under this issue because the equipment is comparatively expensive, applicable materials are limited, and it is difficult to fabricate 3D structures [36].

On the other side, increasing the production of micro scale features is strongly required as the miniaturization, integration and compaction trend of devices are increased remarkably in different industries. Specific examples involve electrical connectors, micro-screws of

fasteners used in electronics and telecommunication devices, micro-gears, micro-heat exchangers, micro-fluidic device, etc. [37] as illustrated in **Figure 2-16**.

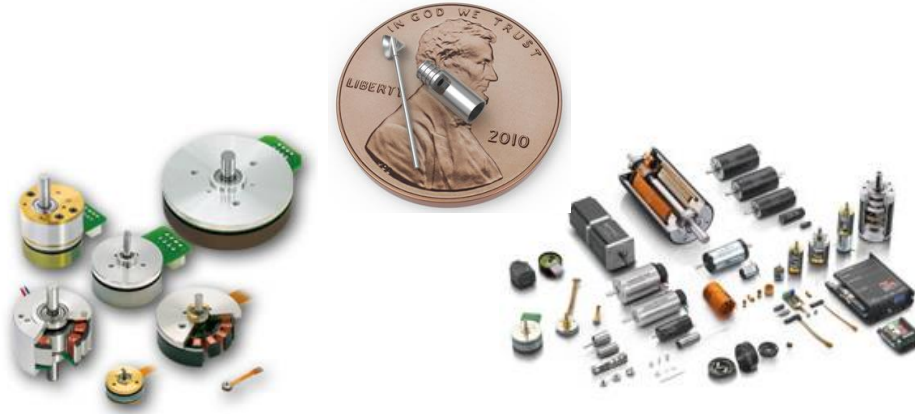


**Figure 2-16.** Typical devices produced through micro forming technology [35, 38]

The production of these components represents a remarkable challenge especially when the precision requirements are just about few microns [37]. Hence, it became very necessary to develop alternative technologies of MEMS to satisfy the industry demands. Previous studies and researches have proved that forming processes are strongly the best choice, in terms of economical fabrication techniques, due to the great advantages that forming processes offer. Of these advantages, which are regarded superior compared to those of other processes, are simplicity, minimized material waste, near-net shape, excellent mechanical properties, high production rate, low manufacturing costs and close tolerances [39]. In general, the micro forming process can be defined as the forming of metallic components with dimensions smaller than 1 mm [36] as seen in **Figure 2-15** and **Figure 2-16**.

Scaling down process configuration, tooling and machine effectively can help greatly in achieving micro forming process. When the dimensions of components/features are miniaturized until micro level for tens or hundreds micros, some complex challenges will be experienced as the accuracy tolerances for the produced parts reduce to just a few microns. Of the major aspects that should be taken in consideration in micro forming processes are characterization of material properties, optimization of the process design, understanding the deformation mode of the material, process modelling and analysis, assessment of forming limits, understanding the contact conditions at material/tool interfaces, etc. with pay significant attention for the size effect issues [32].

Regarding miniature parts made of very thin sheet metals, different types of these products are routinely used in everyday life, and typical examples include electrical connectors and lead frames, micro meshes for masks and optical devices, micro springs for micro switches, micro cups for electron guns and micro packaging, micro laminates for micro motors and fluidic devices, micro gears for micro mechanical devices, casings/housing for micro devices assembly/packaging, micro knives for surgery, etc. (see **Figure 2-17**). Some of the basic configurations of forming processes at macro scale can be utilized in forming miniature and even micro products as long so the related size effects can be addresses successfully.

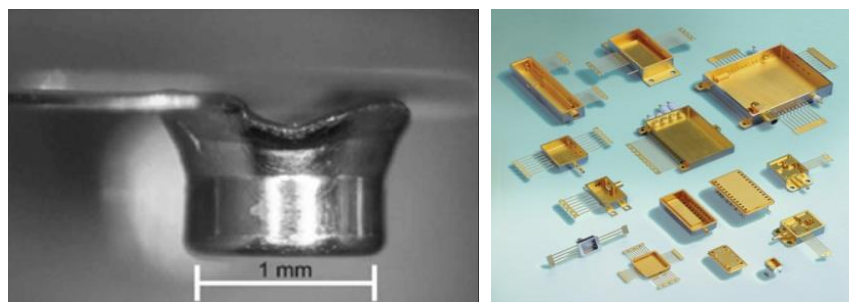


**Figure 2-17. Micro sheet metal products [40, 41]**

In fact different industrial applications have involved forming processes of small and thin products for many years. However, when the main dimensions of parts are scaled down to submillimeter, or some features reduce to just tens microns ( $<100\mu\text{m}$ ), or the precision tolerances required for the miniaturized parts are prescribed by a few microns, new and extremely challenging difficulties arise. As a result of some previous relevant researches, despite additional consideration relation to material, tooling and interface conditions have to be paid attention, conventional macro sheet metal forming processes such as shearing, bending, stamping, deep drawing; stretching, etc. can be equivalently applied for products at micro levels. Moreover, some aspects related to the micro structures and grain boundary characteristics of materials prescribe the formability at micro scale of these materials. The forming limits at such miniaturisation levels differ on those at macro levels, due to so called size effects which depend on the micro structure of the materials [32].

## **2.11 SIZE EFFECTS IN MICROFORMING PROCESSES**

It is known now that it is impossible to scale down the technology of macro forming directly to micro level unless the issues related to so called size effect to be addressed. The



mechanism of material deformation is one of the major aspects in micro forming process, which has to be well understood in order to utilize the micro forming processes. Therefore, deformation mode of a particular material at normal scale cannot provide an indication on the behaviour of this material at micro scale [33]. It is well recognised that the common challenges associated the normal-scaled forming processes are also experienced in micro forming, in addition to new problems which appear as a result of the miniaturized, or in another word size effects. These problems can be in general classified into four main categories related to material, process, tools and equipment.

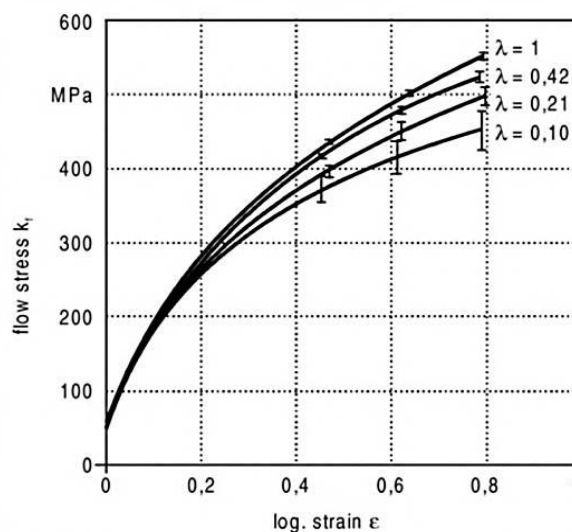


Figure 2-18. Effect of geometric factor on flow stresses [42]

For example Engel and Eckstein [42] have found that increasing the miniaturization level results in decreasing the flow stress of the material as illustrated in Figure 2-18. This decrease can be explained according to the fact that the share of the surface grains in micro parts is higher than that of the inner grains as shown in Figure 2-19. The different mechanisms of dislocation show that the hardening of the inner grain is greater than that of the grains at the surface layers. Hence, the flow stress of materials inversely proportion with the share of surface grains. Another finding here is that increasing grain size and/or miniaturizing level causes an increase in the share of the surface grains. Therefore, one can conclude that the flow stress decreases with increasing the grain size and miniaturizing [42]. Regarding the micro forming processes of sheet metals such as micro deep drawing, micro stamping, etc., the size effects has significant influence on decisive process parameters. It has been investigated that despite of the same forming conditions are adopted then the friction coefficient in micro scale

greater than that at the normal scale. The size effects in micro sheet metal forming can be identified as the following:

- Increasing the surface-to-volume ratio.
- Increasing the influence of adhesion force and surface tension.
- Increasing the influence of grains size on forming micro parts.
- Decreasing the ratio of the closed pockets of lubricant to the lubricating area [43].

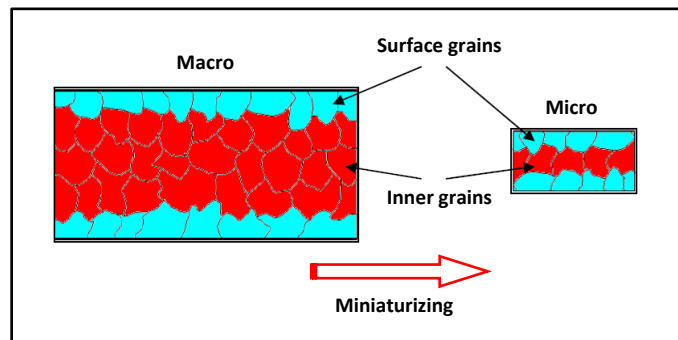


Figure 2-19. Microstructure of a specimen in both macro and micro scale [33]

## **CHAPTER THREE**

# **LITERATURE REVIEW**

\*\*\*\*\*

### **3.1 INTRODUCTION**

Aimed to clarify the different technical concepts that are utilized in deep drawing technology as well as to reveal the influence of the key process parameters on the quality of drawn products, a state of the art review is presented in this chapter. Although the current project is related to sheet metal deep drawing at micro scale, drawing processes at normal scale (macro scale) are discussed in this survey in order to provide a comprehensive guide for the researchers in this area. First, conventional deep drawing and hydraulic pressure-assisted deep drawing are therefore discussed. Then, the technology of using flexible material tooling in sheet metal forming is also taken into account. Afterwards, this survey presents definitions of the so-called “size effects” and the role of these effects on the material behaviour in different forming aspects as well as provides background on micro deep drawing technologies. In the last section of this chapter, a review of micro sheet forming technologies using rubber material tools is included to better understand the deformation mode of both the workpiece and tools as well as to declare the advantages that can be acquired of such rubbery tools in terms of forming quality and production cost.

### **3.2 CONVENTIONAL DEEP DRAWING**

The term “conventional” in deep drawing technology indicates that the drawing process is achieved using a rigid punch, a rigid die and a rigid blank holder at macro scale. Therefore, conventional deep drawing is the simplest technique that can be adopted for drawing cylindrical or box-shaped cups with dimensions at normal geometrical dimension scale. In this section the main key process parameters that have the most significant effects on deep drawing characteristics are discussed.

#### **3.2.1 BLANK HOLDING FORCE (BHF)**

Halil et al. [44] investigated the influence of blank holder force (BHF) on the forming behaviour of aluminium sheet (AA5754-O standard) of 2mm in thickness during deep drawing processes. They developed a new computer-control holding system by which variable blank holder forces can be adjusted accurately in accordance to the required values. FE numerical cups were cut at 0 and 45° to the rolling direction to measure the thickness distribution after

the drawing operation. The different holding forces adopted here ranged from 1 to 18MPa. It was found that the maximum thinning occurs at the cup nose radius at the 45° direction for all cases. The maximum thinning value increases with the increase of the BHF, where broken cups were produced with BHF of 18MPa. High BHFs  $\geq 15$ MPa caused an extreme earing due to the increasing in frictional forces at blank/tool interfaces. The height of the ears increased noticeably with increasing the BHF just over 8MPa. On the other hand, low BHF  $\leq 1.3$ MPa resulted in intensive wrinkles obviously at the side wall. The simulation predictions obtained from the anisotropic model exhibited a well harmony at a rate of 85% with the experimental results. As a result, the numerical and experimental outcomes indicated that the optimum range of the BHF for this material was 5-8MPa [44].

Gharib et al. [45] presented an optimisation study on blank holding force in deep drawing process of cylindrical cups. The main point of this work is to minimize the punch force that is required for producing cups without wrinkling or tearing by utilizing the developed optimization system. The numerical solution espoused in a previous work [46] was used in developing the recent optimization process. The formation of wrinkles can be restricted by the stresses normal to the thickness which increases with increasing the BHF. Nevertheless, broken cups at the side wall and punch profile are usually produced with excessive holding forces [45]. Compared with the results of Saran et al. [47] obtained with 100kN constant holding force, it was indicated that the maximum thinning was reduced by 22% by adopting the current optimization procedure. This result pointed out that cups with more uniform thickness strain distribution were produced. In this study, four different friction coefficients of 0.045, 0.06, 0.1, and 0.13 were used at the blank/die interface for each one of the drawing ratios 1.9, 1.95, 2.0, 2.1, and 2.2. Schemes of the BHF with punch travel were accomplished for different drawing ratios as well as friction coefficients. The curves were above the wrinkling limit regions for all cases. Since the punch load correlates proportionally with the BHF, the minimum punch load was thus because of the minimum BHF passing just above the wrinkling limit. It was observed that the slop of the BHF schemes increase with increasing the drawing ratio. Therefore, the researchers concluded that the BHF scheme slop correlated with the drawing ratio in a linear relation for all coefficients of friction.

Shoichiro et al. [48] carried out a study on the formability of magnesium alloy sheet of 0.5mm in thickness through deep drawing process at elevated temperature of 300°C using variable blank holder forces (BHFs). The main targets of this study were to estimate the limit

drawing ratio (LDR) and to clarify the fracture mechanism of the magnesium sheet. The blank/tools contact interfaces were defined with friction coefficient of 0.05. The experimental results indicated that the maximum drawing ration (LDR) of 2.09 was acquired with constant holding force of 5kN. In the case of variable BHF technique, low BHF caused the product to wrinkle, while high BHF resulted in fracture. However, the variable BHF resulted in successful cups and improved the LDR from 2.09 to 2.14 with lower punch load. Regarding the thickness distribution of the drawn cup, the constant BHF caused a thinning along the punch nose until the wall region, while the upper part of the side wall experienced a thickening. Nonetheless, the issue of the thinning and thickening was overcome in the case of using variable BHF leading to more uniform thickness distribution. The FE simulations predictions showed a well correlation with the results obtained from the experiments. It was clear that as the constant BHF increased the corresponding punch load increased, and as a consequence fracture at the side wall of the cups drawn occurred when the holding force caused tensile stresses exceeding the ultimate strength of the sheet material. Also, the thinning at the punch nose radius of the cup drawn with variable BHF was slightly suppressed compared to the constant BHF. In addition, the thickness of the side wall of the drawn cup was significantly depended upon the initial BHF condition [48].

Wifi and Mosallam [25] developed three nonconventional blank holding techniques which characterized by friction actuated, elastic and pulsating blank holders. 3D-FE simulations for the deep drawing processes were performed using the general code ABAQUS/Explicit. The influence of the variable blank holding forces, under consideration in the mentioned techniques, on the sheet metal formability limits was investigated. The blank used in this study was made of Al 5182 alloy. Concerning the friction actuated-blank holding technique, the top part of the device used here consisted of a urethane pad inserted between the upper and lower parts of the forming punch. At the beginning of drawing stroke, the urethane pad expanded radially filling the clearance with the holder wall, and thereafter the friction exerted between them induced the BHF. The results detected that clearance larger than 0.5mm delayed the contact between the rubber pad and the inner holder surface, allowing the blank to form at the early stage without holding force which resulting in wrinkles. Another observation was that the BHF increased with the height of the polyurethane pad as the friction force exerted increased with increasing the contact area between the pad and the holder bore surface. Also, it was noticed that increasing the punch force caused an increase in the BHF. In

the elastic holding force technique, an elastically deformable thin steel annular ring of 1.5mm thickness was used as a blank holder. An initial gap was set up between the elastic holder plate and the blank. A dramatic increase in the height of wrinkles occurred at the flange region was observed when 0.2mm initial gap was adopted. However, less than 0.2mm initial gap was remarkably influential in eliminating wrinkles. For the pulsating BHF technique, it was denoted that the wrinkle height was improved with increasing the pulsation frequency up to a certain value, and however frequency higher than this value had no significant influence on the wrinkling. Moreover, the results confirmed that increasing the loading amplitude reduced drastically the friction force, and consequently improved the wall thinning of the produced cups [25].

### 3.2.2 TOOL GEOMETRY

Hassan et al. [49] presented a new blank holding technique on friction aided-deep drawing process. The blanks used were made of aluminium sheet with 0.5mm thickness. In this work, a metallic blank holder was composed of stationary base with tapered surface and four drawing segments with the same tapered-plane angle of  $5^\circ$ , as shown in **Figure 3-1**. The current situation in this figure caused the blank and the die to lift up and thereby 50% of the blank flange in the B-direction was unsupported by holding force as seen in **Figure 3-1b**.

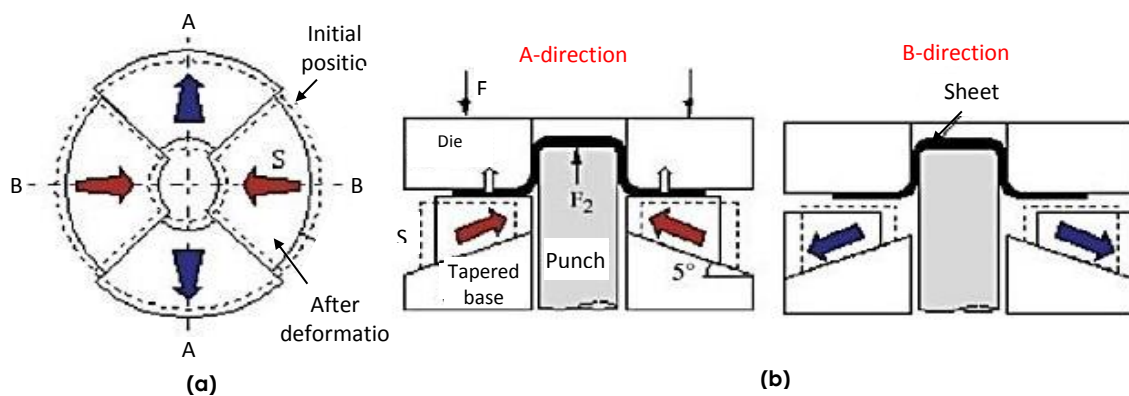


**Figure 3-1. Schematic of construction and movement of tapered blank holder [49]**

For the conditions of 1mm radial segments displacement and 4kN drawing force, it was observed that no increase in the cup height was produced after 20 drawing steps for BHF of 40kN. This result is because this BHF value induced friction forces at the blank/holder interface insufficient to draw more blank material into the drawing die. Nevertheless, it was detected that increasing the BHF caused the height of the final cups to increase with the number of the

drawing steps. Moreover, the results revealed that deeper cups could be produced with increasing the radial displacement of the holder segments. However, an excessive radial displacement resulted in wrinkles of height larger than the value that can be suppressed over the next drawing step. Therefore, holder displacement of 1mm was recommended to establish a balance between avoiding wrinkles and increasing cup height. For drawing operations with 100kN BHF and 1mm holder displacement, it was deduced that for a given number of drawing steps, the cup height increased with the punch force. The results denoted that maximum wall thinning occurred at the punch profile due to the bending at this region was induced by tensile force. The cup bottom had a slight thinning and however a uniform distribution for the thickness strain was observed. Moreover, it was detected that thinning at the side wall gradually decreased and the thicker part of the formed part was at the flange [49].

Due to the low formability of the commercial magnesium alloy, the limiting drawing ratio that can be obtained from a cold deep drawing is relatively low and limited between 1.2-1.4. High temperature annealing process of the magnesium alloy can contribute in increasing this drawing ratio to 1.7. To draw cups with small corner radius especially with square shape, the limiting drawing ratio of 1.7 is still not sufficient. Therefore, a two-stage technique for cold deep drawing process of magnesium alloy AZ31 sheets of 0.5mm thickness annealed to 500C° was developed by Mori et al. [50].

In the first stage, an inner punch of large corner radius was used to form the flat blank into the preliminary cup. Since no extravagant deformation occurred at the large punch profile, the tearing was avoided in this stage. The second drawing stage involved reducing the large corner radius of the cup through compressing the side wall at the rim thickness by an outer punch. Hence, the apprehension of failure by fracture could be eliminated as the tensile stresses were drastically reduced at the side wall and the small corner of the cup. The FE software ABAQUS was utilized to simulate the drawing operations. The results obtained from the experiments exhibited good matching with the simulation predictions. For cylindrical cups, the corner radius decreased with increasing the compression displacement in the second stage, however, the cup experienced a fracture at its corner for excessive compression of 2.8mm. It was indicated that a compression displacement of 2.6mm resulted in reducing the corner radius 5mm of the preliminary cup to 1.1mm. Also, the reduction in thickness of the final cup was small as only the corners underwent deformation. Through the second drawing stage, the height of the final cup was reduced. In order to increase the height of the cup



produced through the first stage, ironing was carried out. The results pointed out that the maximum ironing ratio possible for the magnesium cup was 20% which increased the cup height from 7.2 to 8.4mm. Another advantage of the ironing process here was to prevent the large increase in the wall thickness at the top edge of the side wall. Regarding the two stages stamping of square cups, the maximum drawing ratio achieved by this technique was 1.44, where broken cups were produced when the drawing ratio was increased to 1.49. Nevertheless, small corner radius of 1.7mm and bottom radius of 0.6mm were obtained for the final cup [50].

In aim to clarify the effect of the geometry of forming tools on formability of sheet metal, Savas and Secgin [26] presented a new design for blank holder and die used in deep drawing processes. In this work, the blank holder and die shoulder surfaces that in direct contact with blank were manufactured oblique with different angles ( $\alpha$ ) of 0°, 2.5°, 5°, 10° and 15°. The blank material was DIN EN 10130-91 of 1mm thickness. The diameters of 46.2mm and 48.5mm, and profiles radius of 10mm and 8mm were used for the drawing punch and die respectively. The influence of the initial angle  $\alpha$  on the blank holding force and the drawing ratio was investigated through drawing experiments in this work. The results indicated that for a constant targeted drawing ratio of 1.75, increasing the angle  $\alpha$  from 0° to 2.5° caused the blank holding force to decrease dramatically from 10362N to 3002N. However, a further increase in the angle  $\alpha$  until 15° had no effect on the blank holder force required for producing successful cups. It could be deduced that using blank holder and die with oblique surfaces help reducing the tensile radial stresses and at the same time increasing the compressive stresses in the circumferential direction. This action allowed for the blank to flow smoothly into the drawing die. Nevertheless,  $\alpha$  larger than 15° resulted in excessive circumferential compressive stresses which turn in cause the cup to wrinkle at the flange portion. Also, it was observed that the limit drawing ratio increased from 1.75 to 2.175 with increasing the angle  $\alpha$  from 0° to 15°. Therefore, it was concluded that the optimum angle value for the condition under consideration in this study was 15° as it caused in the smallest blank holder force of 3002N with the highest drawing ratio of 2.175 [26].

The possibility of improving the drawability of DIN EN 10130-91 sheet with 1mm thickness over deep drawing processes via varying the geometry features of the forming tools was presented by Özek and Bal [28]. Therefore, the blank holder and the die with different

angle ( $\alpha$ ) of  $0^\circ$ ,  $2.5^\circ$ ,  $5^\circ$ ,  $7.5^\circ$ ,  $12.5^\circ$  and  $15^\circ$  for the shoulder portion, and also the punch and die with profile radius (R) of 4, 6, 8 and 10 were utilized.

For profile radius R of 10mm, it was found that as the angle  $\alpha$  increased the drawing ratio ( $\beta$ ) increased as well to reach the maximum value 2.3 at  $\alpha=12.5^\circ$ , with exception of  $\alpha=15^\circ$  where  $\beta$  was just 2.2. This action was attributed to many factors, but the most relevant reason was that when the angle  $\alpha$  increased the radial tensile stresses decreases and circumferential compressive stresses increased, and thence  $\alpha=15^\circ$  caused excessive stresses in the circumference direction leading to heavy wrinkles at the die entrance. The results denoted that an increase in the punch force was reported as the angle  $\alpha$  increased from  $0^\circ$  to  $12.5^\circ$ , and nevertheless the punch force decrease when  $\alpha$  was  $15^\circ$ . In the case of profile radius of 8mm, the same correlation between the angle  $\alpha$  and the  $\beta$  was observed, and the maximum  $\beta$  value of 2.175 was obtained with  $\alpha=12.5^\circ$ , and increasing  $\alpha$  to  $15^\circ$  had no effect on  $\beta$  which remained at 2.175. It was noticed that a further increase in  $\alpha$  resulted in wrinkling. On the other side, the larger value of  $\alpha$  resulted in higher punch force at all. The radius  $R=6\text{mm}$  caused the drawing ratio increased to 2.1 when  $\alpha=7.5^\circ$  from 1.8 when  $\alpha=0^\circ$ . Moreover, the same drawing ratio was produced when  $\alpha$  was increased until  $15^\circ$ , which indicated that there was no advantage, in terms of drawing ratio, of increasing  $\alpha$  above  $7.5^\circ$ . On the other hand, the punch force increased with increasing  $\alpha$  from  $0^\circ$  to  $7.5^\circ$ , thereafter, a reduction was observed as  $\alpha$  increased from  $7.5^\circ$  to  $15^\circ$ . The results of using profile radius  $R=4\text{mm}$  detected that the drawing ratio was 1.8 for the angles  $0^\circ$  and  $2.5^\circ$ , and it increased to 1.9 with  $\alpha=7.5^\circ$ , thereafter this value remained constant even though  $\alpha$  increased to  $15^\circ$ . In addition, the punch force increased as the angle  $\alpha$  increased from 0 to  $7.5^\circ$ , and then it decreased with  $\alpha$  increased to  $12.5^\circ$ . Subsequently, no effect on the punch force was observed with increasing the blank holder angle further until  $15^\circ$  [28].

### 3.2.3 LUBRICANT STATUS

Audy and Evin [51] achieved a study on the efficiency of using uncoated and TiN coated forming tools in deep drawing processes of cylindrical steel cups. The influence of this approach on drawing force, power, friction conditions and press work was investigated via experiments and simulation predictions. The dimensions of the blank were 60mm in diameter and 1mm in thickness.

The experimental results referred to the punch force-stroke curves obtained under the uncoated and coated conditions qualitatively have the same tendency. However, the punch force required with the uncoated tools was higher caused the press work to be greater. The simulation predictions exhibited a good agreement with the experimental results. The clearance adopted in the numerical models was 1.2 greater than the initial blank thickness, while that one in experiments was just equal to the blank thickness. This situation implied that there was no reduction in the blank thickness could occur in the simulation analysis. Therefore, the duration of the maximum punch forces, in terms of drawing stroke, through the experimental work was 10mm to 17mm, while this duration in simulation was much shorter ranging from 10-12mm. In the case of wall thinning, it was observed that the use of the coated tools resulted in reduction in the drawing force and the work obtained with the uncoated by 6.2% and 7.4% respectively. Also, the friction coefficient at the blank-tool interfaces was improved about 5% by using the coated tools. On the other side, the final height of the drawn cups was 20.1mm with the coated tool in return of 19.8mm with the uncoated. This difference in the cup height was due to the earing which increased with increasing the friction coefficients. In addition, during the numerical simulation where no thinning occurred; reductions of 3.5% and 5% were produced in the punch force and friction coefficient respectively due to using the coated tools [51].

The influence of using different lubricants on the expansion of an annular ring die utilised in deep drawing processes was revealed by Allen and Mahdavian [9]. In fact the objective of this study was how to exploit the expansion of a die ring in detecting the lubricant film thickness and evaluating the surface quality of the formed parts. The outer diameter of the die ring used here was 119.9mm, the inner diameter was 63.7mm and the height was 15.4mm with profile radius of 7.5mm. The circular drawing blanks were cut from cold steel sheet (BHP CA3SN-G) of 1mm thickness with diameter of 120mm. These lubricants used in this work were three paraffinic mineral oils which are mineral A, mineral B and mineral C with viscosity of 460, 1070 and 1487.5 CP respectively and Castor oil with 225 CP viscosity at 40 °C.

The results exposed that the negative response of the strain gauge was due to the rotating of the die ring inwards, which is caused by the frictional shear stresses at the blank die interface. In this work, the maximum punch force was employed as an index to evaluate the friction force levels that were classified from lowest to highest by lubricant as oil C, oil B, Castor, oil A, none. Where the punch forces 72.3, 73.3, 74.2, 75.8 and 83.1kN were obtained

for the lubricants oil C, oil B, Castor, oil A and none respectively. The wall thickness of a drawn cup was measured at four points 90° apart around the central vertical axis of the cup and at three points of 15, 25 and 35mm heights on the side wall. The results showed that the reduction in wall thickness increased as a higher friction levels between the blank and die were adopted. As the frictional shear forces increased the axial stresses excited in the blank material increased as well, and consequently higher elongation occurred causing further thinning of the cup wall. The thickness of the cup drawn using the mentioned lubricants with exception of oil A increased with decreasing maximum punch force [9].

It was validated experimentally that the surface roughness ( $R_a$ ) increased with the increase in the viscosity of the lubricants used with exception of oil A. Therefore, a significant increasing in the  $R_a$  was observed on the surface of the cups drawn using oil C with comparison of the other lubricants. Also, the results revealed that the reduction in maximum punch force caused an increase in the  $R_a$  value. In addition, the thickness of the blank was increased at the flange portion during the drawing stroke, which caused the forces required to bend the sheet material at the entrance radius of the die increased. It was found that the radial components of these forces caused the die expansion to be directly influenced by the change of the blank thickness. Since the thinning proportionated with the friction levels, thus the die expansion increased with higher friction levels. Furthermore, if the oil film thickness had an impact on the cup thickness reduction, the die expansion then increased directly with increasing the oil thickness. Otherwise, the resulting die expansion was influenced simultaneously by the thickness of both the cup and the oil file [9].

#### 3.2.4 TOOL HEATING CONDITIONS

As is mentioned previously, some of the process aspects included in this chapter is not relevant to the objective of the current study. Despite that, they are taken into account here actually in order to provide a comprehensive guide for the interested in the deep drawing area as well as because these aspects may represent effective aspects in one of the drawing techniques under consideration in the survey. Such these aspects are the heating conditions of the drawing tools, which are presented here to clarify how the working temperature influences on the drawing results.

The formability of sheet material utilized in deep drawing processes can be remarkably improved by adopting the techniques of heating and cooling system for the forming tools.

These activities help in reducing the flow stresses prevailing at the blank part between the blank holder and die, and also causes strengthability of the sheet to be greater at the part close to the punch region and the cup wall [52].

Deep drawing processes of AZ31 magnesium alloy sheet under various heating conditions for forming tools and blank were performed by Palumbo et al. [10]. Electrical heating elements used to control the temperature were included inside the female die and the blank holder symmetrically in the radial direction. Also, the rigid punch contained channels for cooling water. Circular drawing blanks were cut from AZ31 magnesium alloy sheet of 0.7mm thickness with diameter of 80mm. The simulations of the deep drawing processes were achieved using the ABAQUS/Standard FE code. The preliminary results of the deep drawing processes performed by heating the die with different temperatures of 120°C, 140°C, 150°C, 160°C and 170°C without using the punch cooling system, revealed that the highest drawing ratio of 2.6 was obtained at 170°C.

For the condition of punch cooling and heating the blank holder until the temperature at the blank centre reached to 200°C, there was a noticeable increase in the temperature difference along the blank section through the drawing stroke. This difference was greater for the blank portion in contact with the cooled punch than that for the blank portion in contact with the blank holder. In addition, a case of no punch cooling in which the punch was initially kept at 160°C, and a case of improved cooling efficiency were adopted in this work. The advantage of reducing the blank temperature obtained with the improved cooling efficiency technique was pronounced compared with the absence of the cooling water. However, no improvement on the temperature reduction obtained with the punch cooling due to the small contact area. The second strategy considered heating the die and cooling the punch. The heating level of the die was dictated so that the blank was at 160°C. The reduction in the blank centre temperature was clearly noticed, and nevertheless, increasing in this temperature was recognized with the punch stroke due to the progressive increase in the area of the blank surface in contact with heated die [10].

The drawing experiments were performed with heating the blank holder so that the blank temperature was 250°C. The results reported that the blank temperature was higher for no punch cooling (*P*), and thence the punch load was lower than for punch cooling (*PC*). It was recommended to keep cooling the punch correspondingly to the heating for the blank holder

as the maximum drawing ratio of 3.1 was produced, whereas a fracture occurred at the cup wall in the case of absence the punch cooling [10].

The deformation behaviour of the magnesium alloy AZ31 and AZ52 rolled sheets through deep drawing processes at elevated temperature were investigated experimentally and numerically by Hai et al. [53]. The thickness of the sheets of both the alloys mentioned above was 0.83mm. The punch was kept at temperature of 298K, whereas the temperature of the blank, die and blank holder was ranging from 423 to 523K. The numerical part of this work was achieved using an implicit FE code DEFORM 3D. The experiments and simulation predictions denoted that as the drawing temperature increased the limit drawing ratio for the blank materials under consideration increases until reaching a maximum value at 498K.

The results of the maximum conditions which are LDR of 3 for AZ31 and 2.8 For AZ52 at 498K showed that the temperature of the blank part in contact with the punch nose radius decreased through the drawing stroke. This action was due to low heat capacity of magnesium and the temperature of the blank was significantly higher than that of the punch. Also, a gradual increase in the temperature towards the flange portion was observed, which led to a lower punch force was required to draw the flange into the die cavity. The thickness strain distribution produced through the experiments exhibited well matching with that predicted by simulations. Nonetheless, the maximum thinning obtained from the numerical models was greater than that obtained from the experiments. Since the blank underwent to high temperature at the die shoulder and low temperature at the punch nose radius, therefore, the side wall experienced low yield strength, at which therefore the maximum thinning occurred. Despite the limit drawing ratio produced through the experiments for AZ31 was slightly greater than that predicted by simulation; both of the experimental and numerical activities detected that the fracture occurred at 423K and LDR of 2.8 was at around the punch corner, where the maximum strength of the blank material was lower than the punch force. For the conditions of LDR of 3 and 2.8 for AZ31 and AZ52 respectively at 498K, the results indicated that the punch load curves obtained from the experimental and simulations had the same features. Nonetheless, the experimental maximum punch load value was lower than that predicted by the FE models [53].

### 3.3 HYDRAULIC PRESSURE-ASSISTED DEEP DRAWING

In order to eliminate or at least minimize the common problems encountered in the conventional deep drawing techniques using rigid tools, various drawing processes with using elastic forming tools have been developed. Of these processes is the hydraulic pressure-assisted deep drawing, in which just the punch is the rigid tool and the die cavity contains a pressurized fluid (usually oil). Therefore, the rigid punch is the responsible of the final shape of the formed parts [13].

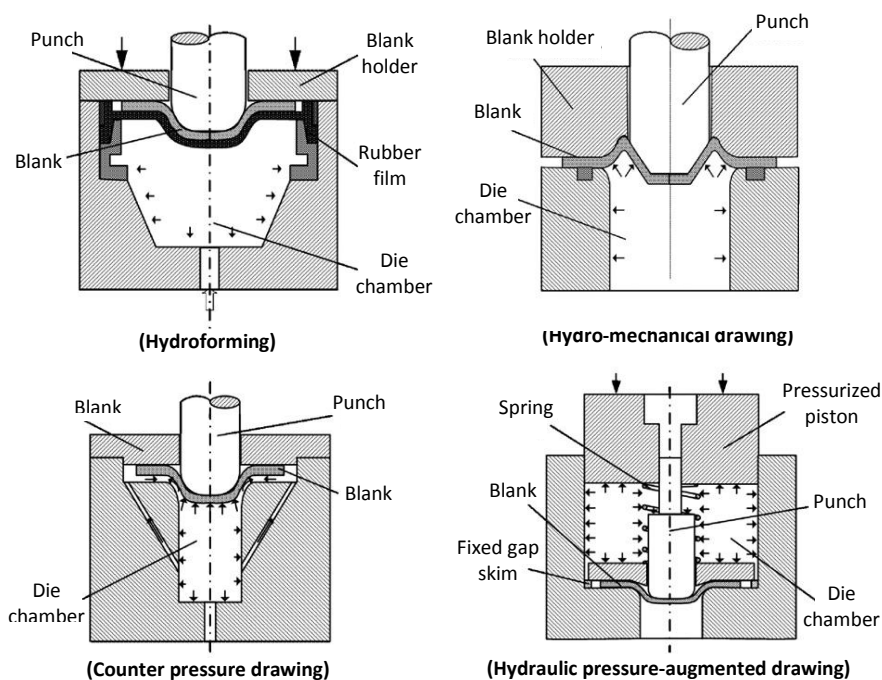


Figure 3-2. Four typical hydraulic pressure-assisted deep drawing methods [54]

The hydraulic pressure-assisted deep drawing processes are classified mainly, in accordance to the way by which the fluid pressure is exploited, into hydro-mechanical drawing, hydroforming, counter-pressure drawing and hydraulic pressure-augmented drawing [13, 54, 55], as shown in Figure 3-2. In addition to the capability of the hydraulic-pressure-assisted deep drawing processes in producing components with complex shape, this technology has several essential advantages such as improvement of the sheet formability, good surface quality, accurate dimensions, reduction of the spring-back effect, and uniformity of product wall thickness. Moreover, since the process is regarded simply, hence the energy will be saved [56, 57].

### **3.3.1 HYDRO-MECHANICAL DEEP DRAWING**

Several studies [24, 58-63] investigated the influence of various parameters, such as initial chamber pressure, peak pressure, blank material properties and sheet thickness, on the formability of blank material in hydro-mechanical deep drawing processes. Singh and Kumar [24] executed hydro-mechanical deep drawing processes on steel sheet of 1mm thickness to clarify the influence of initial pressure and peak chamber pressure on the thickness distribution and surface quality of the final products. The drawn cups were cut at 90° to the rolling direction for measuring the thickness distribution. The thinning occurred at punch corner in conventional drawing processes was reduced in hydro-mechanical deep drawing as low deformation for the blank material took place at this region. Increasing the initial pressure of the chamber liquid resulted in reduction in the necking value as well as moving the necking point to the side wall region. Nevertheless, further increase in the initial pressure make the necking worse at the side wall, which led to fracture. The results detected that the higher the initial pressure, the higher the rate of increase of the chamber pressure. Thus, as the initial pressure increased the peak value of the chamber pressure increased as well. The range of the peak chamber pressure allowed in this work was 80-310bar. It was denoted that the thickness distribution became more uniform with increasing the peak pressure, and therefore the optimum situation was at the value 270bar. Moreover, higher initial pressure, and consequently higher peak pressure, resulted in higher drawing load. As a result, it was very important to attain a compromise between initial pressure and peak pressure. On the other side, increasing the peak pressure from the 80 to 310bar improved the cup surface quality in terms of the roughness reduction. However, for peak pressure higher than a certain value the quality of the product surface deteriorated increasingly. The surface roughness was very slightly influenced by the initial pressure of the fluid in the forming chamber [24].

The effect of pre-bulging on the blank material formability during hydro-mechanical deep drawing process explained by Lang et al. [60]. There are two main parameters corresponding pre-bulging procedure, which are pre-bulging height and pre-bulging pressure value. The results showed that the pre- bulging strategy had a significant influence on the initial forming stage and the middle forming stage. On the contrary, the final stage of the drawing process was not influenced considerably. Increasing the pre-bulging height increased the area of the blank, which was in contact with the punch and consequently the friction at the blank/punch interface increased. This action led to preventing the fracture at that region.



However, excessive pre-bulging resulted in undesirable bending at the punch corner causing fracture. Moreover, increasing the pre-bulging pressure caused the increase in the die cavity pressure to be higher. Also, it can be concluded that when the drawing ratio increases the pre-bulging should increase [60]. As well as, the researchers in another work [64] investigated the effect of the liquid pressure in the die cavity forming behaviour of aluminium alloy sheet. In this work, the uniform liquid pressure in the die cavity was applied on the rim thickness. They found that the high pressure resulted in high thickness reduction. The blank anisotropy had a drastic influence on the drawn product quality in terms of thickness distribution, fracture type and earing occurrence.

### 3.3.2 HYDROFORMING DEEP DRAWING

The fundamental tools used in this technique consist of a rigid punch, a blank holder, a pressure chamber and a rubber diaphragm as shown in **Figure 3-2**. The rigid die employed in the conventional deep drawing process is replaced here by the rubber diaphragm, which is utilized also to seal the oil in the pressure chamber [65]. The process parameters have been investigated through many previous works [13, 27, 66-68].

Choi et al. [66] a new methodology based on FE analysis for warm hydroforming deep drawing of magnesium alloy AZ31B sheets so as to determine the optimum conditions of the hydraulic pressure and the blank holding force under various forming speed. The important advantage of the hydroforming under warm condition is to reduce the friction significantly around the punch nose radius. It was found that the sensitivity of the flow stress to the strain rate increased with forming temperature. The blank holder force increased in accordance with the increase in the hydraulic pressure, and as a result both of the thickness reduction and punch force increased. It was observed that for higher punch speed, the blank sustained higher strain rate and flow stress. Also, the increase in the punch speed caused the strengthability of blank material at the die corner to decrease and thence excessive thinning was produced.

In order to eliminate the problems concerning the life of elastomer diaphragm using in hydroforming deep drawing technology, Vollertsen et al. [67] presented a new method to produce successful cup drawing by employing multiple elastomer membranes as flexible forming tools as shown in **Figure 3-3**. The result revealed that increasing the internal oil pressure contained inside the elastomer membranes during the drawing caused decreasing in the frictional coefficient between the blank and the membranes. Also, the increase in the

internal pressure from 20MPa to 30MPa caused the exerted strain to change from 0.63 up to 0.66. Moreover, a slight increase in the friction coefficient was observed with increasing drawing velocity.

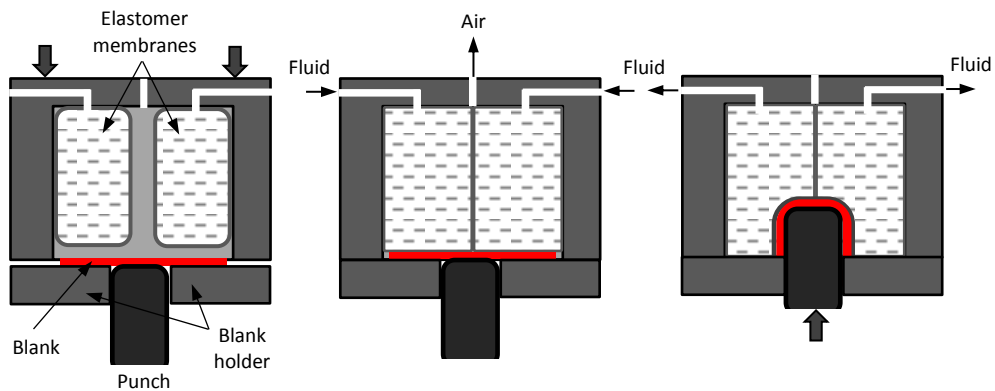


Figure 3-3. Hydroforming process using multiple membranes [67]

In context of using new techniques in hydroforming deep drawing technology with a view to forming cups with a satisfactory quality, Esfahlan et al. [27] presented a novel idea of using a floating rubber disk in a trial to overcome wrinkling and tearing that normally occur during drawing processes. The blanks utilized in this work were made of Ti6Al4V sheet with 1.08mm thickness. The results indicated that decreasing the punch radius the increased the initial pressure just when the punch onset moving into the fluid chamber. Also, for low holding force and/or low fluid pressure wrinkles were observed to occur at different stages depending on the pressure values. As the blank holder force increased the chamber pressure increased, and hence at a particular value fracture occurred at different region in dependence on the pressure level. The high rigidity of the floating rubber disk had important role on reducing wrinkle height and the hydraulic pressure required during the operation. It was denoted also that higher fluid pressure resulted in higher roughness of the drawn cup surface.

### 3.3.3 DEEP DRAWING AGAINST HYDRAULIC COUNTER PRESSURE

The principles of the hydraulic counter pressure-assisted deep drawing process are the same that of the previous techniques. However, as illustrated in **Figure 3-2**, in this process, radial push is applied on the blank periphery by an amount of the fluid contained inside the pressure container, flowing through special passages. Therefore, the radial compression applied on the blank periphery equal to that of the pressurized fluid. In addition, this fluid reaching to the gap between the upper die surface and the blank holder lubricates both sides of the cup flange that is being formed [65]. The effects of the key process parameters such as

the pre-bulging, fluid pressure, gap between die and blank holder, product quality, drawing velocity of the hydrodynamic deep drawing assisted by radial pressure have been detected by many researches [69-72].

Experimental and theoretical investigations on wrinkling obtained in hydroforming deep drawing of Al6111-T4 aluminium alloy sheets with 1mm thickness were implemented by Abedrabbo et al. [71]. Comparative results revealed that the isotropic material model gives no accurate prediction for the failure shape, so the anisotropic model was adopted to simulate the wrinkling behaviour during the drawing operation. The results detected that an obvious increase in the cup height and reduction in springback were attained with increasing the internal pressure up to a certain magnitude. It was also observed that increasing the fluid pressure caused the sheet to stretch in all regions including the flange portion. Hence, this action caused the wrinkles that probably formed during the operation to be ironed. Moreover, uniform thickness strains were produced for the drawn cups.

Lang et al. [69] developed a new technique in hydrodynamic deep drawing process assisted by radial pressure using aluminium alloy (Al6016-T4) sheet of 1.15mm thickness. This technique produced successful cups with maximum drawing ratio of 2.46. The fracture obtained from this work divided into three types in dependence on the drawing stage at which the fracture occurred, and the wrinkling divided into two types in accordance with the region on which the wrinkling took place. The interesting observation was that high and low values for both of the holder/die gap and fluid pressure resulted in fractures with different modes. It was found that the optimum conditions were for the gap about from 0.98 to 1.035mm and for the pressure of 325bar. The pre-bulging height and pre-bulging pressure had a significant effect on sheet forming, and the optimum values detected for the conditions under consideration were 0 mm and 200 bar respectively.

#### **3.3.4 HYDRAULIC PRESSURE -AUGMENTED DEEP DRAWING**

As it can be seen in **Figure 3-2** that the point of this drawing process is that there is no hydraulic fluid pressure in the female tool cavity to counter the rigid punch. The hydraulic pressure here is exploited for providing drawing force and blank holding force simultaneously through getting the fluid in a direct contact with both of the punch and blank holder. Therefore, the punch force and the blank holding force proportional to the fluid pressure generated in the device [65]. However, in another drawing strategy developed by

Thiruvarudchelvan and Wang [73-75], the hydraulic pressure is also applied on the periphery thickness of the blank. Thus, drawing the cup is achieved by a pull activity, by the tensile stresses exerted by the rigid punch action, a push activity, by the radial compressive stresses exerted by the fluid pressure.

An innovative procedure for deep drawing process of aluminium blanks (Al 1100-H14) of thickness 1mm, assisted by hydraulic pressure is conducted by Thiruvarudchelvan and Wang [74]. The hydraulic pressure in this study is employed for three main functions, applying drawing force through a rigid punch, applying blank holder force through cover plate, and applying uniform pressure on the periphery of the blank. It was indicated that as the drawing ratio and/or friction coefficient increased the maximum fluid pressure required in forming stroke increased. Also, the results elucidated that the maximum thickness strains occurred at the cup corner radius, and increasing the drawing ratio caused increasing in the thickness strains. The strange finding was, unlike the previous drawing processes, that for drawing ratio of 3.3 the thickness of the flange region decreased to 0.1mm. This issue was due to the high holding force excited by the hydraulic pressure especially at the latter drawing stroke. In order to obviate this issue, a spacer can be used at the periphery of the blank, which allow the sheet thickness to decrease just to 0.9mm. Moreover, it was revealed that the maximum hydraulic pressure and the pressure ingredient increased with the increase in the initial blank diameter [73]. In this work, the theoretical and experimental results exhibited a good correlation in terms of thickness strain distribution and maximum hydraulic pressure with each blank thickness. It was observed the bottom region of the formed cup underwent obviously reduction in thickness whereas slight thinning occurred at the cup rim. However, the rest of the formed part had some thickening.

### **3.4 FLEXIBLE SHEET METAL FORMING TECHNOLOGY**

Various innovative strategies were introduced into the forming processes of metallic components during the last fifty years. The innovations actually came of using unconventional forming tools such as hydraulic pressure and flexible materials, and techniques such as finite element methods for process design and CAD/CAM for die design [14]. The use of flexible tools in metal forming has a powerful contribution in different industrial applications due to the numerous interesting advantages that can be gained. In flexible forming processes (FFP) just one rigid former (punch or die) is required and it can be made of low cost material such as

epoxy, wood, aluminium, steel, etc. Several rubber materials, such as natural rubber, polyurethane rubber, silicon rubber, can be used for the flexible tool in this forming process. Therefore, the time and cost in terms of tool materials and machining can be significantly reduced. Different and complicated component shapes can be produced by using the same flexible block tool. Moreover, the surface of the workpiece in contact with the flexible tool is definitely protected from any scratching, which implies that this surface can be painted or polished without any protective coating. The difficulties of aligning the male and female tools, which are commonly found in the conventional forming processes, are obviated. In addition, there is no need for using lubricants with flexible forming technology and usually more uniform thickness distribution is obtained for the final products [14, 15].

On the other side, forming parts using such tooling exhibits some disadvantages which include the high press capacity required compared that required with the conventional forming processes, the limited working life of the flexible materials (in dependence on the severity and maximum pressure level of forming), the low temperature range at which the flexible tool can be used, and the low production rate which make it more appropriate for applications of short series [76].

Many forming techniques using flexible tooling technology have been revealed, including Guerin process, Marforming, Verson-Wheelon process, bending, roll forming, blanking and piercing, embossing and Maslennikov' technique. Thirumarudchelvan presented the mechanisms of these processes with details in his work [15]. Various studies and investigations have been achieved to analysis the characteristics of flexible forming technology [14, 15, 76-87]. Ramezani et al. [77] presented theoretical approaches which can be used to simulate the static and kinetic friction at blank/tool interfaces in rubber-pad forming process. The predictions obtained from the FE simulations were validated through experiments. The blank was made out from AA6061-T4 with 1mm thickness and 40mm diameter. The soft pad was made out from natural rubber with Shore hardness 50A and diameter of 40mm. The theoretical simulation was executed by exploiting the commercial software ABAQUS/Standard. The die was defined as a rigid part, whereas both the blank and the flexible pad were modelled as deformable parts. Mooney-Rivlin model was utilized to describe the hyperelastic behaviour of the nearly incompressible natural rubber. In order to define the friction coefficient as a function of contact pressure and sliding velocity, the slip-rate dependent and contact-pressure dependent options provided in ABAQUS were adopted. The result showed that there was

remarkable decrease in the coefficient of static friction with increasing the applied drawing load. In a comparison with the Coulomb friction coefficient (i.e. constant coefficients of static and kinetic friction, the results indicated that use of the static friction model resulted in an accurate prediction for the punch load compared to the Coulomb friction models. For the kinetic friction models, increasing the sliding velocity and normal load caused a decreasing in the coefficient of friction. Here, different values of Coulomb friction coefficients were used beside the coefficient of kinetic friction taken as a function of contact pressure and sliding velocity. It could be denoted that the kinetic friction model had good results at higher forming velocity. Moreover, more accurate prediction obtained with the kinetic friction model than that with Coulomb models.

A numerical investigation using the commercial FE software LS-DYNA on the forming process of an aluminium aeronautic component by utilizing polyurethane rubber pad was achieved by Prete et al. [78]. The influence of forming strategy, part geometry, rubber pad hardness and sheet thickness was explored in this work. The blank material was defined by an isotropic elasto-plastic model with different thicknesses of 1.1, 0.81 and 0.53mm. The material of the flexible pad was polyurethane rubber with 50, 70 and 90 Shore A hardness. The hyperelastic behaviour of the polyurethane material was modelled using Mooney-Rivlin formulation. The first indication of the results was that the interaction between the initial sheet thickness and the rubber hardness had a considerable role to identify the accuracy of the product dimensions. The smaller of the formed part was obtained for the thinner sheet and harder rubber pad. Also, it was deduced that the maximum forming force required under particular conditions decreased significantly with reducing the rubber hardness. However, the initial thickness of the aluminium sheet had just a slight effect on the forming force. It was recommended to adopt polyurethane rubber pad with 90A hardness with blank of 0.53mm thickness to produce the best configuration for the forming process.

The rubber material characteristics have important effect on the deformation mode of blank material. It was found by Ramezani et al. [79] that the maximum thickness reduction with using natural rubber was higher than the one produced with silicone rubber. In this study, it was pointed out that no significant change on the product thickness was observed through increasing the forming velocity. Moreover, a significant increase in the maximum punch load was observed when the silicone rubber pad was replaced by natural rubber. The results proved that for large number of cycles and product with sharp edges, urethane and natural rubber are

the most appropriate choice. The maximum tensile stresses increased with increasing the urethane rubber hardness, and however this action had no influence on the thickness distribution. On the other hand, smaller rubber pad thickness caused an increase in the maximum Von-Mises stress as well as the maximum thickness reduction. It was found that the friction conditions at the blank/tool interfaces had an important role on the success of the forming operation. As the friction coefficient between the rigid die and the blank increased the thickness reduction increased as well. However, higher friction coefficient at the blank/rubber interface resulted in decreasing the thinning.

Wang et al. [80] presented an experimental study to explain the viscous pressure forming process characteristics of corrugated thin sheet metal. This study included evaluating the effect of the drawing pressure and the blank holder force on the dimensional accuracy, thickness strain distribution, and sealing during drawing of nickel-based super alloy and stainless steel sheets with very small features about 2.3mm radius. A soft material such as polyurethane rubber, was used as a flexible punch because their high resistance to high pressure. Two cases of blank holding loading were considered in this study, these were; optimal loading case in which the blank holder force is the smallest and the second case was at higher blank holder force than that with optimal case. The experiments proved that with case 1 the dimensional accuracy meet approximately with the required conditions and the corrugated surface was easier to be formed. Also, the surface quality was similar to that of the original sheet blank. Concerning the thickness distribution of the product, it was observed that the maximum thickness strain was occurred at the corrugated surface and it was smaller with loading case 1 than that with case 2. The highest value of the thickness strain was 15% for the super alloy specimens and 14% for the stainless steel. In addition, decreasing the cup flange width/the original flange width ratio caused decreasing in the thickness strain which means good quality and dimension accuracy of the final product. Finally, the high strength of the metal resulted in making the deformation to be very difficult especially with small features.

Dirikolu et al. in their previous work [81] explained that some of key process parameters and their combinations need to be adjusted before actual forming operation. The parameters taken under consideration were the rubber hardness, blank material, contact conditions and die design. It was revealed that as the rubber hardness increased from 50 to 70 Shore A, the maximum vonMises stress increased for both blank materials used. This prediction was in agreement with the result explored by Wang et al. [80]. Also, a slight reduction in the von Mises

stress was observed when increasing the friction coefficient at the blank/rubber interface and using the hard polyurethane [81].

Liu et al. [82] achieved a theoretical study on sheet forming process using viscous medium. Three forming strategies were examined using the FE simulation code (DEFORM), which are viscous medium over the blank, viscous medium over and under the blank with outlet hole at the die centre, and viscous medium over and under the blank with outlet holes at the die corners. This study explained the role of the die medium viscosity, location of the outlet port, bottom medium, counter pressure, and interface friction force, owing to improve the drawability of the sheet material. Through this work, two types of the viscous polymeric material namely C11 and C12 with different viscosities were used. The results showed that the use of the lower viscosity medium resulted in more uniform thickness distribution. However, cups with poor quality and nonuniform stretching were produced when the outlet port was positioned at the die centre. On the other hand, outlet port at the die corner caused the cup to be fractured at the side wall. When the softer medium (C11) was used only on the upper surface of the sheet, complete contact with the die surface could be occurred. Whereas, if the viscous medium C11 used also under the blank then the trapped amount at the around die corners allowed to increase the formability of the sheet. Furthermore, the results detected that as the friction coefficient at the sheet/medium interface increased the thickness strain decreased and the traction was larger.

### 3.5 SIZE EFFECTS ON MICRO FORMING

Due to the technological revolution of miniaturized devices utilized for different applications of electronics, energy storage, medical activities, micro system-enhanced heat and mass transfer, etc. In the last decade, the need for producing components with micro features such as channels, arrays, etc. has been extremely increasing. Many studies have proved that metal forming processes are considered to be the best choice for manufacturing these components/features with a competitive quality [42, 43]. The key issue in micro forming technology is to well understand the forming behaviour of the workpiece material at the scale under consideration. The material behaviour observed at macro scale can no longer be expected to occur when scaling the forming process down to micro scale. The deviations of the expected results on that received actually at micro forming are due to the so called "size effects". All of process, material response, tools and even equipment used in the micro



forming process are influenced by the size effects. Due to its significant importance, the size effects attract wide attention of the researchers in the field of micro forming processes which are divided mainly into micro bulk forming and micro sheet metal forming [88]. In micro sheet metal forming, the behaviour mode of the workpiece material can no longer be described basing on homogeneous continuum mechanics as the material microstructure is characterized by a few grains in the thickness direction. Thus the term of “size effects” is referred sometimes by the ratio of grain size to the particular part size. Therefore, the material behaviour is quaintly dictated by its grain size and orientation [89].

On the way, many investigations have been achieved on micro sheet metal forming processes for different materials, and thereafter the results pointed out that the flow stress decreases with reducing the sheet thickness [90-93] see **Figure 3-4**. In general the size effects can be defined as the difference between the actual and expected results of material response when changing the geometrical dimension of a workpiece. The size effects are classified into two types: first order size effects which can be measured through conventional models. For example, when scaling forming process down to micro level the friction effect increases and hence its share in the total forming force increases as well. While the second order size effects cannot be accounted directly, and they occur even if the size similarity and conventional models are used. Owing to reveal and prove its occurrence, a number of material tests and forming experiments are required to be performed at micro level [94, 95]. The micro tests and experiments are designed in accordance to the similarity theory proposed by Geiger et al. [96]. This theory points out that the main process dimensions (i.e. workpiece and tool dimensions) are scaled down with taking into account the geometrical similarity conditions by multiplying these dimension by the same geometrical scaling factor  $\lambda$ . In order for the process time to stay constant, the timescale is chosen for the forming stroke to be 1 [97, 98]. Thus, the same scaling factor  $\lambda$  can be utilized for the strain, strain rate and strain distribution, and therefore in accordance to this action the same tendency for the stress strain relationship will be obtained with different value of  $\lambda$  [98]. There are two approaches for the size effects to be classified. The first one states that there are two categories for the size effects; grain size effects and feature/specimen size effects. The grain size effects denote that the strengthability of workpiece material inversely proportion with its grain size and this category has been known to follow the Hall-Petch equation [99]. The average grain size in macro scale represents the predominant parameter affecting the material response. The feature/specimen size effects

appear distinctly when scaling the forming process down into micro scale. In fact, the feature/specimen size effects are usually divided into two subgroups; specimen size effect which refer to the dimensions of the specimen/workpiece e.g. rod diameter in micro bulk forming of cylindrical part and blank thickness in micro sheet metal forming. While, the feature size effects come from the dimension of the features that intentionally formed on the final products [37, 98].

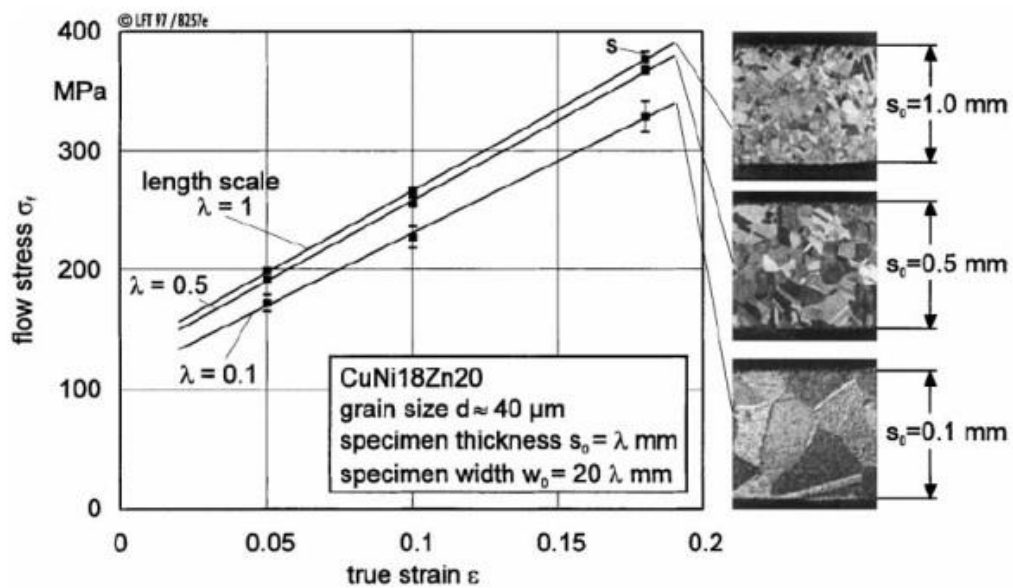


Figure 3-4. Flow curves of CuNi18Zn20 obtained through tensile test for different thicknesses [97]

However, Vollertsen [100] regarded the previous definition of the size effects is not very precise, and he has proposed the following definition “size effects are deviations from intensive or proportional extrapolated extensive values of a process which occur, when scaling the geometrical dimensions”. This definition was established based on the fact that variables can be commonly classified into two types; intensive and extensive variables. When the variable value is characterized as a function of the mass of the object then it is regarded as extensive variable like heat content, if not then it is an intensive variable like temperature. According to Vollertsen the size effects can be classified into three main categories which are density, shape and microstructure size effects as illustrated in Figure 3-5 [100].

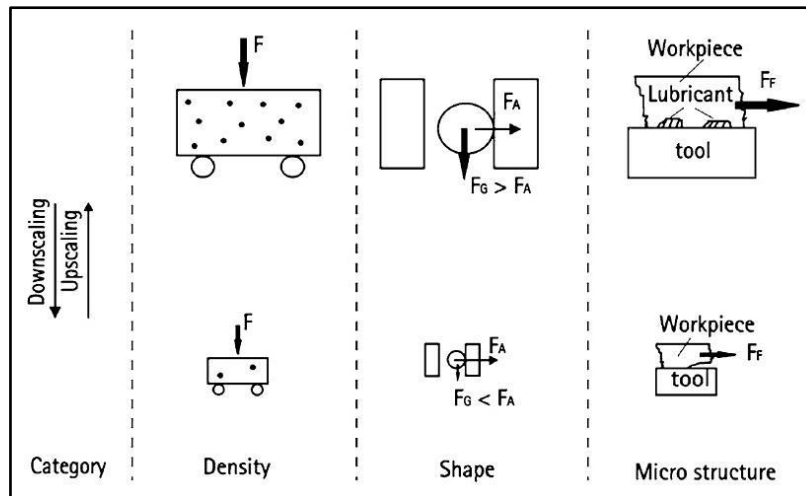


Figure 3-5. Schematic representation of the three main groups of size effects,  $F$  force,  $F_A$  adhesion force,  $F_f$  friction force,  $F_G$  gravity [100]

Geiger et al. [40, 95, 101] studied the material behaviour in sheet metal forming when the specimen dimensions were scaled down to micro scale using various materials. The results revealed that the flow stress of the workpiece decreases with increasing the miniaturization level through scaling down the geometrical dimensions. A number of tensile tests were achieved on CuZn15 samples with different average grain sizes and miniaturization levels through scaling down the cross section area of the samples. The flow stress was observed to decrease as the gross section of the tested sample was reduced. Also, there was no any observable role for the strain hardening on the scaling effects. For a particular constant grain size, it was found that the flow stress value depends on the share of the surface grains which become higher than the inner volume grains with miniaturizing [95]. Moreover, Raulea et al. [102, 103] clarified the occurrence of the size effects through tensile tests and bending experiments of aluminium DIN 1747 by two approaches, firstly by using samples with different initial thickness and constant grain size, and thereafter with various grain sizes with samples of the same thickness. It was pointed out that reducing the thickness of tensile test samples causing a reduction in the yield and tensile strength. As the thickness decreases the volume fraction of the surface grains increases, and they become the predominant factor on the material behaviour. The bending experiments were carried out on specimens of thickness 1mm with different grain sizes. As a result, reducing the grain size resulted in an increase in the maximum load that the sample can sustain without failure (i.e. higher flow stress) [102] see Figure 3-6.

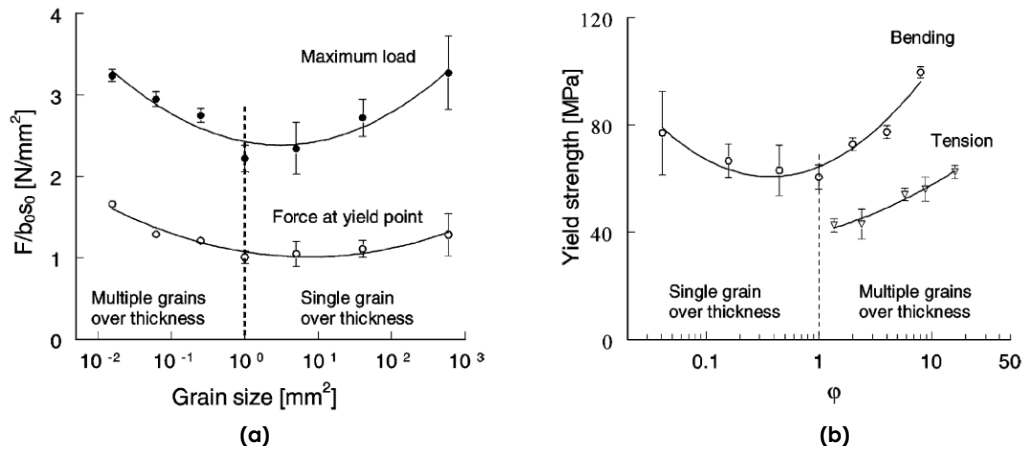


Figure 3-6. Variation of (a) maximum load and yield point load with grain size and (b) tension and bending yield strength with thickness to grain size ratio [103].

Although, increasing the miniaturization level causes the flow stress of specimen materials to decrease, however, Raulea et al. [103] and Gau et al. [104] discovered an interesting observation through bending experiments on aluminium and brass at micro scale. The results showed that increasing the miniaturization until the sheet thickness was less than its grain size resulted in an increase in the yielding point of the specimen material. Also, it was denoted that reducing the sheet thickness to grain size ratio led to reduction in the material formability.

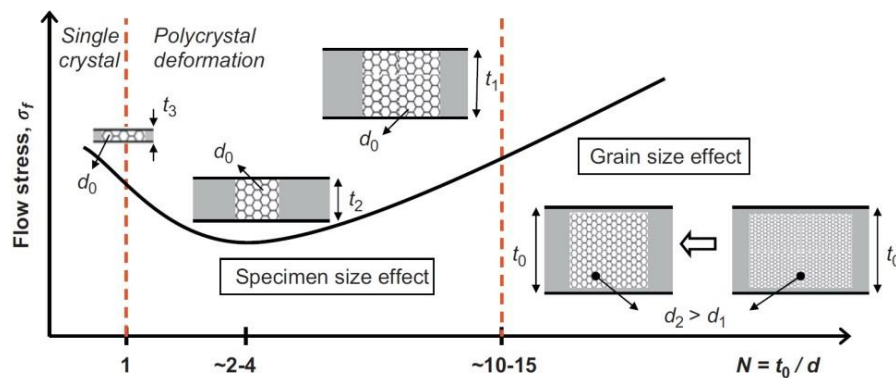
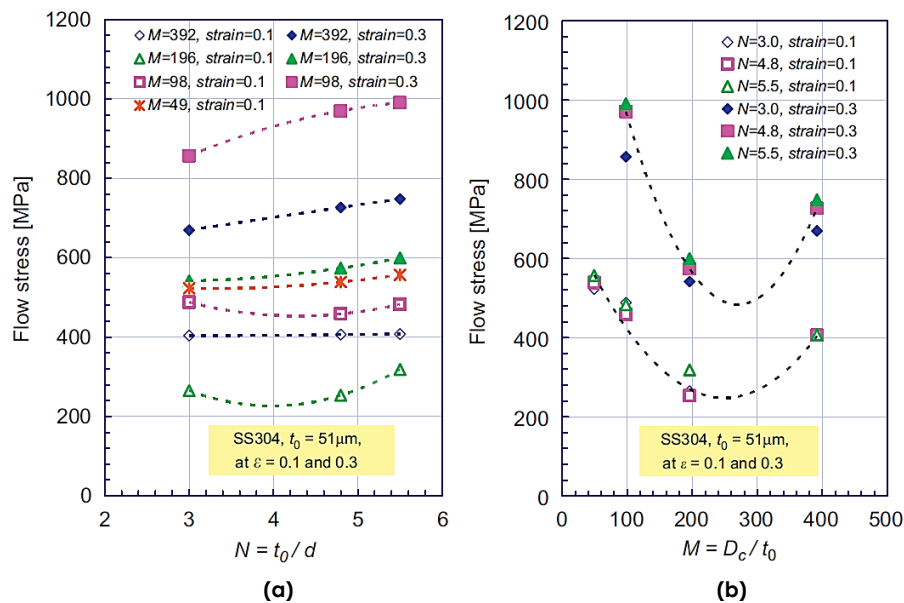


Figure 3-7. Effect of  $N$  (thickness to grain size ratio) on material flow stress [37]

It is known that the surface grains are characterized by lower forces of constraint in the sample surface and exhibit less hardening compared to the inner volume grains. Therefore, as the share of these grain increases with reducing the initial thickness or/and increasing the grain size, thus the strengthability of the material will decrease [42] see Figure 3-7.

In order to detect the interactive effects between the specimen, feature and the grain sizes, Sasawat and Koç [37] studied the flow curves of stainless steel 304 thin sheets obtained from hydraulic bulge tests. The ration of the sheet thickness to the grain size ( $N$ ) and the ratio

of the bulge die diameter to the sheet thickness ( $M$ ) were used as representative parameters of the interactions between the size effects under consideration. This work detected that for strain level of 0.3, increasing the  $N$  value resulted in continuous increase in the flow stress. However, a slight difference on this action was observed at strain level of 0.1, that is, when the ( $N$ ) value decreased from 4.8 to 3.0 the flow stress had a small increase as shown in **Figure 3-8**. On the other side, for both strain levels 0.1 and 0.3 there was a critical value of ( $M$ ) to be between 100 and 200, where the flow stress decreases with the ( $M$ ) value and over it the flow stress exhibited an inverse response [37].



**Figure 3-8. Effect of (a) specimen/grain size ( $N$ ) and (b) feature/specimen size ( $M$ ) on material flow stress [37]**

### 3.6 MICRO DEEP DRAWING TECHNOLOGY

In industry, the production cost plays an essential role in identify the optimum manufacturing processes so long as fulfilling a compromise between the cost, in terms of money and time, and the quality level required for the products.

In order to realize the volume of the growing demand on miniaturized devices, it is necessary to know that from 2004 to 2009 the estimated rise in turnover was approximately from 10 to 19 billion US dollar which spent to fabricate micro formed parts for these devices. Therefore, it can be understand the reason of why a great intention of researchers and manufacturers have been paid towards the micro forming technology rather than the expensive fabrication processes such as micro electro-mechanical systems (MEMS) [105]. As the deep drawing at micro scale is one of the most important processes for producing

miniaturized cup-shapes components, understanding the fundamental characteristics of this technology and thereafter improving the micro drawn parts are needed. Although the theory of similarity can provide a clear guideline for designing the geometrical issues, however, the size effects related to the material, process dimensions and also the tribology conditions cause in unexpected results. As the deformation mechanism in deep drawing differs to that in the conventional stamping processes, hence the role of the size effects may be different as well.

### 3.6.1 BLANK AND TOOL GEOMETRY

Shim [39] presented a study on developing miniature-scale stamping through improving the formability of blank materials. The new method proposed in this work based on optimizing the process aspects in terms of initial blank shape and the material aspects through annealing temperature. The work hardening exponent and the depth of final products were utilized as measures of the material formability and process severity respectively. The blanks that were used here for the drawing process were taken from cold-rolled STS316L sheets with two thicknesses of 50 and 100 $\mu\text{m}$ , and from cold-rolled 99.9% copper with thickness of 100  $\mu\text{m}$ . Owing to identify the optimum annealing temperatures at which the formability of the blank material was observed to be improved properly through tensile tests, several annealing trials were carried out. The temperature adopted for the STS316L sheets were 980°C, 1000°C, 1020°C and 1080°C, while that used for the copper sheet were 160°C, 580°C and 680°C. The optimum conditions and the cases investigated in the experimental were shown in **Table 3-1** presented below.

Cases	Material	Thickness ( $\mu\text{m}$ )	Holding force (N)	Drawing depth (mm)	Flange width (mm)
Case 1	Cu	100	50	1.0	1.0
Case 2	STS316L	50	50	2.0	1.0
Case 3	STS316L	100	60	2.2	1.0
Case 4	STS316L	100	60	2.5	0.65
Case 5	STS316L	100	60	2.7	0.65

**Table 3-1.**Cases investigated in the experimental work [39]

The numerical simulations for the drawing processes were built using the eta/Dynaform 5.6 code. First, the optimum initial blank shape for each case considered in the above table was obtained through the numerical models. Afterwards, the drawing experiments were performed using the optimum blank shapes and square blanks. The results obtained from the

simulations revealed that the thickness strain distributions of the cups drawn for the optimum blanks were more uniform than that for the square blanks. Also, optimizing the blank shape led to reducing the thinning, this means improving the formability of the blank materials. However, except case 1 where the product was shallow for just 1mm in depth, fractures occurred for the square blanks over the experiments, while the simulations predicted successful cups. In general, forming strokes further than 2.7mm caused the blank to fracture, and when the target flange for the final products of 0.6mm resulted in wrinkles [39].

Experimental investigations were conducted by Saotome et al. [106] on very thin metal sheet to demonstrate the material drawability during micro deep drawing process. The foil material was low carbon steel SPCE with different thicknesses ( $t$ ) of 0.05, 0.1, 0.2 and 1mm. In order for the anisotropy of the work materials to be considered, the mechanical properties of each foil thickness at rolling, 45° diagonal and transverse directions were obtained through tensile tests. The theory of similarity was used in this study, where the same miniaturization scale of the blank thickness was used also for the associated tool dimensions, starting with punch diameter ( $D_p$ ) of 10, punch radius ( $R_p$ ) of 2.5, die diameter ( $D_d$ ) of 12.5 and die radius ( $R_d$ ) of 5mm at blank thickness of 1mm. The results demonstrated that the increasing in the ( $D_p/t$ ) value resulted in decrease of the limiting drawing ratio ( $\beta$ ). It was denoted that the effect on the blank holder force was observed to be clear when  $D_p/t > 40$ , where the blank holder force increase with decreasing the ( $D_p/t$ ) value. The experimental results of drawing blank of 0.1mm thickness were shown in Figure 3-9.

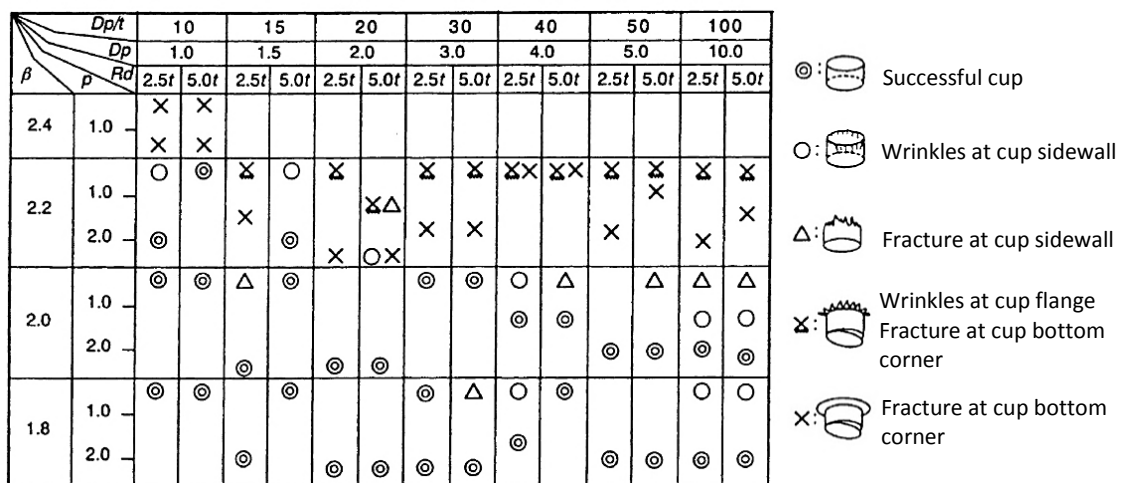


Figure 3-9. Micro deep drawing results for 0.1mm blank thickness,  $\beta$ =Limit drawing ratio [106]

In addition, only with  $(D_p/t)$  values below of 15, the effect of die radius on the process characteristics can be noticed, where with decreasing  $(R_d/t)$  from 5 to 2.5 the blank holder pressure required to produce successful cups increased from 0 to 2MPa. Moreover, it is observed that the maximum punch load is larger and more distributed with increasing the  $(D_p/t)$  value. Finally, the anisotropy factor had important effect on the drawability of blank material, where it is noticed that the maximum relative cup height occurred  $90^\circ$  to the rolling direction [106].

Of the major targets in deep drawing technology at miniature scale are to suppress the development of wrinkling and the decrease in the limiting drawing ratio. Marumo et al. [107] investigated the effect of sheet thickness on the wrinkling occurrence-related aspects that are blank holder force and friction coefficient, in order for the material drawability of very thin metallic sheets to be improved through micro deep drawing process. In this study, three different approaches were utilized for applying the blank holding force (BHF); these are, BHF=constant, BHP=constant and BHP=varying. The results demonstrated that due to decreasing the blank thickness the blank holder force needed to overcome the wrinkling in both cases BHP=C and BHP=varying increases. The same behaviour was observed in the case of BHP=varying, but after a certain punch stroke inverse trend was observed, where the holding force decreased progressively with drawing stroke. In addition, reducing the friction coefficient caused the blank holder force to increase. On the other hand, lower limit drawing ratio was obtained for the thinner sheets, and a drastic reduction in the limit drawing ratio was noticed with sheet metal of thickness less than 0.04mm. As the thickness decreased the influence of the friction coefficient on the limit drawing ratio strongly increased. The researchers deduced that a proper controlling for the variable holding force had an important role in improving the drawability of the sheet material [107].

Chen et al. [108] conducted experimental and analytical investigations on some key parameters of micro deep drawing processes using stainless steel 304 sheets. Of the process-related aspects taken into account were the sheet thickness and the ratio of thickness to average grain size ratio  $(T/D)$ . The influence of these parameters on the limit drawing ratio (LDR) was clarified. Four stainless steel 304 sheets with different thicknesses of 20, 50, 100 and 150 $\mu$ m were used for the workpiece in this study. In order to provide a variety for grain size of the blank materials, annealing treatments were utilized. The set up used in experiments was composed of a rigid punch with diameter  $(D_p)$  of 2mm and punch tip radius of 0.25mm, a rigid



die with diameter of  $(1.1 \times \text{foil thickness} \times 2 + D_p)$  and die shoulder radius is four times of the foil thickness, and oblique position ring to locate the blank and guide holder and punch. The results indicated that at the same annealing temperature, the drawing force required to draw complete cups decreases with decreasing the foil thickness. As is well known, the grain size changes in accordance with the annealing temperature, that is, annealing at the same temperature implies the same grain size is produced. Therefore, it was deduced that the drawing force was observed to decrease with reducing the  $(T/D)$  ratio. Also, increasing the sheet thickness or the  $(T/D)$  ratio with the same grain size caused the limit drawing ratio to be higher. Moreover, the limit drawing ratio was noticed to increase as the sheet thickness increased with the same  $(T/D)$  ratio. The empirical equation which is usually used for predicting the maximum forming load and the limit drawing ratio was applied successfully in this study just with sheet of thickness not less than  $150\mu\text{m}$  as the percentage error between the experimental and predicted results was  $\pm 5\%$  [108].

Hirt et al. [109] carried out experiments and theoretical models in purpose of realizing the roles of size effects in micro deep drawing process. The essential issues of this study are to identify the limits of FE numerical methods in the design of micro deep drawing process and characterize the influence of some material and process-related parameters. The **Table 3-2** illustrates the dimensions of the tools used in this study.

Parameter	Normalised to Punch diameter	Scaling factor $\lambda$			
		1/8	1/4	1/2	1/1
Punch diameter ( $d_0$ )	1/1	1.00mm	2.00mm	4.00mm	8.00mm
Foil thickness ( $s$ )	3/80...4/100	0.04mm	0.08mm	0.15mm	0.30mm
Blank diameter ( $D_0$ )	2	2.00mm	4.00mm	8.00mm	16.00mm
Die radius ( $D_1$ )	43/40	1.08mm	2.16mm	4.30mm	8.60mm

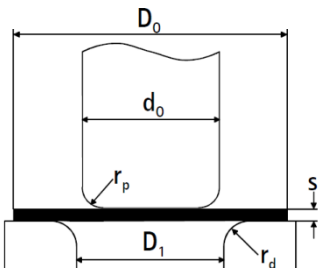


**Table 3-2. Tool data table: geometry parameters of tool sets [109]**

The working blanks were cut from CuZn37 sheets with different thicknesses ranging from 0.04mm to 0.3mm. The deep drawability, in addition to the grain size can be changed by heat treatment, of this material make it adequate workpiece in micro deep drawing process. The dimension aspects that were associated to the punch diameter of 8mm and 4mm were used in initial tests in a view to give a good prediction of relevant process variables affecting the micro deep drawing process. The results indicated that successful cups were produced from foils of 0.15 and 0.3mm initial thicknesses for final normalized drawing depth (depth/punch diameter) of 0.75. As it can be seen in **Figure 3-10**, the punch force curves have two peaks; the first one

was due to the drawing action while the second peak was caused by ironing. It was observed that the maximum forming force with punch diameter of 4mm was higher than the one with punch diameter of 8mm [109].

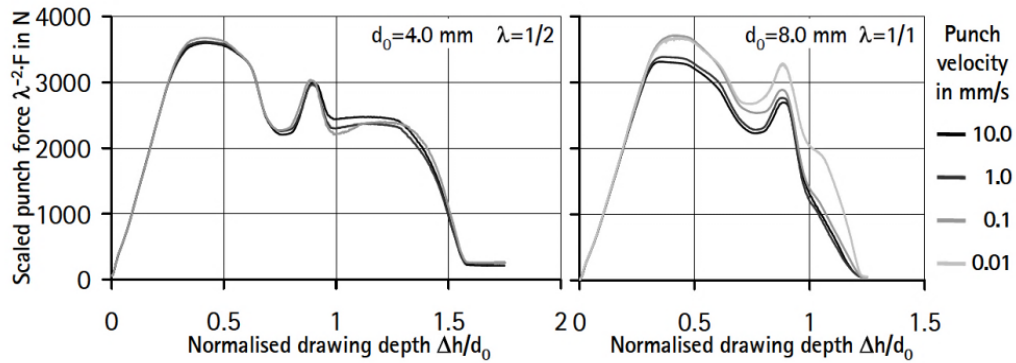


Figure 3-10. Punch force versus normalised drawing depth [109]

Ju et al. [110] presented an experimental study on the influence of die cavity dimensions on strip U deep drawing process. A number of experiments were executed under different process conditions to clarify how the product surface quality and sheet thickness reduction are affected by the process parameters of female die width and radius, initial thickness and blank holding force. The working sheets used in experiments were made of copper T2 with 0.05 and 0.09mm thicknesses, and the dimensions of the forming blank were 10mm length and 5mm width. In addition, the female die was machined to 1mm in width as well as 0.1mm and 0.3mm in shoulder radius. The clearance between the female die and the punch walls was equal to the initial foil thickness. . And the velocity of drawing operation was 10mm/s [110].

The results showed that reducing the female radius caused the punch load to increase. The rate of this increase was found to be larger for the higher blank holder force. This action was rationalized that the reducing the female radius resulted in a decrease in the bending radius which consequently increased the plastic deformation at this critical region and thus a larger load was needed. Also, increasing the blank holder force resulted in higher friction forces which need to be overridden by an increase in the drawing load. Concerning the effect of foil thickness, though the punch load increased with increasing the blank holder force for both the foil thicknesses of 0.05 and 0.09mm, however the increasing range in the punch load with the thicker blank was larger than that with the thinner one. This result was because the plastic deformation of the thicker foil is greater which require a larger drawing load to be form. It was detected that as the blank holder increased the U-shaped product angle increased, this in turn increase the severity of the spring back action. Moreover, the increase of the blank holder force

resulted in increasing the thickness reduction as well as the scratch at the final product surface especially at the die corner [110].

Marumo et al. [111] proposed a new technique of foil-lap blanks in a contribution of improving the deep drawability of stainless steel foils. In this experimental work, a stainless steel foil was lapped by aluminium sheets, through three different approaches, and thereafter all the foil and sheets were formed together in micro deep drawing process. B-sheet type (two-ply foil-lap blank): in this way the stainless steel foil was mounted by an aluminium sheet at the holder side. D-sheet type (two-ply foil-lap blank): in this way the aluminium sheet was lapped the foil at the die side. The third approach was the sandwich type in which the foil was lapped by the aluminium sheets at the both sides. The rigid punch used in experiments was 8mm in diameter, and the same profile radius of 0.5mm was used for the die and punch. The clearance between the punch and die walls was  $1.2 \times$  (foil thickness + lap-sheet thickness). The drawing stainless steel foil was 0.015mm in thickness, while the aluminium lap sheets were selected from pure hard and soft aluminium with 0.2 and 0.5 mm thicknesses. The limit drawing ration obtained without lap-sheets was just 1.25. However, in the B-sheet type this value increased to 1.4 when the aluminium lap-sheets, weather the hard or the soft one, were used as well as the produced cups were free of wrinkles. It was detected that using the hard lap-sheet with thickness of 0.2mm improved the deep drawability of the foil more than the other cases. Despite wrinkling was observed on the products, using the D-sheet type caused the limit drawing ratio to increase to 1.7 for the soft aluminium sheet with 0.5mm thickness and to 1.6 for the hard aluminium sheet with 0.2mm thickness. The results indicated that the B-sheet type played more effective role in the elimination of the wrinkles than the D-sheet type. The efficiency of the sandwich type was remarkable to produce cup of 1.6 limit drawing ratio without wrinkling and fracture, but with aluminium lap-sheet of 0.2mm thickness. It was observed that wrinkles occurred when the lap-sheet of 0.5mm was used, and this action was because the bending radius at the die shoulder increase with the sheet thickness. Furthermore, the drawing force required with the D-sheet type was lower than that for the b-sheet type, and also for both these two types the drawing force increased with increasing the aluminium lap-sheet thickness [111].

Hu and Vollertsen [112, 113] investigated the role of optimization aspects of blank shape in micro deep drawing of rectangular products through experiments and FEM simulations. The sheet materials used for the drawing blanks were Al99.5 of 0.02mm thickness, E-Cu58 of

0.02mm thickness and stainless steel of 0.025mm thickness. The commercial software ABAQUS6.9.3 was used to perform the FE models. The blank material was defined as deformable part with 8-node linear brick 3D-stress element C3D8R. The friction function illustrated in **Figure 3-11** was used in this study.

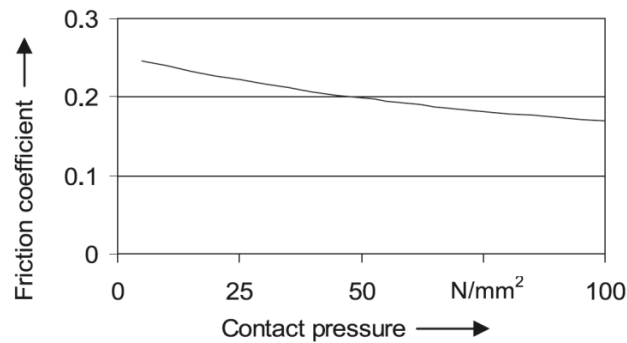


**Figure 3-11.** Friction function of micro deep drawing process with a punch diameter of 1mm [112]

First of all, the simulation results showed that fracture occurred for the drawn parts with excessive holding force, while very low holding force resulted in wrinkling. Also, it was found that successful drawn parts were produced using holding pressure range of 1-3 MPa when the optimum blank shape shown in **Figure 3-12b** was utilized.

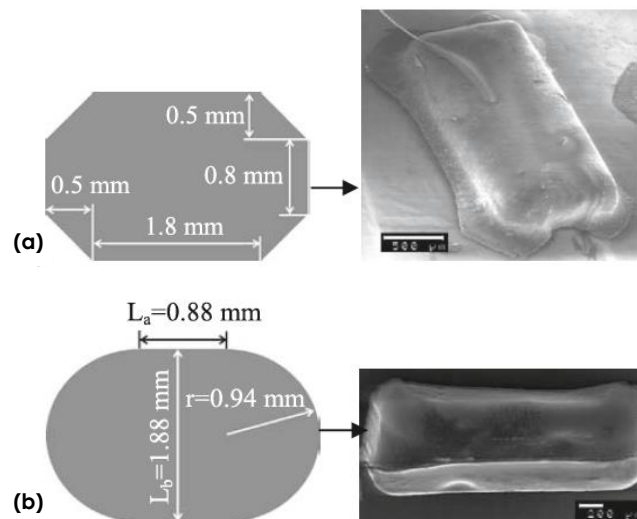


**Figure 3-12.** Drawn parts out of (a) non-optimized and (b) optimized blank shapes for Al99.5 [112]

The dimensions of the optimized blank shape were established using the FE models so that the formed parts of these blanks were flange free compared to the one drawn with non-optimized blank shape [112] shown in **Figure 3-12a**. Moreover, the optimised shapes of the blanks taken from different materials were not similar even they were drawn to the same depth. The

holding pressure had a significant influence to the geometry of the final parts even if the optimized blank shape was used. For example, using holding pressure of 2 MPa resulted in successful parts with equal height on both the short and long edges. Whereas, reducing the holding pressure to 0.5 MPa caused the short edge to be drawn faster than the long edges which produce a difference in height of about 0.1mm [112].

In a contribution to reduce the difficulties of adjustment the very small blanks used in micro deep drawing processes, which in turn save the cost and time for the manufacturing of tinny deep drawn parts, Fu et al. [114] presented a compound process of micro blanking and deep drawing. In this work, several experiments and FE simulations for the entire operation were carried out on thin copper sheets. The process was scaled down based on the similarity theory using different dimensional scales of 0.25, 0.5 and 1 as seen in **Table 3-3**. The influence of the punch radius was investigated to declare that for the sheet of the same grain size, reducing the punch radius resulted in an increase in the material flow stress. Also, it was discovered that for copper sheets with different grain sizes, the flow stress of the material characterized by fine grain size was affected less significantly by the punch radius. The small punch radius caused a significant reduction in the copper sheet thickness of coarse grain size especially at the bottom corner.

Dimensions of the die set (mm).

	Large punch radius (3.75t)			Small punch radius (2t)			
	Set 1 $\lambda=0.25$	Set 2 $\lambda=0.5$	Set 3 $\lambda=1.0$	Set 4 $\lambda=0.25$	Set 5 $\lambda=0.5$	Set 6 $\lambda=1.0$	
D1	1.05	2.1	4.2	1.05	2.1	4.2	
D2	0.75	1.5	3	0.75	1.5	3	
D3	1.65	3.3	6.6	1.65	3.3	6.6	
R1	0.2	0.4	0.8	0.2	0.4	0.8	
R2	0.375	0.75	1.5	0.2	0.4	0.8	
C	0.15	0.3	0.6	0.15	0.3	0.6	
t	0.1	0.2	0.4	0.1	0.2	0.4	

D1, Diameter of drawing die; D2, diameter of drawing punch; D3, diameter of blanking punch; R1, radius of drawing die; R2, radius of drawing punch; C, drawing clearance.

**Table 3-3. Description of the process dimensions used in this study [114]**

This action was because for smaller punch radius the material bending deformation was characterized by a high severity. Hence, products with good quality could be obtained with relatively large features and fine-grained sheet materials. In addition, the maximum forming force was increased with the decrease of the punch radius. As well as the maximum force point was reached earlier through the drawing stroke with using the smaller punch radius [114].

A very interesting investigation was presented by Hu [115] on the application of size dependent FEM-simulation for rectangular part-micro deep drawing process. As is well known, in manufacturing fields a particular tolerance is always needed, and thus there are a certain difference “deviations” between the real dimensions and the required dimensions for the produced part geometry. In order to reveal the influence of these deviations with miniaturizing sheet metal forming processes, deep drawing experiments of Al99.5 rectangular parts were scaled down from (20X10mm<sup>2</sup>) and (0.2mm) to (1.5X0.75mm<sup>2</sup>) and (0.015mm) for the punch dimensions and blank thickness respectively. The four scaling factors of 1, 0.5, 0.1 and 0.075 were used in this work. The size dependent FEM-simulations were carried out by utilizing the software ABAQUS 6.9.3. For the scaling factors of 1 and 0.075, the drawing experiments were repeated many times. As a result, various maximum punch forces were obtained for each process dimension. Also, it was found that the coefficient of variation increased from 2.2% to 7.8% with the miniaturization of the deep drawing process. Concerning these activities, the simulation predictions exhibited a good correlation with the experimental results [115]. Moreover, the simulations rendered to optimize the initial blank shape, so that rectangular parts were obtained without flange, which very beneficial issue especially at micro scale. That gave an indication that the size dependent FEM-simulation had a great potential to identify the optimum conditions for the micro deep drawing [113, 115]. At micro scale, the relation dimensional deviation was not similar and it was very difficult to clarify the reasons. Through the numerical simulations with punch of (1.5X0.75mm<sup>2</sup>), it was indicated that deviation of 25µm for the die corner radius resulted in an increase in the maximum drawing force up to 5%, while deviation of -25µm reduce the maximum punch force about 4%. A different observation for the drawing die radius was that the maximum punch force increase by approximately 9% when a decrease of 21µm was measured, in contrast a reduction about 10% in the punch force with enlargement in dimension of 21µm [115].

### 3.6.2 CONTACT SURFACE CONDITIONS

Tribology aspects can be understood well just when the status of the surfaces in contact is clarified and what happening at the contact interfaces is realized. **Figure 3-13** shows a scheme for the contact situation between a smooth tool surface and a rough specimen surface. The interface configuration seen in the figure is because of the fact that the structure of the surface is considered to be constant during miniaturization. In the case of macro dimensions, when the

lubricant is entrapped inside the closed packets, a fraction of the normal load will be applied on the pressurised liquid leading to a decrease in the total transferred through the contact asperities.

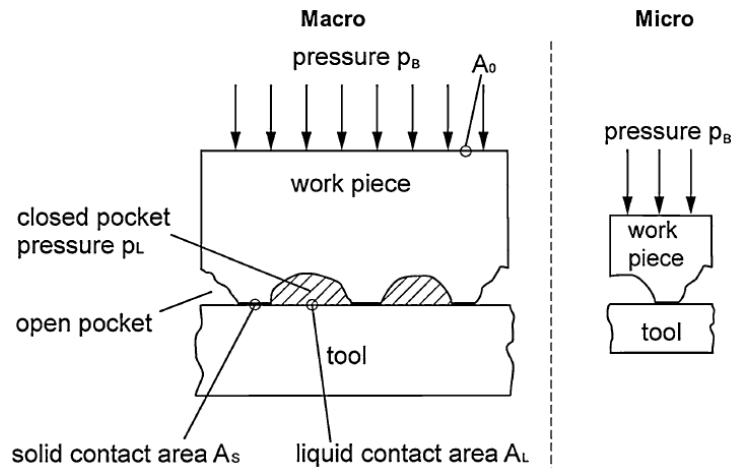


Figure 3-13. Lubricant pocket theory for the coefficient of friction [116]

Nevertheless, during scaling down the process dimensions, the nature of the lubricant packets will change from closed to open causing the number of the closed packets to decrease. This action results in the applied load will be totally transferred through the solid asperities implying the entire load will be employed for the friction activity [116]. As a result, the friction forces increase with reducing the process dimensions which is called “tribological size effects” [115].

Manabe et al. [117] presented an experimental investigation and finite element simulation for a two-stage deep drawing process of milli-scale cylindrical cup. In the experiments, a circular stainless steel 304 blanks with 16.5mm diameter and thickness 0.3mm was used. The surface roughness of the blank was  $R_a=0.42\mu\text{m}$ , whereas polished and unpolished tool sets were used to explain the effect of tool surface roughness. In this survey a cup with diameter of 10.5mm was obtained through the first stage of the process, whereas a redrawing process was implemented to produce the final cup with diameter of 7.5mm. The explicit finite element code, LS-DYNA was exploited to carry out simulations for the drawing process. In these simulations, the static and kinetic coefficients of friction were defined to be 0.15 and 0.1 respectively. The roughness of the tools and blank surfaces, that ranging between  $10^{-4}$  to  $10\mu\text{m}$ , was modelled in a view of a cyclic concave-convex configuration [117].

It was noted that using the unpolished or polished tools resulted in successful cups through the first drawing stage, and however, unsuccessful cups were produced in the second

stage just with the polished tools. In general, the thickness reduction of the drawn parts was obviously noticed at the corner region, and the maximum thinning with unpolished tools was higher than that with polished tools. The results revealed that increasing the surface roughness caused the friction forces to increase. In addition, when the punch with high roughness was used the thinning at the cup corner was reduced. While, the thickening at the cup wall edge decrease considerably when die and holder with small surface roughness were used. In order for the accuracy of the drawn cup surface to be improved, drawing tools with small surface roughness were recommended to be utilized. Furthermore, as the initial blank roughness was small, its effect on the cup surface accuracy was less [117].

Gong et al. [118] conducted an experimental work to reveal the effects of friction conditions on the success of micro deep drawing process and also to identify the proper lubricant for contact surfaces. In this study, the influence of the properties of different lubricants on punch force-stroke curves, limit drawing ratio and product surface quality were investigated. The workpiece was taken from a copper alloy CU-FRHC strain hardened rolling sheet with thickness of 40 $\mu$ m and diameter of 2mm. Also, the surface roughness of the blank was 0.6 $\mu$ m. The drawing operations were carried out at room temperature with drawing velocity of 0.1mm/sec. The friction activities utilized in the micro drawing experiments were no lubricants, lubrication with polyethylene film of 7 $\mu$ m thickness, soybean oil and castor oil. In order for various limit drawing ratios, rigid punches with different diameters were used to form the working blanks. Successful cups were produced through the micro drawing experiments, and slight wrinkling however was observed at the cup rim when small punch diameter (large drawing ratio) was used. The same result was obtained by the researchers [119] when a carbon (DLC) film was utilized in seated of the PE film. This action was due to adopting the same holding force for the different drawing ratios. It was found that the deformation severity of the wrinkles increased with increasing the drawing ratio. The results clarified that for drawing with soybean oil and castor oil, the punch forces were slightly lower than that when no lubricant was used. However, using the polyethylene PE film, the drawing load was reduced of approximately 20% [118], in contrast of 15% for the lubrication of DLC film [119]. That is because most of soybean oil and castor oil were overflowed from the blank and tool interfaces due to the friction size effect. So, the cup drawing with polyethylene film provided the best lubrication conditions compared to the soybean oil and castor oil. Moreover, since the dynamic viscosity of castor oil is higher than that of soybean oil, it was more difficult to overflow the castor oil



through the micro deep drawing. Therefore, the castor oil was regarded superior to the soybean oil. Consequently, the few scratches that appeared at the rim of the cups drawn with no lubricant or under the lubrication of soybean oil and castor oil were eliminated by utilizing the PE film as lubricant [118, 119]. Therefore, the maximum limiting drawing ratio of 2.2 was produced when the polyethylene film was used, in contrast of 1.8 with no lubrication and 1.9 under the lubrication of soybean oil and castor oil [118], while using the DLC film resulted in 2.1 [119]. It can be deduced that it is possible to eliminate the friction size effects by adopting very thin lubrication films such as FE and DLC in micro sheet metal forming process instead of oils.

Shimizu et al. [36] clarified the role of the surface roughness of blanks and tools in micro deep drawing process over experiments and FE simulations. In the experiments, blanks of stainless steel (SUS304) foils were utilized with initial thickness of  $20\mu\text{m}$  and surface roughness of  $0.11\mu\text{m}$ . Two drawing stages were conducted in this work, the first one was to produce a cup of  $700\mu\text{m}$  diameter which was thereafter redrawn in the second stage to the final diameter of  $500\mu\text{m}$ . The FE simulation was performed by modelling the surface roughness by means of cyclic concavo-convex configuration on the surface elements of the blank and the tools, see **Figure 3-14**.

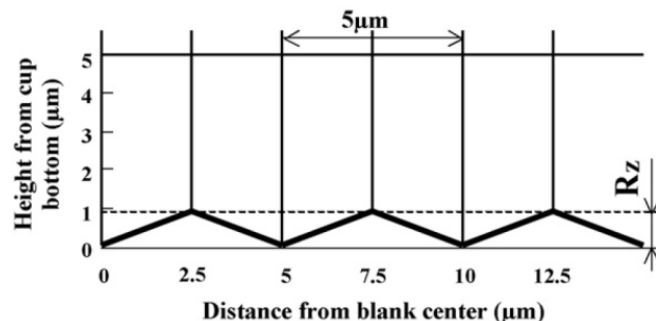


**Figure 3-14.** Example of surface roughness model (undersurface of blank) [36]

In regards of the cup profile, the experimental results exhibited a good agreement with predictions of the proposed model. The results of the first stage revealed that the cup corner and sidewall underwent thinning, while the thickening occurred at the cup rim. In the second drawing stage, the thickening region experienced ironing which turn in resulted in increase in the final depth of the drawn cup. This behaviour was predicted very well by the simulation. The surface roughness of the cup produced through the first and second stages was measured and it was obvious from the results shown in **Figure 3-15** that there are noticeable differences in some regions between the FE simulations and experimental results [36].

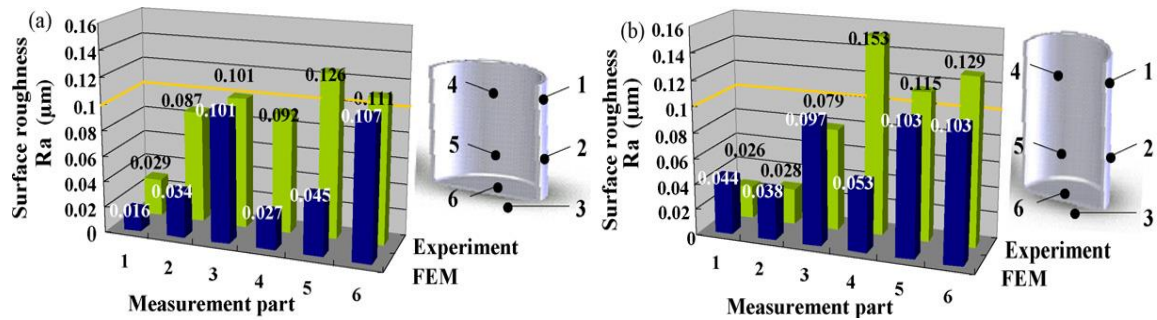
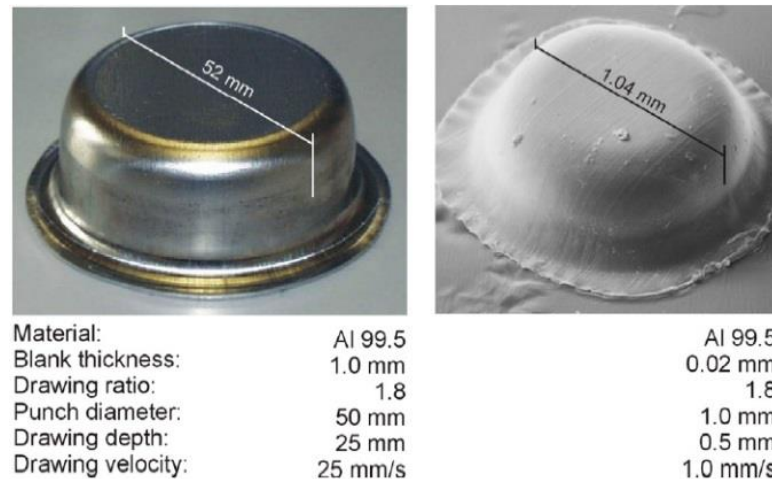


Figure 3-15. Surface roughness of the micro cups drawn through (a) first-stage (b) second-stage [36].

In order to facilitate the deep drawing process of very thin metallic foil as well as to understand how the surface properties of blank and/or rigid tools affect the material drawability and the product quality, Murashige et al. [120] conducted FE simulations and experiments for micro deep drawing of tiny cups with different surface asperities. The work blanks were taken from stainless steel (SUS304-H) foil of  $23\mu\text{m}$  thickness. Air-blasting treatments were carried out on the drawing blank in order to varying the surface asperities. Also, the surface of the micro tools were treated using air-blasted and ion-irradiation processes. As the surfaces of the drawing tools were smoother, the effectiveness of the blank asperities then became higher. It was indicated that the effect of the blank surface asperities depended on the tools surface conditions. In the case of untreated “smooth” tool, the drawing process denoted that the punch force required with the air-blasted blanks was lower than the one with as-received blanks. Also, it was detected that the friction forces excited at the contact interfaces were greater when blanks of rough surfaces were used compared with the smooth blanks. The dimension accuracy, product quality and material drawability were significantly affected by the relative ratio of tool and sheet metal surface roughness to the outer dimensions. The friction forces between blank/tool contact surfaces in sheet metal forming increased in accordance with the roughness of these surfaces [120].

Hu and Vollertsen [112] investigated the effect of the friction coefficient on the optimized blank shape proposed in this study. In the FE simulations for Al99.5 micro deep drawing, two different friction coefficients of 0.05 and 0.4 were adopted. The results showed that the geometrical profiles of the final drawn cups were affected by the change of the friction coefficients. However, the maximum punch force was significantly affected, where an increase from 2.4 to 5.9kN was observed with increasing the friction coefficient from 0.05 to 0.4. This action indicated that increasing the friction coefficients has a great influence on the drawability of the drawing blank material in terms of the limit drawing ratio [112].

Vollertsen et al. [43] achieved micro deep drawing experiments on Al 99.5 and mild steel foils with initial sheet thickness of 20 $\mu$ m and 25 $\mu$ m respectively. The drawing punch was used with diameter of 1mm and profile radius of 0.19mm, while the profile radius for the die was 0.12mm. The micro cups produced through these drawing processes were compared with others obtained at macro level as shown in **Figure 3-16**.



**Figure 3-16. Comparison of micro and macro deep drawing cups [43]**

The results revealed that some slight wrinkles were observed at the flange region of the micro cups whereas the macro cups were clear. Also, it was found that using lubricants caused the friction force between the blank and tools to decrease at both macro and micro drawing scales. The amount of the lubricant used played an important role on the friction status for the micro and macro forming. The maximum limit drawing ration that can be obtained for the mild steel blanks at macro scale was 2.2, in contrast of 1.7 at micro scale when no lubricant was used. Hence, it was denoted that the decrease of the friction forces with lubrication was higher at micro forming. In regards of the drawing forces, the maximum force required for micro cups in the experiments was greater than the calculated value. However, for the macro drawing scale there was nearly no difference between the experimental and calculated values. This action indicated that the friction coefficient in micro-scaled drawing is much greater than that at the macro drawing [43].

Micro deep drawing experiments and simulations were carried out by Witulski et al. [121] using different friction coefficients. In order to reveal the relation between the aspect ratio (punch diameter to drawing stroke ratio) and the miniaturisation level, a variation of punch diameters was utilized in this study with various scaling factors as shown in **Table 3-4**. The

results detected that as the friction coefficient increased, an increase in the drawing forces was observed.

tool set	punch diameter $d_0$ in mm	die radius $D_1$ in mm	sheet thickness $s_0$ in mm	blank diameter $D_0$ in mm *
a	1.0	1.08	0.3	2.0
b	2.0	2.16	0.15	4.0
c	4.0	4.3	0.08	8.0
d	8.0	8.6	0.04	16.0

\* drawing ratio  $\beta = 2$  for all tool sets

Table 3-4. Tool data table [121]

It can be seen in Figure 3-17 that the punch force curves have two peak points, the first maximum punch force was due to the drawing activity, however, the second maximum force was due to ironing the cup wall. Also, it was observed that over a particular friction coefficient value, the maximum punch force of ironing was higher than the drawing punch force. As well as, the increase rate of the ironing-maximum punch force with the friction coefficient was higher progressively than that of the drawing force [121].

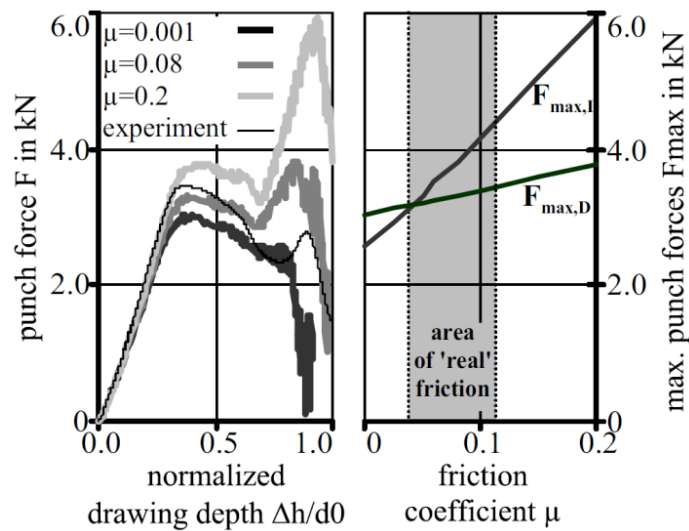
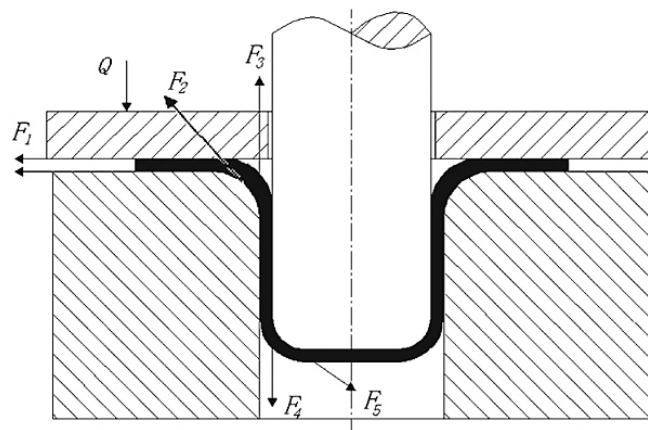


Figure 3-17. Variation of friction  $\mu$  for punch diameter 8 mm [121]

Wang et al. [122] conducted micro deep drawing experiments on a pure gold thin sheet with 40 $\mu$ m thickness using lubrication in means of diamond-like carbon (DLC) film and polyethylene (PE) file as lubricants. The researchers explained how these types of lubrication films render to reduce friction as well as the effect of this action on punch force, surface quality, thickness distribution and accuracy of the inner diameter of the drawn cups. As the

accurate alignment to the central axis of the forming tools is very difficult issue in micro deep drawing, a blanking-drawing combination operation was developed in this study. The diameters of the working blank and punch were 2mm and 1.1mm respectively which implied that the limit drawing ratio was 1.8. The initial roughness of the blank surface was intended to be  $0.1\mu\text{m}$ . **Figure 3-18** shows the kinds of frictions occur through deep drawing process. The friction  $F_1$ ,  $F_2$  and  $F_3$  have a harmful role in the micro deep drawing as they lead to thinning the sheet metal which may cause fracture with excessive values for these frictions. On the other hand,  $F_4$  and  $F_5$  can improve the drawability of the blank materials as they overcome the thinning in the cup wall [122].



**Figure 3-18. Frictions in deep drawing [122]**

The use of the DLC film as a lubricant resulted in a reduction in the maximum punch force of about 28.7% less than that obtained with PE film. This was because the PE film was broken when the tensile stress exceeded its strength and afterwards accumulated at the die corner. This action led to reduce the punch-die clearance, which turn in increases the force required draw the sheet into the die cavity. Moreover, the blank surface roughness of  $0.43\mu\text{m}$  was reduced to  $0.32\mu\text{m}$  with utilizing the PE film, whereas a slight increase was obtained for the cups drawn with DLC film to be  $0.48\mu\text{m}$ . A quantitative improvement was obtained for the thickness of the drawn parts, in terms of maximum thinning, with PE film.

However, micro drawing with the DLC film produced cups with more uniform thickness as shown in **Figure 3-19** as thickening up to 37.5% was observed at the upside part of the micro cup drawn using PE film [122]. The mentioned results give an indication that attractive advantages of low punch load and high quality for the produced cups in terms of surface conditions, thickness distribution and diameter accuracy can be acquired through micro deep

drawing process with using DLC film as a lubricant. The same results were found by Hu et al. [123] through micro deep drawing on stainless steel (X5CrNi18-10) sheet blanks of 0.025mm thickness. The experiments were carried out with two techniques of lubrication: DLC-coated tools and uncoated tools lubricated with mineral oil HBO. It was observed that using the DLC film led to a significant decrease for friction coefficient. Consequently, the maximum punch load required with the coated tools was lower than that recorded for the uncoated tools [123].

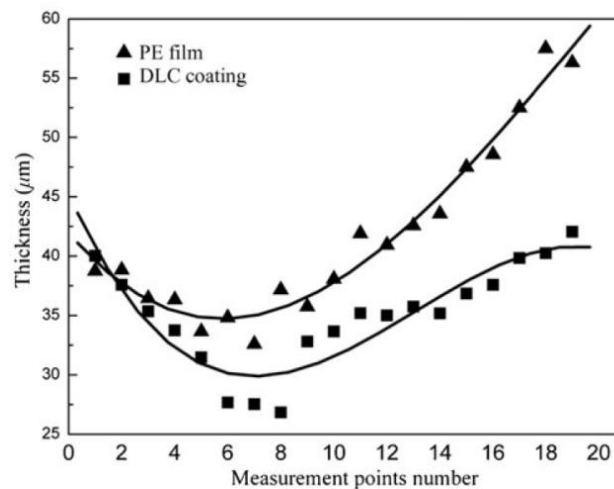


Figure 3-19. Sheet thickness of various measurement points [122]

Moreover, Horiuchia et al. [124] investigated the deep drawability of A5052 aluminium alloy sheet at elevated temperature with utilizing DLC coating. The drawing experiments were performed under three lubrication conditions: a DLC film-coating, lubrication with GM100 (Nihon Kohsakyu Co., viscosity=38.38mm<sup>2</sup>/s at 40°C) and no lubricant. In order to improve the formability of the A5052 aluminium alloy sheet, the drawing operations were carried out at 200°C as well as at room temperature. It was revealed that the friction coefficient obtained with the DLC film was lower than that of the lubricant GM100. Also, the friction coefficient was observed to decrease considerably with increasing the working temperature for both lubrication conditions. As a result of the activities mentioned later, for the experiments achieved at 200°C the maximum punch load for DLC film was lower about approximately 55% than that for the GM100. This result implied that the sheet formability was improved as the punch load was reduced with using the DLC film lubrication technique. While, at room temperature the difference in the punch load was 18%. That indicated that the efficiency of the lubrication action of the DLC film increased significantly with increasing the drawing temperature [124].

### 3.6.3 CHARACTERISTICS OF BLANK MATERIALS

Chen et al. [108] presented an experimental and analytical study on micro deep drawing of stainless steel 304 foils in order to reveal the influence of foil thickness, normal plastic anisotropy, grain size, and T/D (thickness to average grain size ratio) on the limit drawing ratio (LDR) of the blank material. The stainless steel 304 foils used for the drawing blank were selected with different thicknesses of 20, 50, 100 and 150 $\mu\text{m}$ . These foils were annealed at different heating conditions of 900°C, 950°C, 1000°C and 1050°C for 3 minutes. As a result of those treatments, different grain sizes and consequently different T/D ratios (number of grains throughout thickness) were acquired for the blank. The experimental set up used in this work was composed of a rigid punch with diameter ( $D_p$ ) of 2mm and punch corner radius of 0.25mm, a rigid die with diameter of  $(1.1 \times \text{foil thickness} \times 2 + D_p)$  and die shoulder radius of four times the foil thickness. The results showed that as the annealing temperature was increased, the grain size of the different sheets increased, which in turn caused a decrease in the yield strength and tensile strength for the sheet material. It was pointed out that increasing the annealing temperature (decreasing the T/D ratio) caused a decrease in the drawing force required for the blanks of the same thickness. Another finding was that for the same annealing temperature, the drawing force decreases with decreasing the foil thickness (i.e. decreasing the T/D ratio). Moreover, the limit drawing ratio of the blanks with the same thickness was observed to increase with increasing grain size. Likewise, higher limit drawing ratio was obtained as the foil thickness was increased with the same grain size [108]. These results exhibit well agreement with that presented by Yeh et al. [125] using copper C1200 foils.

The deep drawability of ultrafine grained copper sheets was investigated by experiments and FE simulations by Ma et al. [126]. The pure copper sheet of 0.4mm thickness used in this study was annealed at 600°C for 2h and thereafter processed through the severe plastic deformation method known Equal Channel Angular Pressing (ECAP) to produce a variety of ultrafine grained microstructure. The minimum limit drawing ratio was observed with one ECAP pass, and with increasing the number of passes up to four the limit drawing increased slightly referring to an improvement in the deep drawability of the sheet material. This action was pointed out in the work of Lapovok et al. [127] achieved on ultrafine grained aluminium sheet. The researcher attributed this result to the increased plastic anisotropy. However, the maximum limit drawing ratio of 2.2 was produced for the coarse grained copper. Compared to the great reduction in the tensile ductility in the UFG copper from 50% for the annealed sheet

to 10% for the ECAP processed sheet, insignificant decrease was denoted for the limit drawing ratio regardless number of passes. Furthermore, the maximum punch force required to form the UFG copper was much higher compared to annealed material [126].

Behrens et al. [128] and Vollertsen et al. [129] examined the drawability of thin Al-Zr and Al-Sc foils through micro deep drawing experiments. The working foils of 15 $\mu$ m in thickness were fabricated by a magnetron-sputtering process with two different materials by applying substrate temperatures of 310K and 433K. In order for a variety in the limit drawing ratio of 1.5 to 1.9, the researchers used circular drawing blanks with different initial diameters. The forming punch was used with 0.75mm diameter and 0.075mm corner radius. The tensile tests revealed that the tensile strength of the Al-Zr foils were drastically greater than Al-Sc foils, although that the elongations of the Al-Sc foils were found higher. The drawing results showed that maximum limit drawing ratio of 1.8 was produced for the Al-Zr foil fabricated with 310K substrate temperature, in contrast of 1.7 for the 433K-processed Al/Zr foil. Exceeding of these drawing ratio values resulted in cups with wrinkles wall and fractured bottom for Al-Zr foil produced at 310K and cups with wrinkled wall for the Al-Zr foil produced at 433K as seen in Figure 3-20.

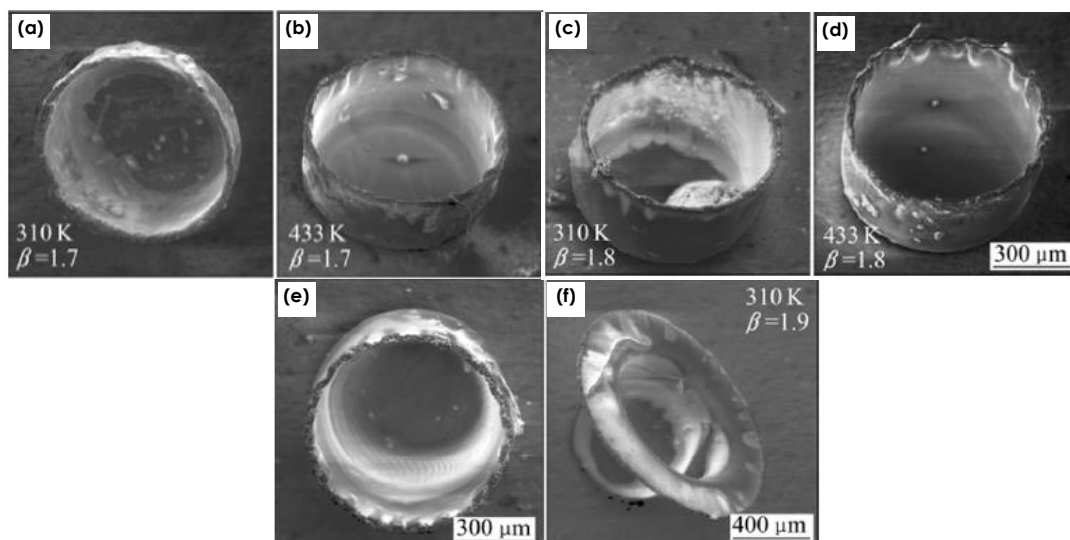


Figure 3-20. Cups drawn of different Al-Zr foils with different drawing ratios [128]

In comparison, the maximum limit drawing ratio obtained by Vollertsen et al. [129] was limited to 1.6. On the other side, it was found that increasing the drawing ratio caused the maximum punch force to increase for both Al-Zr foils fabricated at 310K and 433K. Nevertheless, this action was observed to be higher for the Al-Zr foil produced at 310K [128]. As



the stainless steel 304 micro cups are widely used in different industrial applications especially the miniaturized medical and electronic devices, it is very important issue to produce micro cups with high forming quality. In order to increase the cup height-outer diameter ratio, Gau et al. [130] proposed a drawing process involved one micro deep drawing for a particular stroke and two sequent ironing stages. The stainless steel 304 sheet of 200 $\mu$ m thickness was annealed at different treatment temperature (900°C, 950°C, 1000°C and 1050°C) to investigate the grain size effects on the sheet metal drawability. For the drawing experiments, rigid punch with diameter of 2mm and corner radius of 0.25mm was used with three micro dies that were designed and manufactured to the dimensions shown in **Table 3-5** to perform the whole process. First of all, it was observed the increase of the annealing temperature caused the grain size to increase which in turn resulted in reducing the yield and ultimate strength of the working sheets [130].

Die	Die diameter ( $D_d$ )	Shoulder radius ( $S_r$ )
Die-1	2.44 mm	0.8 mm
Die-2	2.22 mm	0.4 mm
Die-3	2.11 mm	0.2 mm

**Table 3-5. The die diameters and shoulder radii of the three experimental dies [130].**

In general, a quite improvement for the sheet drawability can be obtained when annealing strategy is adopted [108]. In this study, the height of the cups produced through the drawing stroke and the first ironing stage was found to be increased with increasing the annealing temperature. However, at the end of the second ironing stage the largest cup height was for the sheet annealed at 1050°C and the second best height was for the one annealed at 900°C as seen in **Figure 3-21** and **Figure 3-22**. In addition, the ironing technique used here especially through the second stage led to acceptable thinning and however more uniform thickness distribution for the formed cups. Also, it was concluded that the maximum punch force required for each forming stage was mostly reduced by increasing the annealing temperature (i.e. with increasing the grain size), and therefore, the smallest punch force was obtained for the sheet treated at 1050°C [130]. The same results were revealed in the study achieved by Fu et al. [114, 131] on copper sheet through experimental and FE modelled micro deep drawing. They confirmed that smaller punch forces were needed to draw the sheets with larger grain size. Nonetheless, for the sheets characterized by just a few grains in the thickness direction, this action was not considerably pronounced. Fu denoted as well that when using sheets with relatively large grains, inhomogeneous deformation for the blank was received

which led to irregular geometry, as earing and wrinkling defects occurred, and rough surface finish of the drawn cup [114, 131].

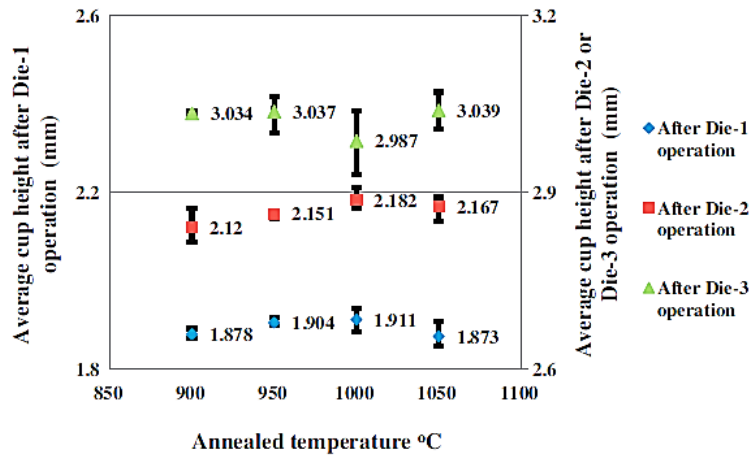


Figure 3-21. The plot of the average cup heights of all cases [130]

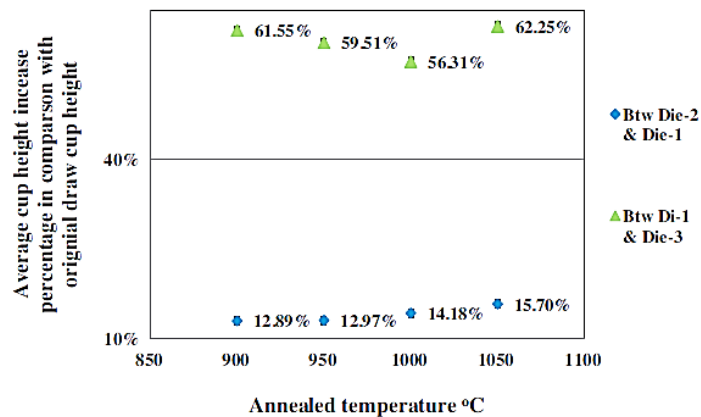


Figure 3-22. The average cup height increase percentage for all cases [130]

### 3.7 FLEXIBLE TOOL-ASSISTED MICRO SHEET METAL FORMING

Unlike the conventional forming process, in micro flexible forming process one of the main tools (punch or die) is made from a soft material. The micro flexible sheet forming technology has many attractive advantages such as its simplicity and the possibility of applying it in prototype process or for low volume production. Also, different complex shaped products can be obtained as easily as the rigid tool is interchanged and the same soft pad is used, reducing the time and cost significantly. As the dimensions of the micro sheet metal forming processes are small so that the clearance between the working tools are about few microns, therefore, these tools may be prone to broken with inaccurate adjustment [77]. Due to these

small dimensions, the cost of manufacturing the tools with the desired quality is very expensive. These issues related to geometrical aspects can be eliminated over using tool made of flexible materials. Furthermore, free scratches-product surface can be obtained that is the workpiece surface in contact with the soft material would be protected. Although these great activities, there is no clear revelation on the principles of micro sheet forming technology enabling one to predict anything related to the soft punch-micro sheet forming technique. Therefore, more investigations and improvements of this technique are needed. When one looking for a robust principles about using the flexible tooling technology in metal forming at micro levels in dimensions, especially for sheet metal forming, he will find just scanty information are available even in the scientific publications [132].

Quadrini et al. [132] conducted micro forming operations on thin aluminium alloy (Al 1200) sheet of 150 $\mu$ m thickness utilizing different flexible material for the working dies. In this work, flexible polymeric materials that are silicon rubber (SR), styrene butadiene rubber (SBR) and semi-rigid polyamide 66 (PA) were used for upper dies combined with aluminium lower die. It was shown that the SR rubber is softer than SBR. The lower dies were designed and fabricated with the following different shapes: a conical die cavity with 20mm and 15mm in maximum and minimum diameters respectively, and 4mm in depth; rectangular section-shaped straight rib dies of 2mm depth, 40mm long with 6mm and 10mm width as illustrated in **Figure 3-23**. Circular blanks with 25mm diameter were used with the conical dies, whereas 30X30mm square ones for the straight ribs [132].



**Figure 3-23. Rigid lower dies [132]**

The upper flexible dies made of SR and SBR was manufactured with flat and shaped geometries, and however only shaped PA dies were intended due to the high stiffness. When different forming rates were adopted in the case of conical die and SR upper die, it was found that a lower distance for the flexible die was required for the higher forming velocity. As a result of this activity, no complete forming stroke as well as no successful part was obtained whether with flat or shaped dies as presented in **Figure 3-24**.

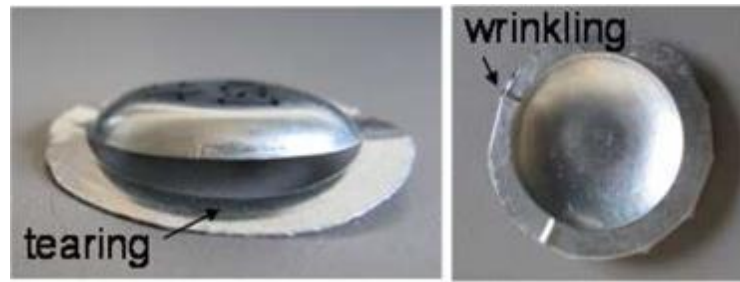


Figure 3-24. Defects of formed cups using SR dies [132]

The same sheet forming trend was observed by using the SBR dies, however, the die durability and the matching ability with the lower die were improved compared with SR dies. Two Experiment strategies were carried out: one by using aluminium lower die with PA upper die and the other both dies were made of PA for straight rib parts. It was noted that reducing the rib width resulted in a decrease in the forming force. Also, the case of PA dies caused a significant reduction in the forming force compared when lower aluminium die was used. In addition, successful products were obtained from the PA dies which exhibited as well a high durability [132]. It was noted that there is nothing mentioned about the surface roughness of the tools used in this work. Due to the friction coefficient one of the most crucial factors which play a major role in the forming results as well as identify the defect mode possibly occur, necessary attention had to be paid for the contact surface situation (i.e. surface roughness degree) especially in the case of rigid/semi rigid dies. As well as, for the flexible dies, lubricants by means of thin films, such as polyethylene film and Teflon film, could be used in order to reduce the friction effects at least for the case of broken products. Thereafter, a comparative study could be achieved to clarify the effects on the process results.

In order to fabricate micro channels and to minimize the total production cost, Peng et al. [133] presented an experimental and numerical investigation on micro forming process achieved by means of a soft punch. The influence of the most important parameters related to the flexible forming technology such as grain size, hardness of the soft material and lubrication conditions were reported in details. In this study, stainless steel 304 sheets were used for the drawing workpieces with thickness of 100 $\mu\text{m}$  and various grain sizes of 25 $\mu\text{m}$ , 60 $\mu\text{m}$  and 100  $\mu\text{m}$ . Polyurethane rubber pieces with different hardnesses of 55 and 70 Shore A was utilized for the soft punch. The process dimensions, shown in **Figure 3-25**, were the grooves span  $s=5\text{mm}$ , the micro drawing angle  $\alpha=15^\circ$ , the upper die radius  $R=0.3\text{mm}$ , the lower die radius  $r=0.2\text{mm}$  and the aspect ratios targeted in this work were 0.5 and 0.75. The FE simulations

were performed utilizing the finite element software ABAQUS-Standard. Elastic–plastic model was used to define the SS 304 sheet material, while hyper-elastic model was adopted for the soft rubber punch. The results proved that the hardness of the rubber punch had no noticeable effect on the stamping process qualitatively and quantitatively in terms of product thickness as the two types of rubber used here had the same capability for transferring the forming load in close space. Also, the thickness reduction was found to be lower with decreasing the grain size of the working sheet. The maximum reduction on thickness was at the corner radius of the rigid die for all cases. In addition, the thickness distribution of the sheet with smaller grain size was more uniform than that of bigger grains. This behaviour was rationalized that the small grain size sheet has higher ability to resist the deformation force and to distribute the forming severity.

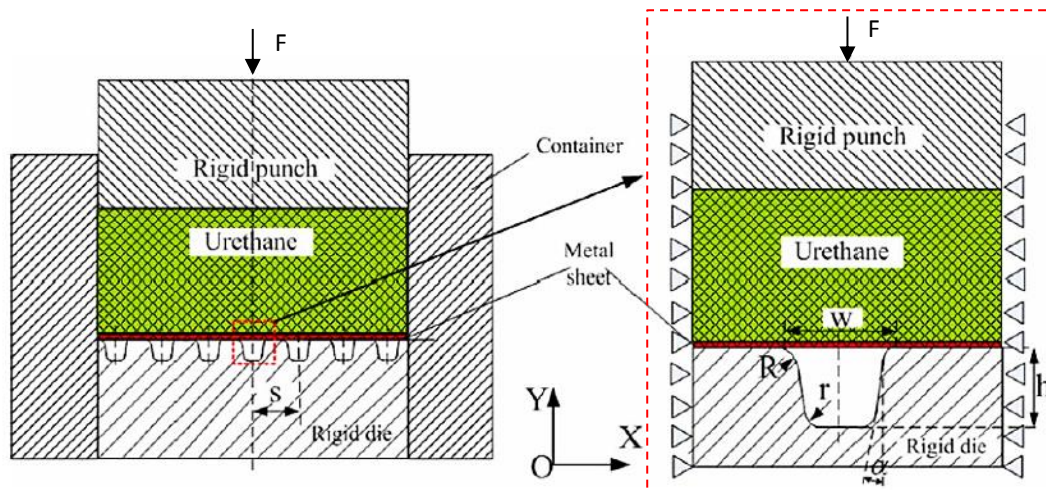
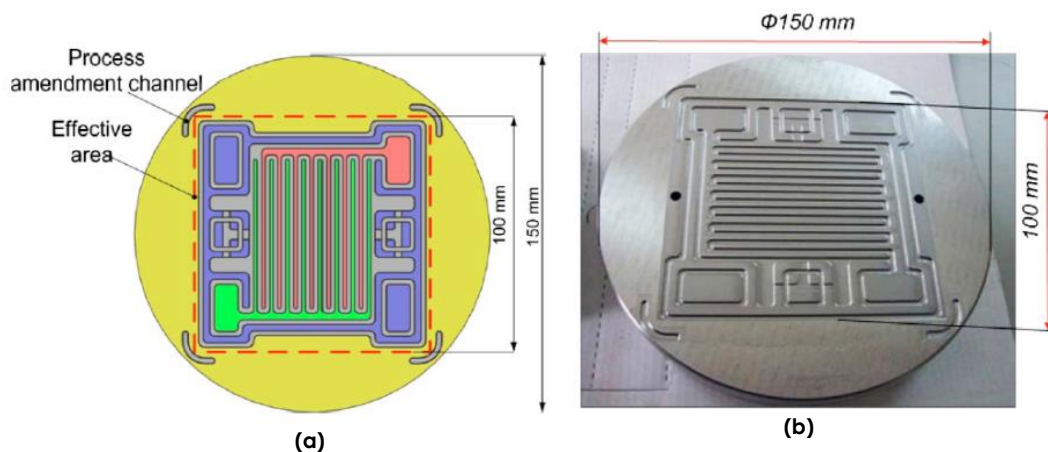


Figure 3-25. Micro/meso sheet forming process to manufacture micro-groove features [133]

Regarding the friction conditions, it was observed that the friction coefficient between the soft punch and the metal sheet was not decisive factor, whereas the friction coefficient between the metal sheet and the rigid die affected the micro forming process considerably. It was clear that increasing the metal sheet/rigid die friction coefficient caused the stress to increase and the stress distribution to become uneven, which in turn implied excessive thinning leading to fracture. All the experimental results mentioned before were predicted very well by the FE simulations [133]. The groove spacing characteristics are very important issue that had to be taken into account in this investigation. No idea could be made directly about what might happen when larger or smaller spacing is adopted between every two adjacent grooves. Also, the surface roughness of the spacing area was another parameter which worth to be examined. It is known that smoother surface will allow for more amount of

the sheet material to flow into the die cavity and turn in may help in this study to produce formed plate with higher quality in terms of more uniform thickness distribution and higher aspect ratio. This work was extended by Peng et al. [134] to fabricate metallic bipolar plate for proton exchange membrane fuel cell. In the FE simulations achieved by using the commercial code LS-DYNA, rubber punch of 70 Shore A hardness and stainless steel sheet of 100 $\mu\text{m}$  thickness were adopted for the forming process.



**Figure 3-26. (a) Process amendment to eliminate the wrinkle at the corner (b) the rigid die [134]**

The mechanical properties obtained from the sheet with grain size of 25  $\mu\text{m}$  were utilized to define the workpiece behaviour in the FE model. In the experiments, all of the rigid die, the soft punch, the initial blank and the inner diameter of the rubber container were used with the same diameter of 150mm and however the effective area was 100X100mm<sup>2</sup> as shown in **Figure 3-26**. As it can be seen in this figure, the flange portion of the circular blank at the corners of the effective area was smaller compared of the other regions around this area. Therefore, the holder force applied by the rubber material at these corners was not high enough to prevent a big amount of the sheet material to flow into the die channels leading to located wrinkling. In order to overcome this action, four process amendment channels were intended outside the effective area to block material flow and as a result the wrinkling was eliminated completely. The numerical simulations and the experimental results proved that the proposed forming technique was feasible in manufacturing the metallic bipolar plate effectively so that some optimization attempts were done until the maximum thinning of the final product was 18% [134].

**Figure 3-27** presents a novel technique for deep drawing process proposed by Maslennokiv [135], which can be achieved without forming punch used in conventional drawing.

In this technique a polyurethane ring is the responsible of drawing the working sheet into a rigid die as it can be seen in the figure. As the container moves downward pressurizing the rubber ring, the later then undergoes a radial extension and this action in turn leads to friction forces between the rubber ring and the sheet. This friction forces are regarded the drawing force which push the sheet into the die cavity. In order to produce deeper and deeper cups, this activity is required to be repeated many times in dependence on the drawing process conditions [15].

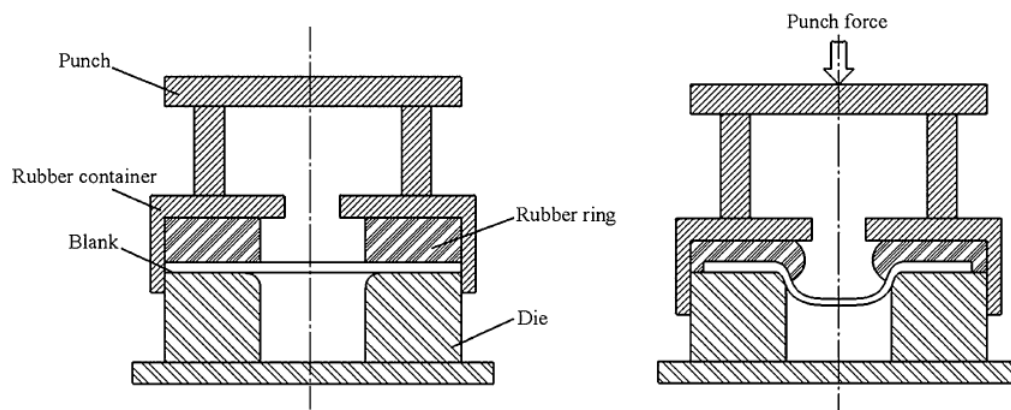
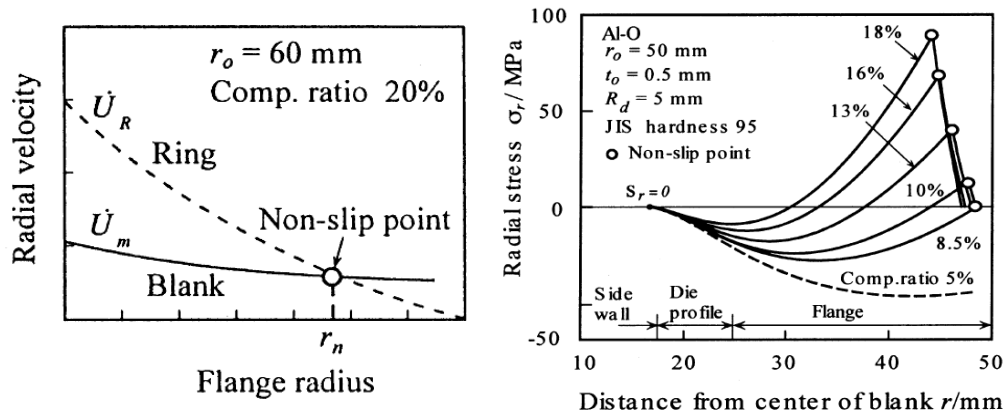


Figure 3-27. Schematic of Maslennikov's process [136]

Hassan et al. [137] modified the Maslennikov's drawing technique by utilizing an auxiliary rigid punch owing to improve the accuracy of the shape and dimensions of the drawn parts. The material of the working sheets was aluminium of 100 $\mu\text{m}$ , 200  $\mu\text{m}$ , 300  $\mu\text{m}$  and 400  $\mu\text{m}$  in thickness. The frictional forces between the die and the blank were reduced through using a polytetrafluoroethylene film (PET). For the punchless deep drawing technique, an increase in the cup height was produced through increasing the die profile radius and the polyurethane ring thickness and reducing the ring inner diameter and the blank thickness. However, this technique was not recommended for drawing thin sheets of 100 $\mu\text{m}$  in thickness as wrinkles were observed at the bottom and the side wall of the drawn cup. To eliminate these defects, a rigid punch was adopted which was found an effective strategy for drawing sound cups from thin blanks with 100 $\mu\text{m}$ . It was detected that the maximum cup height was obtained at the die diameter to the inner rubber diameter ratio of 1.1. Also, larger cup height was produced using thinner sheets and softer polyurethane rubber ring material. In addition, increasing the compression ratio and the thickness of the rubber ring caused an increase in the cup height. The results revealed that the proposed drawing technique was recommended for the very thin aluminium sheets but with small compression ratios of about 10-12% of the polyurethane ring

used [137]. In another publication Hassan et al. [138] clarified that during the drawing operation using Maslennikov's technique, the deformation velocity of the rubber ring at the flange region became equal to that of the blank at a particular point, in terms of flange radius as shown in **Figure 3-28**, called non-slip point as no relative motion between the polyurethane ring and the blank was noted.



**Figure 3-28.** (a) velocity distributions of the polyurethane ring and the blank (b) Variations of radial stress distributions [138]

For a low compression ratio (5%), the radial stress over the flange and profile radius portions of the deformed blank was compressive and then became zero as the compression ratio increased up to 8.5% as seen in **Figure 3-28**. Thereafter, the radial stress was observed prone to be tensile with increasing the compression ratio and reached its maximum value at the non-slip point. For the two types of the polyurethane materials used in this study, it was denoted that the actual drawing deformation with using the harder rubber ring (hardness 95A) was found to begin earlier than with the softer one. Nevertheless, an important observation here was that the maximum cup height obtained for the sheet metal was 4.5mm with the process conditions adopted in this work when the compression ratio the polyurethane ring of 95A hardness was just under of 20% as at which fracture occurred. On the other side, with using the softer ring of 85A hardness a compression ratio exceeded 30 % was reached successfully and maximum cup height of 6.5mm was produced. Furthermore, no difference was observed of using polyurethane rubber with different hardness values for the forming ring when the auxiliary rigid punch was utilized [138].

Ramezani et al. [136] investigated the Maslennikov's deep drawing process through finite element simulation and analytical model. In this study, the researchers proposed a new friction model in which the contact pressure, the material properties and the surface topology on the friction were taken into account. The results taken from this model were compared



with that obtained with adopting the common Coulomb friction model. The coefficient of friction between the blank and the rubber ring was found to decrease as the contact pressure increased so that the friction coefficient reached a particular value and then stayed constant even for more higher pressure. It was clear that a remarkable increase in the height of the drawn cups could be achieved by increasing the rubber ring thickness and reducing its inner diameter. Moreover, using smaller die opening diameter and larger die profile radius had an important role in increasing the cup depth. The predictions taken from the FE simulations exhibited a well agreement with the experimental results. The FE models built using the Coulomb friction model detected a prediction error of 14.3% compared with the experimental results, whereas using the new friction models proposed here the error was 8%. This results referred to the proposed friction model had a high efficiency to be used in the Maslennikov's drawing technique [136]. Two different forming styles were presented by Liu et al. [139] to fabricate longitudinal channels on stainless steel 304 sheet of 100 $\mu$ m in thickness. The two deformation styles are characterized by concave and convex geometries for the former rigid punch. In this study, experiments and FE simulations were achieved for the stamping processes using urethane rubber pad of 70Shore A hardness to optimize the forming conditions and to identify which of the proposed styles is the most proper for fabricating a certain bipolar plate.

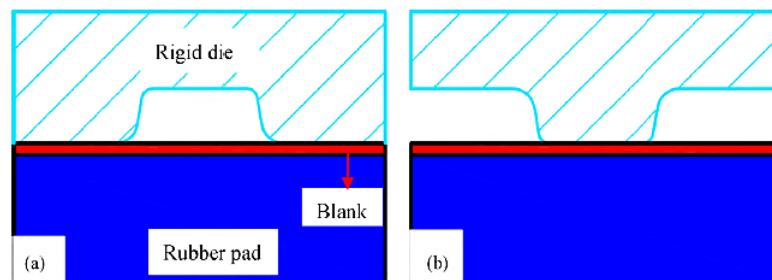


Figure 3-29. Sketch of rubber pad forming: (a) concave die style and (b) convex die style [139].

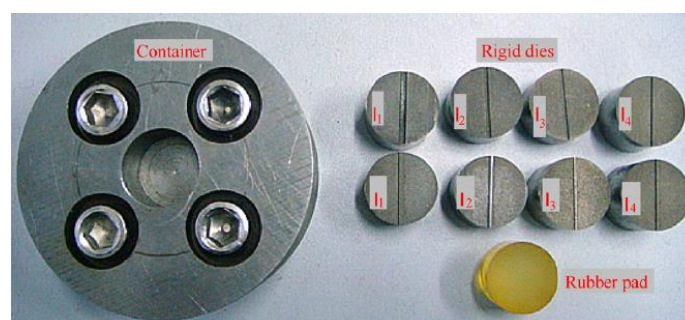
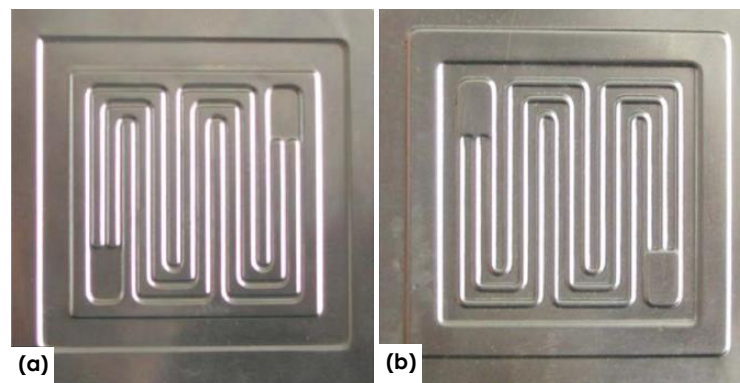


Figure 3-30. Photograph of the forming equipment for the experiment [139].

The concave and convex deformation styles and the set up used in the experimental work are illustrated in **Figure 3-29** and **Figure 3-30** respectively. In the FE simulations, Four-node bilinear quadrilateral plane strain with reduced integration and hourglass control elements (CPE4R) were employed to model the stainless steel 304 material. While, Four-node bilinear plane strain quadrilateral hybrid elements with reduced integration and hourglass control (CPE4RH) were used to define the urethane rubber material. The results indicated a dramatic increase in the forming load for that with using the concave die in compared of the convex one. Also, it was found that the maximum load obtained for the concave style was larger than that for the convex style. It was observed that the thickness at the flange region of formed channel had no noticeable reduction when the concave deformation style was adopted, whereas the maximum thickness reduction of 31.8% occurred at the side wall region. On the other side, the no deformation region for the convex deformation style was at the bottom of the formed channel and the lower maximum thickness reduction of 28.6% was obtained. Moreover, the channels produced with the convex style were characterized by more uniform thickness distribution than that with the concave. For a constant channel depth, reducing the channel width resulted in an increase in the maximum thickness reduction for the concave style as it was very difficult to fill the die cavity. On contrast, for the convex die, smaller channel width caused filling the die cavity easier and the thickness reduction to decrease.



**Figure 3-31. (a) front of the bipolar plate and (b) back of the bipolar plate [139].**

Consequently, the bipolar plate of 150mm X 150mm in dimensions shown in **Figure 3-31** was produce based on the fact that when the ratio of the channel width to the rib width  $w/s > 1$ , the concave deformation style was more properly to be adopted, otherwise the convex was preferred [139]. The design and manufacturability issues for micro channel arrays were also investigated by Mahabunphachai and Koç [140] through hydroforming technology. The most

effective process factors that play crucial role on success of the forming process, such as grain size, internal fluid pressure, die width, draft angle, die corner radius, channel spacing and channel number, were studied in detail. Clarifying the influence of the size effects related to material and process dimensions on the formability of the workpiece materials and providing design guidelines for the researchers in the technology of micro channels fabrication were the major points of this work.

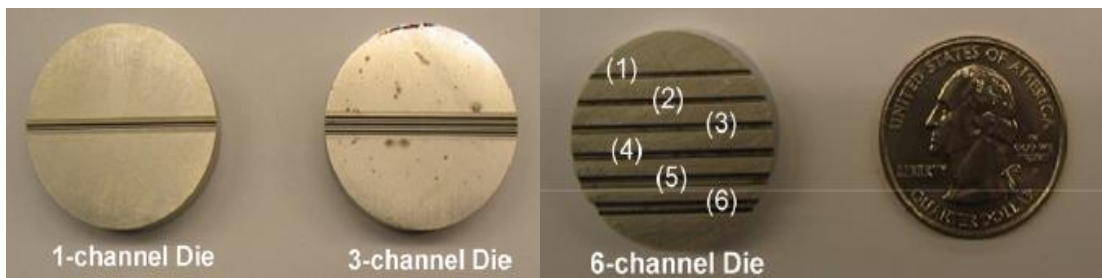


Figure 3-32. Die inserts: 1-channel, 3-channels, and 6-channels die [140]

The stainless steel 304 sheets used for the workpieces had a thickness of  $51\mu\text{m}$  and different grain sizes of  $9.3\mu\text{m}$ ,  $10.6\mu\text{m}$  and  $17\mu\text{m}$ . The three different die sets shown in **Figure 3-32** were manufactured with channel width ranging from 0.46 to 1.33mm and height ranging from 0.15 to 0.98mm. The experimental results denoted that the depth of the channels formed increased with the fluid pressure. Also, in the case of 3-channel die the spacing the employ of spacing distance was observed to cause a decrease in the channel depth. However, the most effective parameter in the case of 6-channel die was the channel width rather than the fluid pressure and the die height. It was indicated that the change in the grain size had unclear role in the forming process. The FE models elucidated that the smaller the channel width the higher the aspect ratio. In addition, the larger die profile radius, larger spacing distance and/or less number of channels had a significant contribution in producing a higher aspect ratio. The increase in the draft angle within the range  $5^\circ$ - $20^\circ$  in combination with the corner radius/initial thickness ration led to noticeable increase in the channel height. Furthermore, the thinnest part of the channel was at the corner radius with 25% thinning while the valley underwent just 4% [140].

## **CHAPTER FOUR**

# **PROPOSED TECHNIQUES**

\*\*\*\*\*

#### **4.1 INTRODUCTION**

With the increasing trend to miniaturization of electronic, medical, energy and other devices, the demand on micro parts especially that fabricated of metallic thin sheets has been growing significantly. Therefore, companies specialist in this field are required to provide competitive products in terms of miniaturizing levels with respect to the formed part quality and production cost. As a result, innovating new and efficient techniques for the forming processes is imperative aspect and hence it has been considerably attracting great attention of researchers and manufacturers. In micro deep drawing technology, one of the challengeable issues is to fabricate drawing tools with dimensional accuracy and finishing quality that particularly needed for certain process conditions. Also, the adjustment between the male and female tool components is another difficulty that causes the cost of the whole forming story to increase with the miniaturization level.

As a novel forming process, flexible forming has significant potential in different industrial applications such as automotive, energy, and electronics. In addition, the numerous advantages mentioned previously provide an insight that the flexible forming could be regarded a feasible technique for fabricating micro deep drawn parts. Up to our knowledgment, this technology is yet not exploited or even investigated worthily. No information has been acquired referring to the flexible tooling, by means of flexible die cavity or punch, is employed for deep drawing process at micro scale. As the difficulties increase with scaling the process dimensions down, the absolute attention is mainly paid towards the size effects related to the behaviour mode and microstructure of the workpiece material, as well as feature dimensions and contact surface conditions with considering the workpiece as a deformable part and the forming tools behave as rigid parts. However, the big question here is how would deal with these size effect categories encountered in micro sheet metal forming when the major tools are made of soft materials. As shown above, the previous research attempts have focused on the stamping process using rubber forming tools to fabricate longitudinal channels on thin sheet metals. Compared to the micro deep drawing, channel forming is considered a simple process as the tensile stresses generated in the sheet material are only along one direction which is the forming path. Nonetheless, deep drawing processes, as it is explained in chapter two, involve much more complicated stress status so that the

necessity of taking into consideration the anisotropic nature of the workpiece material is a clear index to this issue. Consequently, the utilization of flexible forming strategies adopted in micro channels stamping directly for micro deep drawing processes may have probably deficiencies of producing sound cups. For example, when adopting the concave and convex rigid die procedures proposed by Liu et al. [139] through FE models for micro deep drawing of cylindrical cups, no successful drawing operation could be acquired at all even just for aspect ratio of 0.5 which is the minimum binding condition to consider the process as deep drawing [141, 142] as shown in **Figure 4-1**. As the whole simulation models of the micro deep drawing process of both these forming strategies are symmetric, one quarter of each model is therefore adopted and presented in the figure. Also, this activity is intended in order to reduce the computation time required for analysing the FE models.

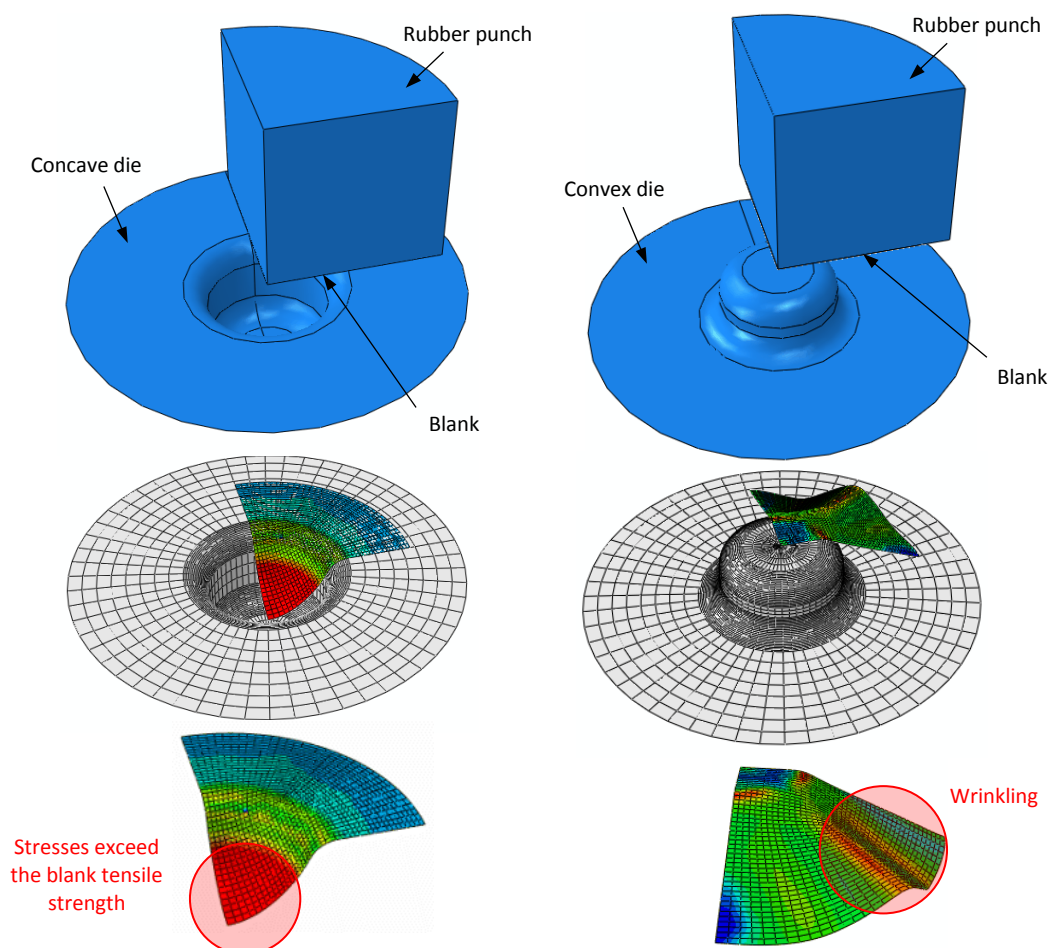


**Figure 4-1. (a) Concave die and (b) convex die drawing strategies**

The concave die resulted in tearing the blank at its central region, whereas the convex die resulted in intensive wrinkles at the flange region of the blank being formed. This action

can be rationalized that for the concave die technique, the rubber pad actually plays the role of the forming punch and blank holder simultaneously. That means that increasing the external load applied on the rubber pad during the operation causes an increase in the holding pressure leading to high constraint on the blank flange. In addition, the drawing pressure also increases especially at the central region of the blank resulting in excessive biaxial tensile stresses which afterwards exceed the tensile strength of the material sheet at a particular drawing stroke. It is well known that through deep drawing processes the blank material experiences radial tension forces which lead compressive stresses in the circumferential direction at the flange portion. In the case of absence a sufficient blank holder force, extravagant compressive stresses compel the flange material to wrinkle and this exactly what happened with the convex die technique. Therefore, it is of most importance to compromise between the two techniques through using a rigid punch, which refers to the convex die technique, and flexible die cavity and blank holding by means of flexible pad pressure, which refers to the concave die technique.

## 4.2 PROPOSED TECHNIQUE

**Figure 4-2** shows the basic schematic configuration of the proposed technique in this study. It can be seen that the tools utilized for the micro deep drawing are rigid punch, blank holder supported by a mechanical spring, gap-adjustment ring and rubber pad as deformable die cavity. The idea of this new technique is to set up an initial gap between the blank holder and the gap-adjustment ring and only through which the blank holder is allowed to move up during the early stroke of the drawing operation.

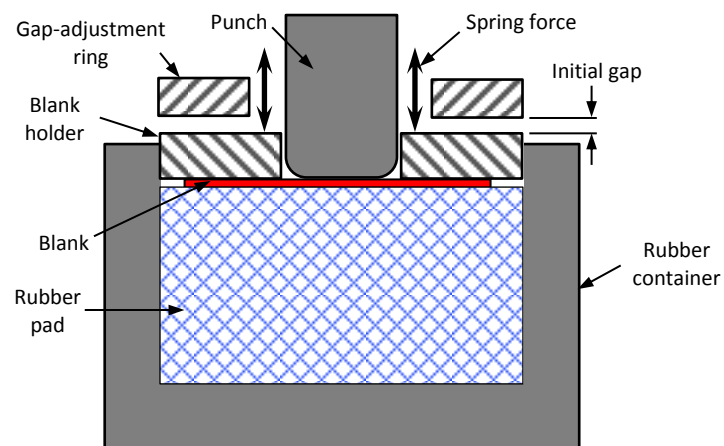


**Figure 4-2.** The basic schematic configuration of the proposed technique

At the beginning, the blank holder is in direct contact with the blank. Also, the spring is initially compressed into a particular distance in order to provide an initial blank holder force. This initial holding force is intended to be just high enough to suppress wrinkling that probably occurs when the blankholder be allowed to move through the initial gap just against the spring reaction. Thereafter, the total blank holder force consequently increases progressively with the drawing stroke in accordance to the stiffness of the holder spring. Depending on what the appropriate application procedure of the proposed technique that can fluently adapt with given conditions for the drawing process, the following three ways are presented in this work.

#### 4.2.1 MICRO DEEP DRAWING WITH POSITIVE INITIAL GAP

First of all, the initial gap value required for drawing products with certain characteristics depends on some key process parameters such as metallic foil thickness, blank diameter, friction situation, rubber material properties and rubber pad dimensions. Therefore, it is of imperative necessity to clarify the role of not only each individual parameter, but also the influence of the combination of these parameters in the drawing process in order to identify the optimum conditions for the successful cups.

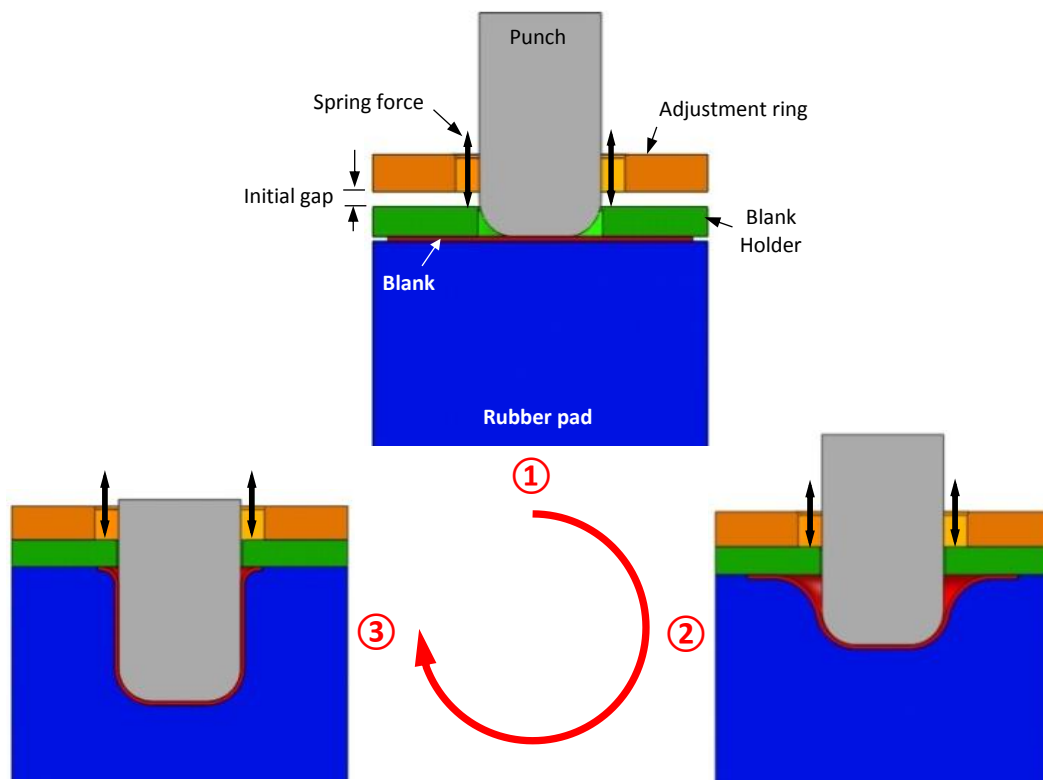


Figure 4-3. The first strategy of micro deep drawing adopted with positive gap



The micro deep drawing procedure with adopting a positive initial gap (see **Figure 4-3**) can be summarized by the following steps:

**Step 1:** At the beginning, the rigid punch is dictated to move downwards just until reaches the blank surface. At this time, the upper surface of the blank is in a direct contact at the central circular region with the punch bottom and at the annular flange region with the blank holder, whereas the lower surface is entirely in a direct contact with the rubber pad surface. The blank holder has not yet moved up, which implies the actual drawing stroke dose not start in this step.

**Step 2:** In this step, the punch is kept moving down leading to thrust the blank into the rubber pad. Therefore, both the blank and the rubber pad are formed simultaneously but only for a particular stroke resulting in shallow profiles. As a result of incompressibility of the rubber material, a hydrostatic pressure is generated in the rubber pad as a consequent to the punch activity. Since the rubber pad is tightly constrained inside a closed cylindrical container; the hydrostatic pressure will be applied totally on the blank which be kept in continuous contact with the holder. In other words, the blank holder will be subjected to the hydrostatic rubber pressure transmitted through the blank material. Thus, the blank holder moves upward against the supporting spring only through the initial gap where this step finishes. Hence, no high forming load is required in this step. Due to this action, the area of the flange portion of the blank is relatively reduced which means that the contact area with the blank holder decreases leading to an improvement in the frictional effects for the next step. Therefore, it can be said that the blank material can sustain higher holding force until the targeted drawing stroke is achieved.

**Step 3:** The final step of this drawing technique starts just at the moment when the blank holder contacts the gap-adjustment ring. At this time the rubber container is completely closed and the blank holder is now prevented of moving any more by the gap-adjustment ring. Thus the only space remaining for the rubber pad to expand is that entrapped between the shallow profile radius, the blank holder and the punch wall. In dependence on the process conditions, a relative high punch

load is needed in this step to overcome the increasing pressure of the rubber pad material. It is important to be noticed here that the process parameters have to be adjusted in a good harmony with each other to provide the optimum conditions that allowing for the rubber pad and the blank to fill in the remaining space progressively with the drawing stroke until producing the desired profiles for the final cup.

#### 4.2.2 MICRO DEEP DRAWING WITH NEGATIVE INITIAL GAP

On the other side, in some cases an initial compression (or negative initial gap) is required to apply on the rubber pad and then the three steps of experimental procedure are shown in **Figure 4-4**.

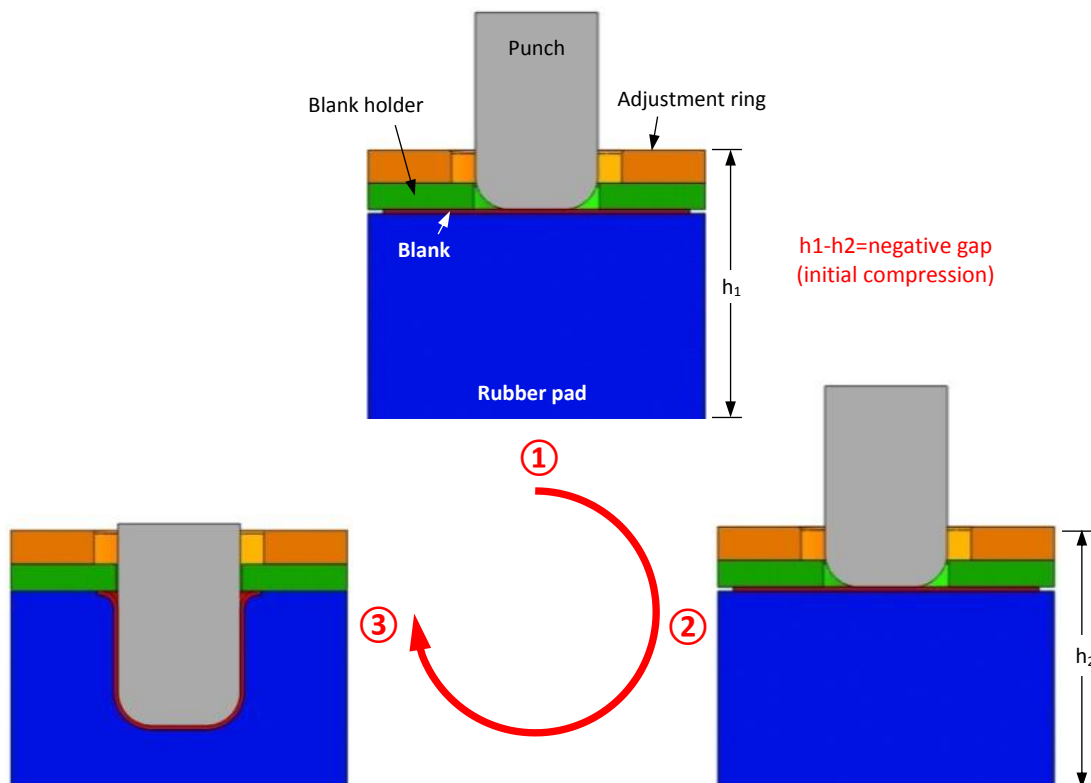


**Figure 4-4.** The second strategy of micro deep drawing adopted with negative gap

**Step 1:** In this step, the rigid punch is sent downwards just to contact the blank surface. The upper surface of the blank is in a direct contact at the central circular region with the punch bottom and at the annular flange region with the blank holder, whereas the lower surface is entirely in a direct contact with the rubber pad

surface. Also, the blank holder is in direct contact with the fixing plate, in other words no space in-between as in the first strategy. The blank doesn't undergo and deformation which means the actual drawing stroke dose not start in the step.

**Step 2:** in the second stage of this strategy of the proposed drawing technique, a negative gap is set. All of the punch, the blank older and the fixing plate are punch down for the same distance which represents the initial negative gap or the initial compression distance. Therefore, the blank will be in a severe contact with the punch and holder at the upper side and with the rubber pad at the lower side. The negative gap in turn causes an initial hydrostatic pressure in the rubber pad due to its incompressibility. The value of this hydrostatic pressure depends on the initial compression distance and rubber properties. It can be seen in **Figure 4-4** that there is no remarkable deformation is performed on the blank in this step.

**Step 3:** In this step both the blank and the rubber are formed by the rigid punch until obtaining a completed cup. As a result of the action in step 2, the punch load-stroke curve exhibits an initial particular load. An important note here is that the increment in the forming load in this technique is higher than that obtained in step 3 of the previous strategy as the rubber pad here is initially compressed.

#### 4.2.3 MULTI SUBSTROKES-MICRO DEEP DRAWING WITH POSITIVE INITIAL GAP

The multi-strokes forming procedure is another strategy adopted to execute the micro deep drawing technique proposed in this study. According to this strategy, the entire operation stroke is composed of two or more sub-strokes as shown in **Figure 4-5** there is a particular initial positive gap allocated for each sub-stroke, through which the blank is drawn partially. In other words, some drawing cases require a large initial positive gap which leads probably to wrinkling at early stages of the drawing process. In order to obviate this action, the drawing operation for the needed initial gap is divided into multi stages with different initial gaps. The execution steps of this strategy are listed following:

**Step 1:** the initial gap for the first stage of drawing stroke is allocated in this step. The same process conditions mentioned in step 1 of the first drawing strategy are specified here, and therefore the blank doesn't undergo any actual deformation.

**Step 2:** the first drawing stroke is carried out in this step. As the rigid punch moves down pushing the blank into the rubber cavity, a hydrostatic pressure is excited in the pad material. Thereafter, this hydrostatic pressure causes the blank holder to raise against the spring force until contacts the fixing plate. This action results in a smaller contact area between the blank and the holder as the blank flows into the rubber cavity. The rigid punch keeps moving down until the partial drawing stroke of this step is finished, producing a shallow cup. As a result, extra hydrostatic pressure will be generated inside the rubber pad material, which results in an increase in the holding force on the flange portion of the shallow cup.

**Step 3:** the major difference with the previous strategies can be detected in this step, where the fixing plate is moved up for a particular distance (second gap). Due to this activity, the blank holder will be again under the effect of the spring force. In addition, as a consequence of the hydrostatic pressure excited in the rubber pad in the previous drawing step, the blank holder will move up for the same distance (the second gap) of the fixing plate. This action causes the blank at its flange to slide on the holder surface flowing into the flexible cavity. As a result, the contact area between the blank and the holder will decrease again which implies reducing the holding pressure and hence the friction forces as well.

**Step 4:** the same scenario, explained in step 3 of the first drawing strategy, is repeated here. The rigid punch keeps moving down to complete forming the shallow cup produced in the previous step. Thus, extra hydrostatic pressure will be excited in the rubber material providing a relative high holding force on the small flange area of the cup. Also, the other function of the pad pressure is to push the blank material, flowing recently into the rubber cavity, towards the rigid punch. This action increases the friction forces at the blank/punch interface so that be able to override the friction at the flange region and then render to draw more material into the rubber cavity. Hence, the final profile of the produced cup is exactly the same of the rigid punch.

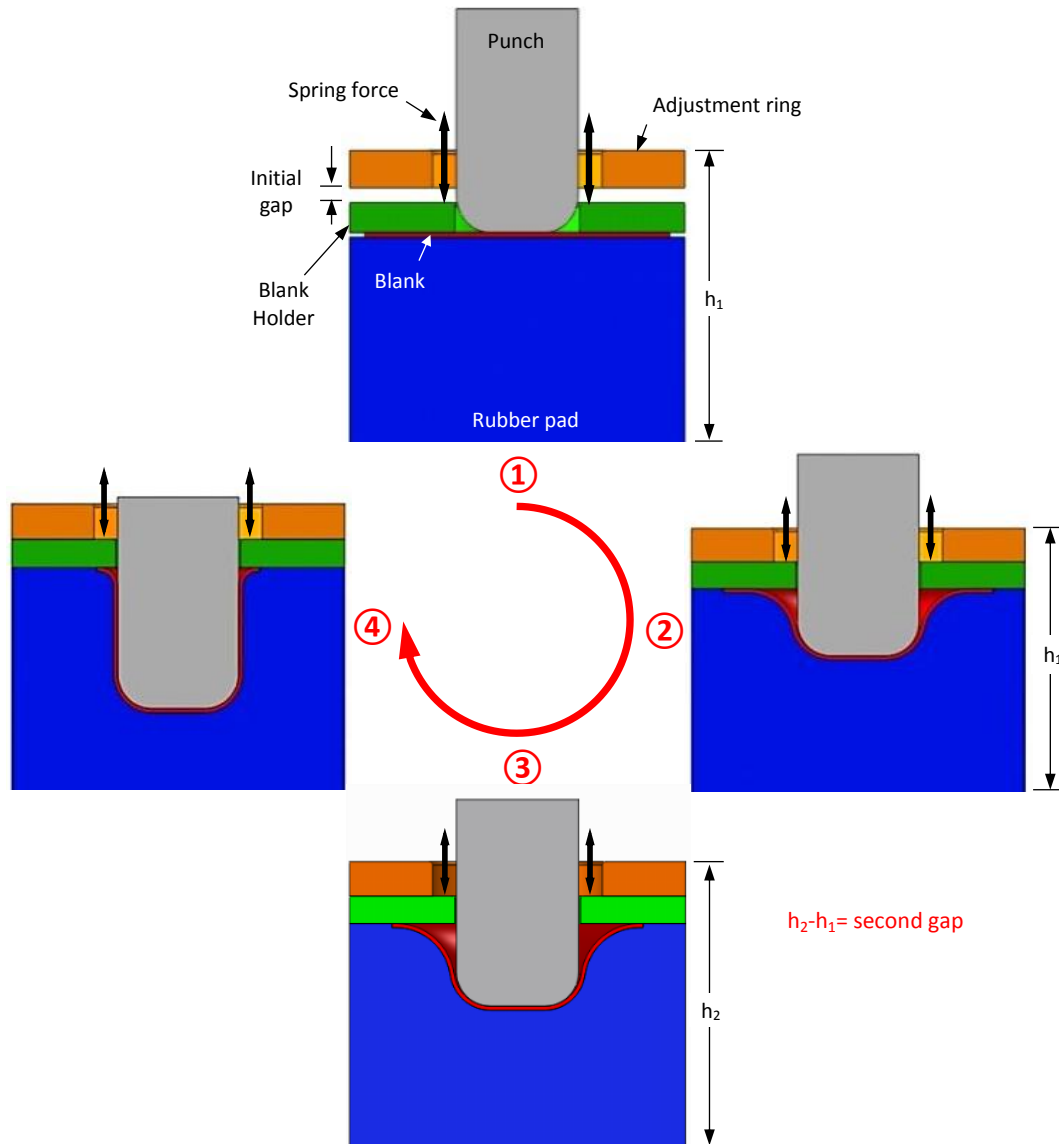


Figure 4-5. The third strategy of micro deep drawing with multi stages

To acquire profound Knowledge of the micro deep drawing proposed in this study, different key process parameters such as sheet thickness, blank diameter, rubber material properties, rubber pad dimensions, drawing velocity, initial gap value, initial holding force and friction coefficients are studied in details. FE simulation models are built for the different strategies of the new technique presented here by using the commercial software ABAQUS/Standard. In these simulations, all the parameters mentioned are taken into accounted. Also, many drawing experimental are achieved in dependence on this technique in order to validate the theoretical predictions. Annealed stainless steel 304 sheets with various thicknesses of  $60\mu\text{m}$ ,  $100\mu\text{m}$  and  $150\mu\text{m}$  are used to supply the drawing blanks. Aimed to

detect whether the rubber properties have any effective role on the drawing process, urethane rubber materials of 40, 63 and 75 Shore A hardness are employed for the flexible forming pads. The mechanical properties and the deformation behaviours of the metallic sheets and rubber materials are characterized in chapter four. Three different scaling factors are adopted in this work for investigating the possibility of use the proposed drawing technique with different dimensional levels. The geometrical parameters of the process tools utilized here as well as the blanks are listed in **Table 4-1**. In addition, blanks with other diameters of 9mm, 11mm and 12mm are used in order to clarify the influence of the initial blank diameter.

Punch diameter $D_p$ (mm)	Scaling factor $\lambda$	Punch corner radius $R_p$ (mm)	Blank diameter $D_b$ (mm)	Rubber diameter $D_r$ (mm)	Rubber height $h_r$ (mm)
4	1	0.8	10	12	10
2	0.5	0.4	5	6	5
1	0.25	0.2	2.5	3	2.5

**Table 4-1. Geometrical parameters for the micro deep drawing of cylindrical parts**

In order to understand how the forming rate may affect the friction status and material behaviour response, a wide range of 0.1, 1, 10 and 100mm/sec is adopted for the punch velocity in this work. Moreover, the initial compression on the holder-supported spring is changed for different cases in order to reveal the influence of the initial blank holder force on the process window. Furthermore, the effect of friction conditions at the interfaces between the blank and the process tools (punch, blank holder and rubber pad) are revealed through adopting different friction coefficients at the contact surfaces. As the mentioned parameters may have various roles relatively on the proposed micro deep drawing technique, it is also of most importance to study the interactions between them especially those affect significantly on the drawing results. The cases for which each one of the drawing strategies presented previously is the most appropriate, are revealed.

**CHAPTER FIVE**

**CHARACTERIZATION OF MATERIAL BEHAVIOURS**

\*\*\*\*\*

## **5.1 BACKGROUND**

In sheet metal forming processes, it is a fundamental activity to characterize the deformation behaviour of the sheet metal and any other material employed in a particular processes. The known tensile test is adopted to define the ss 304 sheet materials, while uniaxial compression and volumetric compression tests are intended for the rubber die materials. This chapter shows the preparation method of the tensile test samples cut from SS 304 sheets of different thicknesses. As well as, the testing procedure is explained and thereafter the calculation steps of the anisotropy factors of the sheet metals are demonstrated. Finally, this chapter illustrates the compression tests of the rubber materials and afterward the hyperelastic and compressibility parameters are determined.

## **5.2 TENSILE TEST OF SS 304 SHEET MATERIALS**

The mechanical properties of the sheet metals employed in forming processes strongly influence the metals flow and therefore the final product quality. The properties differ from one sheet to other, thus in order for control part quality and obtaining robust production it is essential to characterize the deformation behaviour of each sheet metal. In finite element (FE) simulations, accurate stress-strain relationships are usually used as input data. For this purpose, a reliable test is required to estimate the formability of the formed sheet and to define the true stress-true strain data for the FE models. The tensile test is commonly utilised for determining the flow stress of the sheet materials for such process simulations.

### **5.2.1 PREPARING THE TESTING SPECIMENS**

Stainless steel 304 (SS 304) is considered the most common chromium-nickel stainless steel grade. SS 304 sheets are currently used in a wide range of industrial applications such as automotive, chemical equipment, cooling coils, nuclear vessels and components, etc. [143]. With the growing demand on miniaturized devices especially in medical and electronic fields, the need to use micro cups made of SS 304 sheets has been increasing drastically. However, micro cups with high aspect ratio (cup height to cup diameter ratio) cannot be produced through one stage in deep drawing process because of the constraints of the drawability (limit drawing ratio) of SS 304 [130, 144]. Therefore, annealed stainless steel 304 sheets with different



thicknesses of 60 $\mu$ m, 100 $\mu$ m and 150 $\mu$ m are employed in this work to supply the drawing workpieces. The specified chemical composition of these sheets is shown in **Table 5-1**.

Cr	Mn	Ni	C	Fe
17-20%	<2%	8-11%	<800	Balance

**Table 5-1. Chemical composition of SS304 sheets**

In FE simulations, the mechanical properties of the SS 304 sheets are required, which are utilized as input data for the models to define the deformation behaviour of the workpiece materials during deep drawing processes. Therefore, the well-known tensile test is adopted in this work for this goal. The specimens used in this test are cut to dog-bone shapes and the dimension are determined from the standard ASTM E8 [145] as seen in **Figure 5-1**. The tensile test specimens are cut using the 3D micro computerized cutting machine with maximum rotating velocity of 60000 rpm which is shown in **Figure 5-2**.

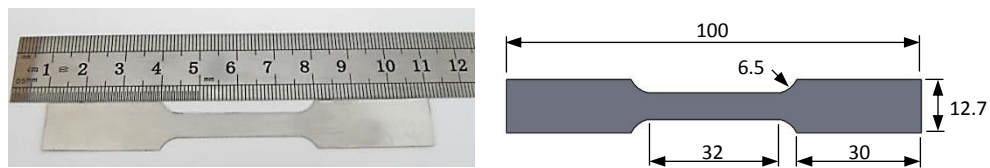


**Figure 5-1. Tensile test specimen**

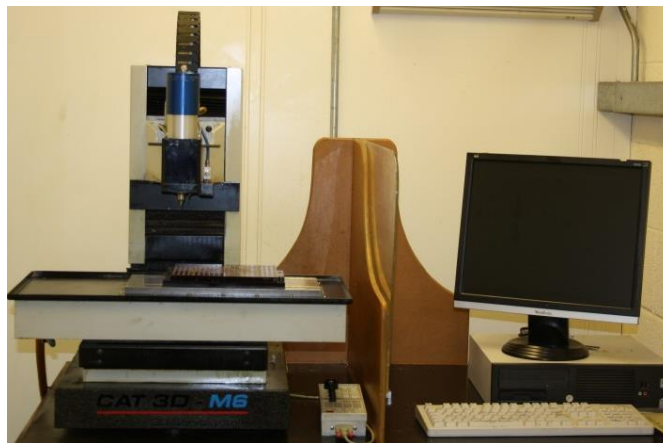


**Figure 5-2. 3D micro computerized cutting machine**

The original sheet is actually put between two parallel Perspex plates of 5mm in thickness which are tightened on each other by a number of screws. This procedure is to avoid moving the metallic thin sheet during the cutting process. The very important issue that has to be paid serious attention is to ensure that the cutting edges of the SS 304 specimen should be

smooth and that what was performed in this study by using the Nikon Eclipse ME600L microscope. In other words, no notches or steps have to left at the cutting line. These imperfections can cause undesired stress constriction which lead to unexpected fracture. Hence, the results obtained from testing such these specimens do not reflect the real behaviour of the tested sheet materials. These aspects are more expectable to occur increasingly with scaling down the sheet size as the grain size to sheet thickness ratio increases.

### 5.2.2 TESTING PROCEDURE AND RESULTS

The supplier company (Goodfellow Cambridge Ltd.) provides the standards mechanical and physical properties of the stainless steel 304 sheets employed in this work. However, since the SS 304 sheets used here are produced using cooled rolling process, the mechanical properties therefore depend on the orientation with respect to the rolling direction. In other words, SS 304 sheets are characterized by an anisotropic behaviour.

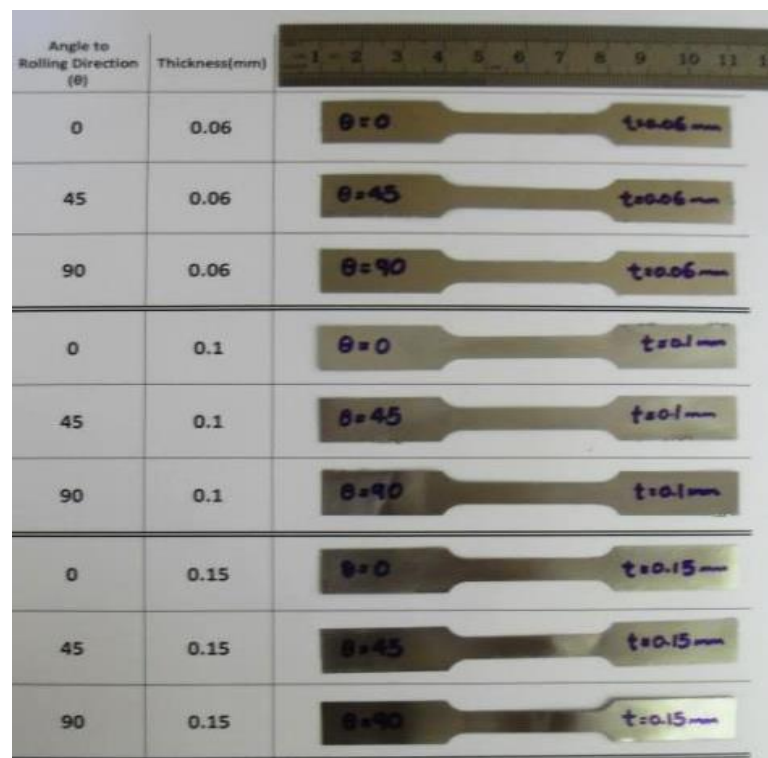
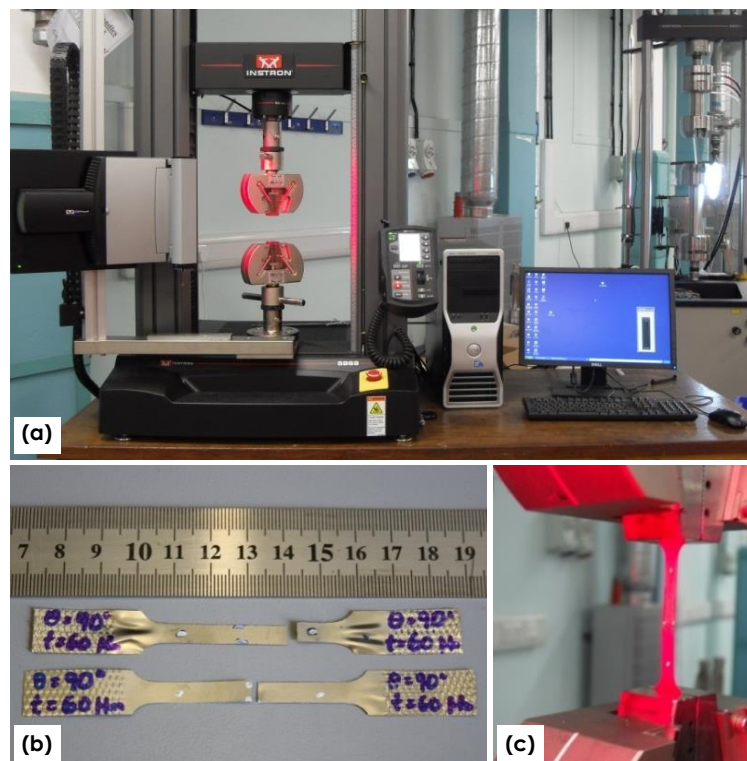


Figure 5-3. Tensile test specimens

Thus, for investigating the effect of the anisotropy nature on the deformation response of the sheet material, the dogbone-shaped specimens employed for the tensile tests are cut at

the rolling, 45° diagonal and transverse directions for each sheet thickness. The sheets of different thicknesses are marked with lines at the rolling direction before the cutting processes, and thereafter the specimens are cut with respect to this direction. That means that the total number of the testing specimens is nine, three for each sheet as shown in **Figure 5-3**. According to the standard ASTM E8 [145], the velocity adopted for the tensile test in this study is 0.1mm/sec. the tensile tests of SS 304 thin sheets are conducted using Instron 5969 universal testing machine with 50kN load cell as seen in **Figure 5-4a**. Non-contacting advanced video extensometer (FOV 200mm) is utilized for measuring the longitudinal and transverse strains simultaneously during the test.



**Figure 5-4.** (a) Instron 5969 machine (b) Tested specimens (c) Broken specimen on the machine

The gripping conditions at the ends of very thin sheet specimens are very important to obtain accurate results. It was observed that that low gripping force and/or insufficient gripping length result in folding the sheet material near to the edges (see **Figure 5-4b**). Therefore, the specimen ends have to be tightened strongly enough as well as sandpaper pieces can be used between the specimen and the grip surfaces to increase the frictional forces. Moreover, the specimen wings gripped by the machine have to be long enough to overcome any probable sliding at the specimen/grip interface as shown in **Figure 5-4c**.

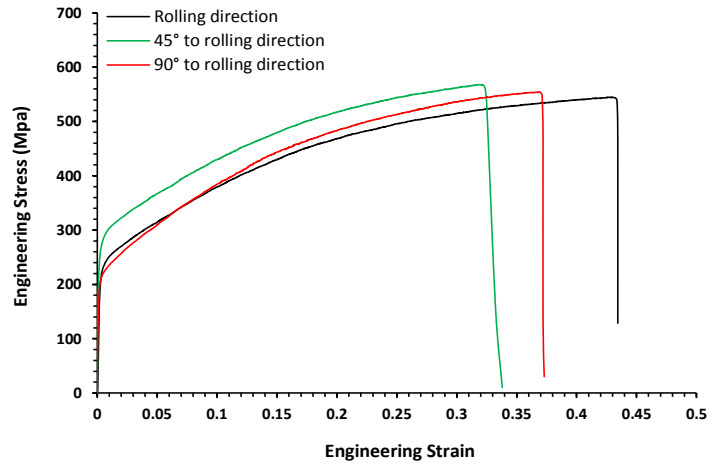


Figure 5-5. Stress-strain relationship for SS 304 sheet of 60µm in thickness at three different directions

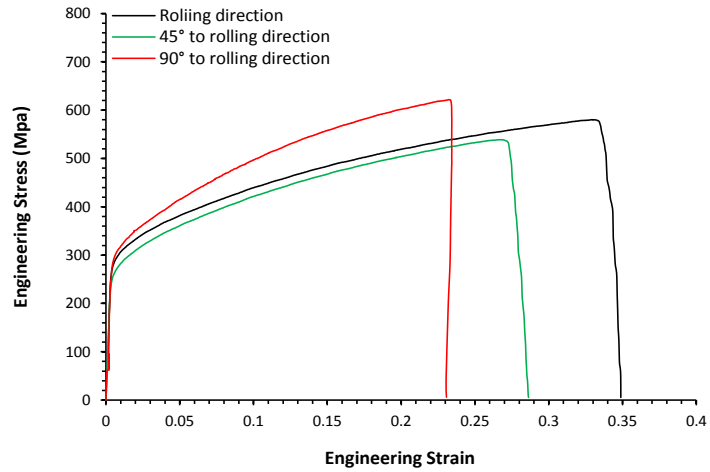


Figure 5-6. Stress-strain relationship for SS 304 sheet of 100µm in thickness at three different directions

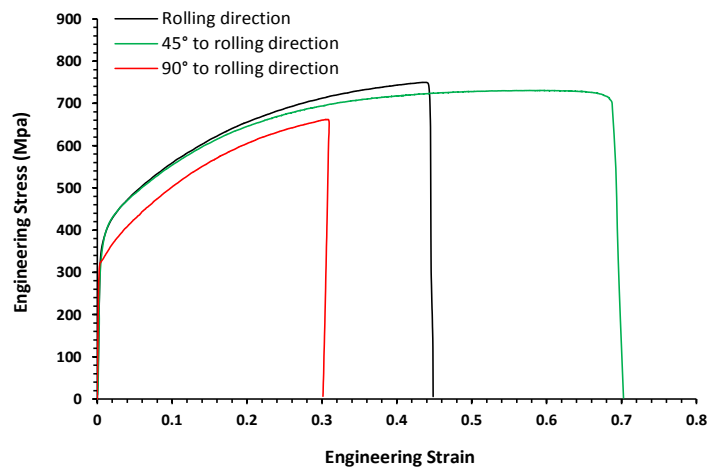


Figure 5-7. Stress-strain relationship for SS 304 sheet of 150µm in thickness at three different directions

The engineering stress-strain relationships obtained from the tensile tests at the three different directions of the SS 304 sheets of 60 $\mu$ m, 100 $\mu$ m and 150 $\mu$ m in thickness used in this work are presented in **Figure 5-5** to **Figure 5-7** respectively. Also, the mechanical properties acquired from these tests are listed in **Table 5-2**

Thickness (mm)	Rolling Direction	E (GPa)	$\sigma_o$ (MPa)	$\sigma_{ult}$ (MPa)	$\epsilon_{ult}$	K (MPa)	n
0.06	0°	128.6	225.4	545	0.42794	1240.5	0.4622
	45°	192.7	273.2	568	0.32075	1249	0.4087
	90°	179	209.8	554.7	0.36925	1329.5	0.4855
0.1	0°	167	277.2	580.5	0.32964	1290.2	0.422
	45°	229.2	252.3	539	0.26787	1263	0.4307
	90°	195	287.3	621.8	0.23202	1444.7	0.4103
0.15	0°	107.5	373	749.8	0.43816	1634.7	0.423
	45°	120.2	327.4	730.7	0.5765	1582	0.4139
	90°	156.8	316.2	662	0.30535	1465.3	0.4104

**Table 5-2. Mechanical properties of SS 304 sheets**

### 5.3 CALCULATING THE ANISOTROPY FACTORS

For the FE simulations, the work hardening of the SS 304 sheet materials is established as a tabular data which are the true stresses and true strains obtained from the tensile tests for each sheet thickness at the rolling direction. The plastic anisotropy which reflects the deformation mode of the sheet material in the other directions (45° diagonal and transverse directions) is introduced into the FE models by utilizing Hill's anisotropic yield criterion. The well-known Von-Mises function is simply extended to formulate the Hill's function that therefore can be expressed in terms of Cartesian stress components as:

$$f(\sigma) = \sqrt{F(\sigma_{22} - \sigma_{33})^2 + G(\sigma_{33} - \sigma_{11})^2 + H(\sigma_{11} - \sigma_{22})^2 + 2L\sigma_{23}^2 + 2M\sigma_{31}^2 + 2N\sigma_{12}^2} \quad 5-1$$

where F, G, H, L, M and N are material constants obtained from test tensile in different orientations and  $\sigma_{ij}$  refers to the stress components [146]. These constants are defined as:

$$F = \frac{1}{2} \left( \frac{1}{R_{22}^2} + \frac{1}{R_{33}^2} - \frac{1}{R_{11}^2} \right) \quad 5-2$$

$$G = \frac{1}{2} \left( \frac{1}{R_{33}^2} + \frac{1}{R_{11}^2} - \frac{1}{R_{22}^2} \right) \quad 5-3$$

$$H = \frac{1}{2} \left( \frac{1}{R_{11}^2} + \frac{1}{R_{22}^2} + \frac{1}{R_{33}^2} \right) \quad 5-4$$

$$L = \frac{3}{2R_{23}^2}, N = \frac{3}{2R_{12}^2} \text{ and } M = \frac{3}{2R_{13}^2} \quad 5-5$$

where  $R_{11}$ ,  $R_{22}$ ,  $R_{33}$ ,  $R_{12}$ ,  $R_{13}$  and  $R_{23}$  are anisotropic yield stress ratios, which can be expressed in the following form:

$$R_{11} = \frac{\bar{\sigma}_{11}}{\sigma^0}, R_{22} = \frac{\bar{\sigma}_{22}}{\sigma^0}, R_{33} = \frac{\bar{\sigma}_{33}}{\sigma^0}, R_{12} = \frac{\bar{\sigma}_{12}}{\tau^0}, R_{13} = \frac{\bar{\sigma}_{13}}{\tau^0} \text{ and } R_{23} = \frac{\bar{\sigma}_{23}}{\tau^0} \quad 5-6$$

where  $\bar{\sigma}_{11}$ ,  $\bar{\sigma}_{22}$ ,  $\bar{\sigma}_{33}$ ,  $\bar{\sigma}_{12}$ ,  $\bar{\sigma}_{13}$  and  $\bar{\sigma}_{23}$  are the measured yield stress values, ( $\sigma^0$ ) is considered as a reference yield stress for the formed material. In sheet metal forming, as the thickness dimension is very small compared with the other sheet dimensions, thus the plane stress conditions are adequately adopted. That means that no shear stresses have to be considered in the thickness plane and as a result just four plastic stress ratios ( $R_{11}$ ,  $R_{22}$ ,  $R_{33}$  and  $R_{12}$ ) are taken into account [53, 147]. Within the FE code Abaqus, the anisotropic yield stress ratios are expressed in accordance to the general anisotropy concept in terms of the width to thickness strain ratios  $r_0$ ,  $r_{45}$  and  $r_{90}$ , which called also Lankford's r-values, as shown below:

$$R_{22} = \sqrt{\frac{r_{90}(r_0+1)}{r_0(r_{90}+1)}}, R_{33} = \sqrt{\frac{r_{90}(r_0+1)}{r_0+r_{90}}} \text{ and } R_{12} = \sqrt{\frac{3r_{90}(r_0+1)}{(2r_{45}+1)(r_0+r_{90})}} \quad 5-7$$

where  $r_0$ ,  $r_{45}$  and  $r_{90}$  are width strain to thickness strain ratios of the workpiece material at the rolling, 45° diagonal and transverse directions respectively [53, 147, 148]. These strain ratios ( $r$ ) depend on the values of the plastic strains. The plastic thickness and width strains used in determining the r-values are obtained from the tensile tests and should be measured when the elongation strain is 20% [148, 149]. In order to determine the values of these strain ratios, the following procedure used for the SS 304 sheet of 60µm in thickness can be adopted as well for the other sheet thicknesses.

- **The width to thickness strain ratio at the rolling direction ( $r_0$ )**

- » **Engineering strains**

- Engineering length strain ( $\epsilon_L$ ) = 0.2

- Engineering width strain ( $\epsilon_w$ ) = -0.073248333

» **Correction procedure of plastic strains**

The common procedure to determine the r-values through tensile tests is to deform up the specimen to the maximum allowed strain (20%), and afterwards the test machine is stopped and the specimen is picked out from the machine grips. At this unloading case, the length and width of the specimen gauge length are accurately measured according to standard recommendations. Nevertheless, in this study the length and width strains are measured simultaneously which causes measuring the plastic strains to be more difficult as the specimen is still under loading. Therefore, there is an imperative need to correct the strain values through eliminating the elastic portion of strains [150] as following:

$$\text{Length plastic strain } (\varepsilon_L)_{\text{plastic}} = \text{Length true strain } (\varepsilon_L)_{\text{true}} - \text{Length elastic strain } \left( \frac{\sigma}{E} \right)$$

$$(\varepsilon_L)_{\text{plastic}} = 0.2 - \left( \frac{518.8978}{167012} \right) = 0.19689305$$

$$\text{Width plastic strain } (\varepsilon_w)_{\text{plastic}} = \text{Width true strain } (\varepsilon_w)_{\text{true}} - \text{Width elastic strain } \left( \nu \frac{\sigma}{E} \right)$$

$$(\varepsilon_w)_{\text{plastic}} = -0.073248333 + 0.3 \left( \frac{518.8978}{167012} \right) = -0.07231625$$

where  $\sigma$  is the engineering stress corresponding to the elongation of 20%.

» **Calculating the true strains**

$$(\varepsilon_L)_{\text{true}} = \text{LN} \left( 1 + (\varepsilon_L)_{\text{plastic}} \right) = \text{LN} (1 + 0.19689305) = 0.17972908$$

$$(\varepsilon_w)_{\text{true}} = \text{LN} \left( 1 + (\varepsilon_w)_{\text{plastic}} \right) = \text{LN} (1 - 0.07231625) = -0.07506439$$

the plastic strain ratios (r-values) are very sensitive to the strain magnitudes. Since it is very difficult to obtain accurate measurements for thickness strains during the tensile test of very thin sheet metals, the thickness strain thus can be expressed in terms of the length and width strains according to the principle of material volume constancy which states:

Increase in length = Reduction in width + Reduction in thickness

$$|\text{Length strain}| = |\text{Width strain} + \text{Thickness strain}|$$

OR:

$$|\text{Thickness strain}| = |\text{Length strain} - \text{Width strain}|$$

» Plastic strain ratio in the rolling direction ( $r_0$ )

$$r_0 = \frac{\text{Plastic true width strain}}{\text{Plastic true thickness strain}}$$

$$r_0 = \frac{|(\varepsilon_w)_{\text{true plastic}}|}{|(\varepsilon_L)_{\text{true plastic}} - (\varepsilon_w)_{\text{true strain}}|} = \frac{0.07506439}{0.17972908 - 0.07506439} = 0.717189264$$

The same calculation steps can be used for the r-values at the 45° diagonal and 90° transverse respective to the rolling direction; hence the values  $r_{45}=1.00371091$  and  $r_{90}=0.77824150464$  are obtained. Now, it is easy to determine the anisotropic yield stress ratios as following:

$$R_{22} = \sqrt{\frac{r_{90}(r_0+1)}{r_0(r_{90}+1)}} = \sqrt{\frac{0.77824150464(0.717189264+1)}{0.717189264(0.77824150464+1)}} = 0.9453293037$$

$$R_{33} = \sqrt{\frac{r_{90}(r_0+1)}{(r_0+r_{90})}} = \sqrt{\frac{0.77824150464(0.717189264+1)}{(0.717189264+0.77824150464)}} = 1.0236559507$$

$$R_{33} = \sqrt{\frac{3r_{90}(r_0+1)}{(2r_{45}+1)(r_x+r_y)}} = \sqrt{\frac{3 \times 0.77824150464(0.717189264+1)}{(2 \times 1.00371091+1)(0.717189264+0.77824150464)}} = 0.9441621249$$

The r-values and the plastic strain ratios of all SS 304 sheets calculated using the procedure presented above are listed in **Table 5-3**.

Sheet thickness ( $\mu\text{m}$ )	$\Theta$	r-values	Anisotropic yield stress ratios			
			R <sub>11</sub>	R <sub>22</sub>	R <sub>33</sub>	R <sub>12</sub>
60	0°	0.975608271				
	45°	1.076671656	1	0.97129434	0.97700096	0.94738359
	90°	0.891692687				
100	0°	0.717189264				
	45°	1.00371091	1	0.945329304	1.02365595	0.944162125
	90°	0.77824150464				
150	0°	0.759571919				
	45°	0.92150833	1	0.98879011	1.06229062	1.01572242
	90°	0.949827615				

**Table 5-3. The r-values and anisotropic stress yield ratios of SS 304 sheets**



#### 5.4 CHARACTERIZATION OF POLYURETHANE RUBBER PROPERTIES

Beside the several advantages of using flexible materials tooling in the technology of sheet metal forming, Polyurethane exhibits outstanding characteristics and abilities compared with other elastomers. Polyurethane is considered extremely durable and has the highest tensile strength among all rubber materials as it stretches up to 650% prior failure [151, 152]. Polyurethane provides excellent resistance to impact, abrasion, shear and tear as well as to chemical compounds even at working temperature ranging from  $-30^{\circ}\text{C}$  to  $+100^{\circ}\text{C}$ . In addition, Polyurethane is available in abroad hardness range 10 shore OO to 85 Shore D [151]. Therefore, it can be said that Polyurethane is a unique elastomer material as it can combine the elasticity of rubber materials and the durability and toughness of metals. In this study different Polyurethane materials are utilized for the forming rubber pads in order to investigate the influence of pad material deformation mode on the micro drawing processes.

#### 5.5 UNIAXIAL COMPRESSION TEST OF URETHANE RUBBER MATERIALS

Polyurethane rubber is characterized by hyperelastic behaviour. The “hyperelastic” term used to define the nonlinear behaviour of a material when subjected to very large strains. The hyperelasticity then refers conveniently to both material nonlinearity and large reversible shape changes. As a conclusion, the behaviour attributes of the materials under consideration of this definition are to be ideal elastic which actually means the stresses depend only on the current strains and also there is no net work done on the material when subjected to cyclic loading under adiabatic conditions [153].



Figure 5-8. Measuring the rubber hardness using Durometer Shore A

The polyurethane rubber materials used for the forming pads in the current study have different Shore A of 40A, 63A and 75A which are measured using Durometer Shore A as shown in **Figure 5-8**. In order to model hyperelastic materials in finite element models, experimental test data have to be provided. Therefore, owing to obviously understand the deformation response of the materials characterized as hydrostatic, the following experimental tests can be adopted: uniaxial tension and compression, planar tension and compression, and volumetric tension and compression. Since the simulation results that obtained from finite element models involved hyperelastic materials can be strongly improved in dependence on the accuracy of the experimental test data provided. Consequently, it is recommended strongly for these data to be taken from tests which are more relevant to the deformation mode occurring in the considered simulations. Therefore, uniaxial and volumetric compression tests are adopted for the current work as the rubber pads undergo compression loading in the proposed micro drawing technique. The volumetric compression test is explained in the next section. Regarding the uniaxial compression test the Instron 3956 machine with 50kN load cell shown in **Figure 5-9** is utilized to perform this test.

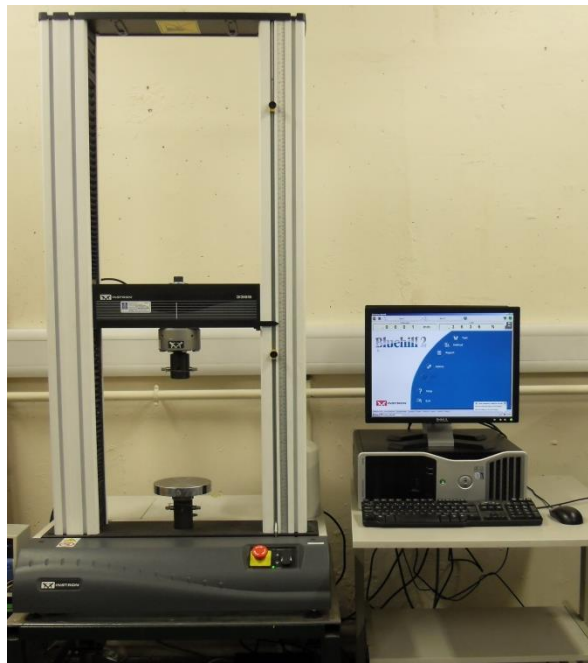


**Figure 5-9.** Instron 3956 machine used for the uniaxial compression test

The dimensions of the disc-shaped test specimens are determined according to the standard ASTM D575 [154] where the diameter is  $28.6 \pm 0.1\text{mm}$  and the height is  $12.5 \pm 0.5\text{mm}$  as seen in **Figure 5-10a**. The standard test specimens with these dimensions are obtained

usually either by casting liquid rubber compounds in rigid dies of exactly the same dimensions required for the final specimens or by cutting them from large pieces of rubber slabs or rods. Consequently, there is a possibility that the specimens cut of different rubber types might have some deviation in their dimensions especially when several dies are used for the casting processes or when the specimens are cut of different slabs of rods for the even the same rubber type. Three specimens for each polyurethane rubber type are therefore tested in order to compare the obtained results and then to acquire the final results from the one with the more accurate dimensions. The testing procedure followed for the uniaxial compression test is to specify a deflection, which is 8mm in this study, and then the force is applied to produce a compression rate of 12mm/min. In order to condition the specimens, each specimen is initially compressed for two cycles and afterwards the readings are taken from the third one.

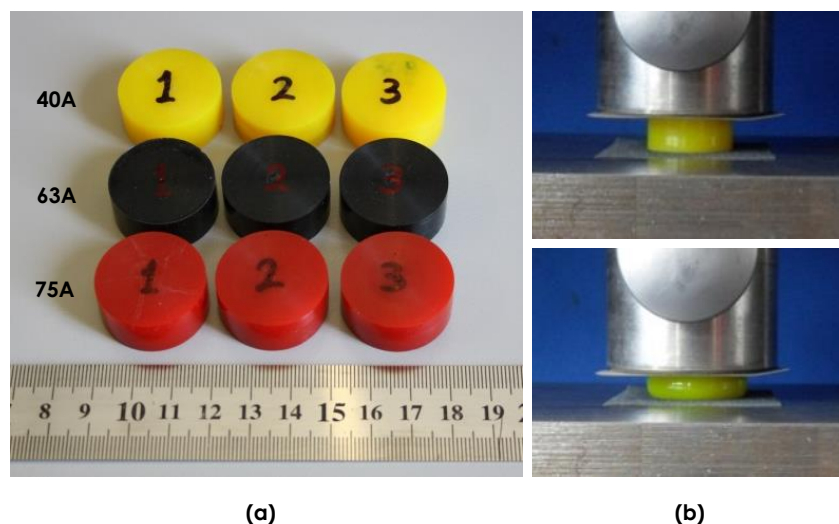


Figure 5-10. (a) Rubber specimens (b) Rubber 40A specimen under compression load

In the uniaxial compression test, there is a very important issue which is to prevent the lateral slippage of the rubber specimen on the machine platens. Therefore, sheets of sandpapers are placed between the rubber surfaces and the platens as can be observed in Figure 5-10b. Figure 5-11 to Figure 5-13 present the load-displacement curves obtained from the uniaxial compression tests for the rubber specimens of 40, 63 and 75 Shore A hardness respectively. Figure 5-14 presents the testing result adopted for the finite element simulations. It can be observed that as the rubber hardness increases, higher force is required to achieve the specified deflection.

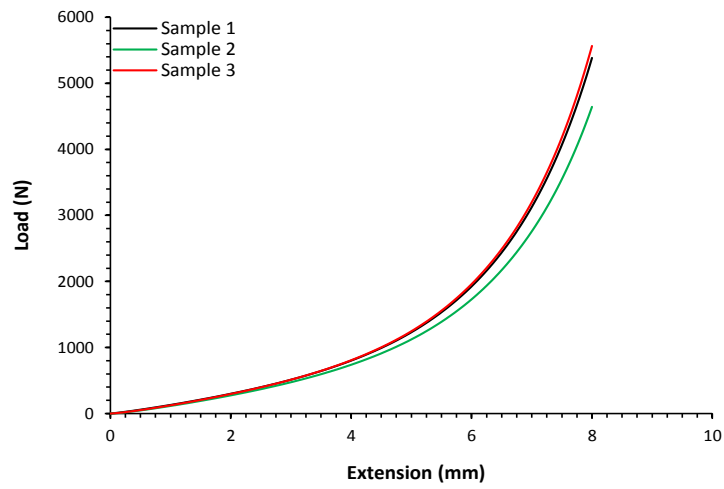


Figure 5-11. Uniaxial compression load-displacement relationships of 40 Shore A rubber hardness

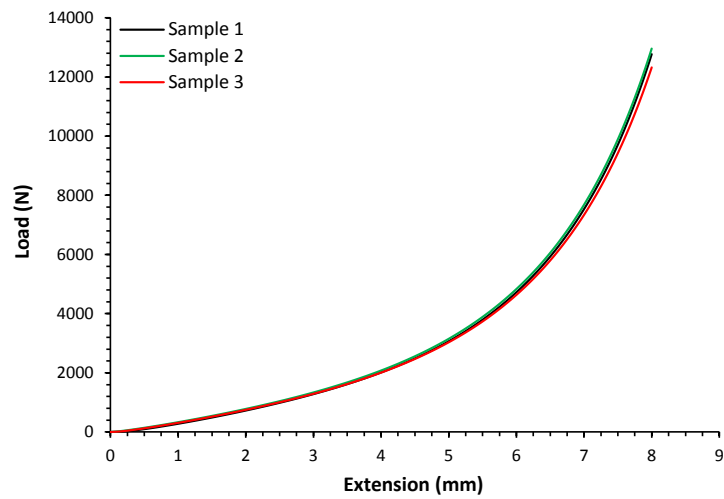


Figure 5-12. Uniaxial compression load-displacement relationships of 63 Shore A rubber hardness

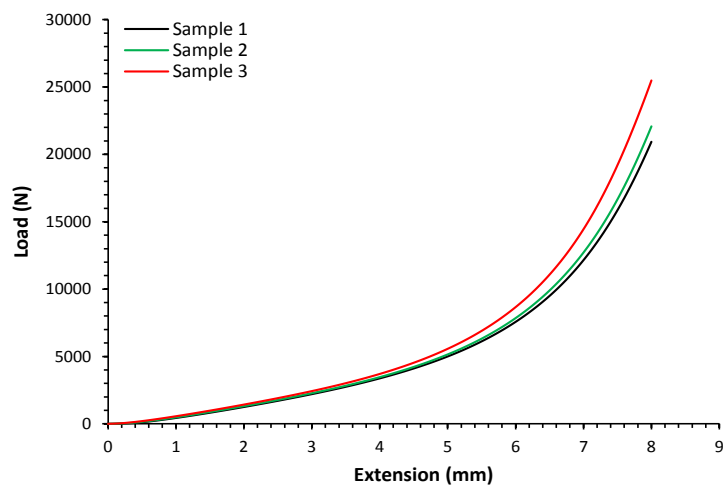


Figure 5-13. Uniaxial compression load-displacement relationships of 75 Shore A rubber hardness

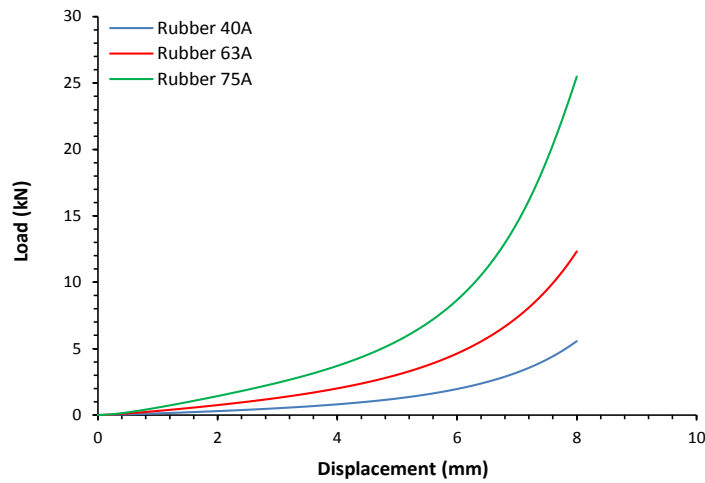


Figure 5-14. Uniaxial compression load-displacement relationships of rubber materials with different hardness

## 5.6 VOLUMETRIC COMPRESSION TEST OF URETHANE RUBBER MATERIALS

Unlike their shear flexibility, rubber materials are characterized by very little compressibility. In accordance to the forming application, the degree of compressibility has a relative influence on the deformation response. For the cases when the rubber materials are loaded under high restriction conditions such as rubber seals and rubber gaskets the compressibility must be modelled correctly and accurately. In such application situations the degree of compressibility though is very small, plays a significant role on the material behaviour mode. On the other side, when the rubber compressibility is not crucial parameter in particular applications, for example when the rubber is not highly confined, it can be conveniently assumed that the rubber material is fully incompressible. The compressibility term refers to the change in material volume under external loading conditions, and therefore it is related to directly to the Poisson's ratio.

In order to model the compressibility of the rubber materials used in this study in FE simulations, experimental data of volumetric compression tests are acquired. The volumetric testing is conducted according to the procedure presented by Gregory et al. [155]. The same rubber specimens that were used in the uniaxial compression test are employed for this test as well. The volumetric compressing tests are carried out on the same Instron 3956 universal testing machine shown in Figure 5-9. The simple device shown in Figure 5-15 is manufactured for the volumetric test. The die cavity dimensions are 29mm in diameter and 20 mm in height, while the punch diameter is approximately 28.98mm. It can be noted that the clearance between the punch and the die cavity is very small due to the high importance of avoiding any

space for the rubber specimen to extrude during the test. This strategy is to ensure that the test specimen will be highly confined [155]. The height of the die cavity is larger than the thickness of the testing specimen. This aspect is to allow the rigid punch to go safely through the die opening before contact the rubber surface. The experimental data of the volumetric compression tests are taken for the same specimens considered in the uniaxial compression test. **Figure 5-16**, **Figure 5-17** and **Figure 5-18** present the applied load-extension curves obtained from the volumetric compression tests for the rubber specimens of 40, 63 and 75 Shore A hardness, respectively. The experimental force-displacement relationships that are used in the FE simulation to define the rubber material behaviours are presented in **Figure 5-19**. It can be observed from this figure that the force needed to achieve the required deflection decreases with increasing the rubber hardness. This action indicate that the compressibility of the rubber materials do not depend on the rubber hardness.

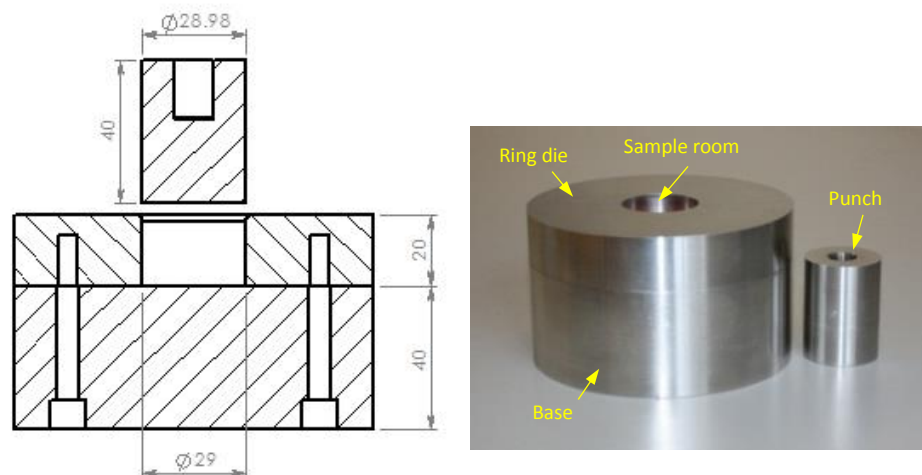


**Figure 5-15.** Experimental device for the volumetric testing

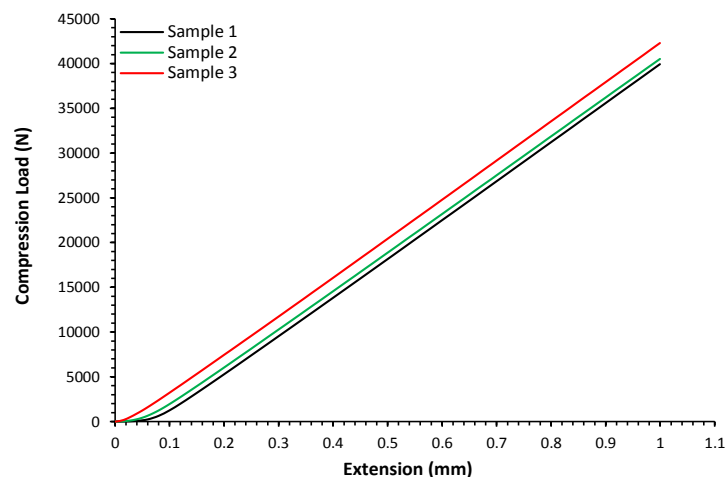


**Figure 5-16.** Volumetric testing load-displacement relationships of 40 Shore A rubber hardness

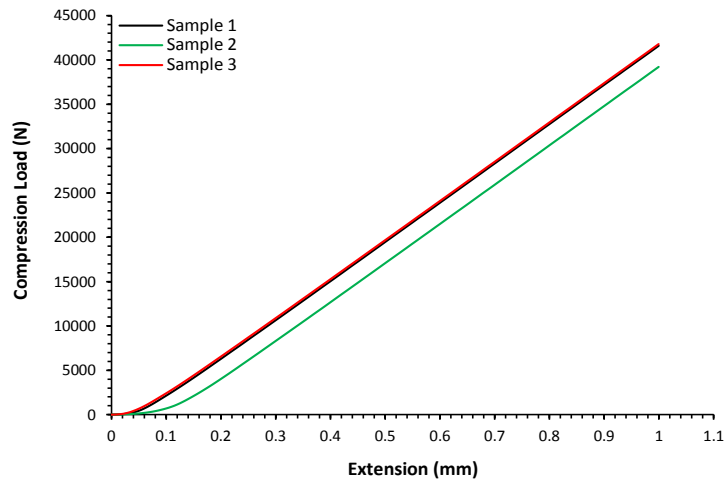


Figure 5-17. Volumetric testing load-displacement relationships of 63 Shore A rubber hardness

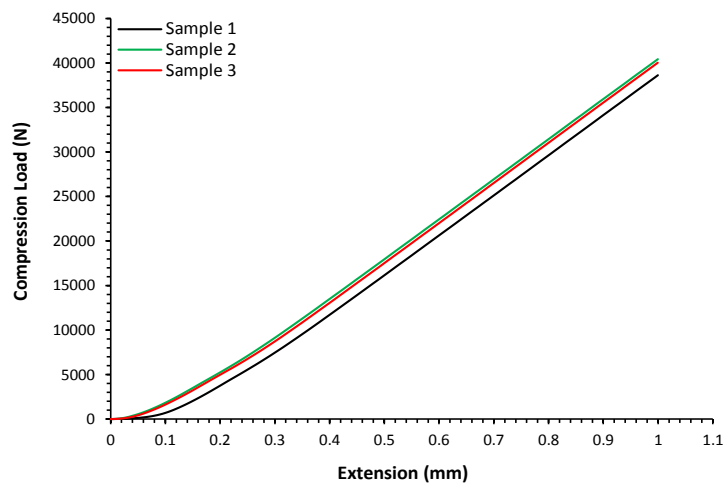


Figure 5-18. Volumetric testing load-displacement relationships of 75 Shore A rubber hardness

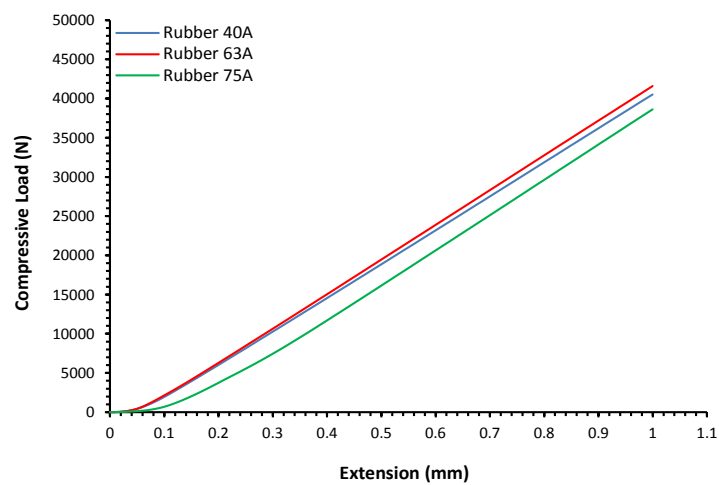


Figure 5-19. Volumetric compression load-displacement relationships

## 5.7 CALCULATING THE RUBBER MATERIAL PARAMETERS

Elastic behaviour indicates that the material subjected to external loading does not undergo a permanent deformation. In other words, the material that returns to their original shape when the applied load is removed is characterized by an elastic behaviour or recoverable behaviour. Usually the simple elastic deformation can be defined by a linear relationship between the stresses and strains such as in the case of metals. For the isotropic materials that have such this deformation mode are completely defined by the Young's modulus and Poisson's ratio and their mechanical properties can be obtained simply from the well-known tensile test [156]. However, in the case of rubber materials, describing the stress-strain relations is difficult. For such these materials the deformation behaviour is typically elastic but with high linearity, and therefore a special formula is needed to define the stress-strain characteristics. In Abaqus, strain energy potentials are employed to relate stresses to strains for hyperelastic materials. There are several different forms for the strain energy potentials, which are in a polynomial model, such as the Ogden model, the Arruda-Boyce model, the Marlow model, the van der Waals model, the Mooney-Rivlin model and neo-Hookean model. The generalized polynomial form of the strain energy potentials is:

$$U = \sum_{i+j=1}^N C_{ij} (\bar{I}_1 - 3)^i (\bar{I}_2 - 3)^j + \sum_{i=1}^N \frac{1}{D_i} (J_{el} - 1)^{2i} \quad 5-8$$

where  $U$  is the strain energy potential (strain energy per unit of reference volume),  $N$ ,  $C_{ij}$  and  $D_i$  are temperature-dependent material parameters.  $C_{ij}$  are the material parameters that describe the hyperelastic behaviour,  $D_i$  are the parameters that introduce the compressibility,  $\bar{I}_1$  and  $\bar{I}_2$  are measures of the distortion in the material,  $J_{el}$  is the elastic volume ratio [147, 153]. The simpler forms of the polynomial models of the strain energy potentials are the Mooney-Rivlin and neo-Hookean which are used appropriately with  $N=1$  due to the difficulty of fitting such large number of material properties to the experimental data with  $N>2$  [133, 153].

In this study the first order Mooney–Rivlin hyperelastic model is adopted to describe the stress-strain relation characteristics of the polyurethane rubber materials used for the flexible forming dies. For this model the material parameters  $C_{ij}$  are usually expressed by  $C_{01}$  and  $C_{10}$  which describe the hyperelasticity nature of the modelled materials. Therefore, the Mooney-Rivlin strain energy potential with  $N=1$  can be written in the form:

$$U = C_{01} (\bar{I}_2 - 3) + C_{10} (\bar{I}_1 - 3) + \frac{1}{D_1} (J_{el} - 1)^2 \quad 5-9$$



For this strain energy potential form, the three strain invariants  $I_1$ ,  $I_2$  and  $J$  can be given in terms of the principle stretch ratios  $\lambda_1$ ,  $\lambda_2$  and  $\lambda_3$  as following:

$$\bar{I}_1 = (\lambda_1)^2 + (\lambda_2)^2 + (\lambda_3)^2 \quad 5-10$$

$$\bar{I}_2 = (\lambda_1)^2(\lambda_2)^2 + (\lambda_2)^2(\lambda_3)^2 + (\lambda_3)^2(\lambda_1)^2 \quad 5-11$$

$$\bar{I}_3 = (\lambda_1)^2(\lambda_2)^2(\lambda_3)^2 \quad 5-12$$

The three Mooney-Rivlin coefficients  $C_{01}$ ,  $C_{10}$  and  $J$  can be determined using the experimental data obtained from the experimental testing. In order to determine the parameters  $C_{01}$  and  $C_{10}$ , the convenient way is to supply the Abaqus software with the experimental data taken from the uniaxial compression test in form of tabulated values of the nominal stresses and strains. However, regarding the parameter  $D_1$  which allows for the compressibility to be taken into account the experimental results of the volumetric compression tests are required to be provided in the form of tabulated values of the applied pressure versus the corresponding volume ratios. The pressure applied on the rubber specimen during the uniaxial testing can be calculated as:

$$P = \frac{F}{A_0} \quad 5-13$$

where  $P$  is the applied pressure,  $F$  is the applied force and  $A_0$  is the original cross section area of the rubber specimen. While the volume ratios can be calculated as:

$$\text{Volume ratio } (V) = \frac{V}{V_0} = \frac{\pi r^2 h}{\pi r^2 h_0} = \frac{h_0 - \text{punch displacement}}{h_0} \quad 5-14$$

where  $r$  is the radius of the rubber specimen,  $V$  and  $V_0$  are the final and initial volumes of the rubber specimen respectively,  $h$  and  $h_0$  are the final and initial heights of the rubber specimen respectively. Since any machine has a particular compliance and in order for accurate displacement readings, the compliance of the Instron 3956 machine used for rubber testing had to be eliminated from the displacement data before the calculation procedure explained above. The machine compliance refers to the measured vertical displacement that is usually resulted due to the flexibility of the used machine. In the rubber compression tests, the compliance has a significant role on the test accuracy as the rubber properties acquired using the testing data are sensitive to the measured displacement especially when the rubber specimen suffers a high load such in volumetric compression. The machine compliance was

measured by getting the upper and lower platens in a direct contact with each other, without rubber specimen, a specified load, which was just higher than the maximum load recorded previously for the compression tests, was applied. The same configuration as if a specimen was being tested was adopted for this activity. Afterwards, the experimental data resulting of this test were plotted as displacement versus load, and the displacement, which represents the machine compliance, was expressed as a function of the applied load using a polynomial curvefit. The formula was used to calculate displacement values by substituting the load values obtained from the material compression tests. Then, the calculated displacements were subtracted from the corresponding ones, which are associated to the same load values, obtained from both the uniaxial and volumetric testing.

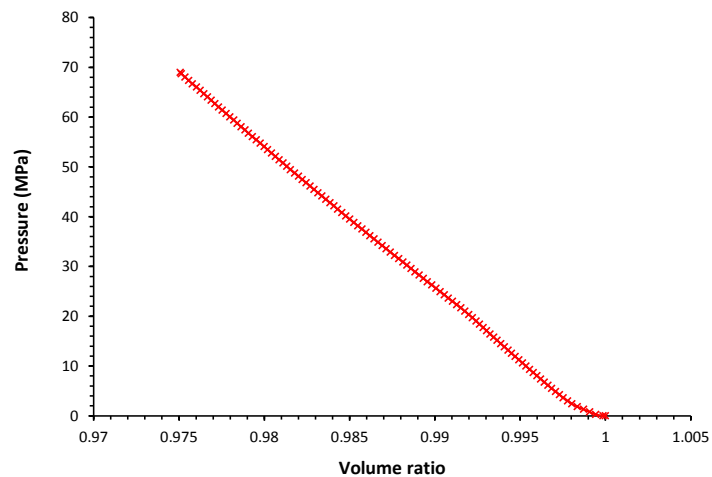


Figure 5-20. Pressure versus volume ratio relationship for rubber 40 Shore A

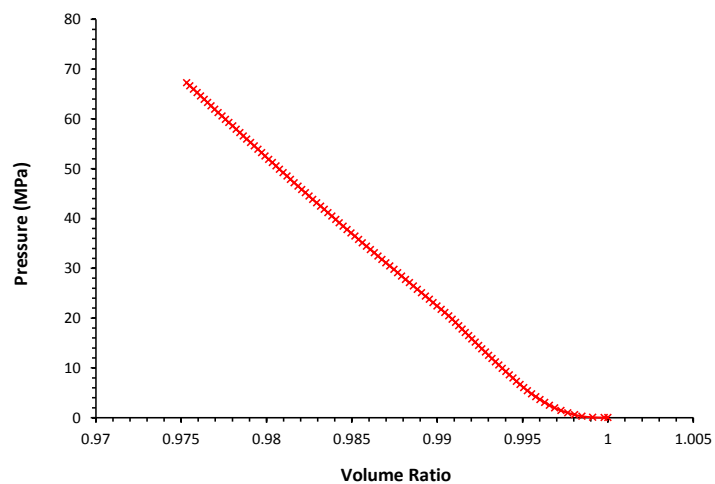


Figure 5-21. Pressure versus volume ratio relationship for rubber 63 Shore A

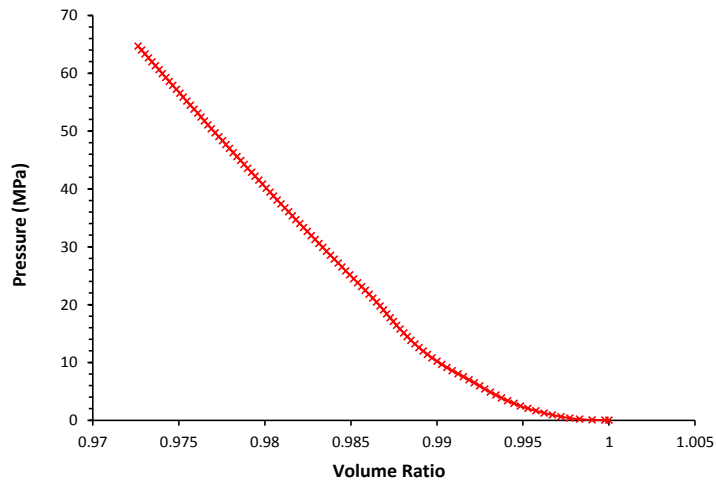


Figure 5-22. Pressure versus volume ratio relationship for rubber 75 Shore A

The final results were used for calculating the nominal stresses/nominal strains of the uniaxial testing and the pressure/volume ratios of the volumetric testing. The relationships between the calculated pressure and volume ratios are shown in **Figure 5-20** to **Figure 5-22** for the rubber materials of Shore A hardness 40A, 63A and 75A respectively. Thereafter, the calculated values of the nominal stresses, the nominal strains, the applied pressure and the volume ratio were tabulated into the Abaqus software to determine the Mooney-Rivlin coefficients  $C_{01}$ ,  $C_{10}$  and  $D_1$  for the rubber materials used. There are two indicators can be used for assessing the relative compressibility of a materials, which are the ratio of its initial bulk modulus ( $K_0$ ) to its initial shear modulus ( $\mu_0$ ) and its Poisson's ratio ( $\nu$ ). The ratio between these parameters can be written in the form:

$$\nu = \frac{3(K_0/\mu_0) - 2}{6(K_0/\mu_0) + 2} \quad 5-15$$

where the Initial bulk modulus ( $K_0$ ) and the initial shear modulus ( $\mu_0$ ) can be calculated as:

$$K_0 = \frac{2}{D_1} \quad 5-16$$

$$\mu_0 = 2(C_{01} + C_{10}) \quad 5-17$$

Table 5-4 presents the mechanical properties of the Polyurethane rubber materials used in this work:

Polyurethane Rubber	Hardness Shore A	M-R Coefficient $C_{10}$ (MPa)	M-R Coefficient $C_{01}$ (MPa)	M-R coefficient $D_1$ (MPa)	Poisson's ratio ( $\nu$ )
Type 1	40	0.22951454	0.107316286	7.4485635E-04	0.499874
Type 2	63	0.586163925	0.146237297	7.7934112E-04	0.499715
Type 3	75	0.94299882	0.310333528	9.5950628E-04	0.499399

Table 5-4. Mechanical properties of different Polyurethane rubber materials

**CHAPTER SIX**

**FE NUMERICAL INVESTIGATION OF MICRO FLEXIBLE  
DEEP DRAWING**

\*\*\*\*\*

## **6.1 INTRODUCTION**

In order for an appropriate optimization for microforming processes of thin sheet metals, it is of high significance to identify the key process parameters that affect the material deformation behaviour at such size scale. This aspect in fact causes researchers to well understand the size effects on micro forming results and also how to successfully control the considered parameters to improve the quality of the obtained products. In this study, the initial gap allocated between the blank holder and the adjustment ring is the main parameter by which parts can be formed with similar final profiles under the influence of specified process parameters. The parameters taken into account in the current work are initial gap, rubber die material, rubber die dimensions, blank thickness and diameter, friction coefficient at different contact interfaces, punch travel and scaling factor. The major objective of investigating the aforementioned parameters is to characterize the effectiveness grade of each of them on the formability of the thin SS 304 sheets and to identify the optimum process conditions that can be ultimately adopted for various applications of micro deep drawing technology. Worthwhile, the influence of each of the considered parameters was studied separately and then the influence of combined process parameters was analysed in order to establish a clear insight on the proposed forming technique.

## **6.2 BASIC CONCEPTS OF FINITE ELEMENT METHOD**

Today one of the most essential and convenient technique that can be used for the computer solution of different complex problems is the finite element method (FEM). The main reason of the great importance of the finite element method is because it can be confidently utilized for a wide variety of engineering fields such as mechanical engineering, civil engineering, biomedical engineering, nuclear engineering, hydrodynamics, heat conduction, geo-mechanics, etc. From other side, several studies proved that the finite element method is a powerful tool for solving differential equations governing different physical problems as well as for simulating various application processes. The basic solution procedure steps of the finite element method, which include the formulating the problem in variation equations, the finite element discretization of these formulations and the assembly of the resulting equations to obtain the effective solutions, are the same whatever the

problem that is under consideration. The finite element procedures provide a quite approach to engineering analysis by using thankfully the digital computers [157]. Therefore, the finite element method can be defined as a numerical solution technique that can be used for solving different problems through formulating them in a form of differential equations. It can be used over a great range of equation and also a great of loading conditions. Moreover, the finite element method can be employed to analysis linear systems and non-linear systems as well as to solve static problems and dynamic problems [158].

In order to clarify what the finite element method means, it can be said that for a particular domain that its behaviour cannot normally be determined by using the analytical procedures, the finite element method is employed to approximate this domain behaviour by idealization. To do that the geometry and behaviour of the domain are represented by a finite number of subdomains called elements. Then, the behaviour of these subdomains can be estimated one by one. For this purpose, a finite number of points are utilized to define and construct the subdomains and the values of the objective equations and their derivatives are specified at these points, called nodal points. Thereafter, the main domain is approximately represented as a finite collection of the subdomains (elements), the finite elements together with the nodal points compose a mesh [159, 160] as shown in Figure 6-1.

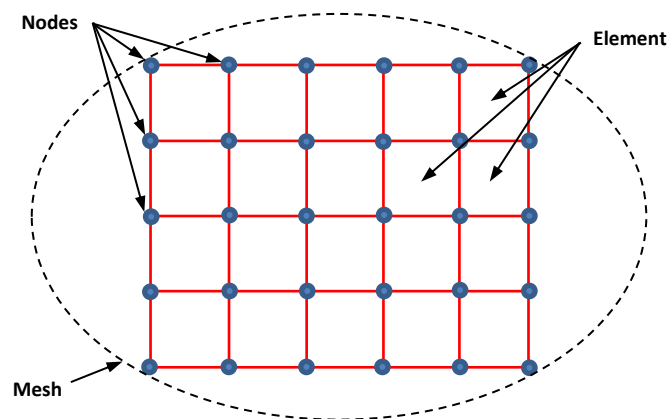


Figure 6-1. Relation of nodes, elements and mesh

### 6.2.1 HISTORICAL BACKGROUND

The first effective approximate solution of the problems related to solid deformation mechanics was presented by Ritz in 1909. The approximation method is based on known functions and unknown coefficients. The unknown coefficients can be determined by solving

the equation sets that are obtained through minimization of functional in relation to each unknown. However, the restriction of the Ritz method was that the resulting functions have to satisfy the boundary conditions of the situation under consideration [157]. In 1943, Courant introduced special linear functions to the Ritz method, which contributed in increasing the possibilities of this method. The linear functions were defined for triangular elements and then the Ritz method was applied for the solutions of torsion problems. Courant found the values of these linear functions at the nodal points of the triangular elements and afterwards the unknowns were determined. The term “finite element” was introduced for the first time in 1960 by Clough. He proposed a finite element method which is similar to the Ritz method together with the modifications presented by Courant [157, 159].

Since 1960, the application of the finite element method for the solution of complex engineering problems has been increasingly growing due to simultaneously the significant development in the digital computers that offer the high computational specifications required by finite element analysis [157, 159].

### 6.2.2 OBTAINING THE STIFFNESS MATRIX

In the finite element method, the quality of the obtained results depends significantly on the element density (number of the finite elements). In other words, the finer mesh, which is composed of finite elements and nodal points, produces more accurate results quantitatively and qualitatively. Nevertheless, as the number of the finite elements and nodal points increases the number of the corresponding objective equations that have to be solved increases as well causing the computation time to be longer [160].

In the case of stress analysis, the parameters such position, displacement, velocity, acceleration and forces are determined at the nodal points (nodes). Whereas, strains and stresses are calculated at the elements. In order to know how formulate the problem in a variational form, it is appropriate to consider the basic element structure shown in **Figure 6-2**:

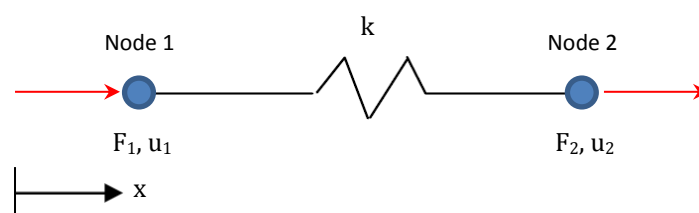


Figure 6-2. Basic element structure



It can be seen in this figure that the main structure element is represented by a spring with two connection points (nodes). The entire system is allowed to move only in the x direction, which implies that there is one degree of freedom for the considered nodes [161]. The relationship between the known forces and the unknown displacements at the nodes affecting on the spring element can be determined as:

$$F_1 = k(u_1 - u_2) = ku_1 - ku_2 \quad 6-1$$

$$F_2 = k(u_2 - u_1) = -ku_1 + ku_2 \quad 6-2$$

Now, in order to obtain the stiffness matrix the equations 6-1 and 6-2 can be written in matrix form as following:

$$\begin{Bmatrix} F_1 \\ F_2 \end{Bmatrix} = \begin{bmatrix} k & -k \\ -k & k \end{bmatrix} \begin{Bmatrix} u_1 \\ u_2 \end{Bmatrix} \quad 6-3$$

the matrix  $\begin{bmatrix} k & -k \\ -k & k \end{bmatrix}$  is the “stiffness matrix” of the system under consideration, which can be written in another form:

$$[k] = \begin{bmatrix} k & -k \\ -k & k \end{bmatrix} = [k_{ij}] = \begin{bmatrix} k_{11} & k_{12} \\ k_{21} & k_{22} \end{bmatrix} \quad 6-4$$

in the resulting stiffness matrix, the component  $k_{ij}$  is defined as an influence coefficient, which represents the response of the element  $j^{\text{th}}$  to the force at the  $i^{\text{th}}$  node [160]. Finally, by using matrix notation, the equation 6.3 can be written in the form:

$$\{F\} = [k]\{u\} \quad 6-5$$

where  $\{F\}$  is the force vector for the given system,  $[k]$  is the global stiffness matrix for the system and  $\{u\}$  is the displacement vector for the system.

### 6.2.3 FORMULATING THE SHAPE FUNCTION

It is of high importance in the finite element analysis to characterize how to relate the nodal response to the total element response. To achieve this activity in term of “nodal displacement”, it can consider the basic element system shown in **Figure 6-3** with the local coordinate system. In order to estimate the influence of the nodal displacement on the element, the so called “shape function” is required to be defined which governs the element displacement.

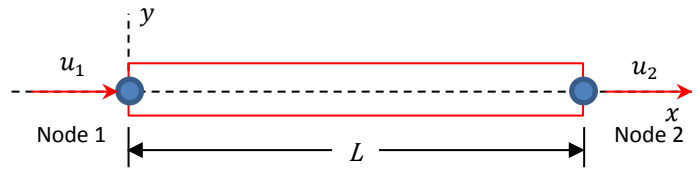


Figure 6-3. A simple element with local coordinate system

It can be assumed that the variation of nodal displacement ( $u_x$ ) is:

$$u_x = \alpha + \beta x \quad 6-6$$

the unknown coefficients ( $\alpha$ ) and ( $\beta$ ) are called the “general coordinates”. These coefficients can be determined by applying the relevant boundary conditions as following:

$$\text{at } x=0 \text{ (node 1)} \quad u_x = u_1 \quad 6-7$$

$$\text{at } x=L \text{ (node 2)} \quad u_x = u_2 \quad 6-8$$

So, substituting equations (6.7) and (6.8) in equation (6.6) results in:

$$u_x = \left(1 - \frac{x}{L}\right) u_1 + \left(\frac{x}{L}\right) u_2 \quad 6-9$$

The later equation can be written as:

$$u_x = N_1 u_1 + N_2 u_2 \quad 6-10$$

The matrix form of equation (6.10) can be written as:

$$u_x = [N] \{u\} \quad 6-11$$

where  $[N]$  is known as the “Local Shape Function” which its components define the weight of the nodal deformation on the element.

#### 6.2.4 TRANSFORMING THE LOCAL SYSTEM TO THE GLOBAL SYSTEM

Understanding the procedure of transforming the local system to the global system imperatively necessitates knowing what the difference between these two coordinate systems is. In general, the location of points in the entire structure can be defined by employing the same coordinate system which is known the global system as shown in **Figure 6-4a**. On the other side, it is of necessity in the finite element method to specify a separate coordinate system for each element for the convenience of deriving element properties. This specified system is usually called the local coordinate system [162].

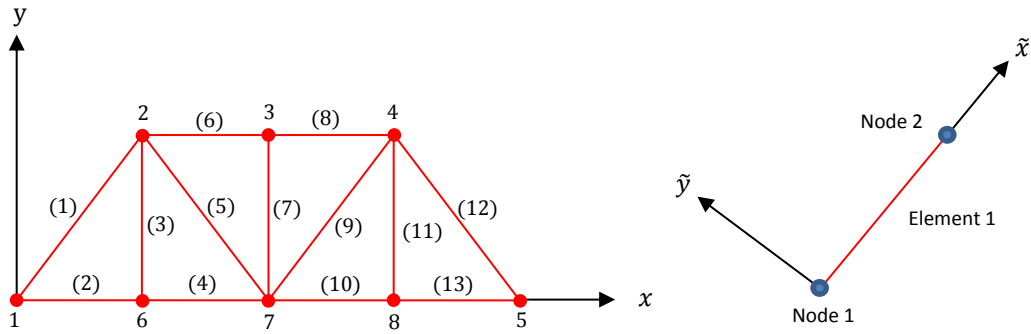


Figure 6-4. (a) Global coordinate system (b) Local coordinate system

The local coordinate system of the element (1) shown in the structure in Figure 6-4a is presented in Figure 6-4b. This section is however because the final objective equation have to be formulated in accordance to the global system. The transformation configuration from the local system to the global system is schemed in Figure 6-5.

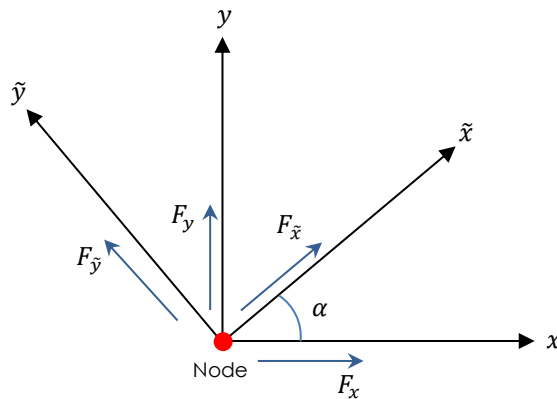


Figure 6-5. Transformation of local coordinate system

In this figure, the local coordinates  $\tilde{x}$  and  $\tilde{y}$  are obtained by rotating the global coordinates  $x$  and  $y$  by the angle  $\alpha$ . The relations of these coordinate systems can be expressed as:

$$F_{x_1} = F_{\tilde{x}_1} \cos \alpha \tag{6-12}$$

$$F_{y_1} = F_{\tilde{x}_1} \sin \alpha \tag{6-13}$$

$$F_{x_2} = F_{\tilde{y}_1} \cos \alpha \tag{6-14}$$

$$F_{y_2} = F_{\tilde{y}_1} \sin \alpha \tag{6-15}$$

The above equations can be written in matrix form as:

$$\begin{Bmatrix} F_{x1} \\ F_{y1} \\ F_{x2} \\ F_{y2} \end{Bmatrix} = \begin{vmatrix} \cos \alpha & 0 \\ \sin \alpha & 0 \\ 0 & \cos \alpha \\ 0 & \sin \alpha \end{vmatrix} \cdot \begin{Bmatrix} F_{\tilde{x}1} \\ F_{y1} \end{Bmatrix} \quad 6-16$$

The general form of the equation (6.16) can be expressed as:

$$\{F\} = [A]^T \cdot \{\tilde{F}\} \quad 6-17$$

where  $[A]^T = \begin{vmatrix} \cos \alpha & 0 \\ \sin \alpha & 0 \\ 0 & \cos \alpha \\ 0 & \sin \alpha \end{vmatrix}$  which is called the "transformation matrix".

The same procedure used above for the force components can be adopted as well for the displacement components, as following:

$$\tilde{u}_1 = u_1 \cos \alpha + v_1 \sin \alpha \quad 6-18$$

$$\tilde{u}_2 = u_2 \cos \alpha + v_2 \sin \alpha \quad 6-19$$

The equations 6-18 and 6-19 can be written in the following matrix form:

$$\begin{Bmatrix} \tilde{u}_1 \\ \tilde{u}_2 \end{Bmatrix} = \begin{vmatrix} \cos \alpha & \sin \alpha & 0 & 0 \\ 0 & 0 & \cos \alpha & \sin \alpha \end{vmatrix} \cdot \begin{Bmatrix} u_1 \\ v_1 \\ u_2 \\ v_2 \end{Bmatrix} \quad 6-20$$

Or in the general form:

$$\{\tilde{u}\} = [A] \cdot \{u\} \quad 6-21$$

Now, substituting equation (6.17) in equation (6.5) yields to:

$$\{F\} = [A]^T \cdot [\tilde{k}] \cdot \{\tilde{u}\} \quad 6-22$$

Thereafter, substituting equation 6-21 in equation 6-22 yields to:

$$\{F\} = [A]^T \cdot [\tilde{k}] \cdot [A] \{u\} \quad 6-23$$

In comparison with equation 6-5, one can deduce that the global stiffness matrix which is [160]:

$$[K] = [A]^T \cdot [\tilde{k}] \cdot [A] \quad 6-24$$

## 6.3 PROCESS SIMULATION BY ABAQUS SOFTWARE

### 6.3.1 INTRODUCTION TO ABAQUS SOFTWARE

Abaqus is regarded a powerful simulation tool that can be confidently used for modelling and analysing a great variety of engineering problems. Abaqus software is not employed just solve problems relatively involve simple linear aspects but it also can deal with those represent the most challenging nonlinear behaviours. A wide range of different element types which can be utilized to model any virtual geometry features are provided by Abaqus. Moreover, Abaqus has an extensive library involving various material models which can define different behaviour modes for the most engineering materials such as metals, rubber, polymers, composites, foams, reinforced concrete and geotechnical materials. Broad variety of engineering problems belonging to diverse areas, such as stress/displacement, heat transfer, thermal management of electrical components, mass diffusion, soil mechanics and piezoelectric analysis, can be simulated and analysed by Abaqus [163]. In the situation of multi-components, Abaqus provides a capability of simulating each component separately associating with definition of an appropriate material model and also specifying component interactions. During the analysis of nonlinear problem, Abaqus adopts a convenient load increment and convergence tolerance so that an accurate solution can be obtained for the considered problem [163].

### 6.3.2 ABAQUS BASICS

The three main stages of any finite element analysis in Abaqus are: preprocessing, simulating and postprocessing. These three stages can be communicated together as in **Figure 6-6**.

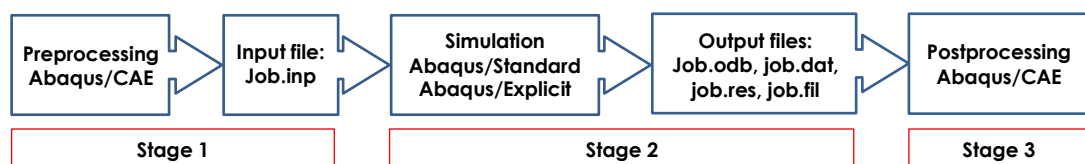


**Figure 6-6.** The main stages of analysis procedure in Abaqus

In the first stage, the preprocessor Abaqus/CAE is used for modelling the physical problem and to create an input file. The simulation stage involves solving the numerical calculations for the fundamental variables of the considered model using one of the main numerical solution approaches Abaqus/Standard or Abaqus/Explicit. The analysis time

required to complete this stage depends on the complexity of the problem under consideration and the specifications of the computer being used. In the last stage, the post processing stage, the evaluation of the final results is generally performed by using the Visualization module of Abaqus/CAE postprocessor. Abaqus offers various displaying options for the obtained results such as colour contour plots, animations, deformed shape plots and x-y plots [163].

### **6.3.3 IMPLICIT AND EXPLICIT NUMERICAL SIMULATION APPROACHES**

The two main solution procedures for the finite element simulations in Abaqus software are Abaqus/Standard and Abaqus/Explicit that can be used for a wide variety of engineering events. For the question of which one of these two procedures is more efficient for a given problem, the answer can be made precisely through well understanding for the characteristics of the implicit and explicit procedures [163].

Abaqus/standard or Abaqus/implicit is defined that the simulation approach which can be efficiently employed for the problems characterized as static and dynamics with low speed conditions. Remarkable accuracy for the quantitative and qualitative results of stress distributions related to the mentioned problems can be obtained from Abaqus/Standard. Abaqus/Standard has the capability of analysing a particular model both in the frequency and time domains. Of the various applications that can be confidently involved in Abaqus/Standard solver are steady-state rolling of a tyre, sealing pressure in a gasket joint and crack propagation in a composite airplane fuselage. On the other side, Abaqus/Explicit is regarded the simulation approach which is extremely effective for brief transient dynamic problems such as ballistic impact, automotive crashworthiness and consumer electronics drop testing. Abaqus/Explicit adopts a solution technique convenient for severe nonlinearity such as the slow crushing of energy absorbing devices [164].

Abaqus/Standard employs the “iteration technique” according to which when the convergence is not obtained for the solution at a particular increment, then one or more iterations will be needed for this increment until attaining the convergence. In some events that may have difficulty converging with Abaqus/Standard due to model complexities weather related to contact conditions or material behaviour, a large number of iterations can be required. This action in turn is expensive in term of time as each iteration includes a large set of linear equation have to be solved. For such cases, the analysis can be more efficient utilizing

Abaqus/Explicit procedure which does not need to iterate to determine the solution but the solution is obtained by explicitly advancing the kinematic state from the previous increment [163]. Therefore, the explicit solution procedure is more effective for reducing the computation time than the implicit procedure.

Both the main solution procedures, explicit and implicit, are frequently used for simulating sheet metal forming processes. However, in order for the solution stability in the explicit method to be obtained, it requires extreme small time steps or artificial adaptations to the model. Another drawback of this method is that the equilibrium is not attained after each time step, causing probably in error in stress distributions and also the product shape can be unrealistic. On the other side, the implicit procedure is characterized by unconditional stability. Reliable results can be produced from this simulation method, since the equilibrium is fulfilled after each time step. The disadvantage of the implicit procedure of increasing the computation time with the model complexity can be estimated by using the iterative solver included in Abaqus instead of the direct solver to solve the linear equations [165].

#### 6.3.4 MODELLING THE MICRO DEEP DRAWING SYSTEM

In this study, FE simulations for micro deep drawing processes of stainless steel (SS304) foils with a flexible rubber die are conducted utilizing the commercial code Abaqus/Standard. Since the deep drawing system used to produce cylindrical cups is normally axisymmetric and due to anisotropic behaviour of the SS304 sheet materials exploited in this work, one FEM quarter model is analysed for the deformable components (blank and rubber pad) involved in the considered system as shown in **Figure 6-7**. This modelling activity is intended in order to enhance the simplicity of the system and to save the computational time as smaller number of elements is required for the simulation of the drawing process. In the case of modelling a system involving multi-contact pairs of components, the rigid surface is always known the master surface whereas the deformable surface is known the slave surface. However, when the two surfaces that are in a direct contact are both deformable and of different materials then the harder one is the master. Otherwise, if both of them are of the same material then the surface with larger area is the master. The very important issue in such situations is to prevent the slave surface from sliding off and falling behind the master surface which turn in causes failing the solution to converge. Therefore, the area of the master surface should be large enough; that is the master surface should be larger than the slave one by a sufficient

area, to avoid this problem. For this purpose, it can be seen in **Figure 6-7** that the diameter of the blank holder is greater than those of the blank, rubber die and even the gap-adjustment ring.

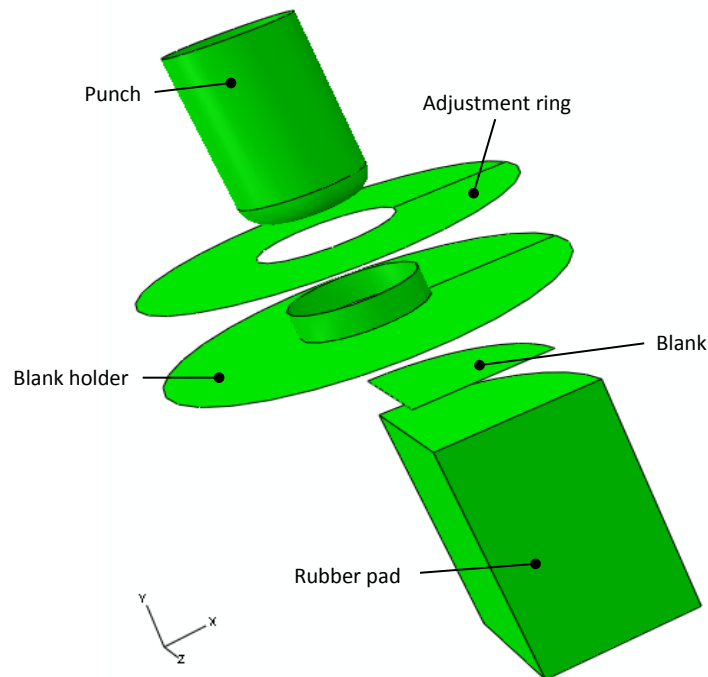


**Figure 6-7.** Scheme of the micro deep drawing system

In accordance with the proposed technique presented in chapter four, all of the punch, the blank holder and the adjustment ring are in general allowed to move in the drawing direction (i.e. along the vertical axis Y) and constrained in the other directions. The cylindrical-shaped rubber pad used in this work experiments as a flexible forming tool is tightly contained in a rigid container. For these conditions to be simulated in the current process model, boundary conditions are defined for the rubber pad so that the nodes on the bottom surface are constrained only in the vertical direction while the nodes on the peripheral side wall are allowed to move only in the vertical direction. On the other side, no constraints are applied on the remaining nodes of the rubber pad model, including those on the upper surface and inside the pad structure, as on their deformation the final geometry of product strongly depends. There are five different contact pairs are simulated in the current model of the micro drawing process. the first pair is between the upper surface of the rubber die and the lower surface of the blank, the second is between the upper surface of the blank and the lower surface of the blank holder, the third is between the upper surface of the rubber die and the lower surface of the blank holder, the fourth is between the upper surface of the blank and the punch surface



and the last one is between the upper surface of the blank holder and the lower surface of the adjustment ring. All these pairs are surface to surface contacts and allow a small sliding between the surfaces. The frictional behaviour of the contact pairs is defined to follow Coulomb's model.

#### 6.3.4.1 FE MODELS FOR PART MATERIALS

In the FE models adopted for the micro deep drawing system in this study, there are two different material models that are defined for the deformable parts. Elastic-plastic material model is utilized to describe the deformation mode of the stainless steel 304 sheets of different thicknesses. This model involves 1260 elements which are four-node doubly curved thin or thick shell, reduced integration, hourglass control elements (S4R) as shown in **Figure 6-8**. It is clear that the blank is modelled with a shell base feature and the thickness is defined in the material module through creating a section for the blank part. It can be seen in **Figure 6-8** that the elements on the side along the x-axis are constrained by the boundary conditions symbolized ZSYMM ( $U_3=UR_1=UR_2=0$ ). These boundary conditions mean that there is no linear motion in translation in the Z-axis direction and no rotation around the x and y axes. Whereas, the elements of the blank model, which are propagated along the Z-axis direction, yield to the boundary conditions symbolized by XSYMM ( $U_1=UR_2=UR_3=0$ ) which refer to no motion along the x-axis and no rotating around the y and z axes.

The uniaxial tensile test in the most simple and common procedure that can be utilized in order to obtain the stress-strain flow curve for sheet metals, which is used in this work as explained in chapter three. However, as is known that the maximum elongation that can be acquired from the tensile test is relatively small due to the necking phenomenon occurring during the testing [166]. In many industrial applications that relate to sheet metal forming processes, the effective strain produced in the sheet material normally exceeds that obtained from the tensile test [113, 121, 166]. Since the deep drawing is categorized one of the sheet metal forming processes that involve high tensile strains especially in the radial direction of the workpiece being formed, the flow curves of the stainless steel 304 sheet adopted in FE model are therefore extrapolated to a maximum true strain of 1.0. The procedure followed to perform to execute this activity is that the true stress-true strain relationships of the sheet materials are acquired directly from the standard tensile tests, and therefore the flow curve of

the plastic deformation regions are extrapolated using Hollomon power law ( $\sigma_f = K \cdot \epsilon_p^n$ ), where  $\sigma_f$  is flow stress,  $\epsilon_p$  is true strain and  $K$  and  $n$  are material constants.

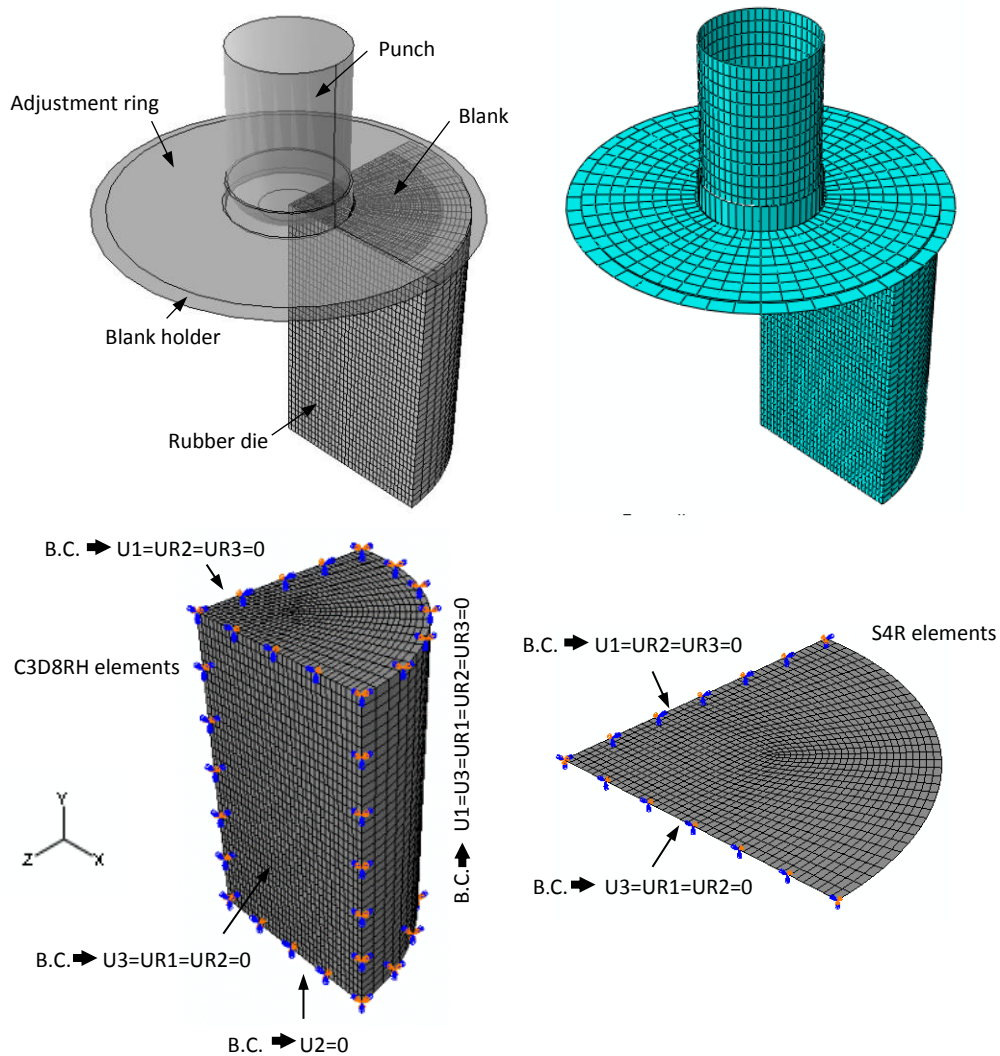


Figure 6-8. FE meshing of the deep drawing components

The deformation mode of the Polyurethane rubber utilized for the flexible forming pads is defined using a hyper-elastic material model. For this purpose, 8100 element are used to build this model. The type of these elements is eight-node linear brick, reduced integration, hourglass element (C3D8RH). The boundary conditions adopted for the pad mode sides parallel to the  $x$  and  $z$  axes are the same mentioned previously for the corresponding sides of the blank model as shown in Figure 6-8. Moreover, in order to control the number of the nodes and elements, all of the punch, the blank holder and the fixing ring are modelled as discrete rigid parts with a shell base feature which do not need material models to be defined.

## 6.4 SIMULATION RESULTS AND DISCUSSION

As mentioned previously, the finite element method (FEM) is regarded an effective simulation method for predicting the deformation response of workpiece materials used in sheet metal forming processes and also for saving the cost and time required for manufacturing operations. In the current study, the working blanks utilized in the micro deep drawing processes are taken from stainless steel 304 sheets which are characterized by anisotropic behaviour.

In **Figure 6-9**, it can be observed the effect of the anisotropic behaviour on the simulation results in terms of final geometry, stress distribution and thickness distribution of the produced parts. This figure shows cups obtained through the simulations achieved using blanks of initial thickness 100 $\mu$ m and diameter of 10mm. These cups are drawn to final depth of 4mm with no initial gap adopted. The geometrical characteristics of the drawing systems utilized here are the rubber pad diameter is 12mm, the rubber pad height is 10mm, the punch diameter is 4mm, and the punch profile radius is 0.8mm. Whereas, the coefficients of friction at the different contact pairs are 0.1 at the blank/holder interface ( $\mu_{BH}$ ), 0.25 at the blank/punch interface ( $\mu_{BP}$ ) and no friction at the blank/rubber pad interface ( $\mu_{BR}$ ).

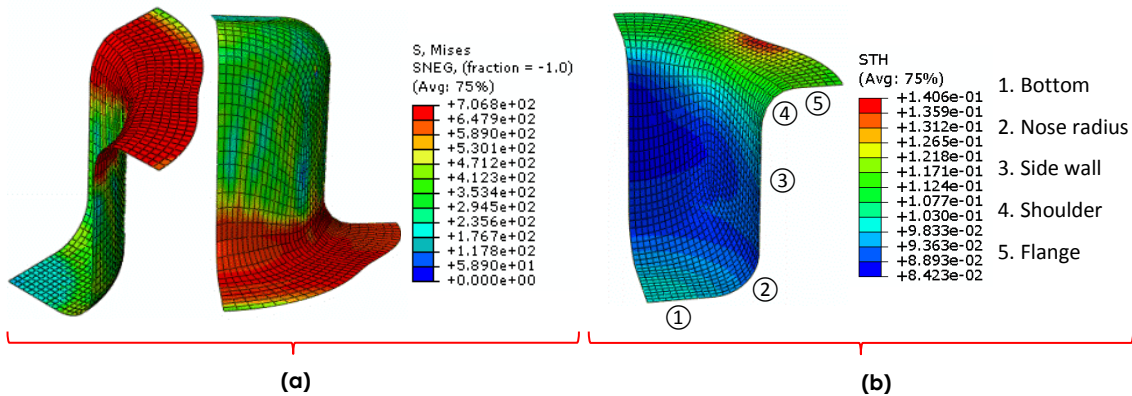


**Figure 6-9. Models of drawn cups obtained from FE simulations (a) Von-Mises stress (MPa) (b) cup thickness (mm)**

**Figure 6-9** reveals that the maximum stresses concentrate at the upper part of the side wall and also at the shoulder corner of the formed cup, while the flange region experiences maximum frictional shear stresses. At a particular stage of the drawing stroke, the side wall of the cup being formed is held at its lower part between the rubber pad and the rigid punch as well as the flange area resists the friction forces with the rubber pad and the blank holder, as shown in the second step of **Figure 4-3**. Therefore, the region in between the side wall and

flange, which involves the upper part of the side wall and the shoulder corner, is subjected to highest tension conditions. Consequently, excessive tensile forces would prevail on these inbetween regions during the forming stroke.

Moreover, the effect of the anisotropic characteristic of the SS304 sheet material on the thickness distribution for the final cups is shown in **Figure 6-10**. In this figure, the thickness distributions along the rolling, diagonal 45° and transverse directions are presented. The first finding in this figure is that the bottom of the formed cup almost remains without changes in thickness. The forming pressure is initially applied on the blank portion underneath the punch nose, and since the friction coefficient at the blank/punch interface is intended to be relatively high, hence the frictional forces excited at this region will overcome any possible relative sliding. This situation implies no high tensile forces are generated at the cup bottom, which keeps the thickness of this region without significant thinning.

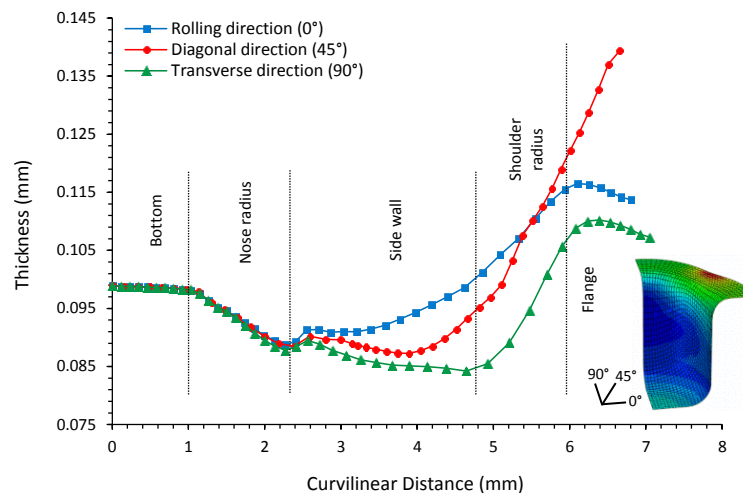


**Figure 6-10.** Thickness distributions at rolling diagonal and transverse directions for a drawn cup

The current technique allows for the blank to form just into a shallow cup in the next step (see **Figure 4-3**), and therefore the cup in this stage undergoes to nearly the same reduction in thickness along the three different directions. Thereafter, once the cup becomes in direct contact with the punch nose corner, the same scenario mentioned above for the bottom region will occur here and then the same interpretation can be adopted for why the differences in thickness at the cup nose remain small. The curves show that the maximum thinning is observed at the transverse direction (90° from the rolling direction); specifically at the upper part of the cup side wall. The result indicates that the rupture region is at the side wall, which is contrary to the conventional deep drawing process where the maximum

reduction in thickness is usually observed at the punch nose radius. This result is due to the excessive tensile stresses concentrated at this critical region, as explained above, which causes an increase in thickness strain.

Figure 6-11 illustrates the distribution of the tensile strains of the produced cup at different radial directions (i.e. rolling, diagonal and transverse directions). It can be noticed that there is no change in the strain values at the bottom portion of the drawn cup as well as no difference in the strain values and distribution trend along the different radial paths adopted in this section. At the corner region of the cup nose, an increase in the strains can be obviously observed in this figure, but in the same tendency along the three directions so that no difference in the strain values between these directions can be recorded. Thereafter, an increase in the radial strains progressively forwards is attained at the side wall portion with higher rate until reaches the maximum values at the upper part of the side wall.

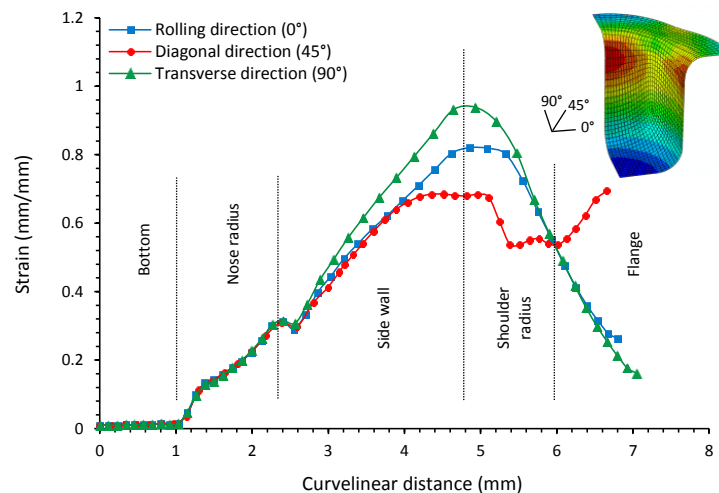
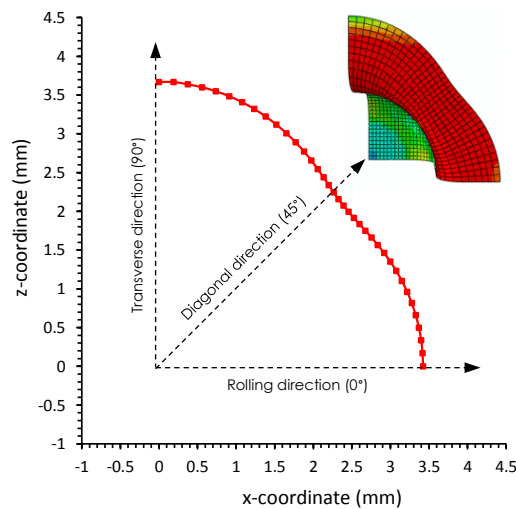


Figure 6-11. Tensile strain distributions at rolling, diagonal and transverse directions for a drawn cup

However, the difference in the strains between the rolling, diagonal and transverse directions commences at the side wall starting from the lower point until reaches the maximum magnitudes at the top portion of the wall. Afterwards, the tensile strains can be observed to decrease drastically over the shoulder corner region for the three radial directions. Nevertheless, it can be seen in Figure 6-11 that the decrease in the strains goes ahead at the flange portion at the rolling and transverse directions. Whereas, at the diagonal direction it can be noticed that that the tensile strain returns again to increase until reaches the maximum value at the last point on the outer periphery. This unexpected increase can be attributed to the high frictional shear stresses excited during the drawing stroke along the

diagonal ( $45^\circ$ ) direction. As is seen in the figure that the radial length of the flange portion along this direction is the shorter compared to that along the rolling and transverse directions. This observation indicates that the flange portion along the diagonal direction slips between the blank holder surface and rubber pad surfaces for a longer distance which implies higher frictional forces (see **Figure 6-12**). This action is due to the difference in the strength of the blank material along the three radial paths considered in this investigation.



**Figure 6-12. Flange region profile**

#### 6.4.1 INITIAL GAP

In order to study the effect of the initial gap, allocated between the blank holder and the adjustment ring, on the quality of produced cups, five cases of different initial gaps -100, -50, 0, 50 and  $100\mu\text{m}$  are investigated under the same process conditions in this section. The drawing system utilized for this purpose is composed of a rubber pad of 12mm diameter and 10mm height, a punch of 4mm diameter and 0.8mm nose corner radius. The coefficients of friction at the different contact interfaces are 0.1 at the blank/holder interface, 0.25 at the blank/punch interface and no friction at the blank-rubber interface. The final profiles of the cups obtained from the numerical models are illustrated in **Figure 6-13**. All of these simulated cups are drawn to final height of 4mm which refers to aspect ratio of 1. It can be seen some differences in the geometrical aspects between the profiles of the produced cups in terms of the shoulder corner radius. It can be seen that increasing the initial gap results in a larger radius for the cup shoulder. Another observation is that the heights of the final cups are slightly different where the cup height increases by the same value of the adopted initial gap.

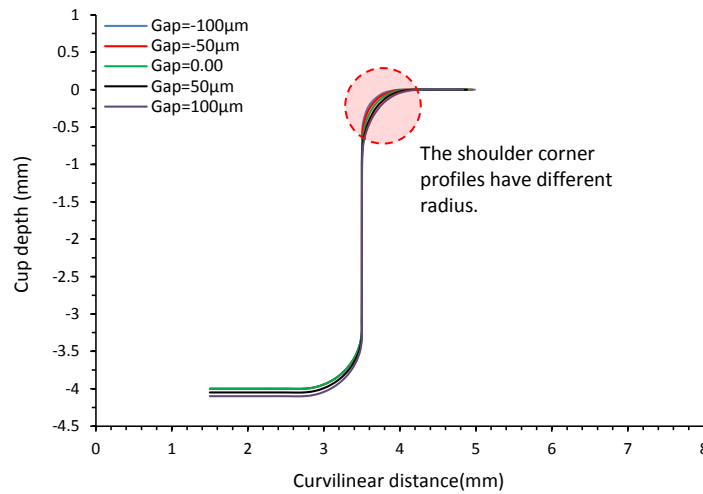


Figure 6-13. The profiles of the final cups drawn with different initial gaps

These observations can be explained that as the initial gap increases more of the sheet material at the flange portion will be allowed to flow into the flexible cavity of the rubber pad. Also, this activity reduces the effect of the constraining conditions on the rubber pad material through allowing it to expand over bigger space corresponding to the increase in the gap.

The thickness distributions along the rolling, diagonal and transverse directions predicted by the simulations of drawing process with different gaps are presented in Figure 6-14, Figure 6-15 and Figure 6-16 respectively. In general, the curves denote that the general tendency of the increment and decrement in cup thickness is the same. The very common feature between all the curves presented in these figures is that no remarkable difference can be seen in the thickness values and even the distribution trend at the bottom and the nose corner radius of the produced cups.

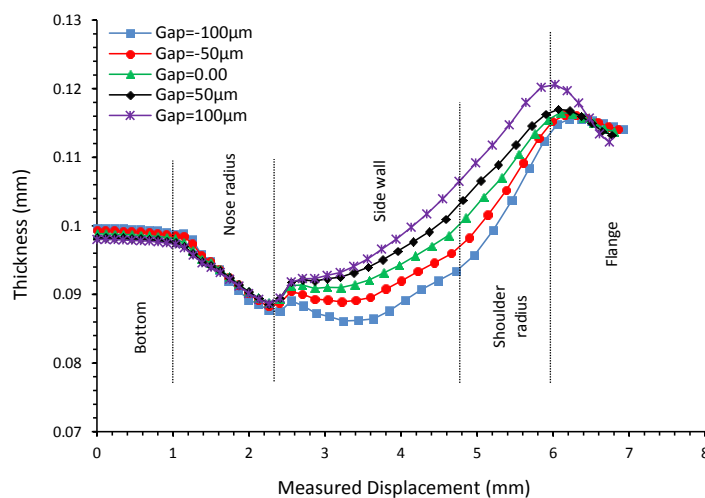


Figure 6-14. Thickness distribution along the rolling direction for cups drawn with different gaps

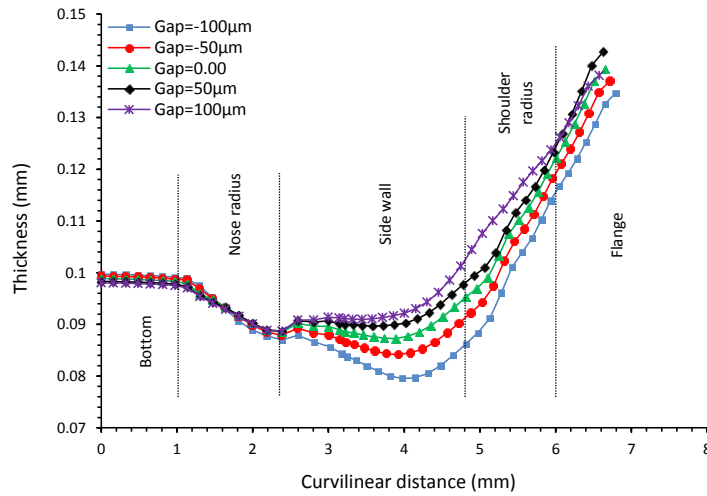


Figure 6-15. Thickness distribution along the diagonal direction for cups drawn with different gaps

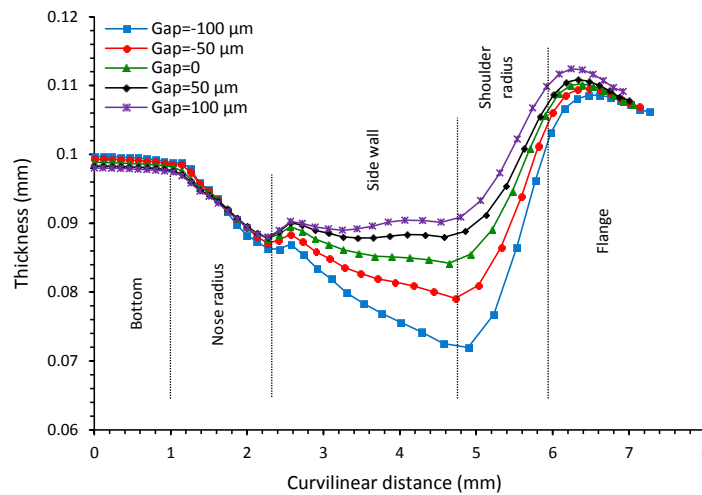
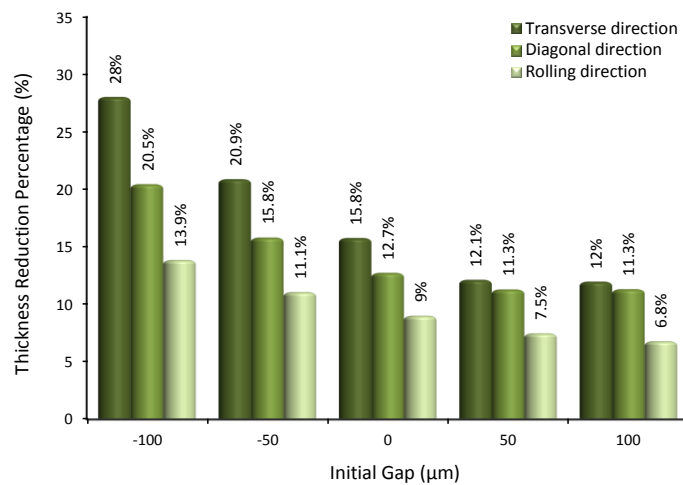


Figure 6-16. Thickness distribution along the transverse direction for cups drawn with different gaps

This finding detects that the initial gap value has no influence on the reduction in the thickness at these regions. However, it can be seen that reducing the initial gaps causes an increase in the thinning highly at the side wall compared to the other parts of the formed cups. If one examines the three groups of curves shown in these three figures, it can be deduced that the rate of thinning at the side wall region that corresponds to the decrease in the initial gap is higher for the curves that represent the thickness distribution along the transverse direction with respect to the other two directions. Moreover, the curves presented in these three figures show that the thickness distribution are fluctuating from the nose corner until the flange region. It can be observed from **Figure 6-14** that the maximum thinning for the cups drawn with the adopted initial gaps are located at the nose corner region except the one with  $-100\mu\text{m}$  where the maximum thinning at the side wall.



On the other side, in the **Figure 6-15** and **Figure 6-16**, the maximum reduction in thickness acquired with 50 $\mu$ m and 100 $\mu$ m initial gaps occurs at the nose corner region while with the other gaps, it found at the side wall. At the side wall, the rate of thickness reduction increases with reducing the initial gap, and consequently the particular initial gaps identified just above are enough to cause the thinning at the side wall to exceed that at the nose corner. The percentages of the maximum reductions in the thickness of the cups drawn with the gaps adopted in this investigation are exposed in **Figure 6-17**.



**Figure 6-17. The maximum reduction in thickness at the transverse direction using different initial gaps**

The results for the thinning along the transverse direction detect that the maximum reduction in the side wall thickness increases from 11.9% to 15.8% by reducing the initial gap from 0.1mm to 0. The interesting attention is that just at this level of initial gap the location of the maximum thinning changes from the nose radius to the upper part of the side wall for the final cups. Moreover, an increase in the thickness reduction from 15.8% to 28% is obtained with reducing the gap from 0 to -0.1mm as seen in **Figure 6-17**. Thereafter, the thickness of the produced cups starts to noticeably increase at the shoulder corner region so that becomes greater than the initial thickness of the original sheet. Afterwards, the thickness progressively increases until reaching the maximum thickening at the flange region.

These issues can be interpreted if it is realized that reducing initial gap implies restricting the rubber pad more and more. As a result of the rubber compressibility, smaller gap causes the hydrostatic pressure applied by the rubber pad, which is in fact regarded blank holding pressure in the current technique, on the blank increases. Thereby, higher tensile stresses therefore generate in the sidewall and shoulder corner of the cup being formed through the

drawing operation, resulting in increase of thickness reduction which leads to failure by fracture. Therefore, it can be said that formability of the workpiece can be improved by adopting higher initial gaps. However, it should be realized that the gap values are limited where the results reveal that using a gap of  $\geq 0.11$ mm produces wrinkling around the shoulder radius. Another finding is that the maximum thickening is at the flange region, and this issue is due to the friction forces at the blank holder interface. These friction forces sweep away the material at the flange against the drawing direction towards the blank rim, and this situation results in increasing the thickness of this region. As a result, it can be induced that the highest rate of the thickness reduction at the side wall region is obviously obtained along at the transverse direction while the smallest rate is at the rolling direction.

On the other side, **Figure 6-18** to **Figure 6-20** illustrate the strain distributions along the rolling, transverse and diagonal directions respectively that are obtained from the simulations of deep drawing processes using the different initial gaps mentioned above. The two groups of curves shown in **Figure 6-18** and **Figure 6-19** reveal similar features in terms of increments and decrements of strain values. It is clear that there is no change in the strain status at the bottom portions of the products, whereas the strain remarkably increase starting early from the nose corner and keep this increase rate over the side wall regions until reaches the maximum value. Afterwards, the strain value declines dramatically over the shoulder corner and flange regions. The curves presented in **Figure 6-18** report that reducing the initial gap has no significant effect on the strain status (i.e. strain values and distribution) along the rolling direction. However, this action is not seen for the strain distribution along the transverse direction, where the curves detect that reducing the initial gap cause an increase in the strains noticeably for the maximum values at the upper part of the side wall. Regarding the stain distribution along the diagonal direction, like in **Figure 6-18** and **Figure 6-19**, the curves in **Figure 6-20** indicate that no change in the strains at the bottom region and however an increase in noticed in the strains over the node corner and the side wall at which the maximum values are obtained for all initial gaps.

Also, one can find that as the initial gap is reduced the maximum strain increases. The interesting finding is that although the strain curves show an obvious dropping down, they return again to increase over the flange region overlapping each other. This action can be attributed to the high frictional forces excited at the flange region at the diagonal direction as rationalized previously, which result in excessive shear strains.

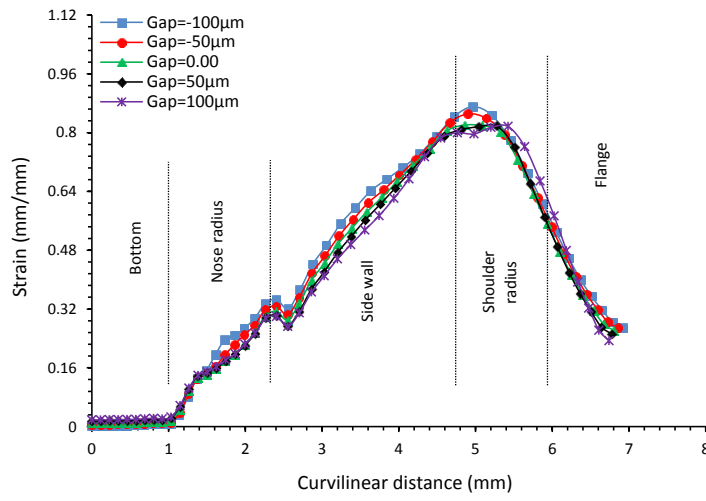


Figure 6-18. Strain distribution along the rolling direction for cups drawn with different gaps

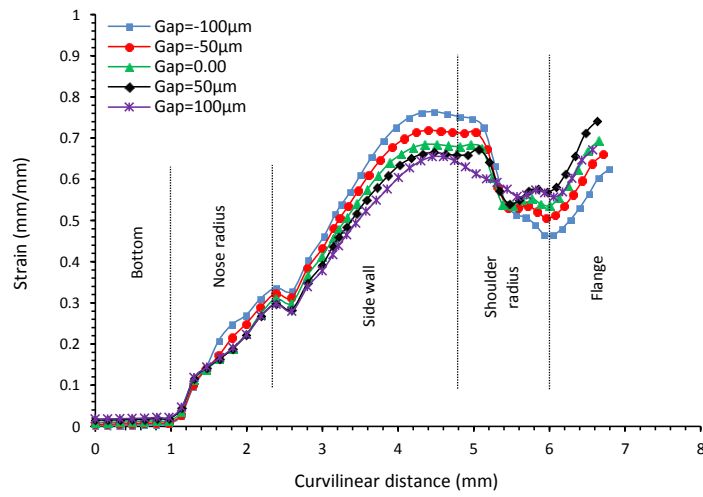


Figure 6-19. Strain distribution along the transverse direction for cups drawn with different gaps

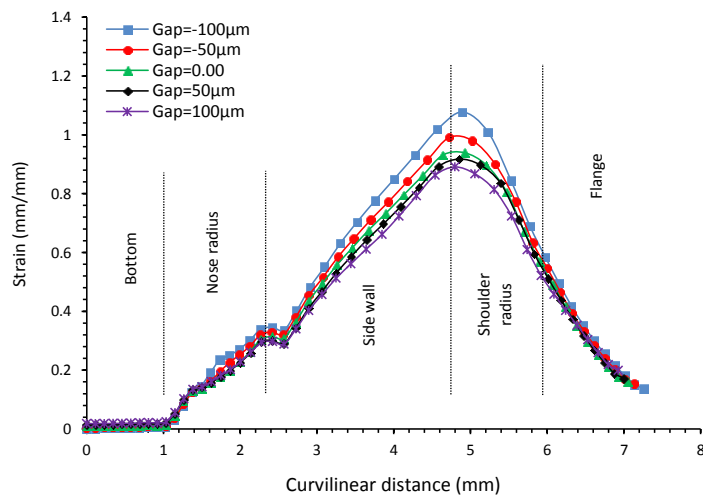
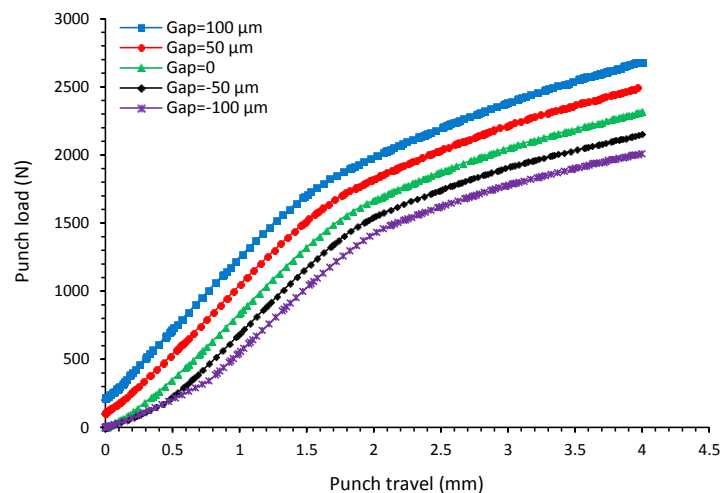


Figure 6-20. Strain distribution along the diagonal direction for cups drawn with different gaps

It can be deduced that the strain distributions can be regarded as reflections for the distribution modes of the thickness stains. In other words, the thickness distributions provide an evident indication on the main features of the strain distribution curves. It can be observed in the results revealed above that wherever high reductions in thickness; that is high thickness stains, are obtained then high tensile strain would be found as well as vice versa as at the at the side wall regions. Therefore, the attitude of the strain distribution can be well understood through realizing the thickness distribution at any [articular direction. **Figure 6-21** shows the punch load-travel relationships obtained from simulations of micro deep drawing using the different initial gaps mentioned previously. The figure reveals that the punch load increases throughout the drawing stroke until a completed cup is obtained.



**Figure 6-21. Punch load-travel relationship for different initial gaps**

However, this increase is actually observed in different rates; that is the punch load-travel curve has different slopes, which depend relatively on the initial gap values. For example, the curve represents the punch load-travel relationship with initial gap of 100μm has three slopes. The first one is due to deforming the blank and the rubber pad through the initial gap, the second slope, for which the increase rate of the load value is the highest, is due to drawing the blank is achieved when no gap is remaining, whereas, the third slope is due to forming the final profile of the cup before which the flange area is significantly decreased resulting in high reduction in the frictional forces there. For this action, it can be noticed that the rate of the increase in the punch load is remarkably lower than that of the previous stage. Nevertheless, the contribution of the first slope in the whole drawing stroke decreases gradually with reducing the initial gap used until disappears completely at -100 initial gap. Also,

another finding in the figure is that the two curves that represent the punch load-travel relationships with the negative gaps start at particular values for the punch load that are 103.83N and 214.47N for the gaps of  $-50\mu\text{m}$  and  $-100\mu\text{m}$  respectively. This result can be rationalized that the negative gaps imply that both the blank and the rubber pad are initially subjected to a certain pressure applied by the blank holder as explained previously in chapter five. Due to this pressure, the punch experiences an initial reaction just once contacts the blank surface whereupon the drawing load is required to be increased to overcome this reaction first before the actual drawing stroke. Furthermore, it can be noticed that the maximum value of punch load decreases with increasing initial gap.

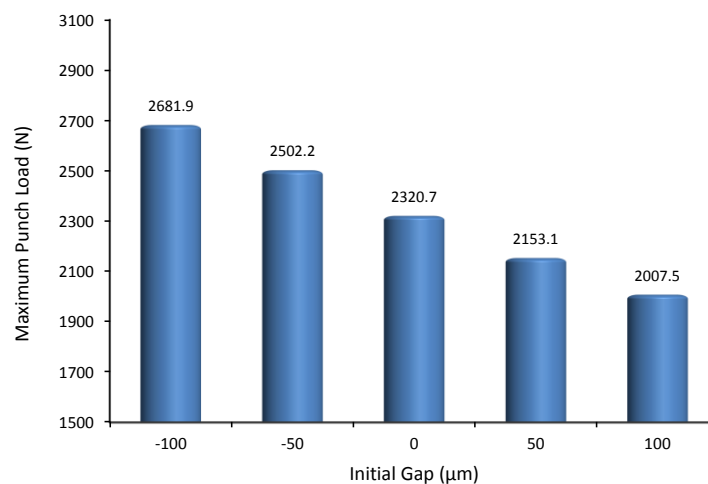


**Figure 6-22. Maximum punch load values obtained from simulations using different initial gaps**

The results demonstrate that the maximum load decreases from 2320.7N for no initial gap case to 2007.5N for initial gap of 0.1mm. Moreover, using a negative gap of  $-0.1\text{mm}$  increases the maximum load to 2682N from 2007.5N for initial gap of 0.1mm as seen in **Figure 6-22**. On explanation of the results above, it can be said that as the initial gap increases, the blank and the rubber pad will have larger space to deform just against the supporting spring. This situation will allow drawing as much as possible of the blank material from the flange region into the rubber die cavity before the blank holder reaches the fixing plate, and therefore the area of the flange region reduces increasingly during the drawing stroke. As a result of that, the friction force at the blank/holder and blank/rubber pad interfaces will decrease which leads to reduction in the maximum tensile stresses generated in the blank. Consequently, thinning and the maximum punch load will be reduced.

### 6.4.2 RUBBER DIE MATERIAL

In this study, three different types of Polyurethane rubber are utilized for the flexible forming die in the micro deep drawing processes. The influence of using these rubber materials on the drawing characteristics in terms of process requirements and product quality is investigated in details in this section through FEA simulations. As is mentioned before, in order for the rubber materials to be modelled in the FE simulation achieved using Abaqus-Standard, the hyperelastic behaviours and the compressibility of these materials are required to be defined.

Parameter	Value
Punch diameter	4mm
Punch nose radius	0.8mm
Blank diameter	10mm
Blank thickness	100 $\mu$ m
Rubber pad diameter	12mm
Rubber pad height	10mm
Blank-Holder friction coefficient ( $\mu_{BH}$ )	0.1
Blank-Punch friction coefficient ( $\mu_{BP}$ )	0.25
Blank-Rubber friction coefficient ( $\mu_{BR}$ )	0
Drawing velocity	0.1mm/sec

**Table 6-1. Process parameters for micro deep drawing simulations using different rubber materials**

Therefore, the contribution of these two properties in the forming mode of Polyurethane rubber and their effects on the final product quality are analysed separately. The process parameters listed in the following table are adopted for the FE simulation of micro deep drawing processes intended in **Table 6-1**. In other word, the Shore A hardness and the Poisson's ratio of the rubber materials are the most important properties needed in the FE models, which play a strong role in predicting the deformation behaviour of these materials.

#### 6.4.2.1 RUBBER TYPE

The three types of rubber materials used here in the FE simulations to model the flexible tool are characterized by different hardness values of 40, 63 and 75 Shore A. To investigate the effect of rubber material on the micro deep drawing quality of SS304 blanks, the process parameters presented in **Table 6-1** are adopted.

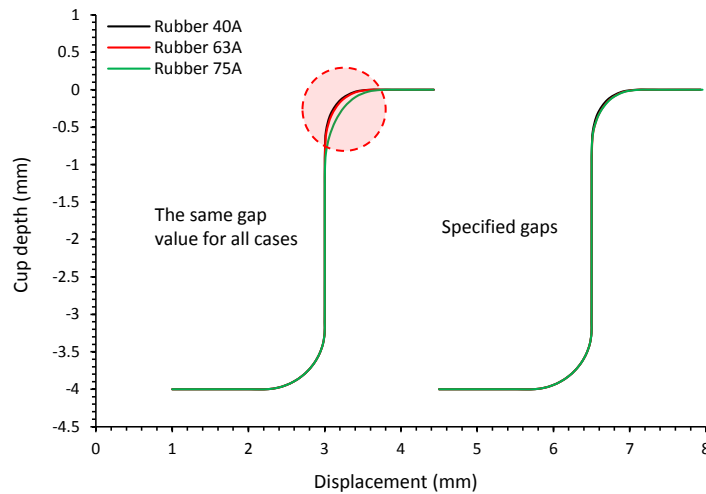


Figure 6-23. Profiles of the final cups produced through simulations using different rubber die materials

The first drawing attempts are carried out with no initial gap using flexible dies made of the three different rubber materials. The results indicate that the cups produced with pads of 40A and 63A hardness have the same final profile, and however the one with rubber of 75A is slightly shallow at its shoulder radius as shown in Figure 6-23. This issue is due to the rubber of 75 Shore A has the lowest Poisson’s ratio (as seen in Table 5-4) which implies the higher compressibility compared to the other two rubber materials. Therefore, the pressure excited in this rubber pad is consequently not enough to produce a cup of profile similar to that obtained using rubber 40 and 63A.

In order to establish a correct comparison between the different rubber materials, an initial negative gap of 100µm (i.e. the second drawing technique, proposed in chapter four, is utilised for the this case) is adopted for the drawing process simulation with rubber pad of 75A to produce a cup with final shape similar to that obtained of the other rubber pads as illustrated in Figure 6-24.

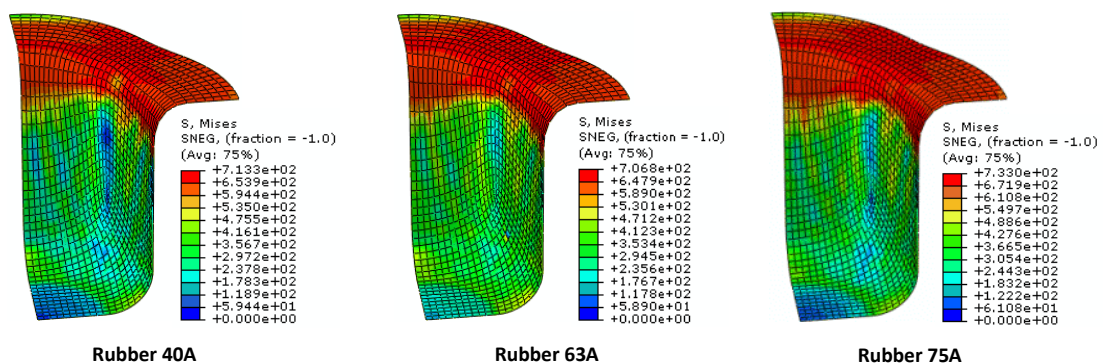
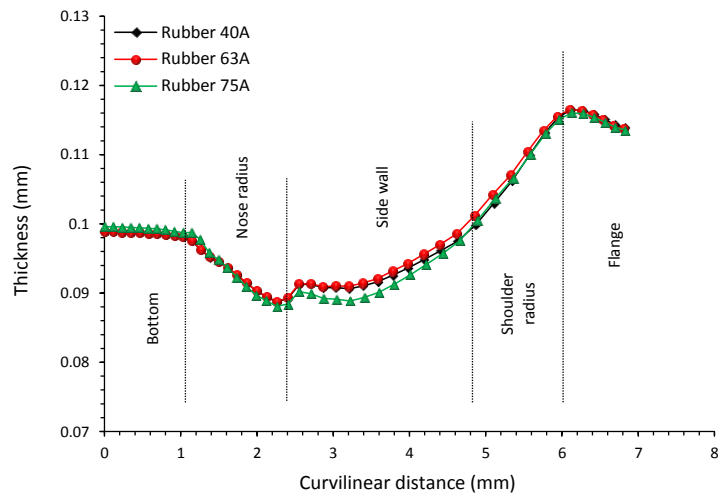
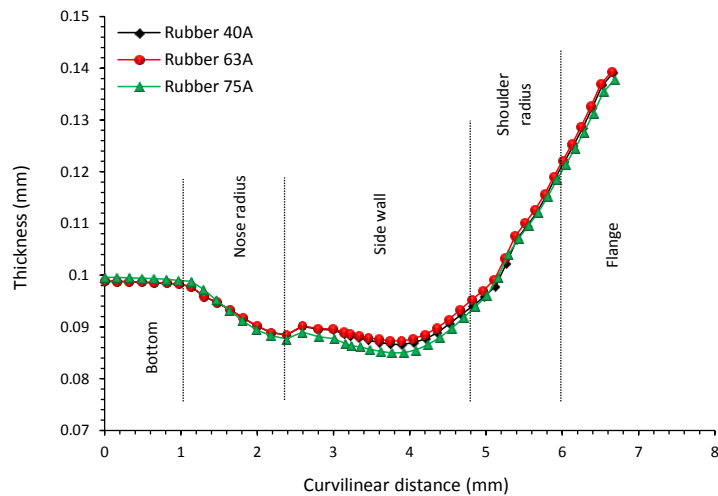


Figure 6-24. Stress distribution obtained from simulation for different rubber materials

In this figure, it can be observed that using different rubber materials for the forming pad tool has no significant influence on stress distributions, where the maximum stresses concentrate at the flange portion and shoulder radius for all cases. The thickness distribution along rolling, diagonal 45° and transverse directions for cups formed using different rubber materials is exhibited in **Figure 6-25** to **Figure 6-27**. It is clear that each group of the curves presented in these figures have the same tendency of the basic features, and very small differences in the thinning values can be observed at the sidewall regions of the products for all directions. These figures expose that the maximum reduction in thickness of the cup produced by using any one of the used rubber materials occurs at the side wall region along the transverse direction.



**Figure 6-25.** Thickness distribution along the rolling direction using different rubber materials



**Figure 6-26.** Thickness distribution along the diagonal direction using different rubber materials



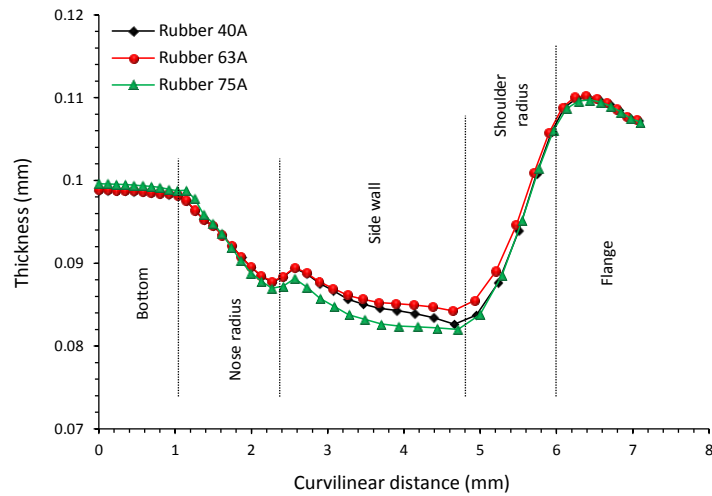


**Figure 6-27.** Thickness distribution along the transverse direction using different rubber materials

For the three groups of curves illustrated in these figures it can be obviously seen that the lower curve is always that obtained with using the rubber material 75A corresponding to the shallow product at the shoulder corner. Thereafter, in accordance to the results related to the wall thickness quality of the obtained products, one can indicate that the best rubber material which can be used for the forming die in this case is rubber 63A which results in minimum thickness reduction of 15.7% in return 17.4% and 18% with 40A and 75A respectively.

**Figure 6-28** demonstrates punch load-travel relationships for the micro deep drawing operations that are carried out using the different flexible tool materials referred to before with no initial gap for 40A and 63A, and  $-100\mu\text{m}$  for 75A. In general, the curves in this figure exhibit similar features related to the distribution mode of the punch load. However, in terms of load magnitudes it is obvious that the curve obtained with using rubber 75 Shore A is higher than the others by approximately the same difference over the whole drawing stroke. As a result, the highest punch load of 2468N is obtained when the rubber 75A is used; 2294N and 2320.7N are acquired with using 40A and 63A rubber materials respectively. It can be realized that the reason behind this action is the initial negative gap  $-100\mu\text{m}$  adopted with the rubber die material 75 Shore A, where the punch load-travel relationships produced by using the same rubber materials but with the same condition of no initial gap refer to different results as shown in **Figure 6-29**.

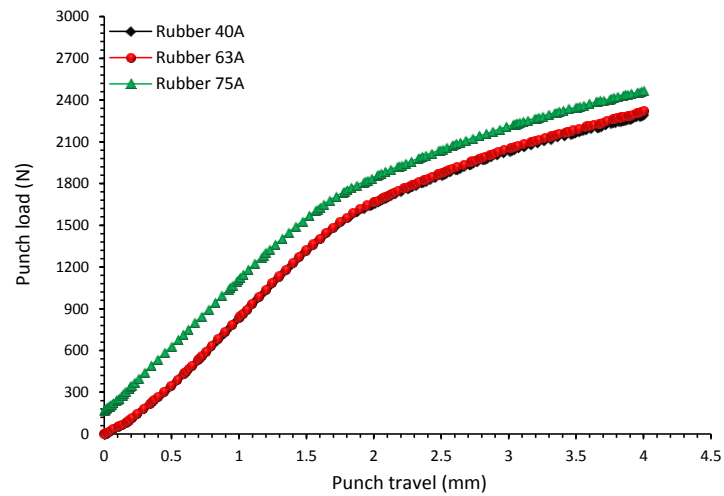


Figure 6-28. Punch load-travels relationships obtained of using different rubber materials and initial gaps

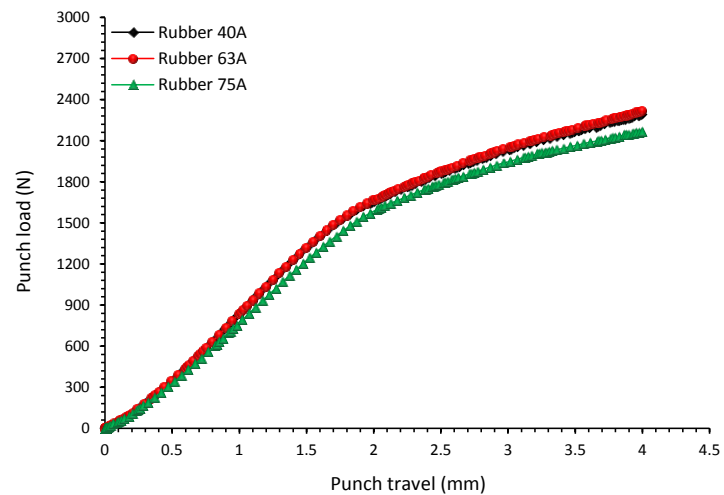


Figure 6-29 Punch load-travels relationships obtained of using different rubber materials with no initial gap

This figure detects that the lower curve represents the punch load-travel relationship for the drawing process achieved using the rubber 75A. The initial negative gap or the initial compression applied initially on the rubber pad generates an initial pressure inside the rubber material itself, which plays a role of reaction pressure on the rigid punch at the beginning of the drawing process and its value depends on the compressibility of the rubber material. This pressure increases correspondingly with the punch stroke during drawing operation.

#### 6.4.2.2 RUBBER HARDNESS

In the previous section, the influence of rubber materials is actually referred by the mechanical properties, that are Shore A hardness and compressibility, specified for each

rubber type in FE simulations in terms of the hyperelastic factors and Poisson's ratio reported in chapter five. The Polyurethane rubber materials utilized for the flexible die in this work are intended to have different Shore A hardness ranging from the soft rubber of 40A to the harder one of 63A and to the hardest rubber of 75A. In accordance to the results obtained for the used rubber materials through the compression tests presented in chapter five, it can be observed that these materials have different hyperelastic behaviour factors as well as different Poisson's ratio values. Therefore, all these characteristics contributed in acquiring the results revealed in the above section. The imperative issue that has to be clarified in this case is how effective are each of these characteristics on this contribution. In other words, how the role that each of these characteristics plays on the final results can be recognised. To answer these enquires, the influence of hardness and compressibility of the rubber materials used in the current study are investigated separately.

Regarding the rubber hardness, the deformation behaviour of the flexible drawing die models in FE simulations are defined using the same Poisson's ratio of 0.499715 (as it intermediates the values obtained for the different rubber material) but with different hyperelastic factors. The FE simulations considered for this investigation are implemented with employing the process parameters presented in **Table 6-1**. Under these conditions, the rubber hardness with the values 40, 63 and 75 Shore A becomes consequently the dominant parameter that controls the rubber material behaviour as well as identifies the final results of the micro drawing process. **Figure 6-30** presents three cups obtained from numerical models using different rubber hardness with no initial gap. It can be seen in this figure that the cup drawn successfully until the entire stroke of 4mm is only the one produced utilizing the rubber die of 63A, whereas wrinkled cup at 2.95mm stroke and fracture cup at 3mm stroke are obtained with of 40A and 75A rubber hardness respectively.

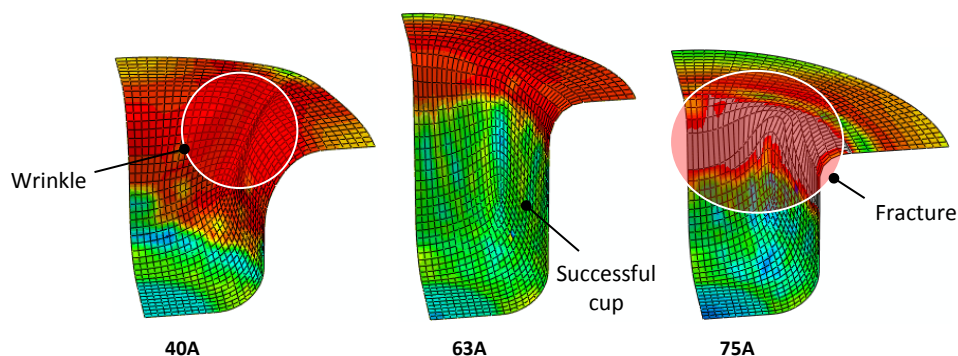
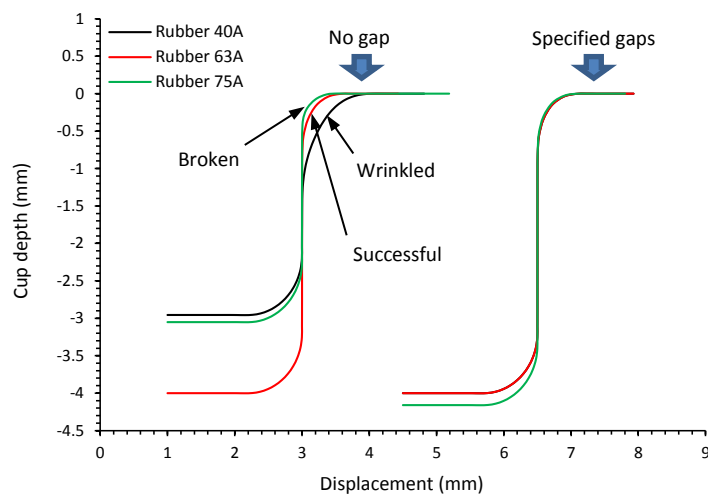


Figure 6-30. Cups Obtained from numerical simulations with different rubber hardness

In the current proposed technique illustrated in chapter four, step 2 of the drawing process exposed in **Figure 4-3** is the most crucial forming stage which identifies whether a complete cup could be drawn successfully or not. As is seen in this figure, the shallow shoulder of the cup being formed is not supported but just by the rubber die at its lower surface. Therefore, under given working conditions, the rubber material is highly responsible on the safety of this region of any failure mode. Hence, the results exposed in **Figure 6-30** can be rationalized that the rubber material of 40 Shore A hardness is very soft with which it cannot overcome the probable occurrence of wrinkling at the shallow shoulder of the cup during the drawing process. On the other side, the hardness of 70 Shore A makes the rubber material to be very tough so that causes an excessive deformation for the cup during the intermediate drawing stage as can be noticed in **Figure 6-31**.



**Figure 6-31. Final profiles of cups obtained from simulations**

Also, the nature of this hard rubber material compels the flange portion of the blank under forming to experience severe contact conditions between its hard surface and the rigid holder surface. This action results in extreme tensile forces at the upper half of the side wall as well as at the shoulder corner, which may lead to failure by tearing as happened for the cup (c) in **Figure 6-30**. If the cup formed using rubber 63A is considered as a reference, then the second micro drawing strategy that adopts negative initial gap is required for the process simulation with rubber material 40A and the first strategy that adopted positive initial gap for the process simulation using rubber material 75A. In order to produce cups of profile similar to that obtained with using rubber material model of 63 shore A hardness, gaps of  $-550\mu\text{m}$  and  $160\mu\text{m}$  are adopted with rubber 40A and 75A respectively. The final profiles of the successful

cups produced through FE simulations adopting these specified gaps are illustrated in Figure 6-31. Figure 6-32 to Figure 6-34 reveals the thickness distribution of cups obtained from FE simulations adopting rubber material models of 40, 63 and 75 Shore A hardness respectively. The results show that the basic trend of the curves is same, where the maximum thinning occurs at the sidewall along the transverse direction ( $90^\circ$  to the rolling direction). Nevertheless, the best results are obtained when using the harder rubber pad of 75A where the maximum reduction in thickness is 13.75%, in return of 15.77% and 20.49% due to using 63A and 40A rubber hardness respectively. From these resultant values, it can be observed that the difference between the maximum reduction percentages in thickness obtained with using 63A and 75A rubber hardness is significantly smaller than that obtained with using 40A and 75A rubber hardness.

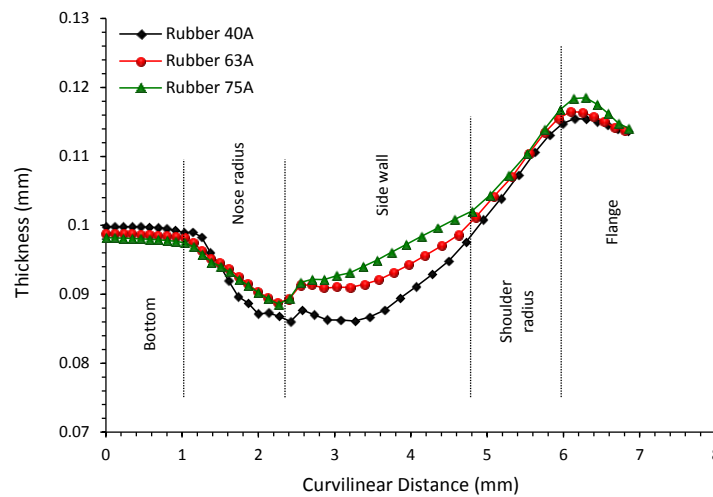


Figure 6-32. Thickness distribution along the rolling direction with using different rubber hardness values

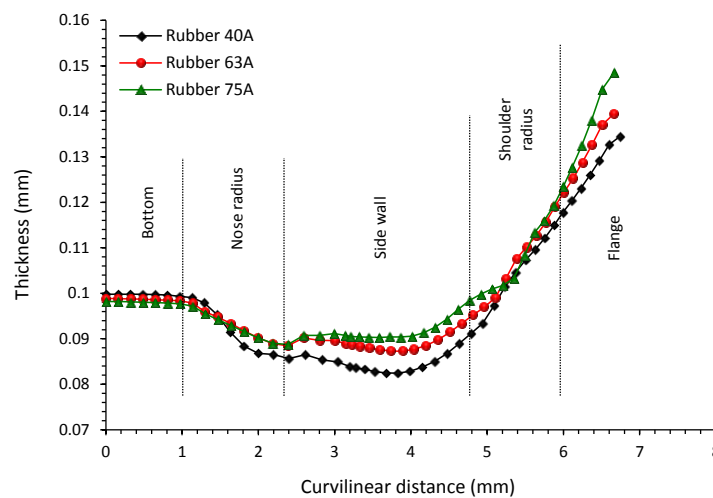
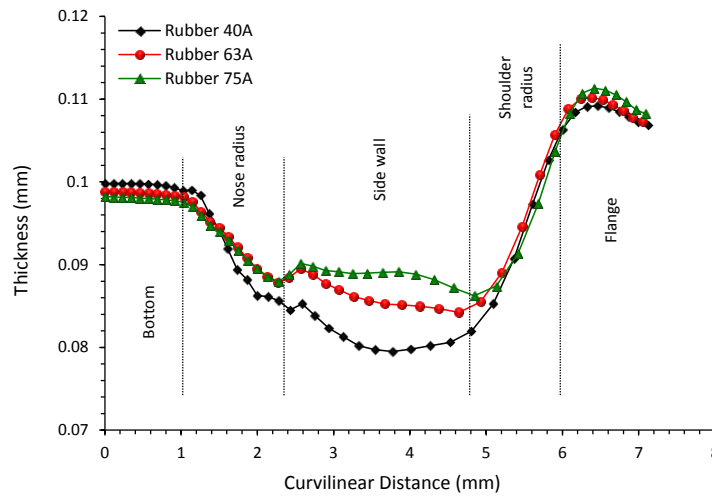


Figure 6-33. Thickness distribution along the diagonal direction with using different rubber hardness values



**Figure 6-34. Thickness distribution along the transverse direction with using different rubber hardness values**

When these results are compared with that obtained with no initial gap, an opposite configuration for the results can be detected. The positive gap utilised with 75A rubber hardness results in producing a cup with the best quality in terms of the reduction values in thickness, whilst a broken cup is produced with no gap. It is clear that the curves represent the thickness distributions acquired with 75A rubber hardness are the higher at the three different directions shown in the figures. On the other hand, the negative gap adopted with 40A rubber hardness causes the acquired curves for the thickness distribution to be lower, which refer to worse thinning. It can be deduced that the reasons for these results are the hardness of the rubber tools and also the initial gap adopted for each rubber material. Thus, it is of high importance for producing successful cups through the proposed technique to provide a consistent compromise between the initial gap and the hardness of the rubber type used for the flexible forming die. As a result, it can be said that the harder rubber material used in this study is the best, in terms of the reduction in thickness, for the flexible tool.

**Figure 6-35** illustrates the punch load-travel relations of drawing operations using different rubber hardness for the forming flexible pad with the required gaps mentioned above. The starting point of the 40A curve at an initial load of 478.4N is a result of the initial pressure applied on the rubber pad due to the negative gap adopted in this case. The curves indicate that as the punch stroke increases, the drawing load required then increases as well. Also, it can be noticed that the punch load at a particular drawing stroke increases with reducing the rubber hardness. That is due to the initial gap values specified as mentioned previously for the drawing processes achieved using rubber die materials with different

hardness. Afterwards, important finding can be denoted for the curves shown in this figure that is the curves overlap on each other after a stroke of approximately 2.83mm, so that the increment in drawing load becomes higher for the harder material.

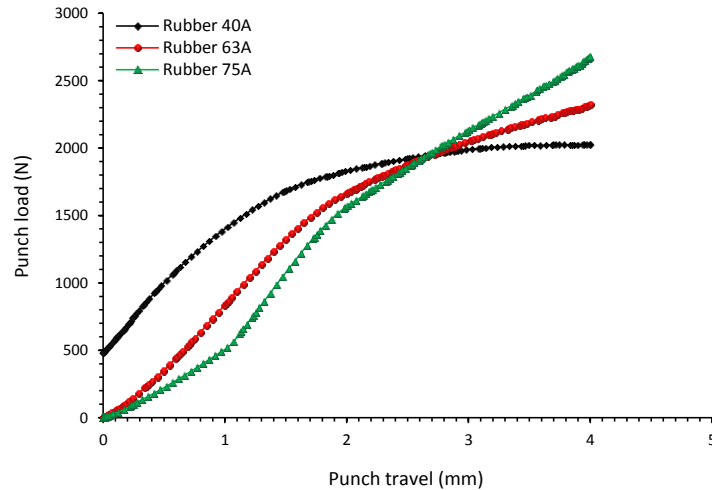


Figure 6-35. Punch load-travel relations with using different rubber hardness

The rationalization for this change in behaviour is that after the particular stroke mentioned before the rubber materials of the forming dies are equally dictated by the same severity of restriction, which consequently eliminates the influence of initial gaps. At this time, the hardness of the rubber die material become the main effective parameter on the drawing process and thereafter the fact of the harder rubber requires higher load to deform is applied. Hence, the main process parameter governing the deformation of rubber pad is its hardness. Likewise the results of the uniaxial compression tests presented in chapter five, the curves in **Figure 6-35** declare that the maximum drawing load required to produce a sound cup increases with increasing the rubber material hardness. The drawing results revealed that maximum punch loads of 2024.7N, 2320.7N and 2677N are required with using rubber die materials with 40, 63 and 75 Shore A hardness, respectively. This result implies that the softer material is optimum in terms of cost of the power required for drawing operation under same conditions. Therefore, the indication that can be deduced from these results is that the softer rubber material used in this study (i.e. 40A rubber hardness) is most appropriate, in terms of the external punch load required for achieving the entire drawing stroke, for the flexible tool.

#### 6.4.2.3 RUBBER COMPRESSIBILITY

To study the effect of compressibility of the rubber tool materials utilized the FE simulations of the micro deep drawing techniques in of this study, different Poisson's ratios ( $\nu$ )

of 0.499399, 0.499715 and 0.499874 are defined for rubber material models with the same hyperelastic factors characterized the behaviour of the rubber hardness of 63 Shore A. As a result of adopting no initial gap condition, a sound cup is drawn successfully using  $\nu=0.499715$ , whereas wrinkled and broken parts are produced with  $\nu=0.499399$  and  $\nu=0.499874$  respectively as shown in **Figure 6-36**.

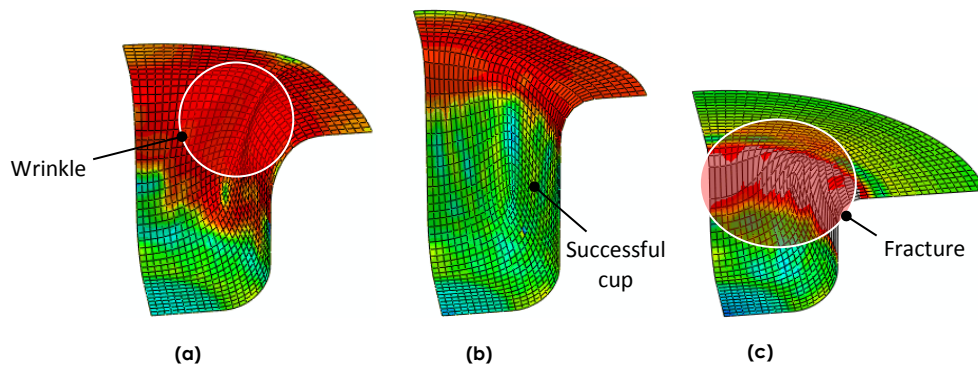


**Figure 6-36. Cups Obtained from numerical simulations with different rubber Poisson's ratios (a) 0.499399 (b) 0.499715 (c) 0.499874**

If the cup formed using rubber die of  $\nu=0.499715$  is considered as a reference, then the first micro drawing strategy that adopts negative initial gap is required for the process simulation in which the rubber material is modelled with  $\nu=0.499874$  and the second strategy that adopted positive initial gap for the process simulation in which the rubber material is modelled with  $\nu=0.499399$ . Likewise in the investigation procedure for the rubber hardness effect, in order to obtain successful cups with final profiles similar to that obtained with  $\nu=0.499715$ , the gaps  $-400\mu\text{m}$  and  $260\mu\text{m}$  are espoused for the cases of  $\nu=0.499399$  and  $\nu=0.499874$  respectively. **Figure 6-37** to **Figure 6-39** presents the thickness distribution along rolling, diagonal  $45^\circ$  and transverse directions of cups obtained from FE simulations using rubber pads of different Poisson's ratios with the specified initial gaps mentioned above. Each group of curves presented in these figures have the same features of tendency, and the remarkable difference in thickness magnitudes between each group of these curves are obviously observed at the side wall region of the produced cups. Also, these figures reveal that the maximum thinning occurs at the three different directions considered when the rubber material model is defined with  $\nu=0.499399$ . This action is due to the negative initial gap adopted for this case which implies that the rubber die is initially subjected to a particular pressure, and this situation leads to extra holding pressure on the flange portion of the cup being formed during the drawing process.



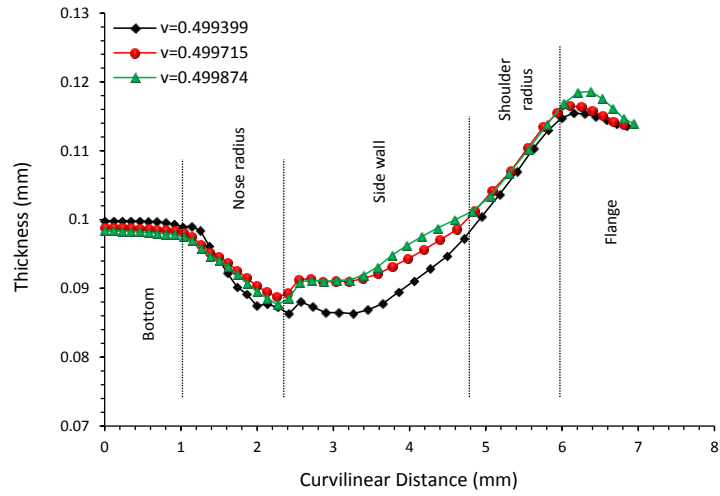


Figure 6-37. Thickness distribution along the rolling direction with using different rubber Poisson's ratios

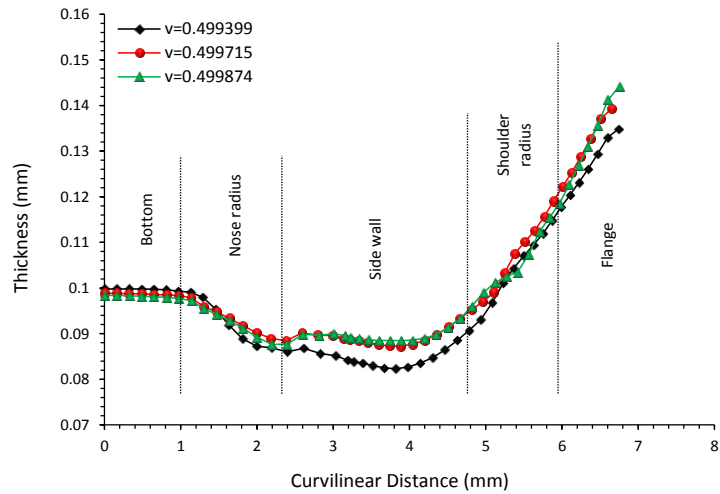


Figure 6-38. Thickness distribution along the diagonal direction with using different rubber Poisson's ratios

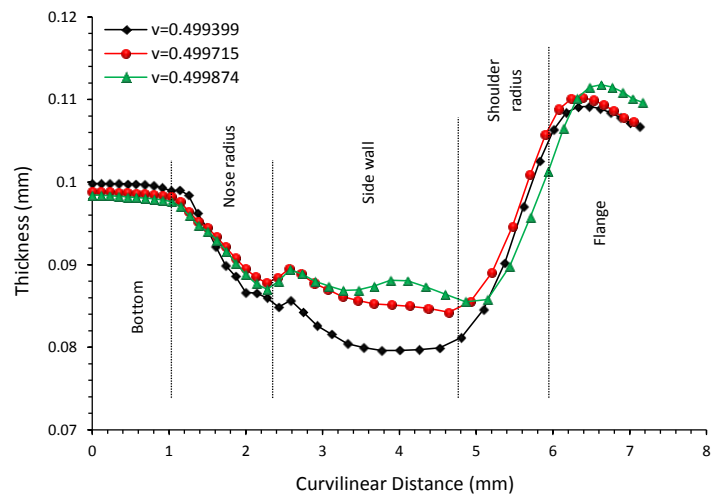


Figure 6-39. Thickness distribution along the transverse direction with using different rubber Poisson's ratios

Furthermore, the maximum thinning is found along the transverse direction identically at the side wall for all cases under consideration. The results reveal that the maximum reductions in cup thickness are 20.4%, 15.8% and 13% using rubber pad material of 0.499399, 0.499715 and 0.499874 Poisson' ratio respectively.

The punch load-travel relationships of drawing operations using rubber pad materials with different Poisson's ratio are shown in **Figure 6-40**. Although the negative gap adopted with  $\nu=0.499399$ , which results in a certain punch load is initially needed, but the maximum load required to produce a completed cup with final depth of 4mm using rubber pad of Poisson's ratio 0.499869 is higher. The results reveal that the maximum drawing loads required in the drawing operation when using rubber pad materials with Poisson's ratios of 0.499399, 0.499715 and 0.499874 are 2209N, 2321N and 2865N respectively. Depending on the slight difference in punch load obtained when using rubber pad-Poisson's ratios of 0.499399 and 0.499715 and due to the late produces cup quality much better in terms of thickness reduction, it can be deduced that the optimum choice is to adopt rubber material with hardness of 63 Shore A and Poisson's ratio of 0.499715 for the flexible forming tool in micro deep drawing under the current conditions. The results above indicate that the best quality in terms of thickness distribution can be acquired for the cups produced by using rubber die material of 75 Shore A hardness, whilst the worse quality associates to the rubber material of 40 Shore A hardness. On the other side, the best results in terms of the punch load required for a particular deep drawing process under given conditions are obtained with using rubber die material of 75 Shore A hardness and the worse results are obtained with using rubber die material of 40 Shore A hardness. In order for identifying the optimum forming parameters it is crucial issue to compromise between the product quality and the total cost of production. For example, it is wrong to produce a part with low cost at the expense of its quality or vice versa. In accordance to this principle, both of the soft rubber of 40A with high incompressibility ( $\nu=0.499874$ ) and the hard rubber of 75A with low incompressibility ( $\nu=0.499399$ ) do not represent wise choice for the flexible forming die in the current micro deep drawing techniques. Thus, the combination of moderate material properties can provide the optimum behaviour for the rubber that can be adequately utilized for the flexible die, and then the rubber material of 63 Shore A hardness and 0.499715 Poisson's ratio can be consequently regarded the most appropriate choice.

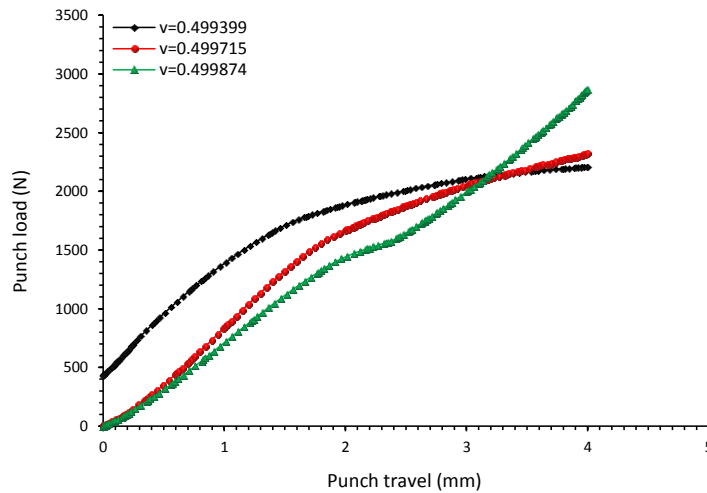


Figure 6-40. Punch load-travel relations with using different rubber Poisson's ratios hardness

### 6.4.3 RUBBER DIE DIMENSIONS

As the rubber materials are characterized by an elastic behaviour even for significantly high strain levels and due to these materials have a limited compressibility beyond which they behave a rigid materials, it is of very importance to investigate whether the geometrical dimensions of a rubber piece have effective role on its material behaviour. In other words, how the geometry dimensions of the flexible die employed in the current study may affect the deformation behaviour of its rubber material which in turn affect, as reported in the previous sections, the product quality and process requirements.

#### 6.4.3.1 RUBBER DIE DIAMETER

In this section, FE numerical simulations for micro deep drawing processes are implemented to study the effect of the rubber die diameter on the drawing results by employing the proposed technique. For this purpose, the process parameters listed in **Table 6-1** are adopted for the FE simulation considered here in exception of the rubber die is modelled with various diameters of 10mm, 11mm, 12mm and 13mm. Also, the deformation behaviour of the rubber die material is defined using the polyurethane 63 shore A hardness characteristics acquired from the compression tests exposed in chapter five. First of all, the FE numerical models are analysed with no initial gap to be adopted for all cases of different die diameters.

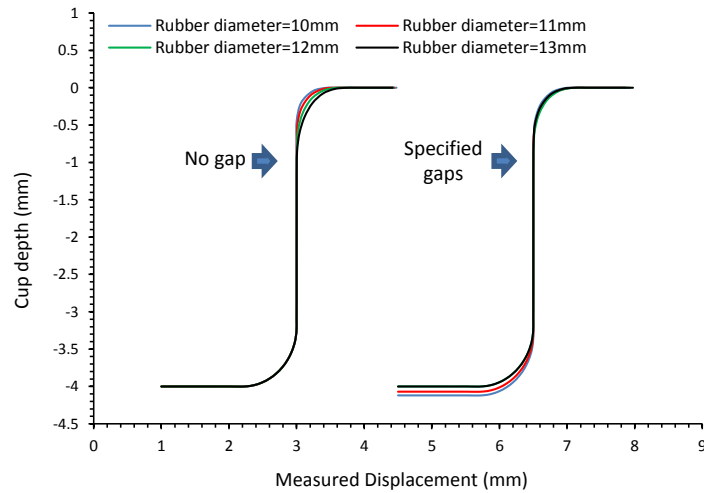


Figure 6-41. Profiles of the final cups obtained with different rubber die diameters

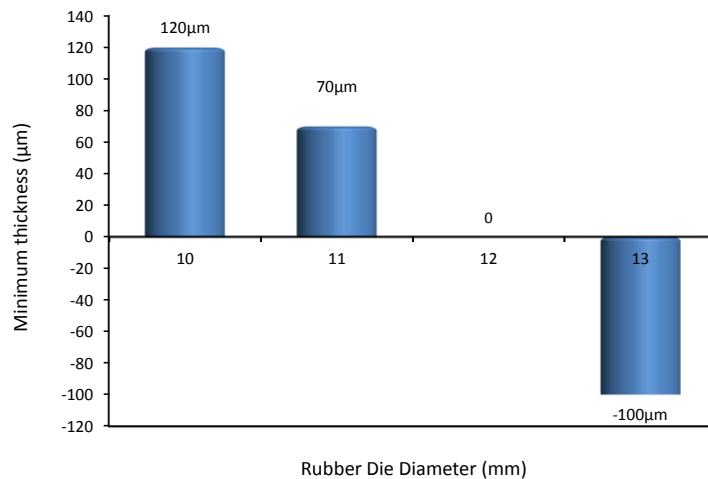


Figure 6-42. The specified initial gaps required to be used with different rubber die diameters

Figure 6-41 shows the section profiles of the final cups produced under the above conditions, where one can recognise the variation in the feature dimensions at the shoulder corner. These profiles indicate that increasing the flexible die diameter cause the cup to be more shallow at its shoulder (i.e. greater shoulder radius). In accordance with these results, the initial gap values revealed in Figure 6-42 should be adopted with the rubber die diameters aforementioned for producing cups with profiles similar to the one obtained by using 12mm die diameter (which is considered as a reference here). The main aim of this activity is in order to establish a correct comparison between the drawing results acquired with adopting varying diameters for the rubber die. The final profiles of the cups obtained from simulations according to this activity are presented in Figure 6-41. Figure 6-43 exposes the Von-Mises stress contours for the final cups, in which the stress distribution of the four cups have nearly the

same trend were the high stresses are concentrated at the shoulder corner and flange regions as explained previously in the effect of anisotropy behaviour.

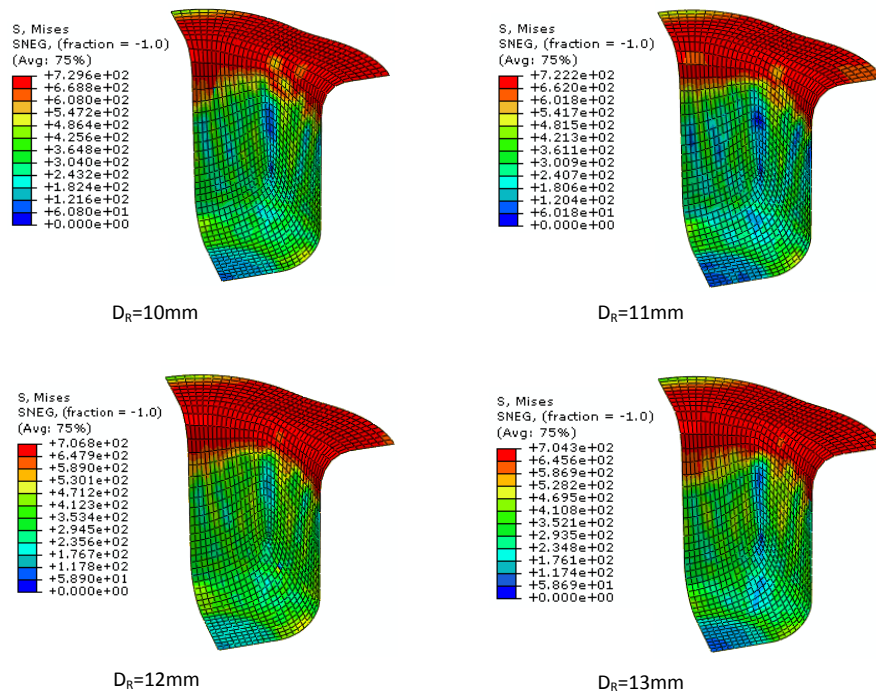


Figure 6-43. Von-Mises stress distributions obtained by using different rubber-die diameters ( $D_R$ )

The results of thickness distributions acquired for the cases of using different diameters for the rubber die in numerical models detect that the maximum reduction in thickness occurs along the transverse direction. Therefore, the investigation of thickness distributions that are taken into account in this section involves only that along the transverse direction. Figure 6-44 presents the thickness distributions along the transverse direction for the cups formed through FE simulations with different rubber-die diameters and no initial gap. It can be observed that the curves in this figure have the same major features in terms of increments and discernments, where no difference in the distribution and values of thickness can be recognised at the bottom and nose corner regions. Moreover, the maximum reduction in thickness occurs at the upper part of the side wall at which the maximum variation in the maximum thickness reduction between the four curves is noticed. Another finding is that the smaller the rubber-die diameter, the higher the maximum reduction thickness. As is revealed in Figure 6-45, the percentages of the maximum reduction in thickness 31.33%, 21%, 15.77% and 12.88% are acquired for the cups drawn using the rubber-die diameters 10mm, 11mm, 12mm and 13mm respectively.

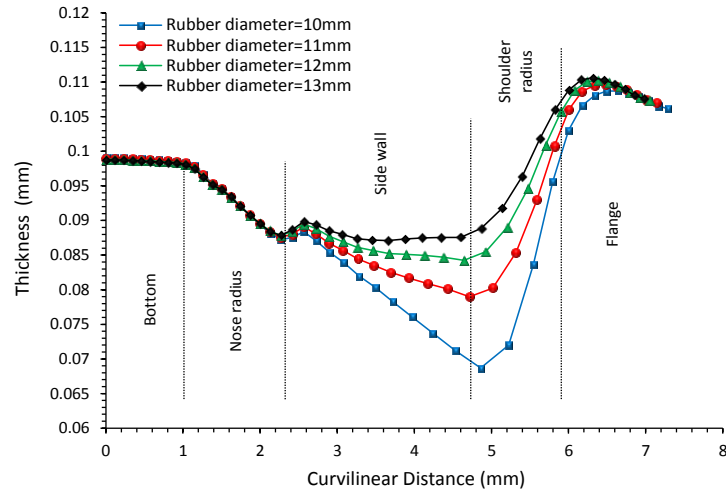


Figure 6-44. Thickness distributions obtained by using different rubber-die diameters with no gaps

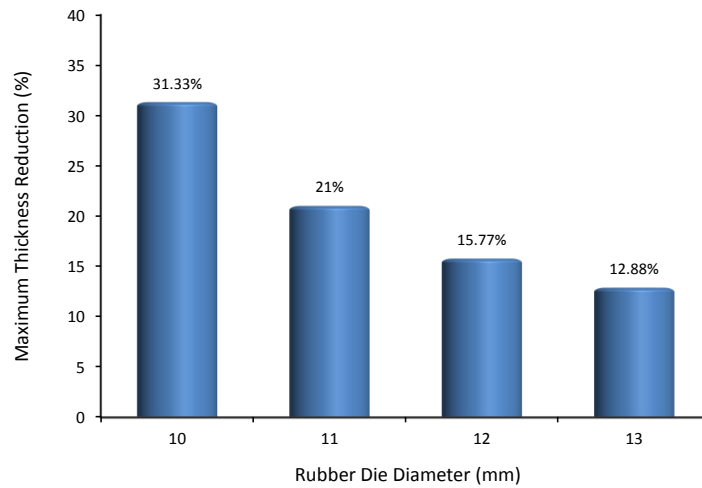


Figure 6-45. Maximum reduction in thickness obtained by using different rubber-die diameters with no gaps

On the other side, **Figure 6-46** illustrates the thickness distribution along the transverse direction taken from drawing simulations using the initial gaps identified for each rubber-die diameter in **Figure 6-42**. It can be noted that the curves expose similar tendency and however the significant difference in thickness can be obviously seen at the side wall region. As shown in **Figure 6-47**, the maximum reduction in thickness of 22.24% is associated to the rubber-die diameter of 13mm and this action is due to the negative initial gap of 100 $\mu$ m adopted with this diameter. Two interesting findings can be indicated in **Figure 6-45** and **Figure 6-47**; the first is the great difference of the maximum reduction in thickness of 31.33% obtained utilizing rubber-die diameter of 10mm with those obtained with other diameters as seen in **Figure 6-45**. Whereas, the second finding that is found in **Figure 6-47** is the reduction in thickness increases

with the rubber-die diameter except the one corresponding to the diameter 10mm although with which the highest positive gap is adopted.

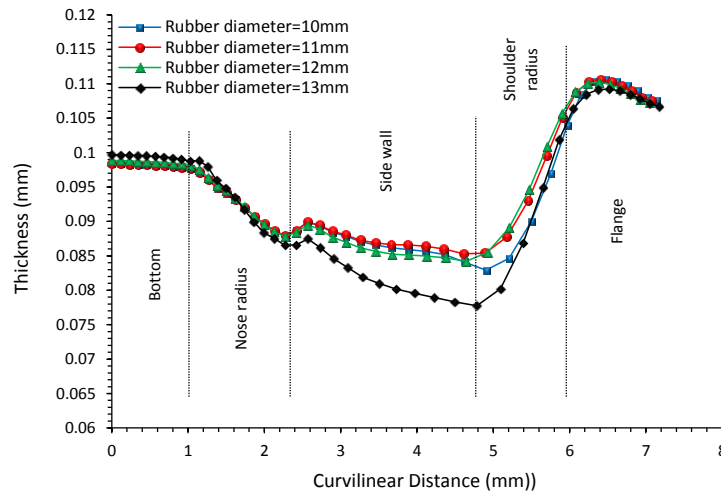


Figure 6-46. Thickness distributions obtained by using different rubber-die diameters with specified gaps

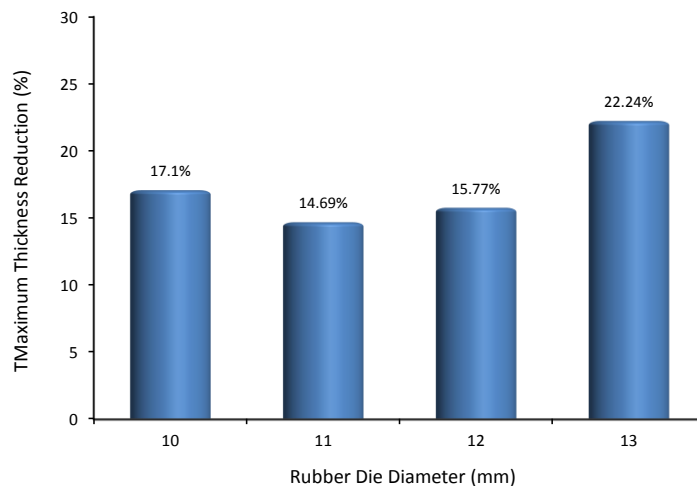


Figure 6-47. Maximum reduction in thickness obtained using different identified gaps

These actions can be attributed to the diameter 10mm of the rubber-die diameter is exactly equal to the diameter of the working blank used for this investigation. This activity implies that initially there is no contact area between the blank holder and the rubber die, which in turn causes the pressure normally excited in the rubber material to be totally subjected to blank. Thereafter, this situation in turn results in high tensile stresses in the blank sheet which consequently undergoes an excessive thinning. Figure 6-48 declares the punch load-travel relationship obtained from the FE simulation utilizing different rubber-die diameters with no initial gaps. It is clear that the curves show similar features of trend in terms of increments and discernments in punch load. The external load required for forming the SS

304 sheet blank increases during the drawing process progressively with the punch travel until reaches the maximum value at the end of the entire stroke.

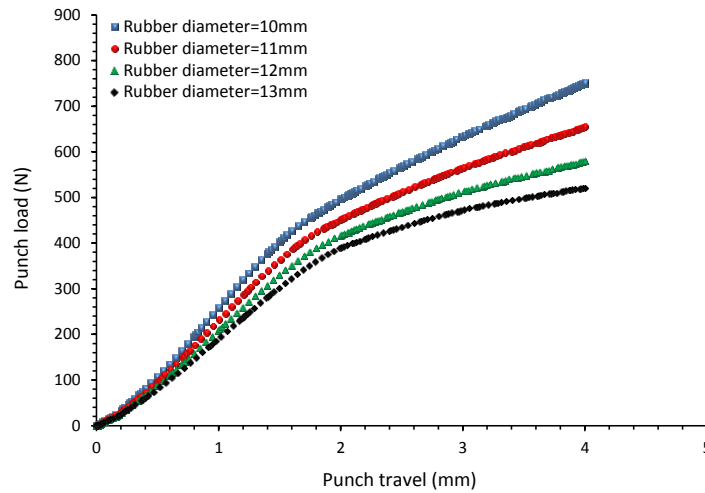


Figure 6-48. Punch load-travel relationships obtained by using different rubber-die diameters with no gap

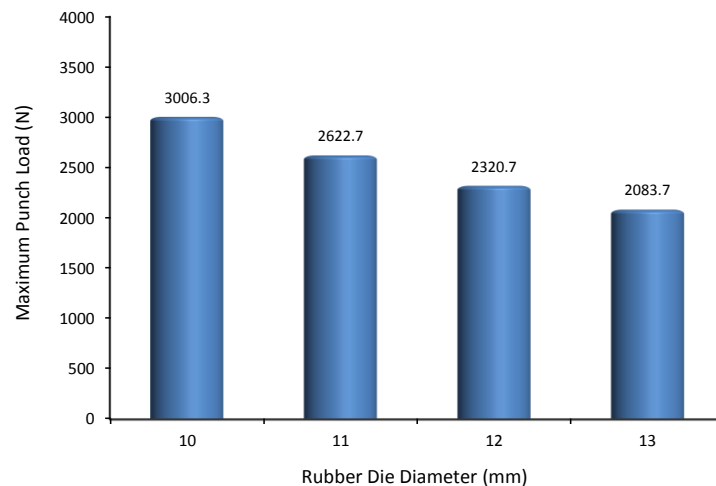
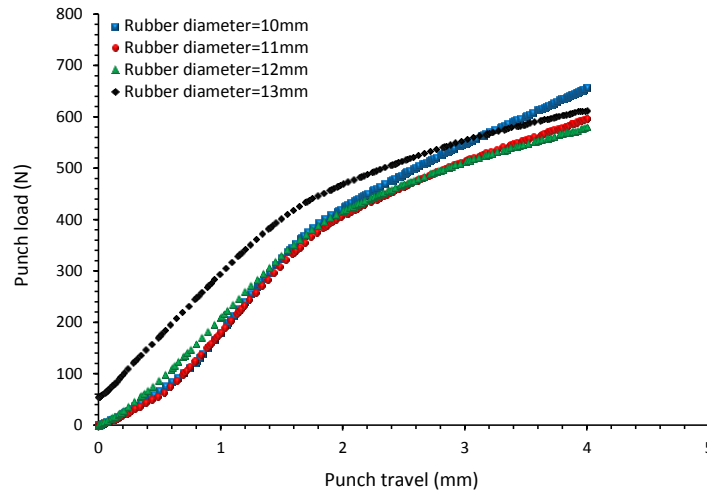


Figure 6-49. Maximum punch load obtained by using different rubber-die diameters with no gaps

The maximum punch load values acquired for the drawing simulation with different rubber-die diameters are presented in Figure 6-49. The results indicate that the smaller the rubber-die diameter the higher the maximum punch load required for performing the drawing stroke completely. This action can be well understood if the result is expressed in other words: for example, as the cross section area of the rubber die increases then the rubber material becomes able to absorb higher pressure which means that the reaction forces resists the punch movement against the rubber material would relatively decrease. Therefore, the punch load needed to achieve a particular drawing stroke is lower for greater rubber die diameter. On the other side, the punch load-travel relationships obtained from the simulation with the



initial gaps identified in **Figure 6-42** are revealed in **Figure 6-50**. The curves corresponding to the rubber-die diameters of 10mm, 11mm and 12mm show no significant difference in the general trend features and even in the punch load values over the drawing stroke of nearly 2.3mm.



**Figure 6-50.** Punch load-travel relationships obtained with different rubber-die diameters and identified gaps

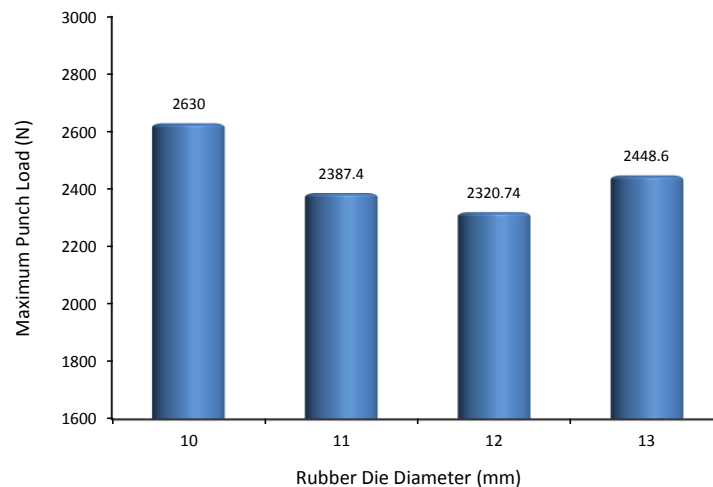


**Figure 6-51.** Maximum punch load obtained by using different rubber-die diameters with identified gaps

Afterwards, an increase in the slope of the curve representing the relationships taken for the die diameter 10mm is evidently reported in this figure although the greater initial gap of 120 $\mu$ m is adopted with this diameter. This issue can be rationalised that the variant gaps that are identified for this investigation cause a kind of compromise with the rubber-die diameters, however, after the punch travel of 2.3mm the influence of the die diameter dictates on the rubber material behaviour and finally to result in the maximum punch loads presented in **Figure 6-51**. Regarding the die diameter of 13mm, the curve starts with an initial value of 214.67N on the load axis, which is due to the negative gap adopted with this

diameter. Thereafter, at punch stroke of nearly 1.64mm the slope of this curve remarkably decreases and however the maximum punch load remains higher than that obtained with the diameters of 1mm and 12mm.

#### 6.4.3.2 RUBBER DIE HEIGHT

In this section, the influence the height of the rubber die employed in the micro deep drawing technique proposed in this study is investigated through FE simulations. For this purpose, the rubber die is modelled with different height of 10mm, 15mm and 20mm as well as the process parameters declared in **Table 6-1** are involved in the process simulations under consideration.

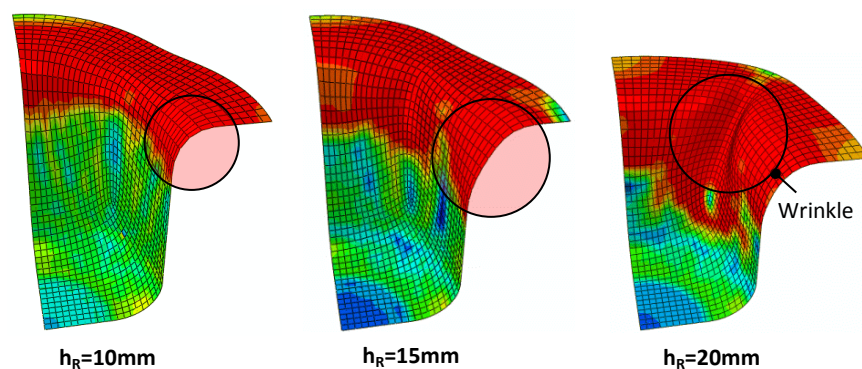


**Figure 6-52.** Cups obtained from simulations with different rubber-die heights ( $h_R$ ) with no gaps

Likewise the analysis procedure followed in the previous section, for the first attempts of drawing processes FE numerical models are analysed with no initial gaps for all cases of varying the rubber die height. The cups produced under these conditions are shown in **Figure 6-52** in which one can see that as the height of the rubber die increases the produced cup becomes shallower at the shoulder region until the height of 20mm results in wrinkled cup. This action indicates that also that reduction of the rubber die diameter results in thicker products. In order to acquire cups with final profiles similar to the one obtained with rubber-die height of 10mm, negative initial gaps of  $-200\mu\text{m}$  and  $-350\mu\text{m}$  are adopted with the rubber dies of 15mm and 20mm in height respectively. The thickness distributions along the transverse direction for these cups are revealed in **Figure 6-53** Error! Reference source not found.. In general, similar features can be indicated for the three curves and also no differences can be recognised between the two curves represent the thickness distributions for the cases of using rubber-die heights of 15mm and 20mm. Nevertheless, the higher curve is

obtained with the rubber die of 10mm height and this action refers to the best result in terms of thinning value.

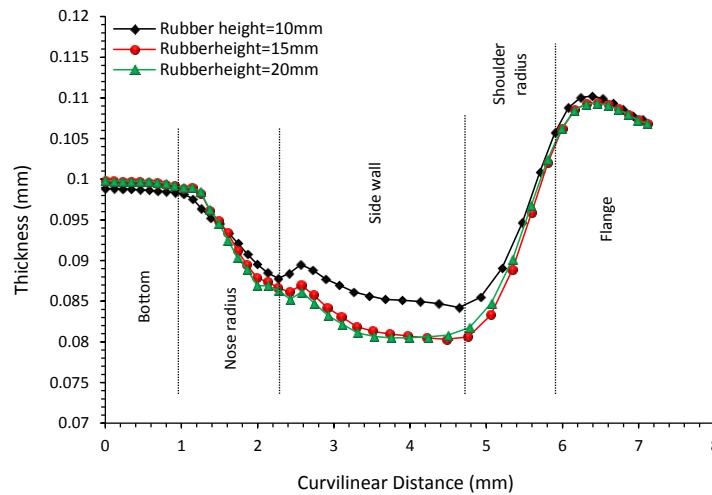


**Figure 6-53.** Thickness distribution along the transverse direction with identified gaps

The results detect that the maximum reductions in thickness of the cups obtained under the process conditions aforementioned are 15.8%, 19.7% and 19.5% with rubber die heights of 10, 15 and 20mm respectively. These values reveal the significant influence of the initial gap combined with the height of the rubber die on the quality of the final products. It can be noticed that the smallest value of the maximum reduction in thickness is obtained for the rubber diameter 10mm as no gap is adopted while the negative gaps for the other two cases caused an increase in the maximum thickness reduction. However, the maximum reductions in thickness observed with the rubber heights of 15mm and 20mm are very close though the considerable different in the initial gaps, which refers to the influence of the flexible die height. Moreover, the effect of the rubber-die height on the punch load-travel relationships obtained from FE simulations with the initial gaps identified above are reported in **Figure 6-54**. As is explained previously, the initial negative gaps results in the elementary values for the punch load observed at the beginning of the curves represents the load-travel relations produced with using the heights of 15mm and 20mm for the rubber die. Afterwards, these curves keep the first slopes until a particular drawing stroke of nearly 1.78mm and beyond which the slopes decreases resulting the maximum punch loads of 2320.7N, 2284.8N and 2182.5N with rubber die heights of 10mm, 15mm and 20mm respectively. These magnitudes report that the maximum punch load increases slightly with reducing the rubber-die diameter.

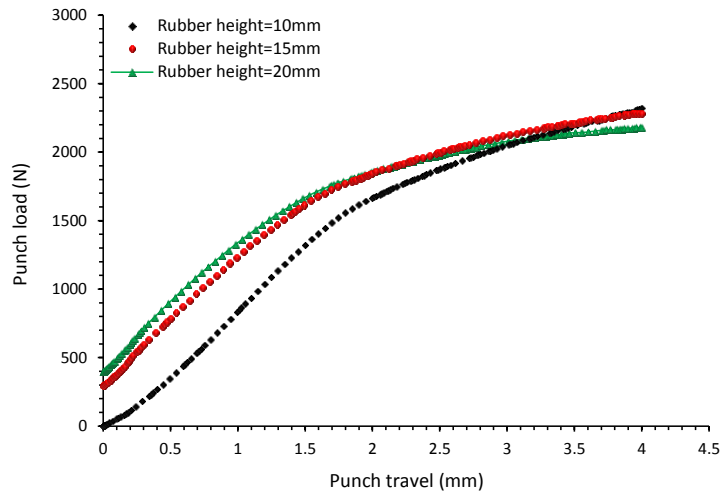


Figure 6-54. Punch load-travel relationships obtained by using different rubber-die heights with identified gaps

#### 6.4.4 FRICTION COEFFICIENTS

One of the crucial parameters in micro deep drawing processes is the coefficient of friction at the interfaces between blank and forming tools due to its significant influence on the formability of the sheet metal used and on the quality of the final products. As a consequence of size effects, the role of the friction coefficients in micro sheet metal forming is much more effective than in conventional processes [134, 167]. The success of deep drawing operations at micro scale depends strongly on the friction status at the interfaces in direct contact.

Parameter	Value
Punch diameter	4mm
Punch nose radius	0.8mm
Aspect ratio	1
Blank diameter	10mm
Blank thickness	100 $\mu$ m
Rubber pad diameter	12mm
Rubber pad height	10mm
Blank-Holder friction coefficient ( $\mu_{BH}$ )	variable
Blank-Punch friction coefficient ( $\mu_{BP}$ )	variable
Blank-Rubber friction coefficient ( $\mu_{BR}$ )	variable
Drawing velocity	0.1mm/sec
Initial gap	50 $\mu$ m
Rubber material type	63A

Table 6-2. Process parameters for micro deep drawing simulations under different friction conditions

The occurrence of excessive thinning and wrinkling to products made of sheet metals for given forming conditions is dictated by the frictional forces excited between the workpiece and

the tools employed. In the micro deep drawing technique proposed in this work, the SS 304 sheet blanks experience a direct contact simultaneously with rigid surfaces of the blank holder and punch and with deformable surface of the rubber die. In order to provide an evident insight on the effect of friction coefficients, three different friction interactions are investigated separately in the current study. These interactions are in order at the blank-holder interface, the blank-punch interface and the blank-rubber die interface. For this purpose, the process parameters declared in Table 6-2 are employed.

#### 6.4.4.1 FRICTION COEFFICIENT AT BLANK-HOLDER INTERFACE

In order to study the friction status at the contact interface between blank and blank-holder surfaces, different values of 0, 0.05, 0.1, 0.15, 0.2 and 0.25 are defined for the friction coefficient ( $\mu_{BH}$ ) at this interface in FE numerical simulations. For this investigation, the process parameters listed in the table shown above are utilized where the friction coefficients at the blank-rubber interface ( $\mu_{BR}$ ) and the blank-punch interface ( $\mu_{BP}$ ) are 0 and 0.25 respectively. The results reveal that the cups produced under the friction conditions considered here are successful except the one obtained with  $\mu_{BH}=0.25$  is broken. It can be observed in Figure 6-55 that the flow stress distribution curves along the transverse direction have the same trend features at the different regions except that at the side wall of the produced cups. At this portion, the tendency of the increment in stresses is prone to increase with increasing the friction coefficient ( $\mu_{BH}$ ) until fracture occurs with the value  $\mu_{BH}=0.25$ .

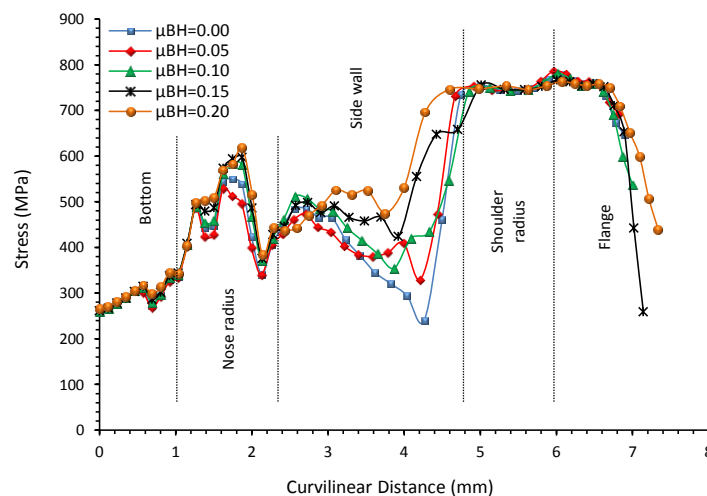


Figure 6-55. Stress distribution along the transverse direction obtained by using different  $\mu_{BH}$  values

This behaviour can be rationalized that with relatively high  $\mu_{BP}$  value used here, increasing the  $\mu_{BH}$  results in an increase in the resistant forces (frictional forces) obstructing to flowing the blank into the flexible cavity die during the drawing process. This activity in turn causes higher tensile stresses at both the side wall and the shoulder corner regions. The results detect that varying the friction coefficient  $\mu_{BH}$  has no effect on the geometrical aspects of the final cups obtained from the FE numerical models.

Figure 6-56 presents the thickness distribution along the transverse direction acquired for cups produced by FE simulations with different  $\mu_{BH}$  values. The significant variations between the curves shown in this figure are obviously measured at the upper part of the side wall as well as at the shoulder of the final products. The interesting observation is that the maximum reductions in thickness for the  $\mu_{BH}$  values of 0 and 0.05 occurred at the nose corner portion and thereafter the maximum reduction position transfers gradually to the side wall portion with increasing the  $\mu_{BH}$  value from 0.1 to 0.2. This action refers to that the friction forces excited at the blank-holder interface with  $\mu_{BH}=0$  and 0.05 are low enough to allow for the blank to flow easily into the flexible die cavity.

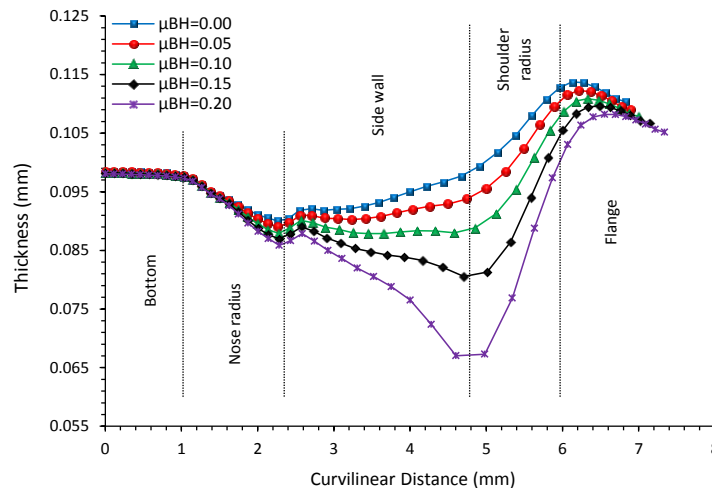


Figure 6-56. Thickness distribution along the transverse direction obtained by using different  $\mu_{BH}$  values

Afterwards, for  $\mu_{BH} \geq 0.1$  the friction forces between the blank and the holder resist more effectively flowing the flange portion of the cup being drawing into the flexible die resulting in excessive thinning at the side wall and shoulder corner portions. Due to this variance in the position of the maximum reduction in thickness obtained from the simulations for the different  $\mu_{BH}$  values, it is of very importance to reveal the magnitudes of the maximum reductions at both the nose corner region and the side wall region as shown in Figure 6-57.

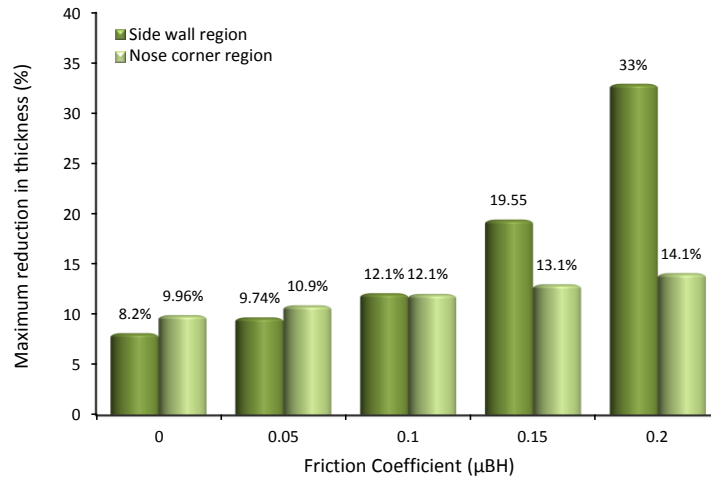


Figure 6-57. Maximum reduction in thickness obtained by using different  $\mu_{BH}$  values

The punch load-travel relationships acquired from the FE numerical models of micro drawing processes adopting the different values mentioned above for the friction coefficient at the blank-holder interface are illustrated in **Figure 6-58**. As it can be seen in this figure, the curve show similar features in the tendency of increasing the punch load with the drawing stroke. Also, due to the same positive initial gap adopted for all cases under consideration in this section, each curve evidently consists of three different slopes.

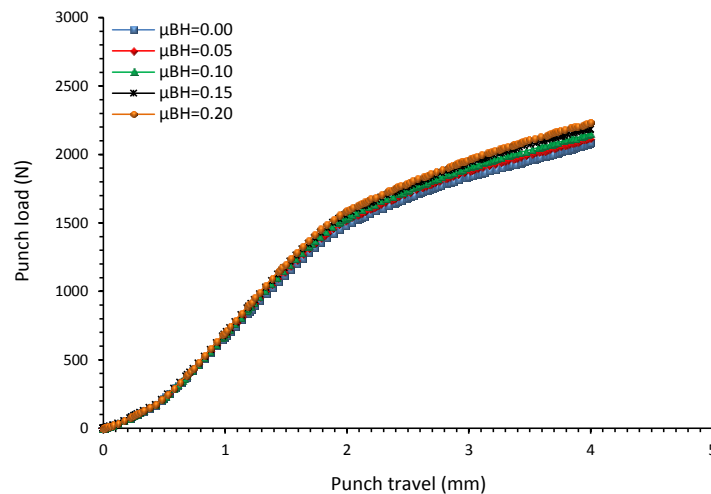
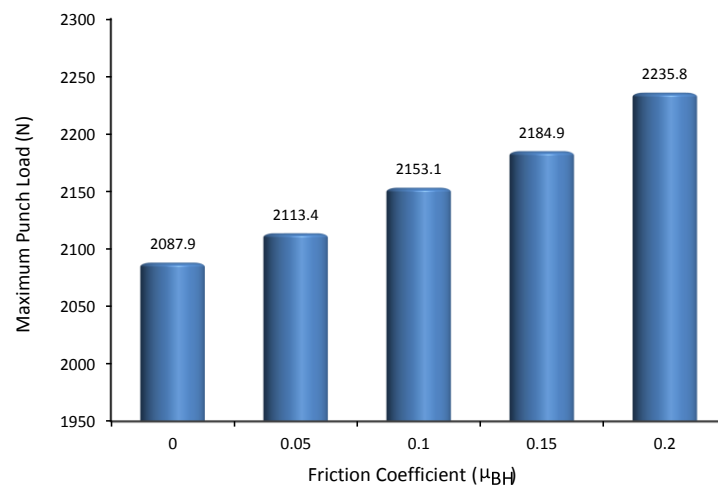


Figure 6-58. Punch load-travel relationships obtained by using different  $\mu_{BH}$  values

The first slope is due to forming the sheet metal just against the spring force by exploiting the positive gap and therefore this slope is relatively slight. Then the second one dramatically increases in the next stage because the rubber material at this drawing stage is deformed inside tightly closed space resulting in high reactive pressure against the rigid punch.

Afterwards, the slope decreases again as the flange area of the cup being formed is remarkably reduced through the previous stages and the main function of the rubber die now is to finish forming the final cup. In general, the punch load increase slightly with increasing the friction coefficient at the contact interface between the blank and the blank holder. The maximum values of the punch loads required to produce successful cups completely are presented in **Figure 6-59**.



**Figure 6-59. Maximum punch load obtained by using different  $\mu_{BH}$  values**

#### 6.4.4.2 FRICTION COEFFICIENT AT BLANK-RUBBER INTERFACE

The influence of the friction conditions at the interface between the blank and the rubber die utilized in the proposed technique is studied in this section by FE simulations. The most interesting point of this investigation is that the interaction occurs during the drawing process is due to a direct contact between two deformable surfaces instead of between one that is rigid while the other is deformable as in the previous section. For this purpose, the friction coefficient ( $\mu_{BR}$ ) at the blank-rubber die interface is defined in the numerical models using the values 0, 0.05, 0.1, 0.15, 0.2 and 0.25. Beside the process parameters illustrated in **Table 6-2**, the values of 0 and 0.25 are utilized for the friction coefficients ( $\mu_{BH}$ ) and ( $\mu_{BP}$ ) respectively. The results detect that changing the  $\mu_{BR}$  value has absolutely no effect on the final geometry of the produced cups. **Figure 6-60** shows the thickness distributions along the transverse direction for cups drawn through the numerical simulations using the different  $\mu_{BR}$  values. It is clear the curves have similar tendency as well as the same features for the increments and decrements in thickness values. Although the curve obtained with  $\mu_{BR}=0$  is slightly the higher, however the differences between all the curves presented in this figure can



be neglected. This activity can be realized through knowing that a maximum reduction in thickness of 10% is acquired for the cup formed with  $\mu_{BR}=0$ , in return of 11.1% with  $\mu_{BR}=0.25$ .

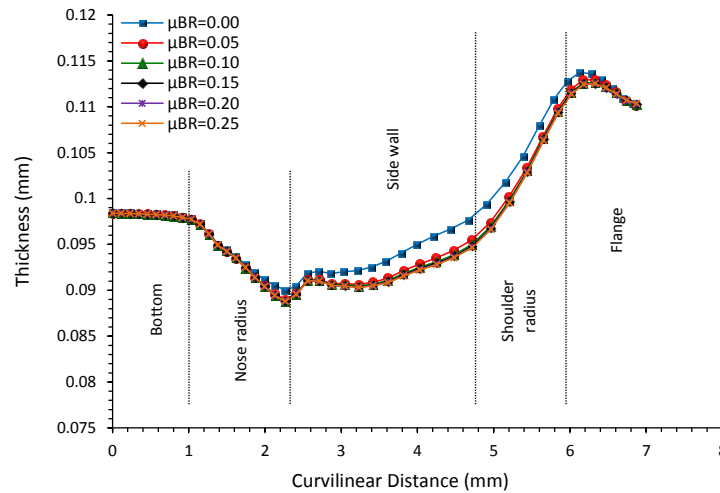


**Figure 6-60. Thickness distribution along the transverse direction obtained by using different  $\mu_{BR}$  values**

On the other side, the punch load-travel relationships of the micro drawing simulations performed using the different values identified above for the friction coefficient ( $\mu_{BR}$ ) are exposed in **Figure 6-61**. The curves indicate that varying the friction coefficient  $\mu_{BR}$  for the given range has no any effective role on the distribution trend of the punch load through the whole drawing stroke. The results indicate that no remarkable difference between the maximum loads obtained with the different  $\mu_{BR}$  values except the one acquired with  $\mu_{BR}=0$ .

The maximum punch loads corresponding to the different  $\mu_{BR}$  values are ranged between 2222.6N and 2235.6N corresponding to  $\mu_{BR}=0.05$  and  $\mu_{BR}=0.25$  respectively, whereas the load value of 2088N is obtained with  $\mu_{BR}=0$ . These results can be interpreted that due to the contact is between the deformable surfaces (blank surface and rubber die surface), then when the rubber material cannot resist the frictional forces at the blank-die contact interface, it deforms along with the blank sheet during the drawing process. This action in turn results in reducing the relative motion between the contact surfaces, causing a significant decrease in the friction forces which supposed to be applied on the blank material. In accordance with the results related to the thickness reduction and maximum punch load, it can be therefore indicated that the friction force excited with adopting  $\mu_{BR} \geq 0.05$  is high enough to provide the conditions for this activity.

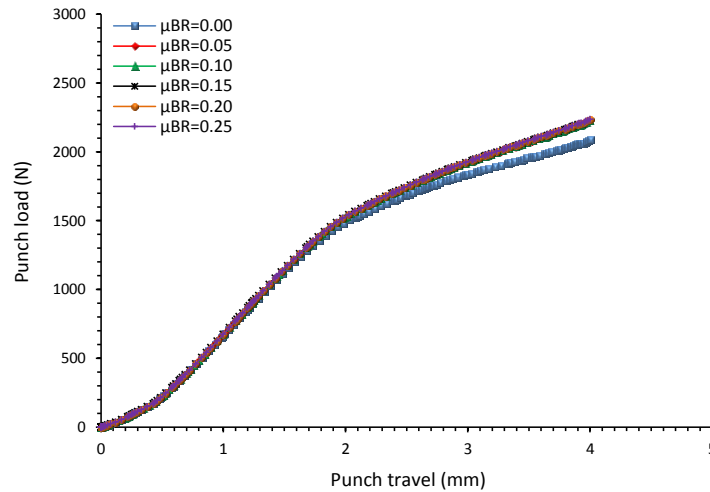


Figure 6-61. Punch load-travel relationships obtained by using different  $\mu_{BH}$  values

#### 6.4.4.3 FRICTION COEFFICIENT AT BLANK-PUNCH INTERFACE

As explained in chapter four, according to the technique presented in this study the cup body being formed is continuously in a direct contact with the rigid punch wall during the micro deep drawing stroke. Therefore, the contact conditions at the interface between the blank and the punch surface is crucial parameters and it is important to investigate its effect on the product quality. In order for this purpose, different values of 0, 0.05, 0.1, 0.15, 0.2 and 0.25 are defined in FE simulations for the friction coefficient ( $\mu_{BP}$ ) at this interface. The process parameters in Table 6-2 are utilized for this investigation and also the values of 0 and 0.1 are defined for  $\mu_{BR}$  and  $\mu_{BH}$  respectively. The results show the geometry of the final cups obtained from the simulations is not affected by the friction coefficient ( $\mu_{BP}$ ). Also, the results show that using  $\mu_{BP}=0$  causes the final cup to be broken at the nose corner region, whereas successful cups are obtained with the other  $\mu_{BP}$  values.

Figure 6-62 presents thickness distribution along the transverse direction, where the maximum thinning occurs, for cups produced varying the  $\mu_{BP}$  values. Unlike the thickness distribution trend resultant with different friction coefficients  $\mu_{BH}$  and  $\mu_{BR}$ , the great variances between the curves obtained for the current investigation are observed at the bottom and nose corner regions. Moreover, the difference between each two sequent curves decreases with increasing the  $\mu_{BP}$  values adopted until the curves represent the thickness distributions with  $\mu_{BP}=0.2$  and  $\mu_{BP}=0.25$  are remarkably coincide. The maximum reductions in thickness that occur at the nose corner and the side wall for the final cups are exposed in Figure 6-63. It can be denoted that with increasing the friction coefficient  $\mu_{BP}$  from 0.05 to 0.25 the position of the

maximum thinning transfers from the nose corner to the side wall. Furthermore, it can be noticed that there is a significant decrease in the maximum thinning value at the nose corner with increasing the  $\mu_{BP}$  values. However, the maximum thinning experiences no important change at the side wall region. The interpretation for these results is that for low friction coefficient  $\mu_{BP}$  values, the blank then is allowed to easily slip on the rigid punch surface and nonetheless its flange portion undergoes relatively high friction forces with the blank holder surface. This action in turn increases the relative motion of the blank with rigid punch especially at the nose corner radius, resulting in high reduction in thickness.

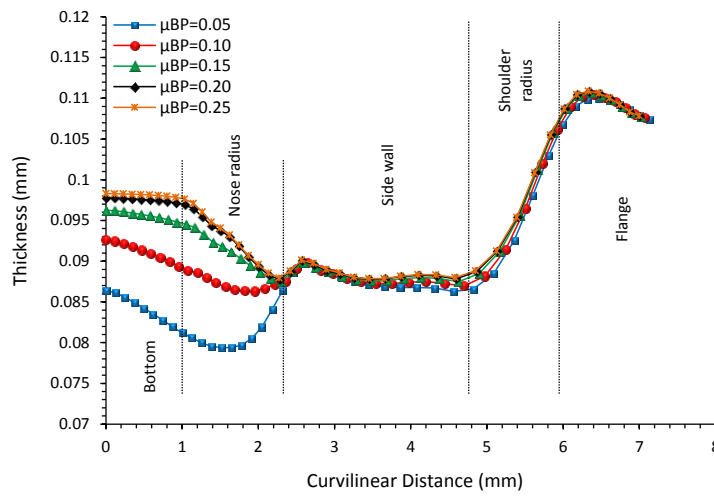


Figure 6-62. Thickness distribution along the transverse direction obtained by using different  $\mu_{BP}$  values

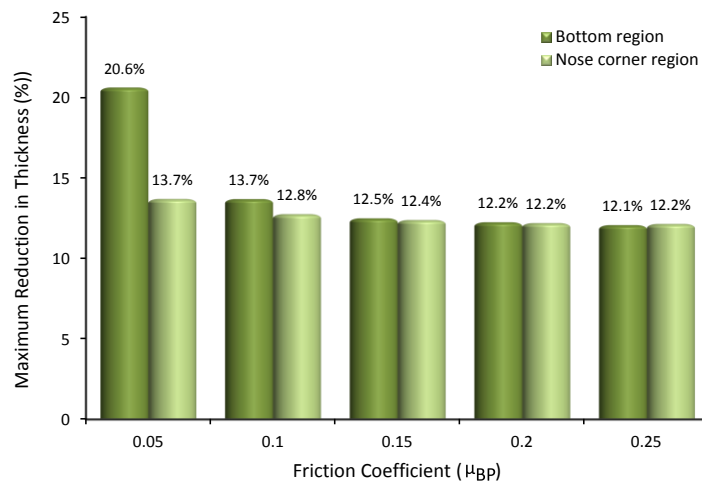


Figure 6-63. Maximum reduction in thickness obtained by using different  $\mu_{BP}$  values

However, the different values adopted here for the friction coefficient ( $\mu_{BP}$ ) have no noticeable effect on the punch load-travel relationships as shown in Figure 6-64. In this figure

one can observe that there is no difference whether in distribution trend or in load values between the obtained curves.

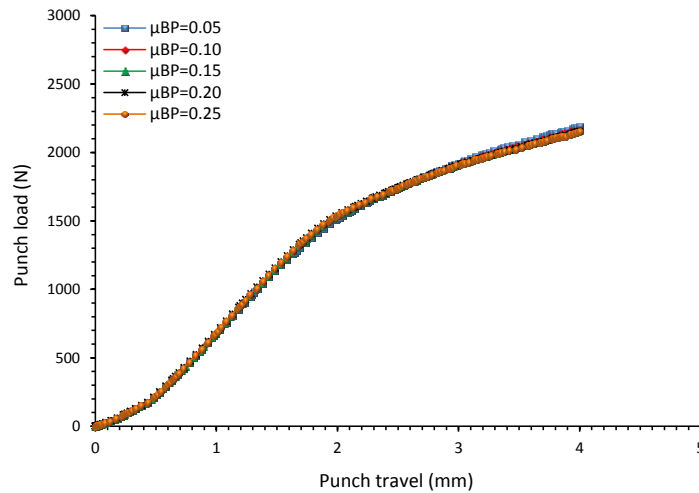


Figure 6-64. Punch load-travel relationships obtained by using different  $\mu_{BP}$  values

## 6.4.5 BLANK DIMENSIONS

### 6.4.5.1 INITIAL BLANK DIAMETER

Initial blank diameter plays a potential role in evaluating the formability of workpiece material utilized in sheet metal forming processes. In deep drawing technology, the friction force depends strongly on the contact area of the blank required to deform with the forming tools. As a result of size effects, it is hence of high importance to investigate the influence of the initial diameter of the blank used in deep drawing processes at micro scale utilizing flexible tools. Therefore, in order to reveal the effective role of the workpiece diameter in the current technique, the SS 304 blanks are modelled in FE numerical simulations with various initial diameters of 9, 10, 11 and 12mm. For this purpose, the process parameters listed in Table 6-2 are adopted in this investigation except that the values 0.1, 0 and 0.25 are defined for the friction coefficients  $\mu_{BH}$ ,  $\mu_{BR}$  and  $\mu_{BP}$  have respectively. In addition, no initial gap is simulated in the numerical models for the first drawing attempts. The results denote that no successful cups can be drawn at all from the blank diameter 12mm for any initial gap, even if no friction is defined for the blank/holder and blank/rubber die contact interfaces. Also, it is found that the conditions of  $\mu_{BH}=0.1$  and no initial gap with the blank diameter of 11mm results in broken cups. These results indicate that as the surface area of the blank increases the holding force applied by the rubber material then also increases. Hence, the holding forces created on the blanks with initial diameters of 11mm and 12mm are high enough to obstruct sliding the blank

being drawn into the flexible forming cavity even if no friction is defined at the contact interfaces.

Consequently, other drawing simulation analysis are carried on blanks of the different diameters of 9mm, 10 and 11mm using  $\mu_{BH}=0.05$ ,  $\mu_{BR}=0$ ,  $\mu_{BP}=0.25$ . Nevertheless, in order for similar profile of the final products, the blank of 11mm diameter is formed with initial gap of 60 $\mu$ m while the other two with no gap. The cup sections shown in **Figure 6-65** are drawn via numerical simulations under these conditions. It can be noticed that the tendency of stress distribution is nearly the same, which means that the initial diameter of drawing blank has no significant influence on distributing the flow stresses on the final products.

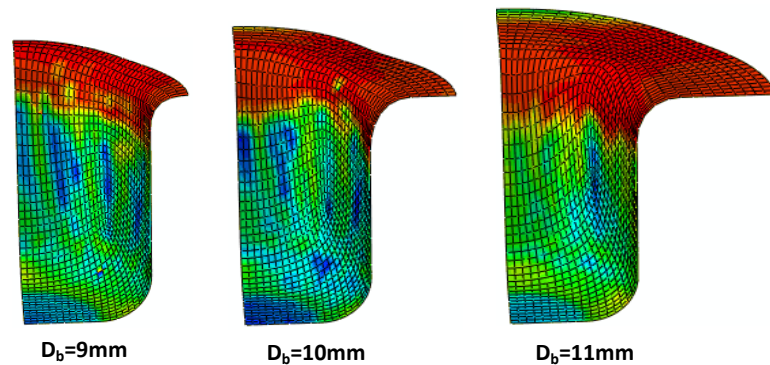


**Figure 6-65.** Cups obtained from simulation with different initial blank diameters ( $D_b$ )

**Figure 6-66**, **Figure 6-67** and **Figure 6-68** display the thickness distributions along the rolling, diagonal and transverse directions of the final cups shown in the figure above. It is clear that the curves in each group are similar in the general tendency of the increment and decrement. However, there are remarkable variations in thinning values between these curves particularly at the side wall and shoulder corner regions. The results detect that the maximum reductions in thickness along the three different directions under consideration in this investigation are acquired at the nose corner region for the cups produced using blank diameters of 9mm and 10mm. While, the reductions in thickness obtained for the cups formed from blanks of 11mm diameter occur at the side wall region. Also, these figures reveal that the maximum thinning is recognised at the transverse direction for all cups produced through the FE simulations using the different blank diameters of 9mm, 10mm and 11mm. Another important observation is that higher values for the maximum reductions in thickness are generally observed on the cups drawn from blanks with greater initial diameters. These results can be interpreted that increasing the initial diameter of the blank used in the micro deep drawing process, with a given punch size, implies greater area for the flange portion of this blank.

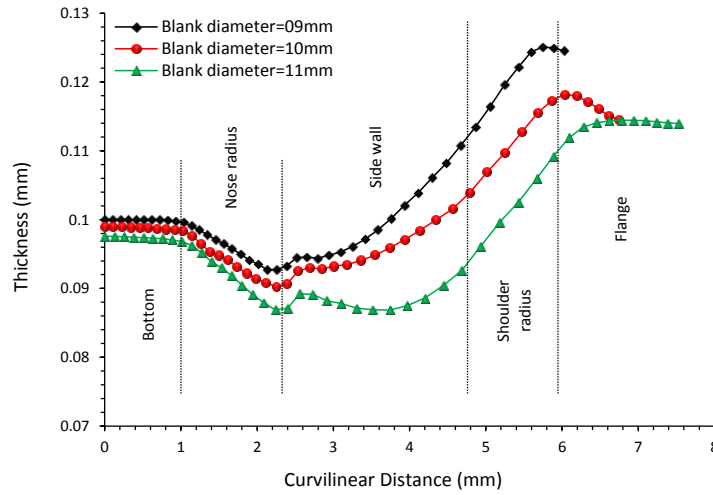


Figure 6-66. Thickness distributions along the rolling direction of cups drawn with different blank diameters

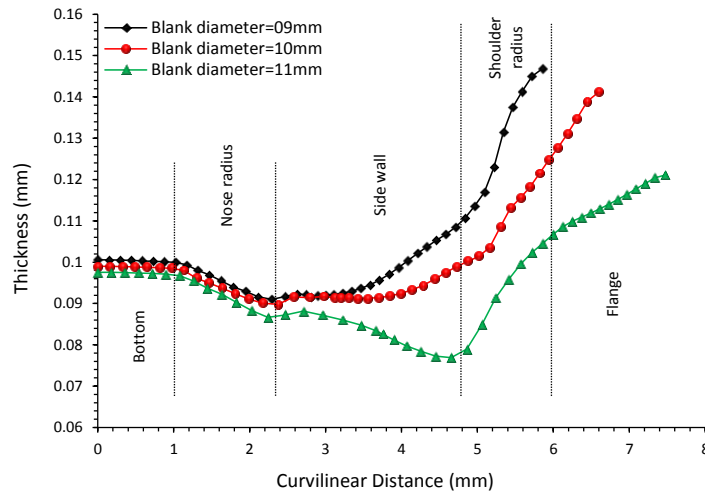


Figure 6-67. Thickness distributions along the diagonal direction of cups drawn with different blank diameters

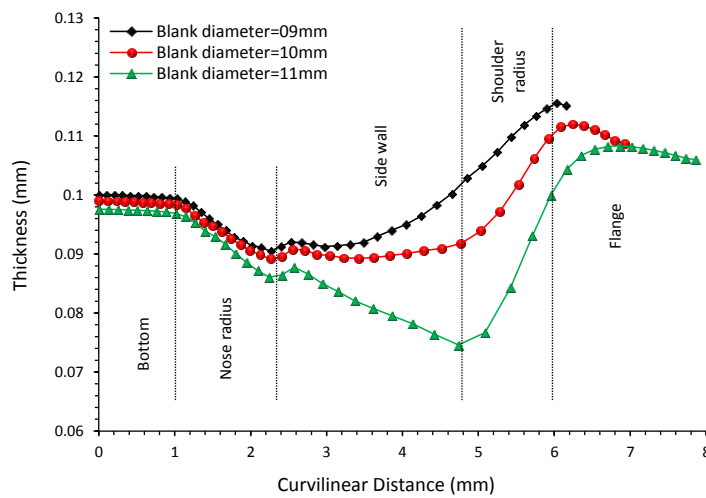
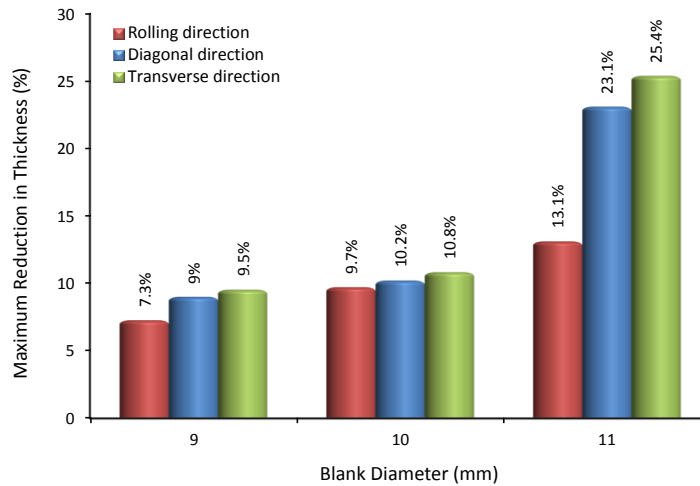
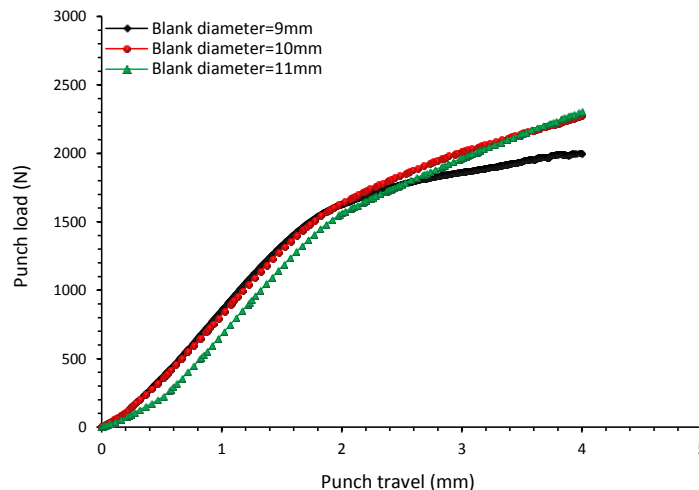


Figure 6-68. Thickness distributions along the transverse direction of cups drawn with different blank diameters



**Figure 6-69. Maximum reductions in thickness for cups formed from different blank diameters**

This activity refers to an increase in the holding force applied by the rubber die as the part of the blank area which is simultaneously in direct contact with both the blank holder and the rubber die is increased. Subsequently, excessive tensile stresses are excited in the sheet material being formed leading to high reductions in thickness identically at the side wall and shoulder corner portions, like what happens with a blank diameter of 11mm. This fact is obviously expressed in **Figure 6-69** where the maximum reductions in thickness along the transverse direction occurred for the blank of the diameters 9mm, 10mm and 11mm are 9.54%, 10.84% and 25.4% respectively.



**Figure 6-70. Punch load-travel relationships obtained using different blank diameters**

**Figure 6-70** reveals the punch load-stroke relationships obtained from the numerical models using different blank diameters. The same basic features can be observed for the curves. Despite the positive initial gap adopted with blank diameter of 11mm, the maximum

punch loads required for producing a successful cup with blank diameters 10mm and 11mm are very close of 2320.74N and 2304N respectively, and however the load corresponding to the diameter 9mm is the lower of 2000.9N. As a final result, the best choice of initial blank diameter, in terms of thickness reduction and drawing load, to be used under the conditions under consideration in this investigation is 9mm.

#### 6.4.5.2 INITIAL BLANK THICKNESS

Concerning the capability of the proposed technique for drawing various blank thicknesses, three different thicknesses of 60 $\mu$ m, 100 $\mu$ m and 150 $\mu$ m are defined for the SS 304 blanks modelled in FE simulations in this study. The final depth to which the blank is drawn in this investigation is 4mm utilizing the friction coefficients  $\mu_{BH}=0.1$ ,  $\mu_{BR}=0$  and  $\mu_{BP}=0.25$ . Likewise in the previous investigations, the first attempts of micro deep drawing are carried out here with the same initial gap for all cases, which is 50 $\mu$ m for the current investigation. The result reveal that the cup of thickness 100 $\mu$ m is sound and the cup of 150 $\mu$ m thickness is just shallow at the shoulder radius, while no sound cup of thickness 60 $\mu$ m can be produced at all with  $\mu_{BH}=0.1$  due to fracture, as shown in **Figure 6-71**.

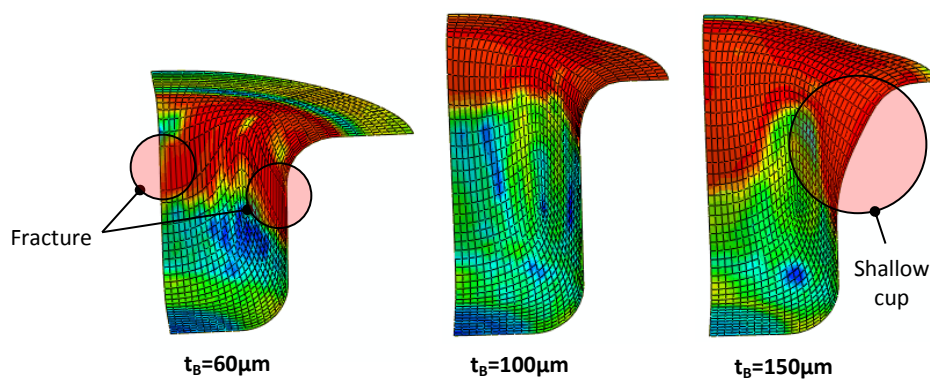


**Figure 6-71. Cups obtained from simulation using different initial blank thickness**

In order to obtain a correct comparison between cups produced from blanks with these different thicknesses, the final profiles of the cups should be exactly the same and the process conditions above therefore should be changed. Thus, the friction coefficients  $\mu_{BH}=0.05$ ,  $\mu_{BR}=0$  and  $\mu_{BP}=0.25$  are adopted with initial gaps of 60 $\mu$ m, 100 $\mu$ m and 150 $\mu$ m for the blank of thicknesses 60 $\mu$ m, 100 $\mu$ m and 150 $\mu$ m respectively. **Figure 6-72**, **Figure 6-73** and **Figure 6-74** show the thickness distribution along the rolling, 45° diagonal and transverse directions for the cups obtained from the numerical models with different blank thickness under these conditions.



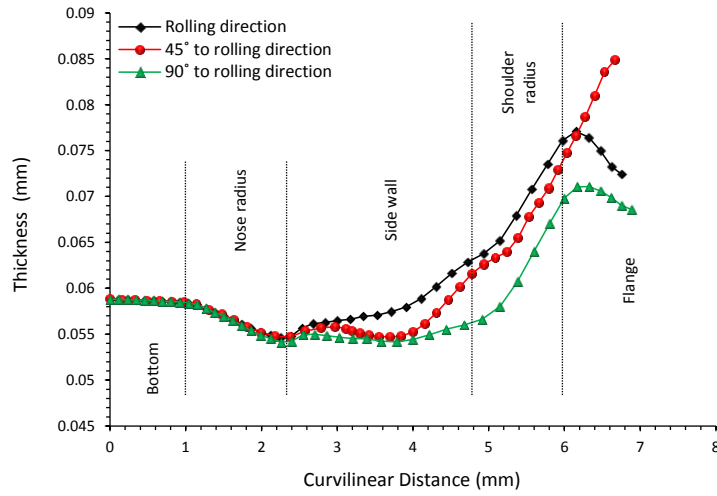


Figure 6-72. Thickness distribution obtained using blank of 60µm initial thickness

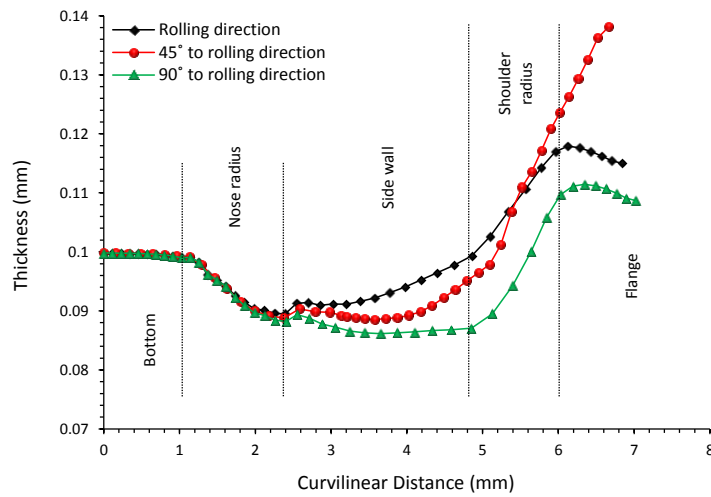


Figure 6-73. Thickness distribution obtained using blank of 100µm initial thickness

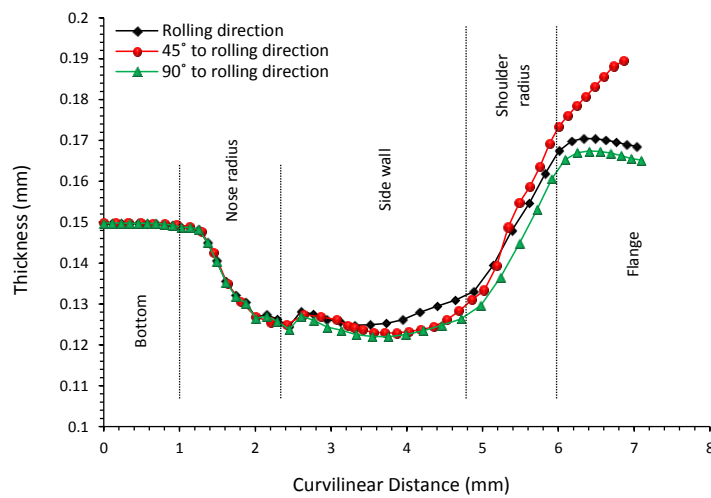
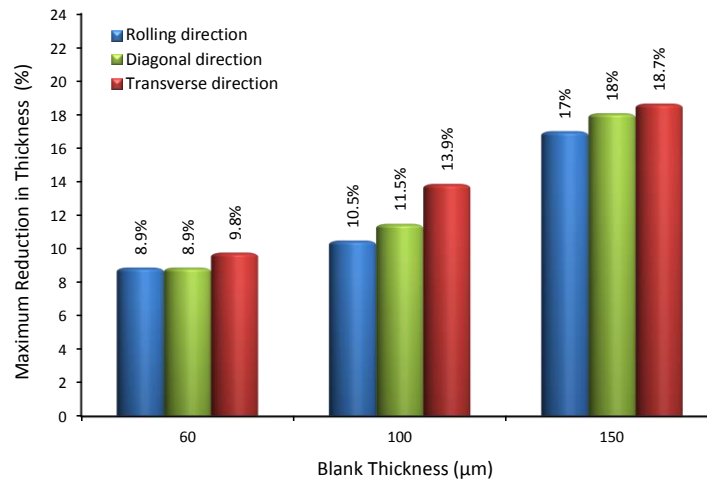


Figure 6-74. Thickness distribution obtained using blank of 150µm initial thickness

The curves acquired for each blank thickness reveal that the bottom and the nose radius of the formed cups remain without remarkable change in thickness valued along the three different directions adopted. The general trends of the curves are quietly similar, where the highest values of the maximum thinning along the transverse direction are observed at the cup side wall for the three curve groups. Also, it can be denoted from the figures that the maximum thinning along the rolling directions occurs at the nose corner regions.

In order to provide a clear view on the influence of the initial gap in combination with the initial blank thickness on the acquired quality of the final products, **Figure 6-75** is presented here. This figure shows the maximum reductions in thickness along the rolling, diagonal and transverse directions obtained for cups formed from blanks of 60 $\mu\text{m}$ , 100 $\mu\text{m}$  and 150 $\mu\text{m}$  initial thickness. The results, that are acquired for a particular blank thickness, refer to the smaller values of maximum thinning occur along the rolling direction whereas the higher values are detected along the transverse direction. Moreover, the interesting finding in this figure is that the greater the initial blank thickness is the higher the maximum thinning. This issue can be mainly attributed to the initial gaps specified correspondingly with the different blank thicknesses. It can be deduced from this action that the influence of the initial gaps is significantly the dominate factor on the drawing quality at the expense of the blank thickness.



**Figure 6-75. Maximum reduction in thickness using different initial blank thicknesses**

Regarding the punch loads required for conducting drawing processes completely, **Figure 6-76** indicates that the maximum load value increases significantly with the increase in the initial blank thickness. The results reveal that the maximum punch loads required to produce similar profiles-shaped cups from blanks of 60 $\mu\text{m}$ , 100 $\mu\text{m}$  and 150 $\mu\text{m}$  blank thicknesses are 1929.5, 2878 and 5158.8N respectively. The important attention in this figure

is that the curves associating the thicknesses 100 and 150 $\mu\text{m}$  start at particular load values (as seen also in some previous figures), and the reason of this issue is the negative gaps adopted for these two cases. By the way, the negative gaps -100 and -550 $\mu\text{m}$  used for the thicknesses 100 and 150 $\mu\text{m}$  causes the loads 332N and 1367N respectively as interpreted previously.

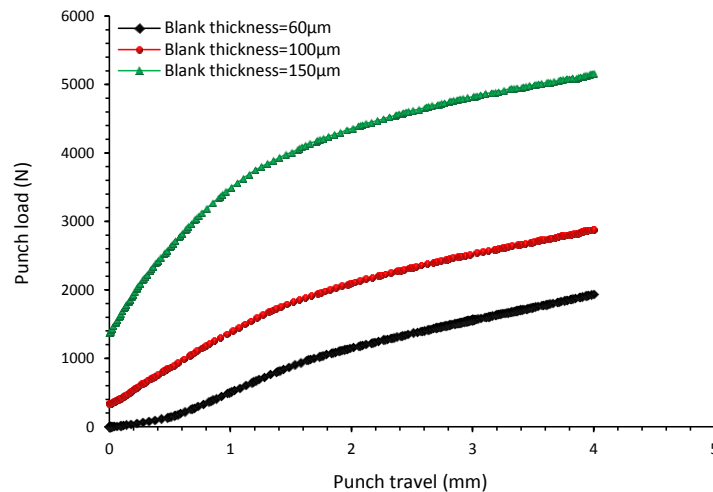


Figure 6-76. Punch load-travel relationships obtained by using different initial blank thicknesses

#### 6.4.6 PUNCH TRAVEL

In accordance with requirements of some industrial applications, micro stainless steel cups are needed to be formed with different depth/diameter ratios i.e. different aspect ratios. Thus the new technique proposed in this study for micro deep drawing processes is examined to produce micro cups with various punch strokes via FE numerical simulations. The process parameters presented in **Table 6-1** are utilized for this purpose as well as the rubber 63 Shore A material is employed for the flexible die tool. Moreover, the aspect ratio targeted in this investigation are 0.75, 1 and 1.25 and as the rigid punch is modelled with 4mm diameter then the drawing strokes corresponding to the mentioned aspect ratios are 3mm, 4mm and 5mm respectively. Aimed to obtained cups with same shoulder corner radius, the initial gaps of -100  $\mu\text{m}$ , -50  $\mu\text{m}$  and 0 can be adopted for the drawing systems of punch strokes 3mm, 4mm and 5mm respectively. The final cups formed successfully under these conditions are exposed in **Figure 6-77** which reveals the stress and thickness distributions obtained from the FE simulations. It can be observed that the influence of the anisotropic deformation response of the blank material becomes more distinct as the drawing stroke increases. This action denotes that there is no feasibility would be acquired of drawing a cup into depth more than 5mm as the material remaining at the flange region (see the cup of 5mm depth in **Figure 6-77**) is not

enough to contribute beneficially in the main body of the final cup. It is clear that keeping form this cup will definitely result in earning for the produced cup at the end of its wall sides.

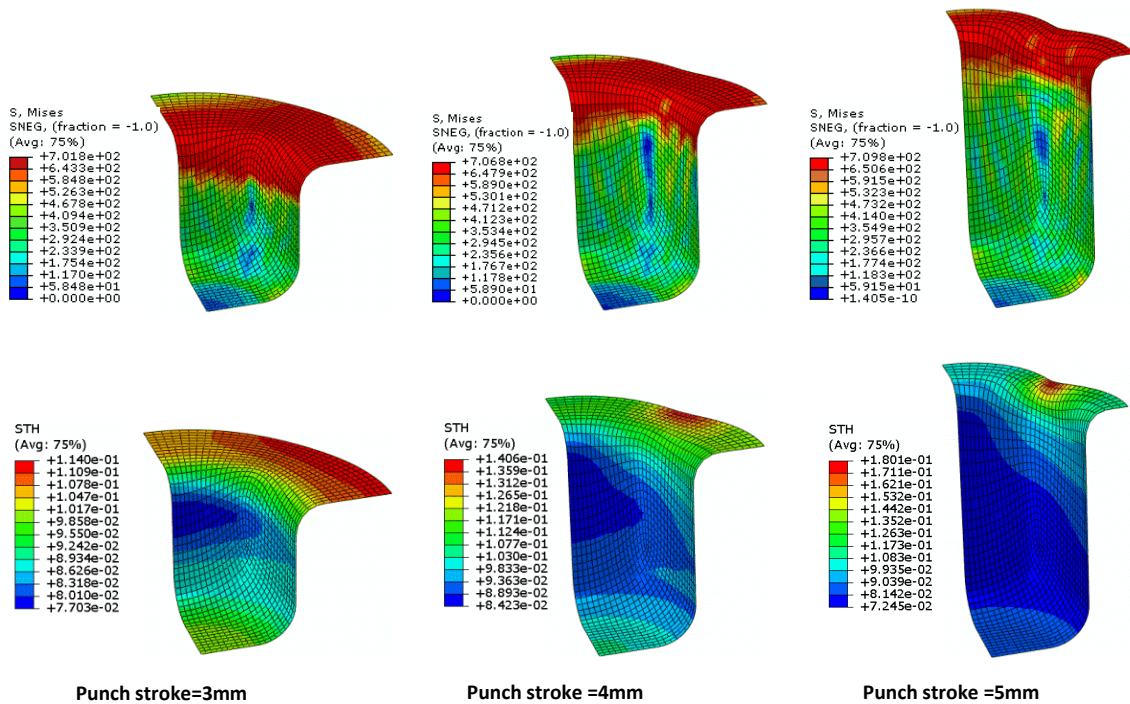


Figure 6-77. (a) stress and (b) thickness distributions for cups obtained from FE simulations with different drawing strokes

As can be seen in Figure 6-77 that the maximum stresses are concentrated at the shoulder corner and the flange portions of the formed cups. The concentration activity is due to the excessive tensile stresses dominating these two regions identically the shoulder corner as explained previously. As well as, the surface shear stresses at the flange part of the obtained cup, which sweep the material along the flange region towards the periphery resulting in noticeable thickening.

Figure 6-78 declares the thickness distribution along the transverse direction, where the maximum thinning takes place, obtained from the numerical models of drawing processes with the different punch strokes. The general tendency of the increments and decrements in thickness is similar for the curves in this figure which indicate that the maximum thinning occurs at the side wall region for the cups corresponding to the drawing strokes 3mm, 4mm and 5mm. It can be deduced that the maximum reduction in thickness increase as the drawing stroke reduces. The results detect that producing cups with 3mm, 4mm and 5mm final depth causes maximum reductions in thickness of 22.97%, 20.9 and 16.1% respectively. This finding can be attributed to the negative initial gaps adopted for the drawing systems of 3mm and

4mm punch strokes. Therefore, it can be said that although the high difference intended between the targeted cup depths, the influence of the initial gap is significantly more effective in terms of maximum thinning than the punch stroke. Unlike this action is observed for the punch load-travel relationships acquired from the FE simulations, where higher maximum punch load is required for the larger drawing stroke. In accordance with this fact, the maximum punch loads of 2385.2N, 2502.17N and 2562.9N are required to completely form cups with final depth of 3mm, 4mm and 5mm respectively. This result can be rationalized that regardless the initial gap effect, as long as the rigid punch is pushed down into the rubber die for a greater distance then a higher forming load will be required to resist the reaction pressure that is increasingly excited in the rubber material.

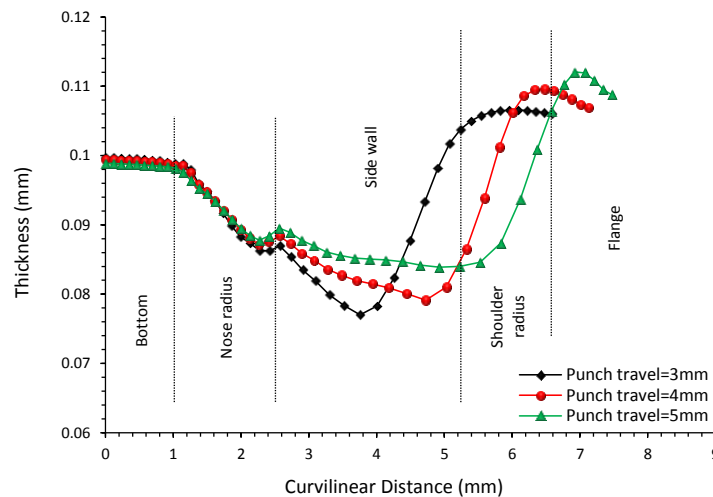


Figure 6-78. Thickness distribution along transverse direction for different punch strokes

#### 6.4.7 SCALING FACTOR

Due to the progressive growing of miniaturization in particular industry fields such as medical and electronic devices, an increasing demands on micro cups made of stainless steel 304 sheets are obviously observed. For such devices, there are imperative needs to produce stainless steel micro cups with high cup height/cup diameter ratio (i.e. cup height/cup diameter ratio is higher than unity) for specific application purposes. However, the limit draw ratio (LDR) of stainless steel 304 is characterized by certain constrains in deep drawing at micro scale, with which it cannot implement micro drawing processes for high cup height/cup diameter ratio at room temperature through a single stage drawing by using conventional rigid tools [130]. Hence, in order to prove that the current study presents a robust technique for various process size scales, the "size effects" category of process dimensions is taken into

account in this work. For this purpose, the similarity theory is employed for the process design, and in dependence on which three size-scaled drawing systems are designed and manufactured corresponding to the scaling factors of 1, 0.5 and 0.25. The geometrical parameters of the blank and forming tools are presented in Table 6-3.

Punch diameter $D_p$ (mm)	Scaling factor $\lambda$	Punch radius $R_p$ (mm)	Blank diameter $D_b$ (mm)	Rubber diameter $D_r$ (mm)	Rubber height $h_r$ (mm)
4	1	0.8	10	12	10
2	0.5	0.4	5	6	5
1	0.25	0.2	2.5	3	2.5

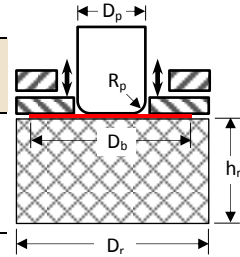


Table 6-3. Geometrical parameters of the micro deep drawing process

FE simulations are performed for the three scales down-drawing systems in accordance with the dimensions listed in Table 6-3 in order to predict the geometrical size effects on the micro deep drawing executed by flexible die tooling. First of all, drawing processes are achieved with no initial gaps are adopted for the different cases of the three scale factors. The final profiles of the obtained cups are shown in Figure 6-79.

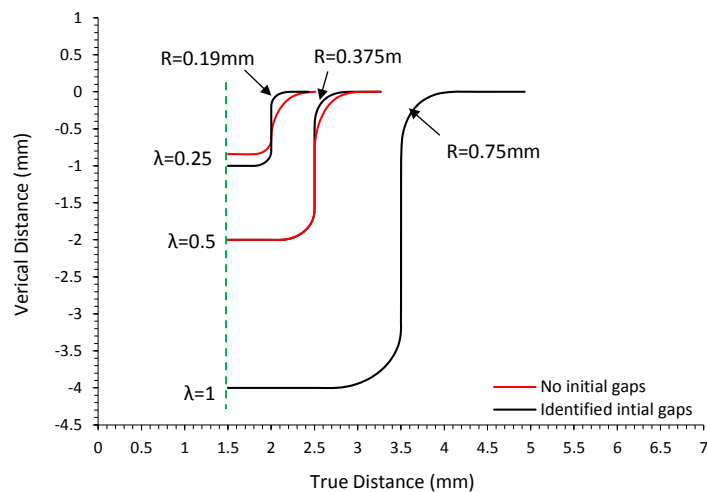
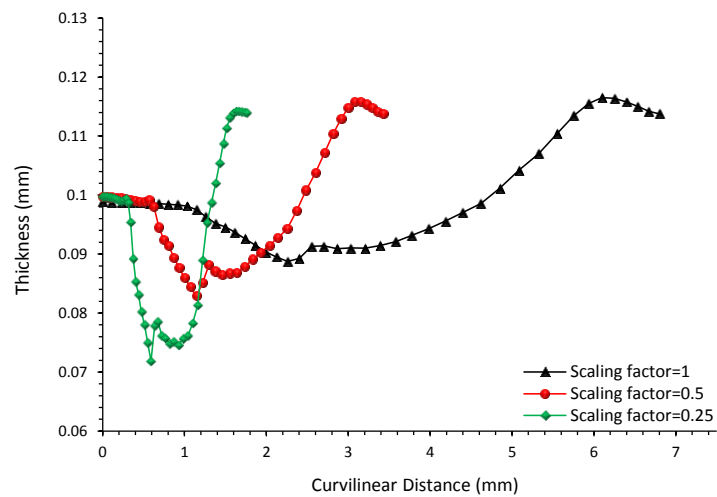


Figure 6-79. Profiles of cups produced with different scaling factors

The results indicate that just the cup formed with  $\lambda=1$  is successful, whereas the one produced with  $\lambda=0.5$  is shallow at its shoulder corner and adopting  $\lambda=0.25$  cause in wrinkles. If the cup profile obtained with  $\lambda=1$  is considered as a reference, then owing to produce micro cups of profiles similar to the reference one, the FE simulations detect that initial negative gaps of  $-170\mu\text{m}$  and  $-100\mu\text{m}$  have to be adopted for the drawing systems corresponding to  $\lambda=0.25$  and  $\lambda=0.5$  respectively (see Figure 6-79). It can be deduced from these results that for a given blank thickness, as the process dimensions in terms of scaling factors are reduced, higher

pressure is required to form a sound cup completely. The ways to increase the pressure excited in the rubber die material are either through using rubber material of higher incompressibility or applying larger initial negative gap on the used rubber die. On the other side, it was elucidated that as the initial gap decreased the reduction in the blank thickness increased during the drawing stroke, and that exactly what happened here. **Figure 6-80**, **Figure 6-81** and **Figure 6-82** reveal the thickness distributions along rolling, diagonal and transverse directions respectively for the cups produced for different scaling factors. The figures declare that the curves in each group have similar features of increments and decrements in thickness values.



**Figure 6-80.** Thickness distribution along rolling direction obtained for different scaling factors

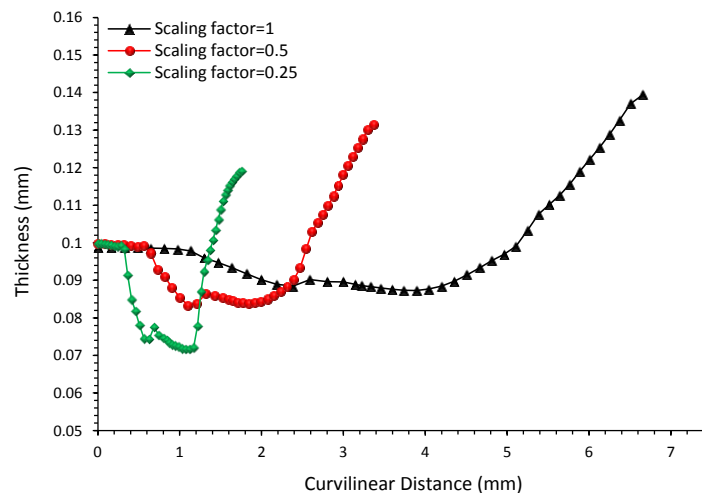


**Figure 6-81.** Thickness distribution along diagonal direction obtained for different scaling factors

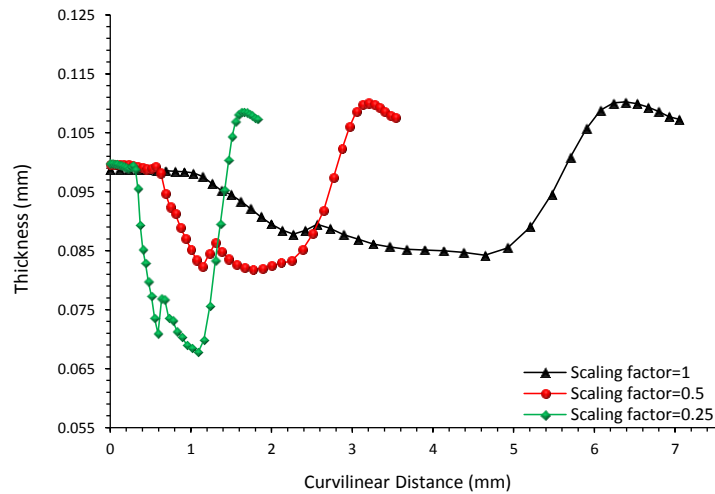


**Figure 6-82.** Thickness distribution along transverse direction obtained for different scaling factors

**Figure 6-83** presents the punch load-stroke relationships obtained from the FE simulations of micro deep drawing systems modelled according to the different scaling factors mentioned above. It can be noted that the three curves have the same trend and that the curves corresponding to  $\lambda=0.25$  and  $\lambda=0.5$  have initial punch loads of 95.4N and 105.64N respectively which are as previously explained due to the initial negative gaps. It is clear that as the scaling factor increases, higher punch load is required to form the larger workpiece. It is of most importance to understand that the loading parameters (punch load and rubber pad pressure) are relative values relating to the scaling levels that are under consideration here. For example, the maximum punch load required with  $\lambda=1$  is greater than that required with  $\lambda=0.25$  indicates that the hydrostatic pressure excited in the rubber pad with respect to  $\lambda=1$  (when the punch stroke=4mm) is greater than that with respect to  $\lambda=0.25$  (when the punch stroke =1mm).

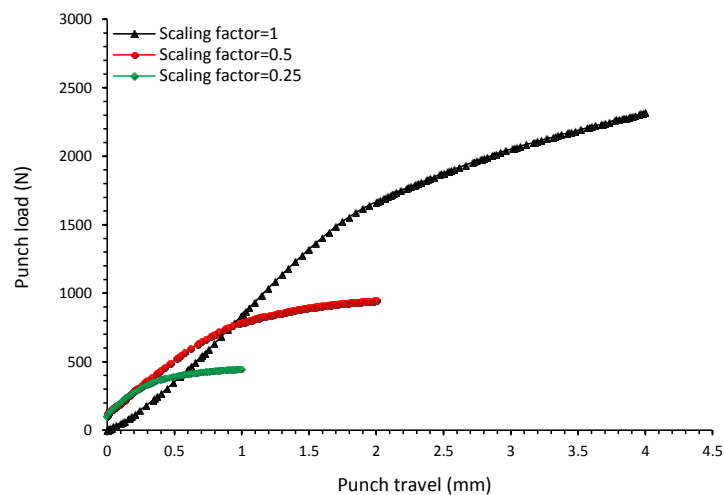


**Figure 6-83.** Punch load-travel obtained with different scaling factors



The fact that can be deduced now is that the maximum thinning remarkably increases with scaling down the process dimensions based on the scaling factors  $\lambda=0.25$ ,  $\lambda=0.5$  and  $\lambda=1$ . As previously revealed that the most crucial parameter that affect significantly on the drawing quality are the initial gap and the friction conditions especially at the blank/holder interface  $\mu_{BH}$ . Because the initial gap values depend on some production requirements such as the geometrical features of the final parts, they cannot be therefore identified as much as appropriate in order for reducing the maximum thinning that probably takes place. Due to this activity, the friction coefficient at the blank/holder interface as the most effective one is defined with different values of 0, 0.05 and 0.1 in FE simulations built based on  $\lambda=0.25$ . The drawing workpieces are modelled in these simulations with initial thickness of  $60\mu\text{m}$ ,  $100\mu\text{m}$  and  $150\mu\text{m}$ . **Figure 6-84** presents the maximum reductions in thickness obtained for the cups produced under these conditions. It can be concluded that in general reducing the friction coefficient  $\mu_{BH}$  improves the cup quality in term of maximum thinning values. The results report in this figure that maximum reduction in thickness obtained for the cups of initial thicknesses  $100\mu\text{m}$  and  $150\mu\text{m}$  noticeably decreases as the friction coefficient  $\mu_{BH}$  is reduced from 0.1 to 0. Nevertheless, just a slight different in the maximum thinning is observed for the part formed from blank of  $60\mu\text{m}$  thickness. These actions are due to the negative initial gaps -  $100\mu\text{m}$  and  $-170\mu\text{m}$  adopted correspondingly with blank thicknesses of  $100\mu\text{m}$  and  $150\mu\text{m}$  respectively in return no initial gap is utilized with the blank of  $60\mu\text{m}$  thickness. Hence, it is recommended to adopt low friction coefficient for the flange portion of the blanks when the size scaled down-drawing processes are restricted with small initial gaps.

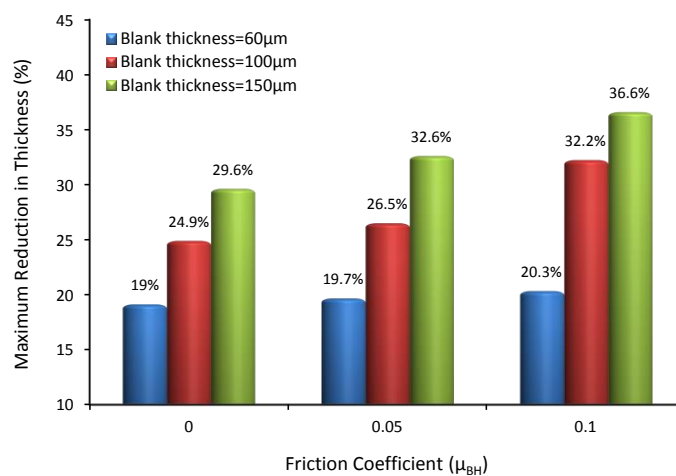


**Figure 6-84.** Maximum reductions in thickness obtained for different friction coefficient  $\mu_{BH}$

One of the main objectives of this study is to examine the feasibility of the proposed drawing technique for producing micro SS 304 cups with higher than unity aspect ratio under the conditions of the scaling factors  $\lambda=0.25$ ,  $\lambda=0.5$  and  $\lambda=1$ . For this purpose, three size-scaled systems are established through FE simulations in which the values 0 and 0.25 are defined for the friction coefficients  $\mu_{BR}$  and  $\mu_{BP}$ , whereas the blank/holder contact interface is defined with  $\mu_{BH}=0.05$  in accordance with the previous results. The aspect ratio that is targeted in this investigation is 1.5, therefore the drawing workpieces are modelled in the current simulations with initial diameters of 2.75mm, 5.5mm and 11mm corresponding to the scaling factors  $\lambda=0.25$ ,  $\lambda=0.5$  and  $\lambda=1$  respectively.

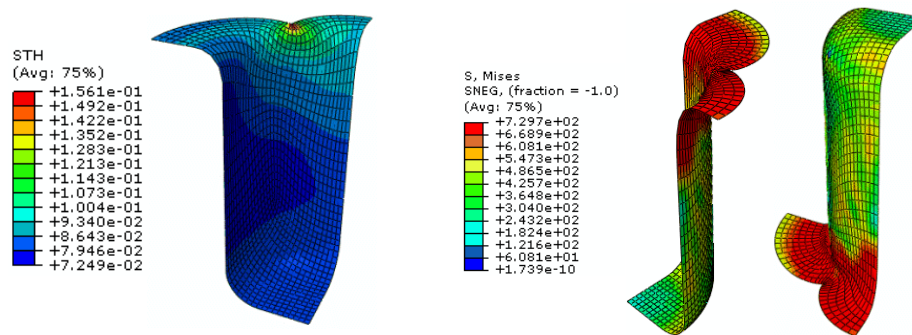


Figure 6-85. Stress and thickness contour distributions obtained with aspect ratio of 1.48 and  $\lambda=1$

The results reveal that it cannot produce a cup with aspect ratio of approximately 1.5 by a single stroke drawing process with  $\lambda=1$ . Therefore, the multi sub-strokes-drawing strategy exposed in chapter four is utilized for the late case. In this technique, the entire drawing stroke is divided into two sub-strokes; the first one is for 4mm with initial positive gap of  $60\mu\text{m}$ , and afterwards all of the punch, the blank holder and the adjustment ring are simultaneously moved up so that the total gap between the original position of the rubber die surface and the final position of the blank holder becomes  $100\mu\text{m}$ . Thereafter, the second sub-stroke of 2mm is implemented with which the total drawing stroke is 6mm. However, the maximum depth to which the final cup is drawn to 5.9mm; i.e. aspect ratio of 1.48, because no enough sheet material remains at the flange portion to produce the targeted depth, as can be seen in Figure 6-85.

On the other side, the first drawing procedure is utilized for the size-scaled forming systems at  $\lambda=0.25$  and  $\lambda=0.5$  and micro cups were produced with 1.5 and 2.98 in depth, respectively. The results indicate that the maximum thinning values for the products obtained at the three scaled systems occurs at the side wall region along the transverse direction.

Figure 6-86 shows the maximum reductions in thickness acquired from the FE numerical models for the final cups. It can be noticed that at the given initial blank thickness of  $100\mu\text{m}$ , the larger the scaling factor is the higher the maximum reduction in thickness. This figure detects that the maximum thickness reduction increases from 19% to 26.3% when the scaling factor increase from 0.25 to 1 respectively. As a result, this action proves the capability and feasibility of using the proposed technique efficiently with scaling down the micro deep drawing systems so long as the process conditions are optimized appropriately.

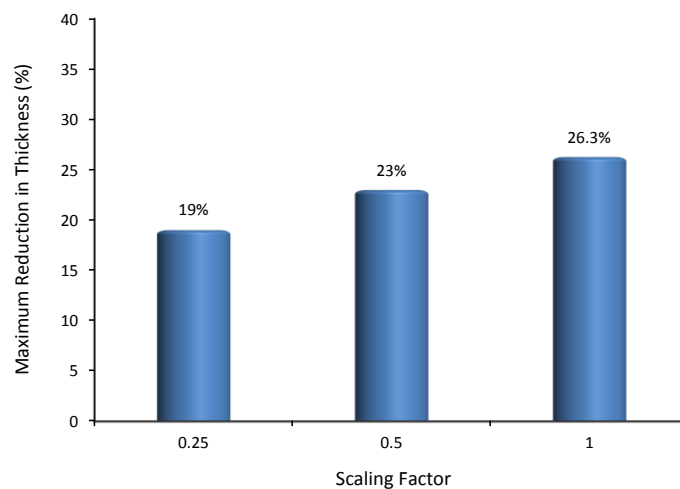


Figure 6-86. Maximum reductions in thickness obtained with different scaling factors for aspect ratio of approximately 1.5

#### 6.4.8 ANALYSIS OF THE INTERACTION OF PROCESS PARAMETERS

After investigating the influence of process parameters in a separate manner, a comprehensive analysis for the interactions between the key forming parameters is considered. The impact that takes place on the thin sheet formability due to the variation of process parameters is characterized by three cases of comparison that take into account initial gap, friction conditions at blank/holder interface, blank thickness, blank diameter and scaling levels as all of them affect the material behaviour. In the first case, the relationship between the initial gap and the friction coefficient  $\mu_{\text{BH}}$  values are presented for the micro drawing system at  $\lambda=1$  under constant blank thickness with various blank diameter as shown in Figure 6-87 to Figure 6-89. It can be deduced that the domain of producing successful parts is wider for the smaller blank diameter.

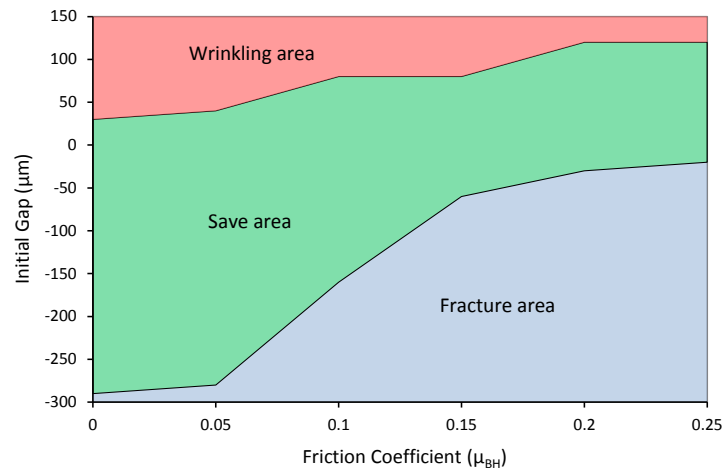


Figure 6-87. Initial gap via friction coefficient relationship for blank diameter of 9mm

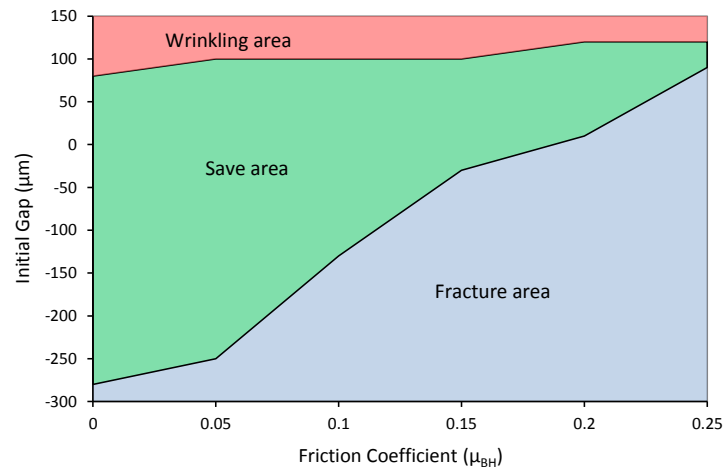


Figure 6-88. Initial gap via friction coefficient relationship for blank diameter of 10mm

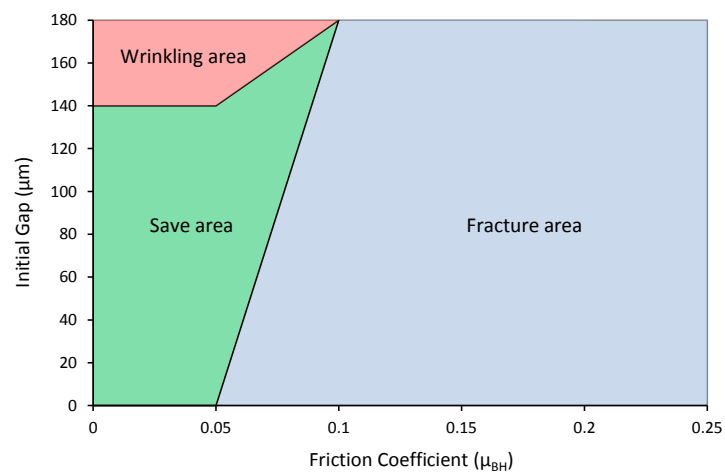
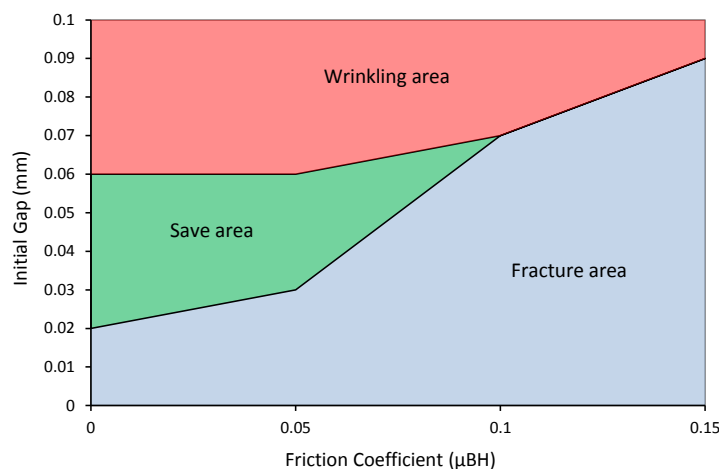


Figure 6-89. Initial gap via friction coefficient relationship for blank diameter of 11mm

The range of the initial gaps values that can be adopted at a particular friction coefficient  $\mu_{BH}$  so that successful parts are obtained is greater in the case of using blank diameter of 9mm compared with the blank diameter of 10mm and 11mm. Another observation is that using blanks of 11mm diameter cause the final product to be under a risk of failure by fracture for  $\mu_{BH} > 0.05$ . Other result report that no sound cups can be obtained over forming blanks of 12mm diameter. This action is because at this case the blank diameter is equal to the rubber die diameter which implies that the hydrostatic pressure excited inside the rubber material is totally applied on the blank instantaneously at the beginning of the drawing stroke. Also, the other effective factor in this result is the relatively high limit drawing ratio cooperating with the ratio of the blank thickness to the rigid punch diameter.

The second comparison case presents the relationships between the initial gap and the friction coefficient  $\mu_{BH}$  again but this time under constant blank diameter with varying the initial blank thickness. In this case, micro deep drawing system at also  $\lambda=1$  is considered where the initial diameter of the blank is 10mm. Moreover, the deformation behaviour of the blank models is defined using the mechanical properties acquired for the SS 304 sheets of 60 $\mu\text{m}$ , 100 $\mu\text{m}$  and 150 $\mu\text{m}$ . By exploring carefully the **Figure 6-90** to **Figure 6-92** it can be noticed the significant variation in the ranges of both the initial gap and the friction coefficient values that are adopted with the different blank thicknesses. In general, the domain of successful cups decreases remarkably with reducing the initial thickness of the used blanks. It can be denoted that the greatest ranges of the initial gap and the friction coefficient are acquired for the case of 150 $\mu\text{m}$  blank thickness, and thereafter these ranges recede for the thickness 100 $\mu\text{m}$  until be significantly limited for the 60 $\mu\text{m}$  thickness.



**Figure 6-90. Initial gap via friction coefficient relationship for blank thickness of 60 $\mu\text{m}$**

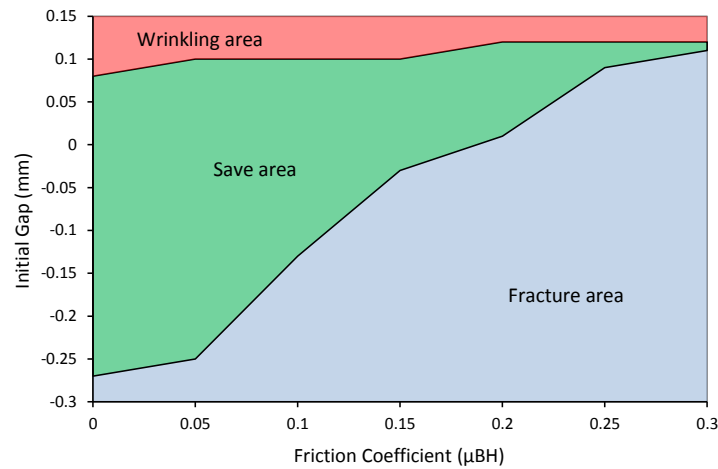


Figure 6-91. Initial gap via friction coefficient relationship for blank thickness of  $100\mu\text{m}$

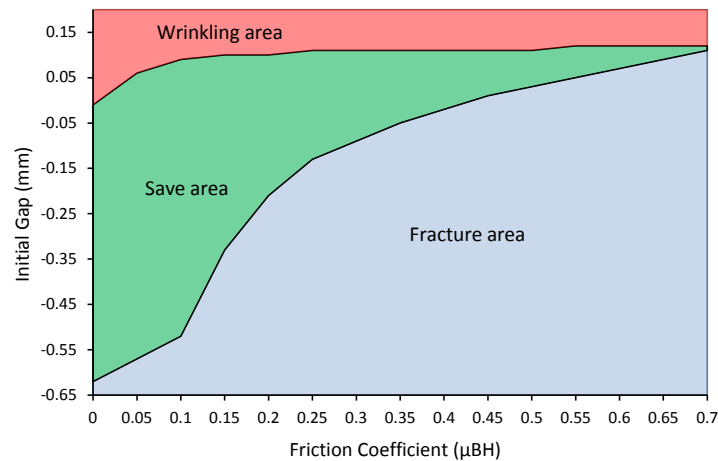


Figure 6-92. Initial gap via friction coefficient relationship for blank thickness of  $150\mu\text{m}$

This action can be rationalized depending on the observations acquired here and in the previous investigation. It can be said that beside the direct influence of the blank thickness, the ratio between the blank thickness to punch diameter as well as the blank diameter and blank thickness ratio contribute in the current window for the drawing process. For example, increasing the punch diameter and/or reducing the diameter of the blank of  $60\mu\text{m}$  in thickness will improve the drawing quality and the final result configuration in accordance with the results obtained above. The last comparison case is made for the maximum thinning and the maximum drawing loads obtained at the scaling factor  $\lambda=1$ ,  $\lambda=0.5$  and  $\lambda=0.25$  with using different blank thicknesses of  $60\mu\text{m}$ ,  $100\mu\text{m}$  and  $150\mu\text{m}$ . for this purpose, FE numerical simulations are established for these conditions so that at each particular scaling factor the working blanks are modelled with the three different initial thicknesses.

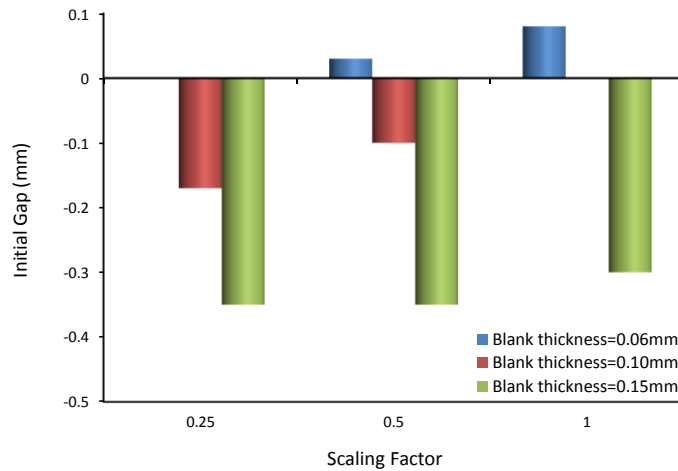


Figure 6-93. Initial gaps adopted at different scaling factors

With respect to the scaling factor, similar process characteristics are considered in these models. In order to fulfil the condition of reasonable comparison for producing cups with similar geometrical features, the initial gaps presented in **Figure 6-93** are taken into account so that the reference profile is that acquired with  $\lambda=1$ , blank thickness of 100 $\mu\text{m}$  and no initial gap. **Figure 6-94** illustrates the maximum reductions in thickness taken from the FE simulations. The general trend is that at a given scaling factor, the maximum thickness reduction increases as the initial thickness of blanks increases. For example, at  $\lambda=0.25$  the maximum thickness reduction of 20.3% that is obtained with 60 $\mu\text{m}$  initial thickness increases to 32.2% with 100 $\mu\text{m}$  thickness and thereafter to 36.6% with 150 $\mu\text{m}$  blank thickness. However, the rate of this increase is clearly higher for the smaller scaling factor. Another finding is that the maximum reduction in thickness of all the cups formed using blanks with the different initial thicknesses adopted in this investigation experience a significant decrease with the increase in the scaling levels. For example, the maximum thinning that occurs for 150 $\mu\text{m}$  blank thickness decreases from 36.6% at  $\lambda=0.25$  to 17.2% at  $\lambda=1$ . These results can be attributed to the ratio of the punch diameter to the blank thickness as well as the initial gaps adopted at each case. At a particular scaling factor, as the blank thickness is increases the punch diameter/blank thickness inevitably decreases which requires a smaller initial gap in order to produce parts with similar final profiles. Consequently, this activity in turn leads to a higher thinning for the obtained cups. Likewise, for the same blank thickness reducing the scaling factor causes the punch diameter/blank thickness ratio to decrease resulting in thinning for the product as smaller gaps are whereupon required.

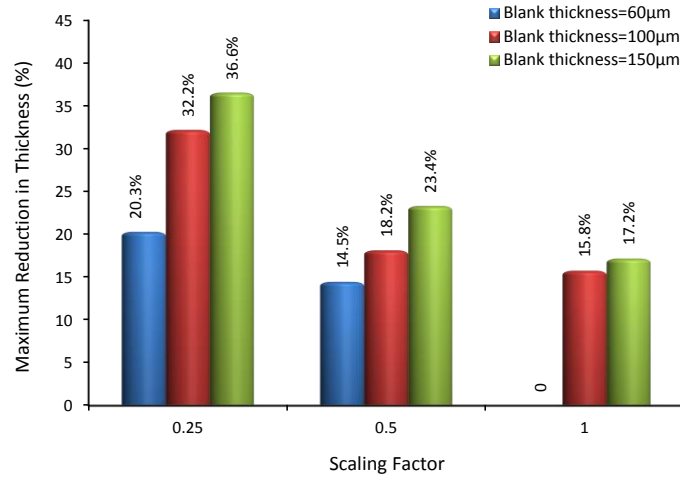


Figure 6-94. Maximum reductions in thickness obtained at different scaling factors

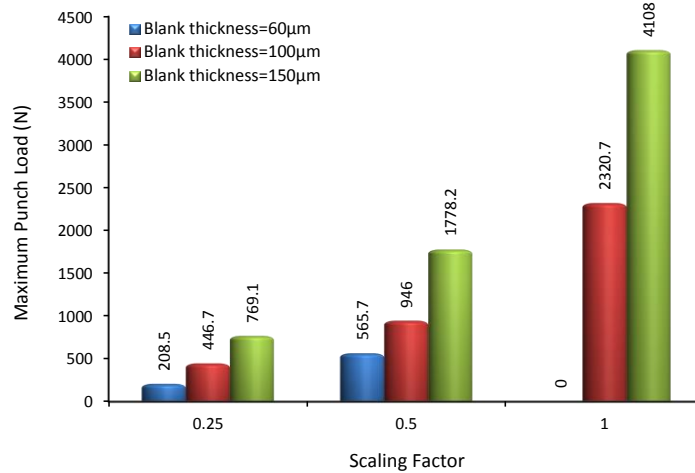


Figure 6-95. Maximum punch loads obtained at different scaling factors

On the other side, it can be evidently seen in Figure 6-95 that the maximum punch load needed for completely drawn cups increases with the increase in the initial thickness of the blanks formed at the same scaling level as well as with increasing the scaling factor even if the same blank thickness is utilized. The action of the former case is due to the smaller initial gaps used for the thicker blanks. Nevertheless, the later action can be rationalized that increasing the scaling factor implies higher drawing stroke which normally needs greater punch load so long so the same rubber material is used for the flexible die.



## **CHAPTER SEVEN**

# **EXPERIMENTAL VALIDATIONS OF FE SIMULATIONS**

\*\*\*\*\*

## **7.1 INTRODUCTION**

Chapter six presented FE simulations for micro deep drawing processes in accordance with the proposed technique. Numerical models were built to predict the effects of different key process parameters. This chapter demonstrates experimental validations for the numerical results obtained under various forming conditions. The preparation procedure of the workpieces cut from stainless steel 304 sheets with different thicknesses is explained in section 7.2. A special set up was developed to conduct deep drawing experiments at micro scale as illustrated in section 7.3. Section 7.4 shows the main drawing tools involving rigid punches, rigid blank holders and flexible dies that are designed and fabricated depending on the different scaling factors adopting in this study. The working procedure that is followed to perform the drawing experiments is clarified in details in section 7.5. Thereafter, owing to measure the wall thickness of final products each cup is cut along two different orientations using a special facility as can be seen in section 7.6. Finally the experimental results are presented and discussed in section 7.6.

## **7.2 PREPARATION OF DRAWING WORKPIECES**

Due to the nature of the devices used for various medical applications, these devices require extremely precise design and fabrication criteria. Some of the medical devices and components employed in surgical instruments to be in direct contact with the body tissues and others are implanted within human bodies, therefore they must be fabricated exactly as designed, without fail. As a result of its properties that meet with these requirements, stainless steel 304 (SS 304) is regarded one of the most appropriate materials to be used efficiently in manufacturing the medial devices [168]. As well as, SS 304 sheets has a wide range of applications in electronic and electricity industries at micro scale such as mini cartridge heaters, micro motor housings, micro vibration/movement and sensors and switches, cartridges for transistors and capacitors, etc. (see **Figure 7-1**). Therefore, stainless steel 304 sheets with different thicknesses of 60 $\mu\text{m}$ , 100 $\mu\text{m}$  and 150 $\mu\text{m}$  are utilized in this study provide various blanks for micro drawing experiments. In order for blanking processes of sheet metals male (punch) and female (die) tools are usually used. For these tools, the die clearance is defined the total difference between the male and female dimensions. The proper amount of

clearance to be identified, a number of variables have to be taken into account such as sheet metal hardness, speed of press, design of tools, finish on punches and dies, etc. The optimum clearance results in maximum tool working life and reduces the cutting pressure required.

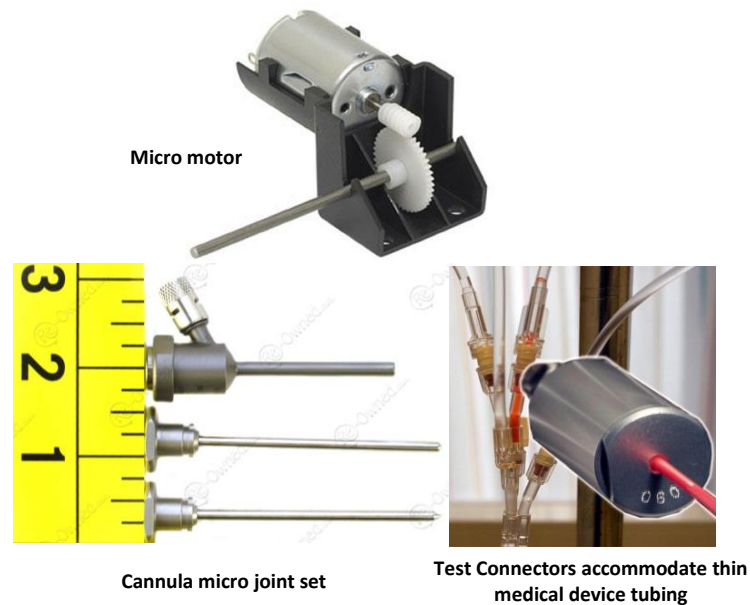


Figure 7-1. Applications of micro stainless steel cups [169-171]

Regarding the materials of high shear strength such as stainless steel, it is recommended to adopt clearance 25% of the initial thickness of the sheet metal [172]; i.e. approximately  $15\mu\text{m}$ ,  $25\mu\text{m}$  and  $37.5\mu\text{m}$  for the current sheets of  $60\mu\text{m}$ ,  $100\mu\text{m}$  and  $150\mu\text{m}$  in thickness respectively). In this work, it was observed that this clearance amount is not efficient enough to produce blanks with smooth cutting edges.

As can be seen in **Figure 7-2**, the blank rim is obviously bent and has evident burrs which refer to tearing action. This situation indicates that the clearance was greater than what must so that allows for sheet metal to go through between the punch and the die and to experience tearing instead of shear. Thus, the clearance was reduced to be 20%; i.e. approximately  $12\mu\text{m}$ ,  $20\mu\text{m}$  and  $30\mu\text{m}$  for the current sheets of  $60\mu\text{m}$ ,  $100\mu\text{m}$  and  $150\mu\text{m}$  in thickness respectively. In order to verify the numerical investigation relating to the effect of blank thickness, blanks of 10mm in diameter are needed to cut from the SS 304 sheets aforementioned. For this purpose, a blanking punch with diameter of 10mm was employed correspondingly with die set that according to the proper clearance aforementioned have the diameters of 10.012mm, 10.02mm and 10.03mm for the sheet of  $60\mu\text{m}$ ,  $100\mu\text{m}$  and  $150\mu\text{m}$  in thickness respectively (see **Figure 7-3**).

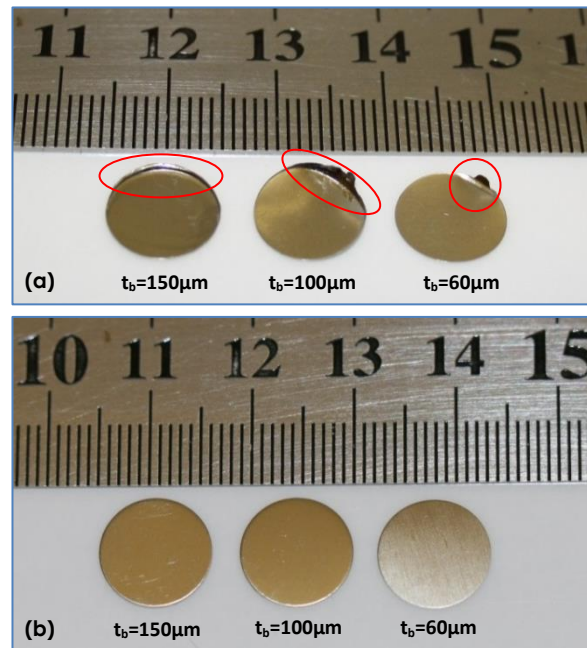


Figure 7-2. Stainless steel 304 blanks of different thicknesses ( $t_b$ ) (a) failed cutting process with obvious burrs (b) Successful blanks

Moreover, the three size-scaled micro deep drawing systems designed in this study based on the scaling factors presented in **Table 6-3**, necessitated providing blanks of 100 $\mu\text{m}$  thickness with initial diameters of 2.5mm, 5mm and 10mm. Furthermore, in order to validate the results obtained from the numerical models related to the effect of blank diameter, blanks with various diameters of 9mm, 10mm, 11mm and 12mm were needed to cut from SS 304 sheet of 100 $\mu\text{m}$  in thickness.

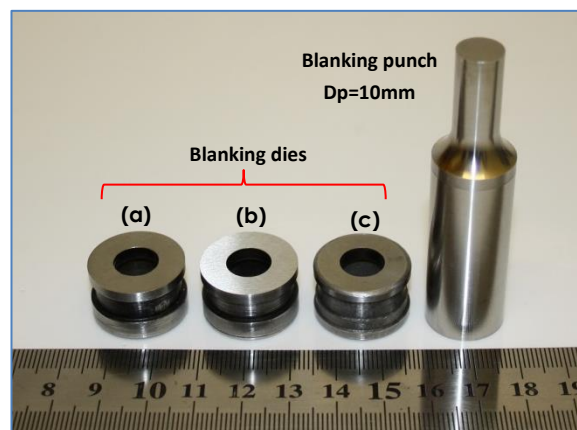
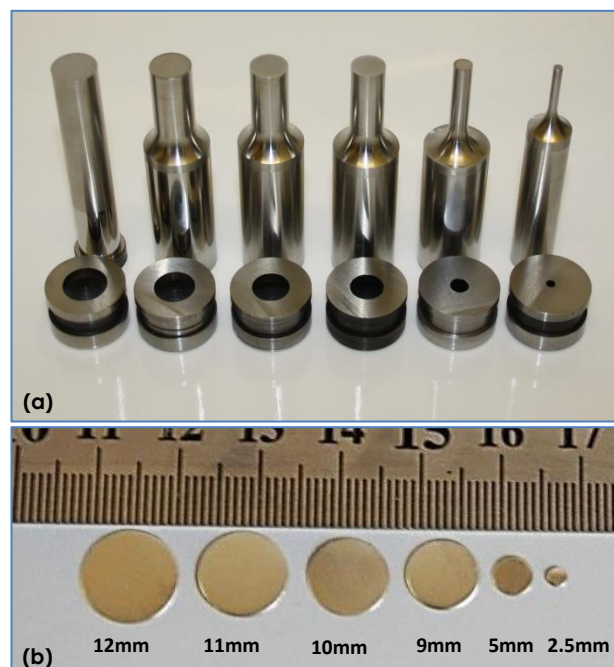


Figure 7-3. Blanking tools, punch of head diameter  $D_p=10\text{mm}$  and dies of opening diameters of (a) 10.012mm (b) 10.02mm and (c) 10.03mm

To fulfil these requirements, blanking punch of 2.5mm, 5mm, 9mm, 10mm, 11mm and 12mm in diameter and correspondingly blanking dies with diameters calculated based on the

clearance 20% were designed and fabricated as shown in **Figure 7-4**. The very important issue in the cutting processes is that the around edges of the blanking punch heads and die openings must be very sharp to provide perfect shearing conditions which consequently lead to clean and smooth cutting edge lines. Actually, these tool pairs were made of carbon steel, and were subjected to hardening conditions at nearly 750°C in order to increase the surface hardness. The cutting processes were carried out through attaching the blanking tools along on the Instron 3956 machine, where the punch is clamped on the upper grip of the machine by using a special; connector while the die is tightly clamped on the lower platen of the working machine.



**Figure 7-4. (a) Blanking punch-die sets tools (b) SS 304 blanks of 100 μm in thickness with different diameters**

### 7.3 DEVELOPMENT OF EXPERIMENTAL SETUP

The experimental set up shown in **Figure 7-5** was developed in this study in order to conduct a series of micro deep drawing experiments to validate the numerical results obtained from the FE simulations. The apparatus is basically composed of two main sets of components; upper set which is movable and lower set which is stationary that are presented in **Figure 7-6**. The upper set is driven by the moving grip of the Instron 3956 machine that is employed for the drawing experiments; therefore this set represents the movable part of the entire apparatus. In fact, the upper can be divided into two groups of components according to the

function performed by each group as illustrated in **Figure 7-6a**. The first group involves upper circular plate, lower circular plate, three supporting springs with their guides, three guide posts and upper connector. Actually, the spring guides are intended here as bolts with threaded length of 20mm, in order to allow the upper and lower plates to connect with each other as well as to provide possibility of compressing the supporting springs into initially an identified distance. Whereas, the second group consists of rigid punches, blank holders, blank holder housing, gap-adjustment ring, holding spring and three studs with twelve nuts (see **Figure 7-7**). The latter group in fact includes the main tools that represent the micro drawing system, which are the responsible on the forming results. The function of the three studs is to connect the blank holder housing and the lower plate but away from each other by a particular distance.

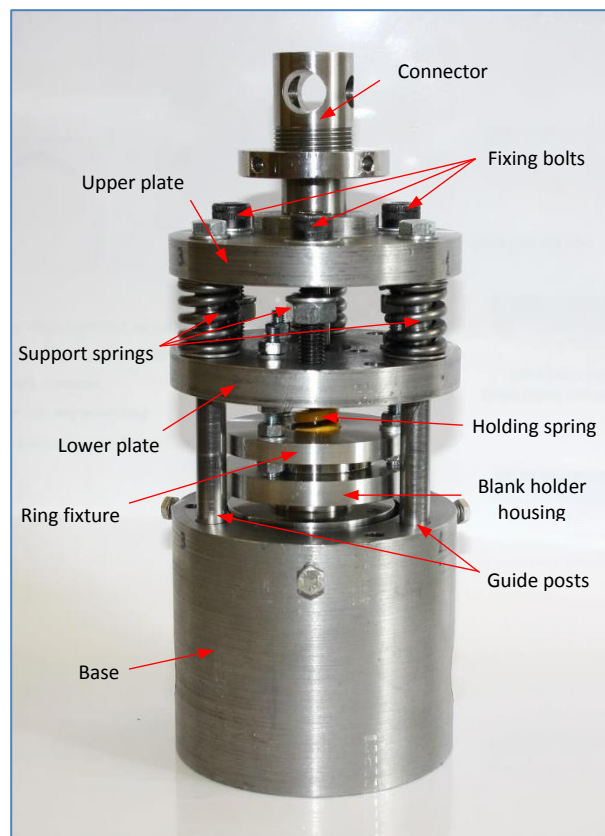


**Figure 7-5. Experimental set up**

However, this distance is changeable depending on how much the initial holding force requires applying on the blank holder. The other function of these studs is to adjust the position of the adjustment ring by which the initial gap with the blank holder that is consistent for a given process conditions can be set. For this activity, three nuts were allocated over the

gap-adjustment ring and other three underneath, and the initial gap can be controlled through raising or lowering the fixing ring (see **Figure 7-8**).

On the other side, the lower set of the current set up is constructed of main base, three screws, cylindrical rubber container, rubber container housing and rubber die as seen in **Figure 7-6b**. The screws were used to adjust the position of the rubber container so that coincide with the blank holder and drawing punch. By this manner, it can avoid any damages probably occurs for these three components. The rubber containers were designed with internal diameter just allows for the rubber die to be tightly inserted. While, the height of the containers is greater than that of the rubber die by nearly 3mm and the height of the blank holder feature is 4mm; i.e. the difference is 1mm which provides a possibility to perform the negative gap-micro deep drawing technique presented in chapter four.

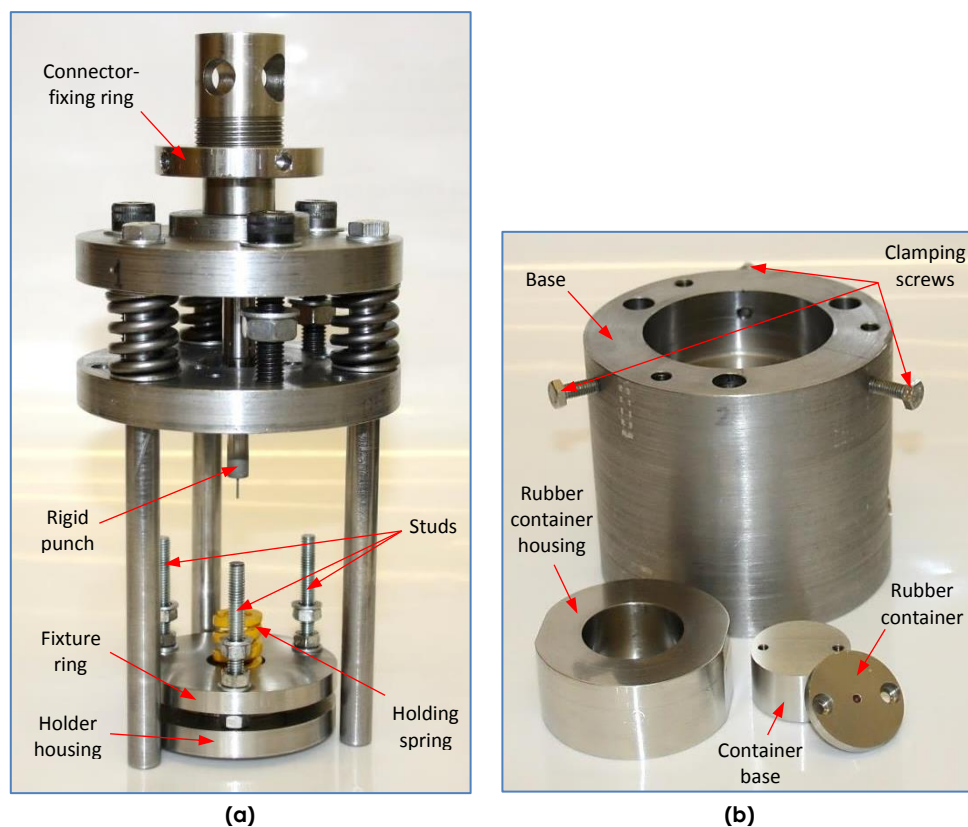


**Figure 7-6. Components of the experimental set up (a) upper component set and (b) lower component set**

The reason behind making the rubber container and the rubber container housing to be separated each other is because various rubber dies with different diameters and heights were used which implied then rubber containers with different dimensions were needed. In order to reduce the cost and time of manufacturing operations, therefore just the small rubber

containers were replaced as the drawing conditions necessitate. Due to this activity, the new part may not coincide precisely with the blank holder feature and the rigid punch. Hence, the advantage of the rubber container housing is to re-adjust these parts together through the three screws disseminated circumferentially around the platform base.



Figure 7-7. Drawing tools

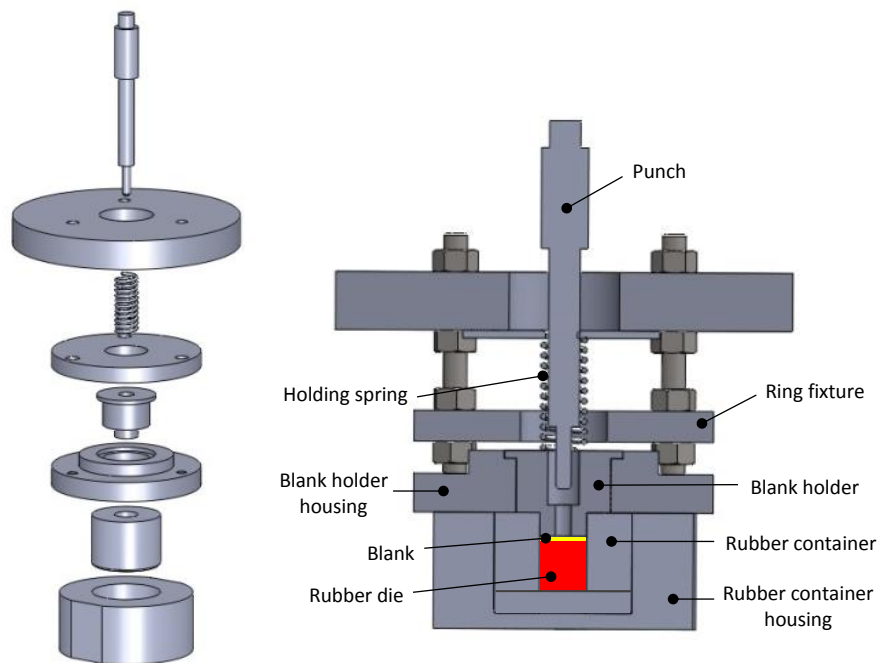


Figure 7-8. Assembly of the drawing tools



This set is tightly clamped by two grapples on the base platen of the experiment machine. The main function of the three supporting springs in the former set is to provide a high supporting pressure to the lower plate to keep it fixed against the holding spring action. For this purpose, these three springs were chosen with relatively high stiffness of 300N/mm which means 900N/mm in total compare to 100N/mm for the holding spring. The geometrical features and dimensions of all components of this set up are provided in appendix A.

## 7.4 DRAWING TOOLS

### 7.4.1 RIGID PUNCHES

One of the targeted points in this study is to investigate the possibility of employing the proposed technique for micro deep drawing processes at different size scales. The numerical results acquired from the FE simulations in chapter six revealed that the conditions of drawing processes necessitate to be changed in accordance with the requirements of each scaling factor that is considered for a particular case. As shown in **Table 6-3** three scaling factors are adopted for the process dimensions in the current work. Based on these scaling factors, three size-scaled micro deep drawing systems were simulated through FE numerical models using ABAQUS code. In order for the simulation results to be verified, the three size-scaled drawing systems are fabricated with taking into account the key dimensions presented in the table. For this purpose, three rigid punches are manufactured with different size scales for the geometry features that identify directly the final profile of the produced cups. **Figure 7-9** demonstrates rigid punches with head diameters 1mm, 2mm and 4mm, which are used in the micro deep drawing experiments carried out at scaling levels of  $\lambda=0.25$ ,  $\lambda=0.5$  and  $\lambda=1$ , respectively.

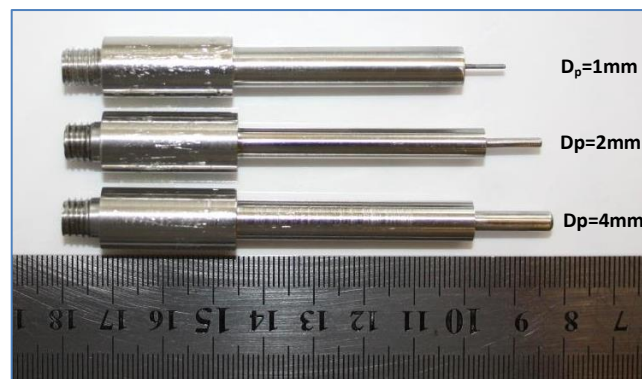


Figure 7-9. Rigid punches of different head diameters ( $D_p$ ) corresponding to different scaling factors

It can be noticed that these punches are designed and fabricated so that the upper ends are featured as threaded parts. These threaded features are utilised to fasten the rigid punches into the central tapped hole made on the lower face of the upper plate. The rigid punch is strongly tightened to keep it perfectly parallel to the main vertical axis of the experiment set up. Moreover, the punch is passed through the lower plate; the holding spring and the blank holder (see **Figure 7-8**). The design of the rigid punches is intended so that the total length is enough to perform the forming strokes achieved in the numerical models.

#### 7.4.2 BLANK HOLDERS

On the other side, the manufactured blank holders that used in the micro drawing experiments as well as their geometrical schemes are presented in **Figure 7-10** with respect to the three scaling level considered in current work. It can be denoted that the clearance intended between the outer wall of the blank holder and the inner wall of the blank holder housing is relatively very small just about  $20\mu\text{m}$  for all scaling factors. As well as, the figure indicate that the clearance between the punch head span and the internal wall of the central cavity of the blank holder is nearly  $40\mu\text{m}$ .

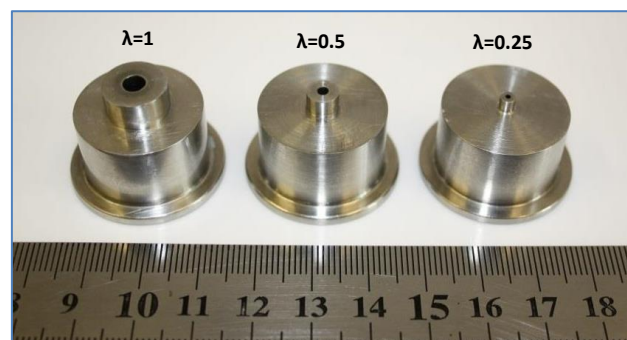
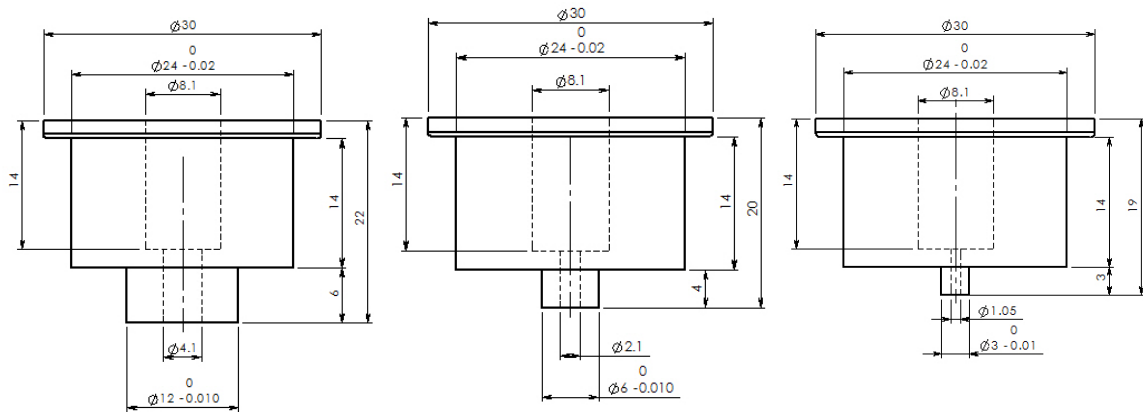
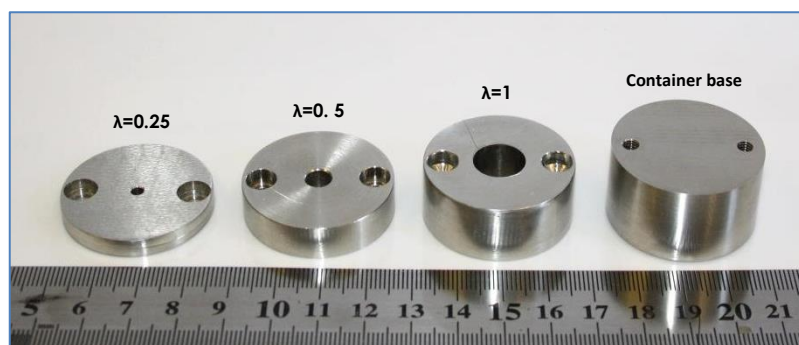


Figure 7-10. Blank holders of corresponding to different scaling factors ( $\lambda$ )

These design aspects are intended to ensure that the rigid punches at all cases of the different scaling factors consistently coincide with the blank holder. By this strategy, it can avoid any damages that probably occur for the drawing tools during the drawing processes. Furthermore, the central cavity of the blank holder is in fact composed of two sequent holes with different diameters and heights with which the blank holder is harmonious with the punch features. It can be seen that the heights of the smaller holes of the three parts illustrated in **Figure 7-10** are 8mm, 6mm and 5mm, whereas the length of the head span of the corresponding punches are 16mm, 12mm and 8mm, respectively at scaling factors of 1, 0.5 and 0.25. These dimensions indicate that the parts of the punch head spans that are actually utilised for forming the sheet metals are 8mm, 6mm and 3mm at the scaling factors aforementioned. That implies that the punch lengths are enough to produce cups with aspect ratios even higher than the maximum value of 1.5 that is obtained from the numerical models.

#### 7.4.3 RUBBER DIES AND CONTAINERES

**Figure 7-11** demonstrates the rubber containers employed for the flexible die during the micro deep drawing experiments at each of the size scaling levels adopted here. The figure shows that each blank holder consists of two parts; base disk and hollow cylinder. This design allows for the rubber pieces to be inserted and pick out very easily.



**Figure 7-11. Rubber containers used at different scaling factors ( $\lambda$ )**

The steps of setting the rubber die starts by inserting the rubber piece into the cavity of the hollow cylinder so that a small part is left out. Thereafter, the base disk is positioned on the lower face of the cylinder pushing up the remaining part of the rubber die into the cavity, and by this strategy it can ensure that the rubber die base is in direct contact with the base disk. Afterwards, the disk is fixed on the hollow cylinder by using two bolts. The rubber pieces

that are used in the experiments as flexible forming dies in accordance with the three scaling factors are shown in **Figure 7-12**.

By comparing the heights of these rubber dies and the depths of the central holes of the corresponding rubber containers, it can be deduced that the differences are 4mm, 3mm and 2mm which represent the space remaining over the rubber dies. On the other side, it can be noticed for the parts presented in **Figure 7-10** that the heights of the features that directly contact the blanks during the drawing processes are 6mm, 4mm and 3mm in accordance with the scaling factors of 1, 0.5 and 0.25 respectively. That indicate that the blank holder features can be used to initially compress the rubber dies by distances greater even than that recommended according to the numerical results.

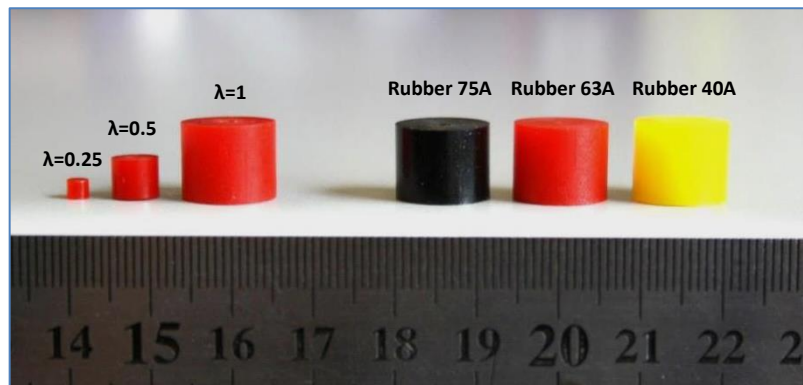


**Figure 7-12.** Polyurethane rubber Pieces used for the flexible forming dies

## 7.5 EXPERIMENTAL PROCEDURE

The micro deep drawing experiments were carried out utilizing the Instron 5965 machine with load cell capacity of 50kN for measuring the deformation load. The key technical specifications of this machine model are load measurement accuracy +/-0.5% of reading down to 1/1000 of load cell capacity option, speed range of 0.001 to 3000mm/min, and automatic transducer reorganisation for load cells and extensometers. The experiment proceedings start when the supporting springs that have a length of 33mm are compressed about 3mm to provide an initial supporting force of 2700N to the lower plate. Afterward, the initial gap is set up as aforementioned by positioning the gap-adjustment ring at the correct position depending on the requirements of the case conditions under consideration. As mentioned previously that the initial gap is one of the most crucial parameters of the proposed micro deep drawing technique, however adjusting the gaps at high standard of accuracy is in fact of

high difficulty in the experimental work of this study. For this purpose, three feeler gauges were utilised in order to obtain precisely accurate measurements for targeted gaps. The feelers of the required size were positioned simultaneously over the blank holder housing at different positions along the circumference direction, and the adjustment ring was then dropped down to be in direct contact with these feelers. Afterwards, the nuts over and underneath the ring fixture were strongly tightened to keep the adjustment ring fixed at its instant position. At this time, the holding spring was compressed between the blank holder housing and the lower plate by tightening the three screw posts to a particular distance so that the proper initial holding force could be generated. Thereafter, the position of the rubber container housing was adjusted manually and then clamped using the three bolts spaced by equal angular spans around the set up based. By this strategy, the rubber container was coincided with the upper set; i.e. importantly with the punch and the blank holder feature. The set up became ready now for drawing experiments, and thus it was attached to the Instron 5965 machine used in this work as seen in **Figure 7-13**.

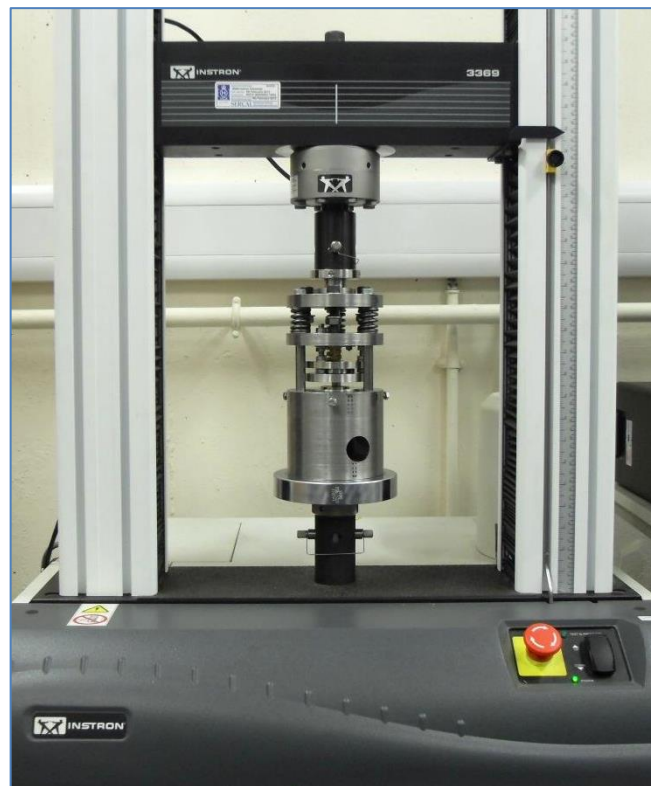


**Figure 7-13.** The experimental; apparatus is set on the Instron machine

The moveable part of this set up was tightly clamped to the machine grip using the upper connector, whereas the lower part was just put over the bottom platen of the machine. The last step prior the actual drawing operation was to position the working blank on the rubber die surface. For this purpose, the positioning rings shown in **Figure 7-14** were utilized. The inner and outer diameters of these rings are depended on the diameter of the blank wanted to form and the diameter of the rubber container opening respectively. The differences between each corresponding pair of the dependent and independent diameters are  $\leq 20\mu\text{m}$ . The positioning rings were introduced into the space remaining inside the container over the rubber die. After that, the blank was inserted into the ring cavity and dropped falling through it down until reaches the rubber surface, then the positioning ring was picked out. At this time, the drawing process began by moving the machine grip a distance that equal the sum of the gap between rubber container and the blank holder plus the drawing stroke targeted for a particular case.

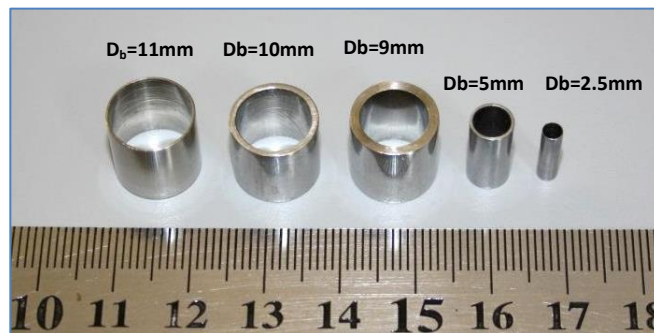


**Figure 7-14.** Tubular-shaped positioning components for different blank diameters ( $D_b$ )

## 7.6 PREPARATION OF PRODUCED CUPS FOR MEASUREMENT

It can be seen in chapter six that the thickness distribution of formed cups is one of the most important factors that represents an index on the drawing quality. Therefore, the wall thicknesses of the final products were measured for all drawing cases that are considered in this study. In order to establish a comparison with the experimental results of thickness distributions, the physical products have to cut at different paths with respect to the rolling direction along which the wall thickness is needed to be measured. For this purpose, the first cutting attempts were carried out by using the laser technology, but unfortunately no facilities were provided in our laboratory that can supply the laser beams appropriate for the SS 304 sheets used in the current work. Thereafter, the other option was to adopt a mechanical

strategy, and hence the high precision cut-off saw machine presented in **Figure 7-15** was employed. The maximum speed of the watering blade attached to this machine is ranging from 1000rpm. A set of sample holders is available with this machine including a rotating holder for round samples. The sample holder is held on a pivoting arm which is moved with a micrometre adjustment. The blade utilized for cutting the metallic cups produced in this work was 0.5mm in thickness.

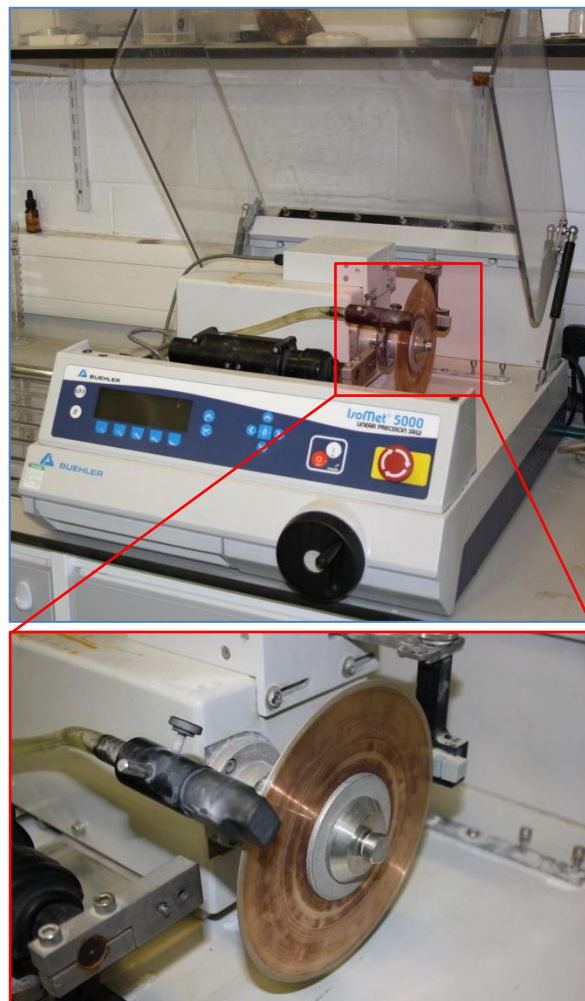


**Figure 7-15. The high precise cut-off saw machine used for cutting the produced cups**

Before forming processes, each of the SS 304 blanks are marked with a line referring to the rolling direction in order to easily identify the direction along which the formed cup wanted to cut. As the cup sizes are small in total and with very thin walls to be held by the sample holders of the cutting machine without proper damages, a special technique was thus required for this purpose. The formed part was positioned inside a cylindrical die so that the cup shoulders spread on the die bottom. The size of this was appropriate to hold the product

by the cutting machine holders. Afterwards, an amount of epoxy liquid mixed with hardener material is carefully poured into the die cavity with taking into consideration not to move the cup until filling up the die. Then the mixture is left for a certain time to dry. After that, the dry epoxy block, which now contains the metallic cup, is picked out of the die. Afterwards, a line was drawn with a permanent pin on the epoxy block face where the cup shoulder is apparent to be as a guide for the cutting process. **Figure 7-16** illustrates a formed cup that is cut along the rolling direction but still assembled to the epoxy block. Although, the cut-off saw machine shown in **Figure 7-15** is designed so that gives a high quality standard for the cut surface without deformation, however little burrs were observed on the cut surface of the cup thickness section. Due to the cut quality is a decisive factor in measuring the thickness distributions, the entire cut surface of both epoxy material and metallic cup was polished by using a very fine sand paper sheet of 1200 grade.

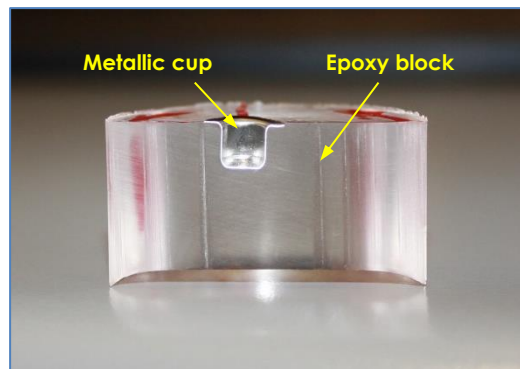


**Figure 7-16.** Cutting section of the metallic cup and epoxy block

## 7.7 EXPERIMENTAL RESULTS AND COMPARISON

This section reports the results acquired from micro deep drawing experiments achieved under different process conditions. Also, a comparison between the results obtained from the FE simulations and experiments in terms of product geometrical profile, thickness distribution and punch load-travel relationship is presented in the current chapter. In order for this comparison to be established, the wall thicknesses of a number of produced cups were measured along the rolling and transverse directions. For this purpose, the Nikon Eclipse ME600L microscope model, which is called Nomarski microscope, using Nikon digital camera DXM1200 was employed for the thickness measurements. The thickness measurements were performed at several points along the curvilinear path of the cut cups. On the other side, the



punch load-travel relations were calculated from the resultant readings taken from the working machine. First of all, the experimental apparatus was set on the machine without rubber die and metallic blank and then this machine was operated to a particular stroke that is targeted when a blank is employed. Thereafter, an actual drawing process was carried out to produce a physical cup under the same conditions. The corresponding values of the punch loads obtained from the former time were subtracted from that recorded at the same travels in the later time. By this procedure, the net punch loads required to form the considered blank was acquired.

Before presenting the experimental investigations of the key process parameters considered in this work, a number of physical cups that were produced under different forming conditions are demonstrated in **Figure 7-17**.

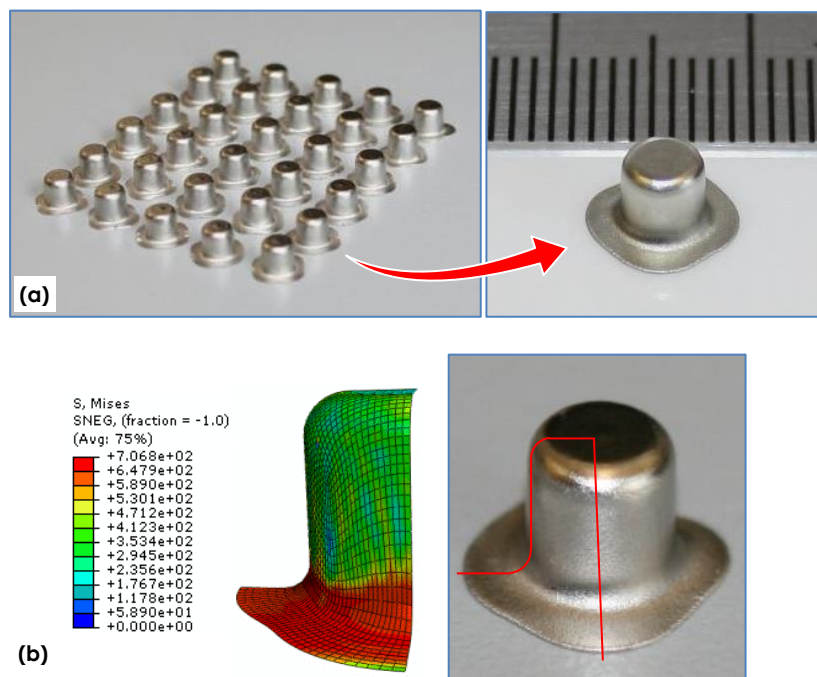


**Figure 7-17. (a) Physical cups (b) Comparison between physical and simulated cups in terms of final profiles**

The first important point that can be indicated from this figure is the capability and the feasibility of the novel technique proposed in the current study for micro deep drawing processes. By the way, it can denote from this figure that the cups obtained from FE simulations well match in terms of the final geometrical profiles with the physical ones produced under the same conditions. The physical cup presented in **Figure 7-17** detects the influence of the anisotropic behaviour of the SS 304 sheet material identically as predicted in the FE models. This action points out two essential issues; the validation of the FE numerical

models that are established in the current study in efficiently simulating the proposed micro deep drawing technique as well as the reliability of the developed experimental set up as a research equipment.

### 7.7.1 INITIAL GAP

#### 7.7.1.1 THICKNESS DISTRIBUTION

The FE numerical results revealed that the initial gap is significantly a crucial parameter in the micro deep drawing technique presented in this study. For the strategy of using a flexible forming die in the drawing system, the initial gap plays the key role in the identification of product geometrical aspects; that is the radius of shoulder corners, of the final products. In order to verify the results obtained from the simulations, a number of micro deep drawing experiments were carried out for different initial gaps of 100, 0 and -100 $\mu\text{m}$ . These three values for the initial gap were specifically identified because at which the differences between the physical cups in terms of geometrical profiles can be visibly recognised.

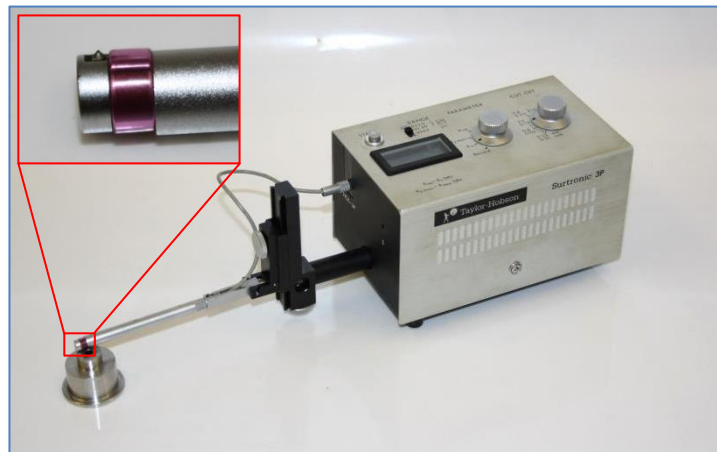


Figure 7-18. Surtronic 3P Taylor-Hobson roughness tester

The forming conditions that were adopted for this investigation are blank thickness of 100 $\mu\text{m}$ , blank diameter of 10mm, initial holding force of 300N and rubber material 63A hardness as well as the process dimensions were specified in dependence on the scaling factor  $\lambda=1$ . Regarding the status of the contact interfaces, the surface roughness of the components that directly influence the drawing results was measured using the Surtronic 3P Taylor-Hobson roughness tester shown in Figure 7-18. The rigid tools were equipped with surface roughness of 1.41 $\mu\text{m}$  and 2.97 $\mu\text{m}$  for the blank holders and the punch respectively, whereas the SS 304

sheets were finished with surface roughness of approximately  $0.64\mu\text{m}$ . The identification of appropriate roughness values for the forming tools required many attempts for surface finishing processes. At each time, the cup produced at particular surface roughness was cut along specified direction. Afterwards, the wall thickness of the cut section was measured and compared with the corresponding thickness distribution obtained from simulation results. In fact, these roughness degrees were reported as the most compatible; in terms of final drawing results regarding cup thickness distributions, to the friction conditions adopted in the corresponding FE models.

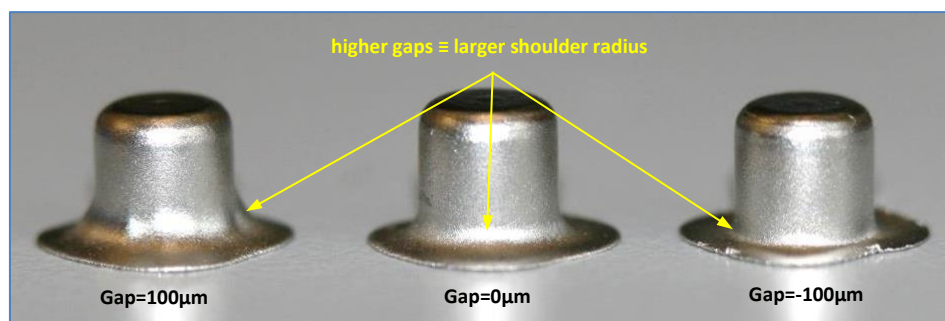


Figure 7-19. Physical parts formed with different initial gaps

Figure 7-19 shows three physical cups formed through micro deep drawing experiments that are achieved with different initial gaps of 100, 0 and  $-100\mu\text{m}$ . The figure reveals the effect of the variation of the initial gap value on the geometrical profiles of final products. Where, it can be observed that as the initial gap increases the shoulder corner radius increases as well. This activity was predicted precisely by the FE numerical models presented in chapter six. To measure experimentally the thickness distributions for the cups demonstrated in the figure aforementioned, they were cut along the rolling and transverse directions as illustrated in Figure 7-20.

Figure 7-21 to Figure 7-23 present comparisons between the thickness distributions of the cups obtained from simulations and experiments that were performed with initial gaps of  $100\mu\text{m}$ , 0 and  $-100\mu\text{m}$ , respectively. In order for this comparison to be confidently considered, the experimental and numerical thickness distributions curves in the figures are taken along the rolling and transverse directions for each case. It can be indicated that the thickness distributions predicted by the simulations well match with that obtained for the physical parts.

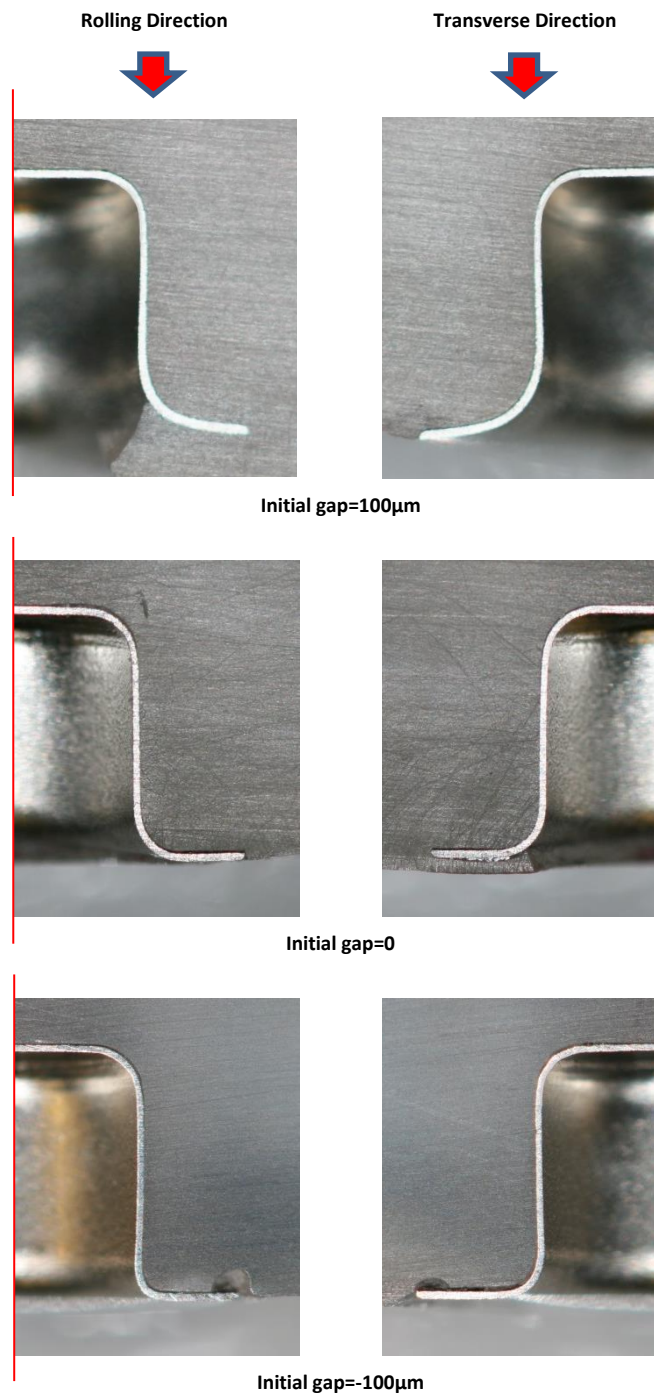


Figure 7-20. Physical cups drawn with different initial gaps and cut along the rolling and transverse directions

The general trend is that the curves representing thickness distributions along the rolling direction are higher than that along the transverse direction for both simulations and experiments. Also, it can be deduced from the figures that the experimental results are well agree with the numerical predictions.

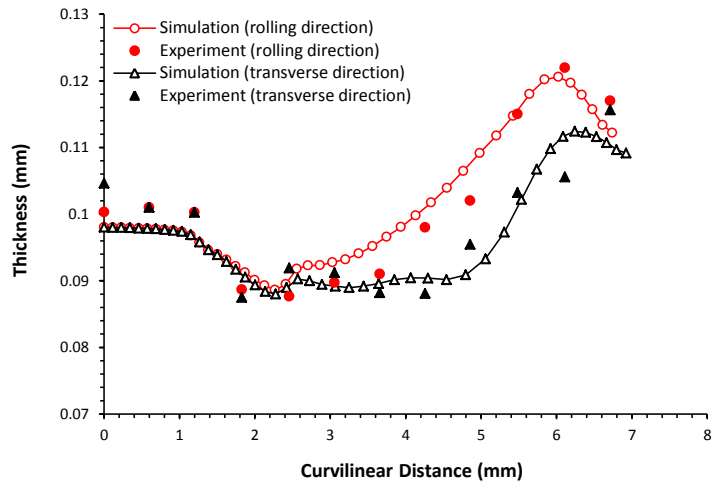


Figure 7-21. Experimental and numerical thickness distributions with initial gap of 100µm

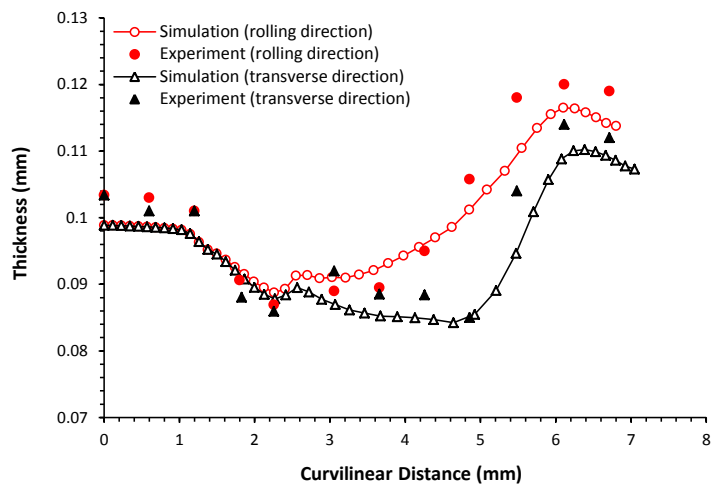


Figure 7-22. Experimental and numerical thickness distributions with no initial gap

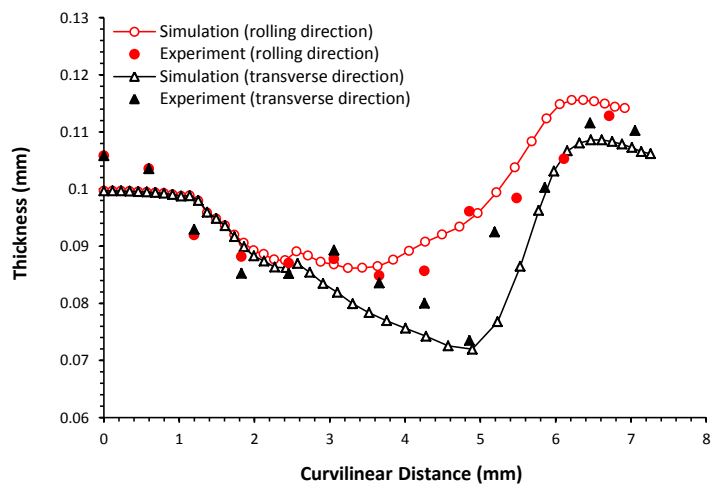
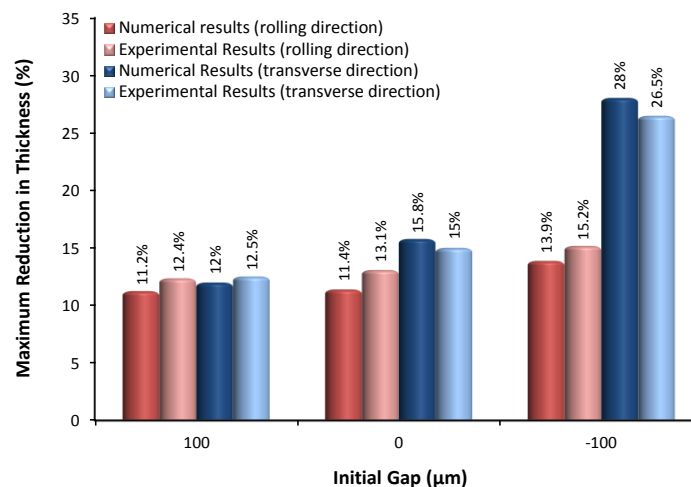


Figure 7-23. Experimental and numerical thickness distributions with initial gap of -100µm

The maximum thinning at the rolling direction occurred at the nose corner, except the case of initial gap of  $-100\mu\text{m}$  where the maximum thinning is observed at the lower half of the side wall. Moreover, the curves relating to the thickness distributions along the transverse direction declare that the maximum thinning are observed at the side wall region of the cups produced through experiments with initial gaps of 0 and  $-100\mu\text{m}$ . Whereas, the maximum value of the wall thinning occurred with initial gap of  $100\mu\text{m}$  is found at the nose corner. These results accurately verify the numerical predictions obtained from FE simulations. Likewise the influence of the initial gap is shown in these figures; the experimental curves also reveal the role of the anisotropic behaviour of the sheet metal on the quality of the final products in terms of reduction in wall thickness. In order to highlight on how the initial gap value affects the maximum reductions in wall thickness of produced cups as well as on the correlation between the experimental and simulation results in this regard, **Figure 7-24** is reported here.



**Figure 7-24. Maximum reductions in thickness with different initial gaps**

This figure detects that the maximum reductions in thickness; whether at rolling or transverse direction, of the cups produced through experiments in general increases as smaller gaps are adopted. For example, the experimental results expose that the maximum thickness reduction at the transverse direction increases from 12.5% at the initial gap  $100\mu\text{m}$  to 15% at no gap and thereafter to 26.5% at  $-100\mu\text{m}$ . It can be denoted that the increase of the maximum reduction at rolling direction is noticeably very slight for both physical and simulated cups. However, the difference between the maximum thickness reductions at the transverse direction acquired with initial gaps of  $100\mu\text{m}$  and 0 is relatively insignificant, but a remarkable jump in this reduction can be observed in the figure when the gap is reduced from 0 to -

100 $\mu\text{m}$ . Furthermore, **Figure 7-24** provide crucial evidence on how the drawing experiments validate the numerical predictions, where one can indicate that the greatest present error in the maximum thickness reductions obtained from the experiments and simulation is 1.7%.

### 7.7.1.2 PUNCH LOAD-TRAVEL RELATIONSHIPS

Regarding drawing loads, **Figure 7-25** illustrates comparisons between the punch load-travel relationships obtained from simulations and experimental work for the different gaps that are adopted for this investigation. It can be seen that the trend of the increase in the predicted punch load reveals good correlation with that of the experiments. However, the experiment curves are in general slightly higher than that representing the numerical results especially for the second half of the entire drawing stroke.

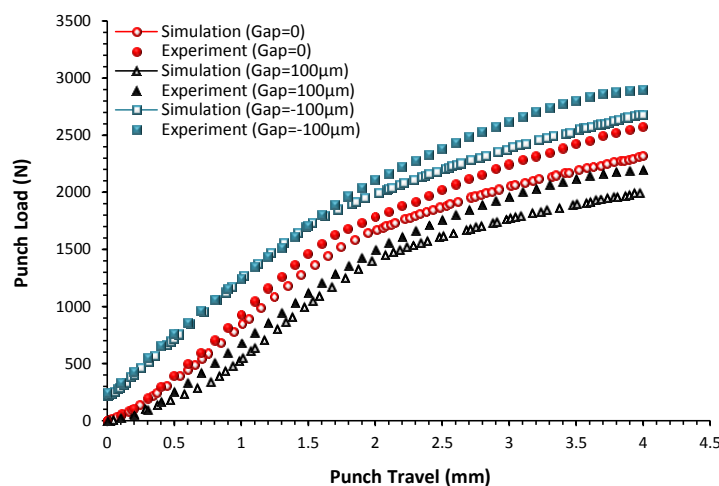


**Figure 7-25.** Comparison between punch load-travel relationships with different initial gaps

Then, the difference gradually increases to reach maximum load magnitudes at the end of drawing operations. Moreover, the initial punch load associating with the negative initial gap -100 $\mu\text{m}$ ; as explained in the numerical results of all negative gaps, is declared in this figure where the experimental value is 243.6N in return of 214.4N predicted by simulations. Another finding is that the maximum punch loads obtained by experiments are higher than those taken from the FE numerical models as shown in **Figure 7-26**. As can be estimated the present differences between the maximum loads exposed in this figure, the measured values are higher by 9.6%, 10.8% and 8.1% than that obtained from the numerical predictions for initial gaps of 100, 0 and -100 $\mu\text{m}$ , respectively. The differences between the drawing load-stroke curves could be due to the difficulty of establishing friction coefficients for the experiments

exactly equal to that adopted in the numerical models. In addition, the set up developed here for micro drawing experiments consists of various parts that are in direct contact with each other, and hence friction between them possibly leads to an increase in the total maximum loads measured by the employed machine.

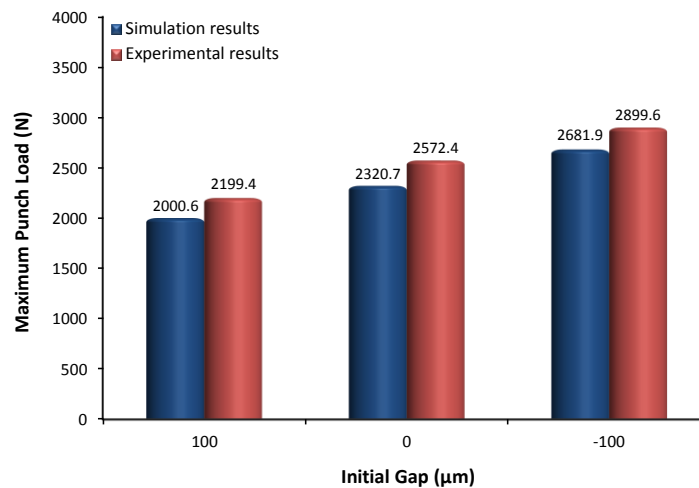


Figure 7-26. Comparison between maximum punch loads obtained from experiments and simulations

## 7.7.2 RUBBER TYPE

### 7.7.2.1 THICKNESS DISTRIBUTION

In order to verify the influence of the deformation behaviour of flexible die revealed via FE simulations in chapter six, Polyurethane rubber materials with different hardness of 40, 63 and 75 Shore A were utilized for the forming die in micro deep drawing experiments. For this purpose, the process conditions adopted for each case of the used rubber materials were blank thickness of  $100\mu\text{m}$ , blank diameter of  $10\text{mm}$ , initial holding force of  $300\text{N}$ , whereas the component dimensions were identified in accordance with the scaling factor  $\lambda=1$  (see Table 6-3). The rigid tools that used in the previous investigation were employed also for the current experiments, and that implies the same surface roughness of the forming tools were specified for the cases under consideration here. In order for a reasonable comparison, the optimum initial gaps adopted for the FE simulations that included corresponding rubber material models were considered for the current experiments. Figure 7-27 demonstrates three cups formed using the different rubber die materials aforementioned with the optimum initial gaps that are  $-100\mu\text{m}$  with 75 A rubber and no gap with 40A and 63A rubber. The geometry profiles of these displayed products well match with the numerical models.



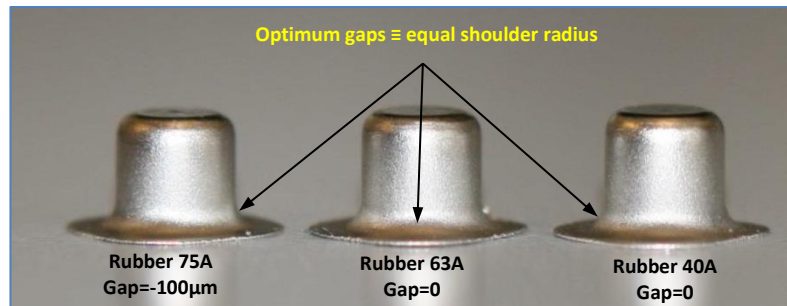


Figure 7-27. Physical cups formed using different rubber materials with different initial gaps

Figure 7-28 presents the physical cups cut along the rolling and transverse directions. The first observation is that the profiles of the sections confirm the agreement between the experimental and simulation results in terms of geometrical aspects of the obtained products. It can be seen that the radius of shoulder corner regions are nearly the same. The thickness distribution of these cut cups are exposed in Figure 7-29 to Figure 7-31. The curves of the experimental results denote well correlation with that predicted by simulations regarding the key features of the increments and decrements in thickness values. The occurrence of maximum reductions in thickness at the nose corner along the rolling direction and at the side wall along the transverse direction are quite validated by the experimental results. It can be indicated that both the thickness distribution curves acquired from experiments and numerical models agree regarding the thickness values along the rolling direction were found higher than that along the other direction.

Figure 7-32 reports the maximum reductions in thickness along the rolling and transverse directions of the cups formed via experiments and FE simulations under the conditions of the different rubber materials 40, 63 and 75 Shore A. It can be noticed that the highest values of the maximum thinning are obtained along the transverse direction and specifically at the side wall regions in return at the nose corner along the rolling direction. Another finding is that the differences between the numerical and experimental values of the maximum reductions in thickness are actually small, where the greatest difference is 3.1% which associated the rubber 40A material at the rolling direction. This action refers to a good match between the results taken from the experiments and simulations. In terms of maximum thinning, the rubber material that is recommended to use for the flexible drawing die in the proposed technique is that with 63 Shore A hardness.

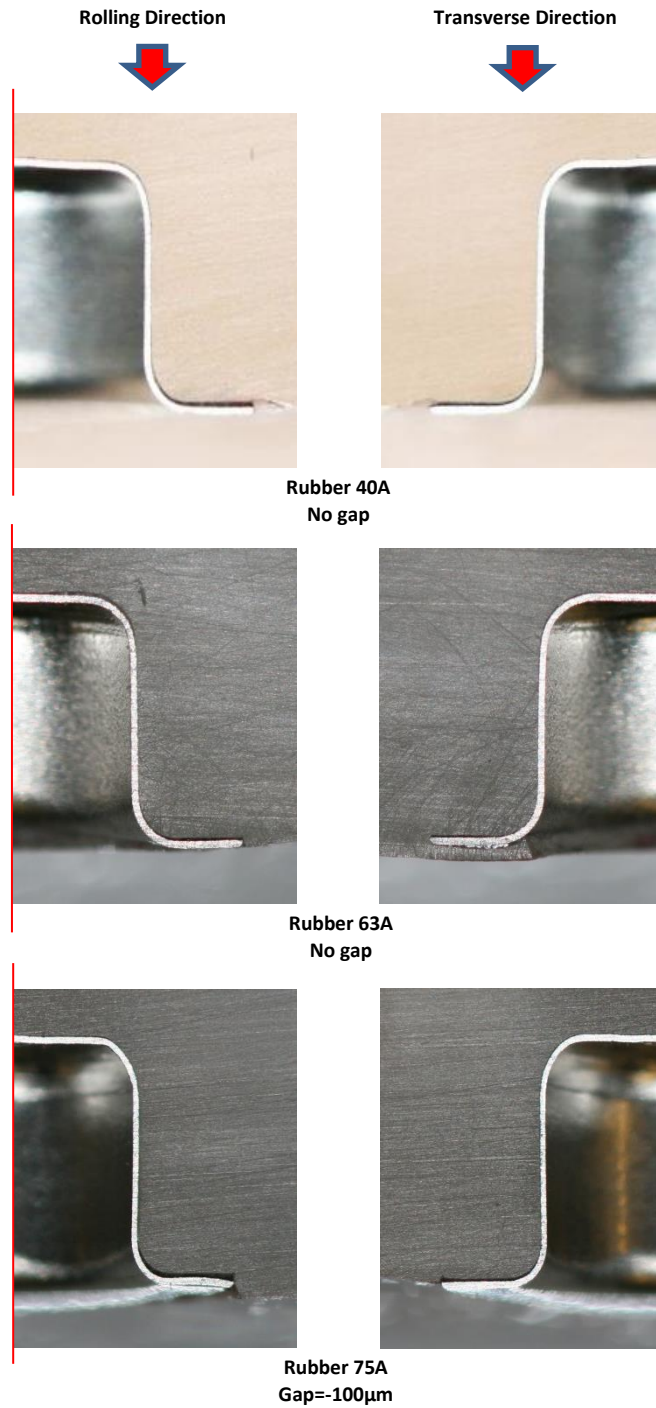


Figure 7-28. Physical cups drawn under conditions of different rubber materials

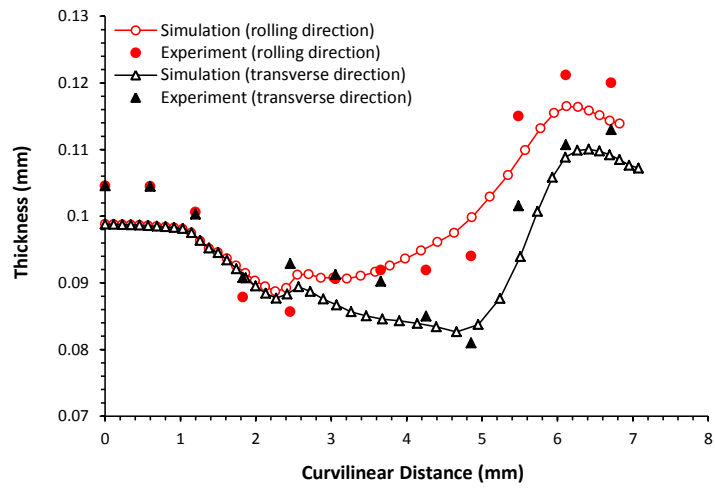


Figure 7-29. Experimental and numerical thickness distributions obtained using rubber 40 shore A hardness

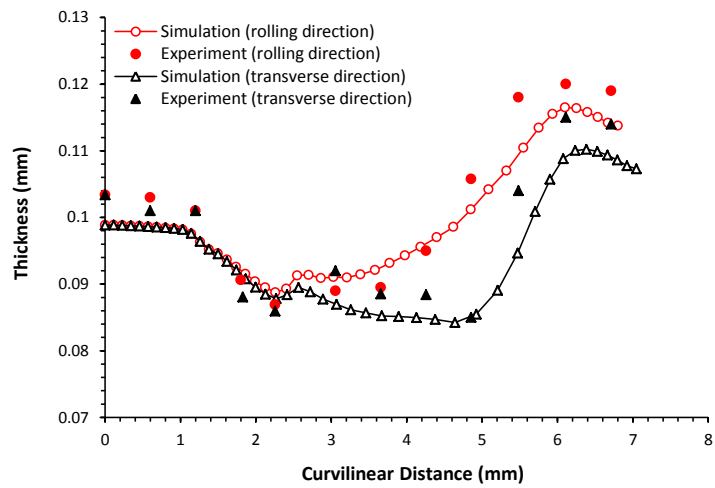


Figure 7-30. Experimental and numerical thickness distributions obtained using rubber 63 shore A hardness

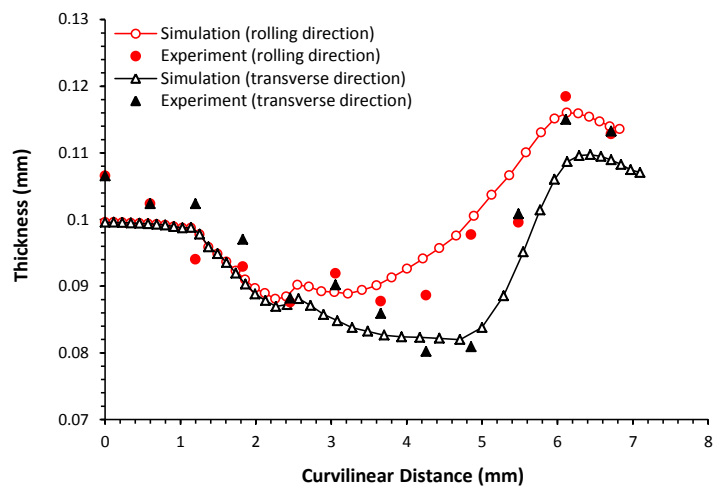


Figure 7-31. Experimental and numerical thickness distributions obtained using rubber 75 shore A hardness

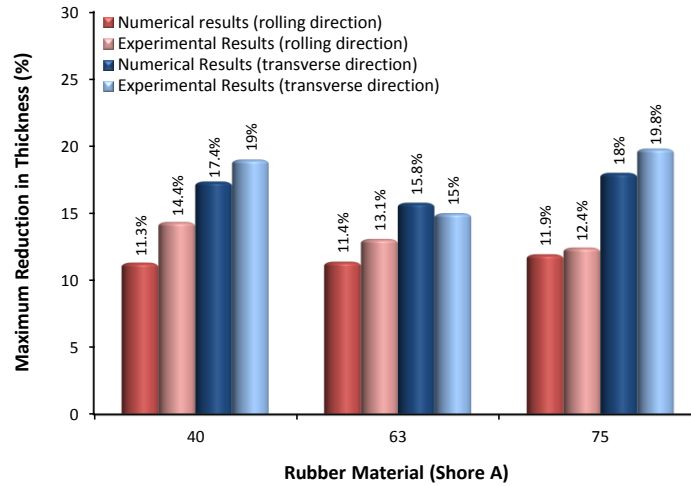


Figure 7-32. Maximum reductions in thickness with different rubber materials

7.7.2.2 PUNCH LOAD-TRAVEL RELATIONSHIPS

Figure 7-33 presents a comparison between the drawing results regarding punch load-travel relationships acquired from the numerical simulation and experiment. It can be observed that the general trend of the curves is the same, where the punch load increases with increasing the drawing stroke. In general, the curves that represent the experimental results are higher than that taken from the FE simulations specifically for the drawing stroke hereafter nearly 2mm. Likewise the predictions provided by FE numerical models, the experiments confirm that there is no noticeable difference between the drawing load curves obtained with using 40A and 63A rubber die materials. Also, it can be seen in the figure that the load-travel curve corresponding to the rubber material 75A is higher than the other two experimental curves by the same deviation through along the whole drawing stroke, and this action was previously declared by the numerical simulation.

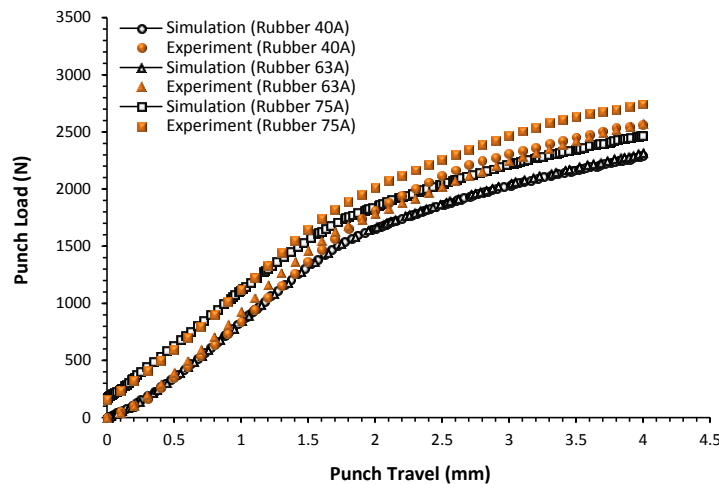
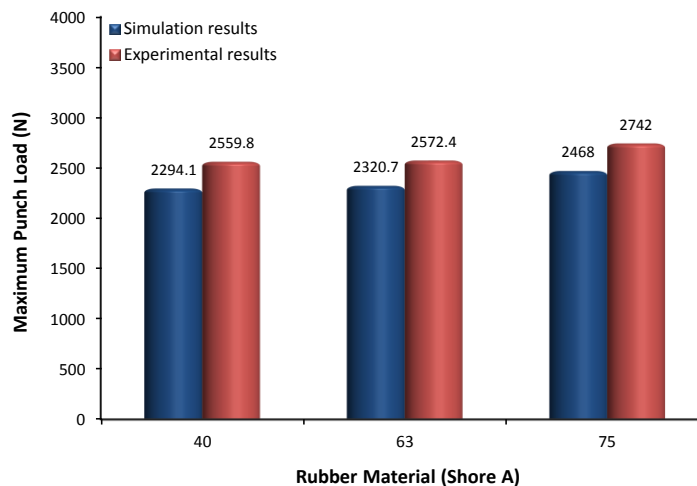


Figure 7-33. Comparison between punch load-travel relationships obtained using different rubber materials

As a result, it is denoted that the maximum punch load values that were required for the micro drawing experiments, which were measured by the working machine, are higher than that predicted by simulations. The maximum punch loads acquired by experiments and numerical models with the rubber materials of 40, 63 and 75 Shore A hardness are exposed in **Figure 7-34**. The increases percentages in the maximum load obtained from the experiments with the different rubber materials used in this study are very close each other.



**Figure 7-34. Comparison between maximum punch loads obtained with using different rubber materials**

It is important to explain here that the deviations observed between the experimental and numerical results are not due to the rubber material only, but also because the initial gap adopted with at each case. Moreover, these differences could be due to the difficulty of measuring friction coefficients experimentally, which results in surface roughness maybe greater or smaller than that required to provide friction coefficients exactly equal to what adopted in the corresponding numerical models. In addition, the set up used to perform the drawing experiments consists of various parts which are in direct contact with each other, and thence that leads to increasing in total load measured by the machined used.

### 7.7.3 BLANK DIAMETER

#### 7.7.3.1 THICKNESS DISTRIBUTION

One of the most important aims of the current study is to investigate the effect of the initial diameter of the working blanks on the drawing quality. Owing to establish a reasonable comparison, the micro deep drawing experiments were carried out in accordance with the process conditions that were adopted for the corresponding numerical models. For this purpose, rubber die material of 63 Shore A hardness, blank thickness of 100 $\mu$ m initial holding

force of 300N were utilized as well as the process dimensions were identified according to the scaling factor  $\lambda=1$ . Also, the blank holder was processed to reduce the effective surface roughness to approximately  $1.09\mu\text{m}$  which was efficiently equivalent to the friction coefficient 0.05 adopted in the numerical models at the blank-holder interface. The SS 304 sheet blanks that were employed for this investigation were cut with different diameters of 9mm, 10mm, 11mm and 12mm. The largest diameter of 12mm was specified as the diameter of the rubber die used according to  $\lambda=1$  was 12mm. The final cups produced utilizing blanks with these diameters were compared with each other in regard of the geometrical features. Therefore, the smallest blank diameter was limited just at 9mm since blanks of a diameter less than this size result in cups formed with no flange and shoulder corner.

The experimental results showed that no successful products were obtained from blank of 12mm in diameter, and this action was exactly predicted by FE simulations. To produce cups with the same geometrical aspects (i.e. same radius for the shoulder corner), no initial gaps was used with the blanks of 9mm and 10mm diameters whereas the blanks of 11mm in diameter were drawn with  $60\mu\text{m}$  initial gap as adopted in the corresponding simulations. **Figure 7-35** presents three cups formed using blanks of 9mm, 10mm and 11mm in diameter.

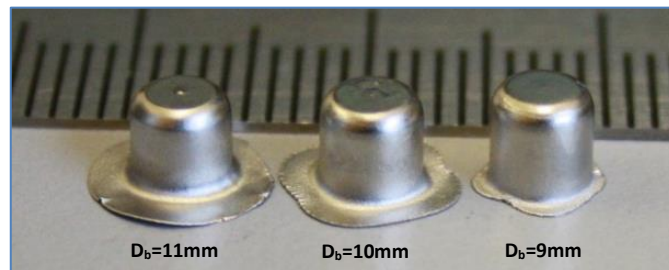


**Figure 7-35. Physical cups formed using blanks of different initial diameters ( $D_b$ )**

These cups were cut at the rolling and transverse directions along which the wall thickness was measured as exposed in **Figure 7-36** to **Figure 7-38**. First of all, it can be indicated from the presented curves that the experimental results quite correlate with the predictions obtained from the FE numerical models. The best homogeneity in thickness distributions measured for the cup walls cut along the rolling direction and the transverse direction is that acquired for the blank of 9mm in diameter. Also, the curves taken from the experiments reveal that as the initial blank diameter increases the deviation in thickness values between the two considered directions increases significantly at the side wall region. These activities were exemplary predicted by the corresponding FE numerical models in chapter six.

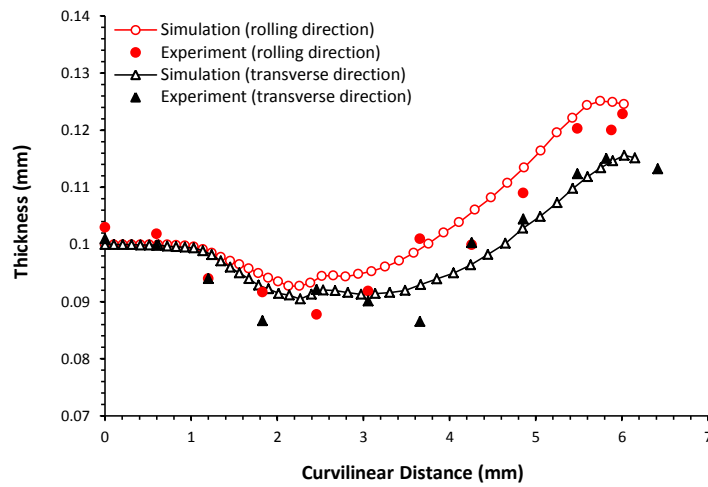


Figure 7-36. Experimental and numerical thickness distributions obtained using a blank of 9mm in diameter

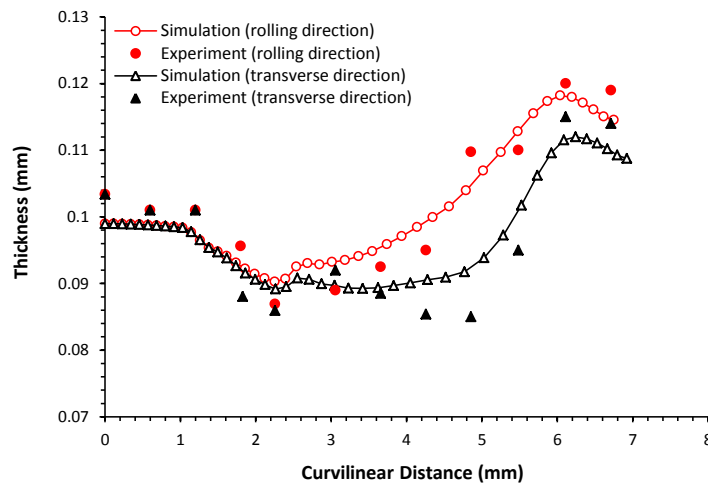


Figure 7-37. Experimental and numerical thickness distributions obtained using a blank of 10mm in diameter

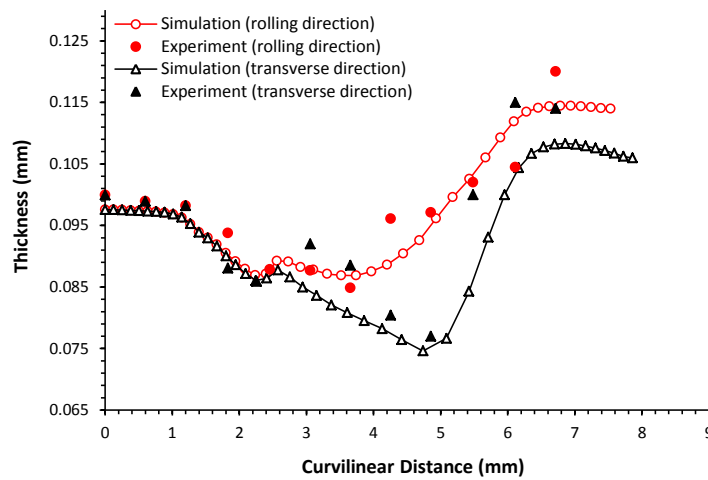
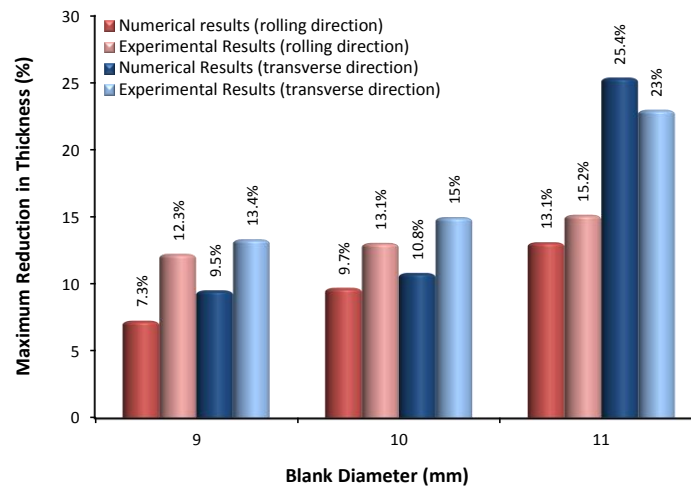


Figure 7-38. Experimental and numerical thickness distributions obtained using a blank of 11mm in diameter

In the above figures declare that the numerical predictions relating to thickness distributions are properly verified by the experimental measurements performed on the physical products. Although that, **Figure 7-39** detects some differences in maximum reductions in thickness obtained from the experiments and the FE simulations at the rolling and transverse directions. In general, the maximum reductions in thickness whether the obtained from the experiments or from the simulations increase with increasing the initial diameter of the formed blanks. It can be observed that differences between the experimental and numerical values of the maximum thickness reductions are slightly higher for the smaller blank diameter. The highest error percentage in the maximum thinning is 5.4% which obtained at the rolling direction for the blank diameter 9mm, whereas the lowest error percentage is 2.4% at the rolling direction for the blank diameter 11mm. Another finding is that the higher maximum reductions in thickness in general occur along the transverse direction for all cases under consideration.



**Figure 7-39. Maximum reductions in thickness with different blank diameters**

Moreover, higher differences between the maximum thickness reductions along the rolling direction and the transverse direction are almost obtained for the greater blank diameters. This action point out the initial blank diameter obviously dictates on the anisotropic response of the ss 304 sheet metal. In other words, as the initial blank diameter is increased the effect of the anisotropic behaviour of the blank martial then becomes more recognisable in terms of thickness distribution and maximum thinning.



### 7.7.3.2 PUNCH LOAD-TRAVEL RELATIONSHIPS

The punch load-drawing stroke relationships acquired from FE simulations and experimental work for drawing operation with different blank diameters are shown in **Figure 7-40**. It can be seen that each pair of the corresponding curves obtained from the numerical models and experiments reveal well matching. The main features in terms of increments and decrements of these curves are quite similar. The interesting observation is that the experimental and numerical curves representing the results taken with blank diameter of 11mm are the lower for the first half of the drawing stroke. Thereafter, they became higher than the other corresponding curves although the higher initial gap was adopted for the mentioned case.

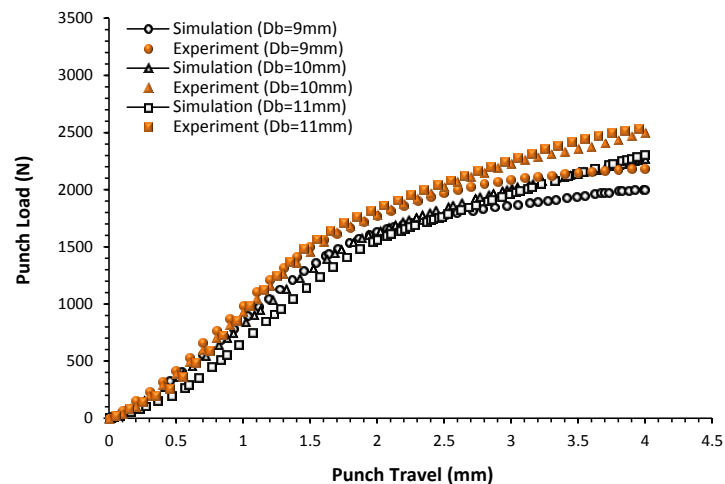


**Figure 7-40. Comparison between punch load-travel relationships obtained using different blank diameters**

Also, it can be indicated from the figure that the maximum punch loads whether that acquired from the experiments or from the simulation increase as the blank diameter increases. In general, the experimental curves are higher than that numerically predicted which implies subsequently that the maximum drawing load obtained from drawing experiments to be higher. These expectations are confirmed in **Figure 7-41** which detects that the maximum load required drawing blanks with initial diameters of 9mm, 10mm and 11mm are 2179N, 2498.3N and 2533N in return of 2000.2N, 2275 and 2304N obtained from the simulations respectively. It is clear that the maximum drawing load required under the same process conditions increases with increasing the initial diameter of the blank used.

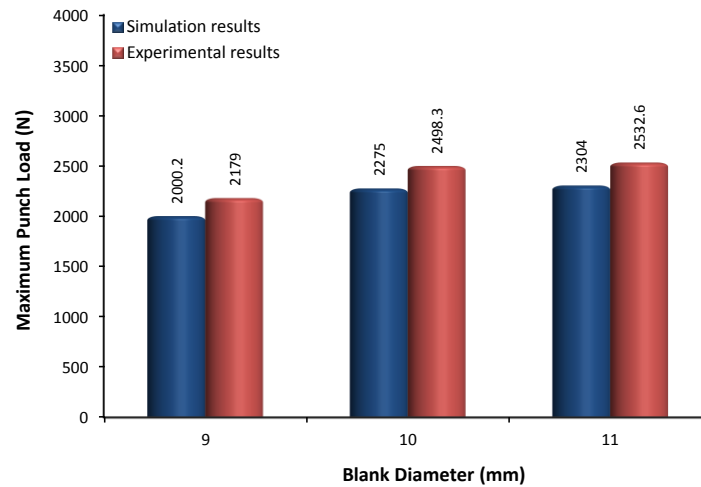


Figure 7-41. Comparison between maximum punch loads obtained with using different blank diameters

## 7.7.4 BLANK THICKNESS

### 7.7.4.1 THICKNESS DISTRIBUTION

Various industrial applications widely involve utilizing micro components made of sheet metals with different initial thicknesses. Therefore, it is essential issue in any sheet forming process to investigate the influence of the initial thickness of workpieces on the product quality. As revealed in the numerical simulations that varying blank thickness necessitates an optimization of the effective process conditions so long as adapt with the considered thickness to produce parts with compatible quality.

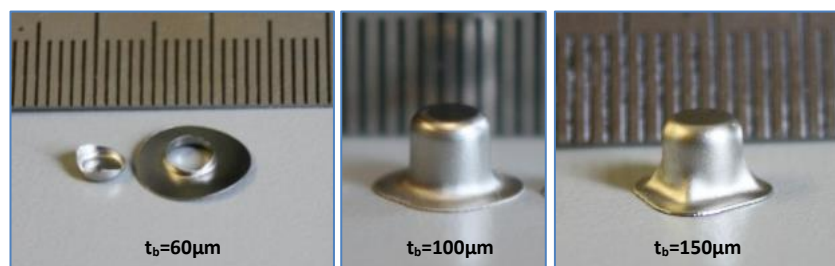


Figure 7-42. Cups formed from different sheet metal thicknesses with no initial gap

Figure 7-42 presents three cups drawn using different sheet metal thicknesses but with no initial gap. It is clear that just the one successful cup was obtained with blank thickness of  $100\mu\text{m}$  whereas the blanks of  $60\mu\text{m}$  in thickness resulted in a broken part and of  $150\mu\text{m}$  in thickness resulted in a wrinkled part. In order for the results acquired from the numerical models to be validated, micro deep drawing experiments were achieved using ss 304 blanks with different thicknesses of  $60\mu\text{m}$ ,  $100\mu\text{m}$  and  $150\mu\text{m}$ .

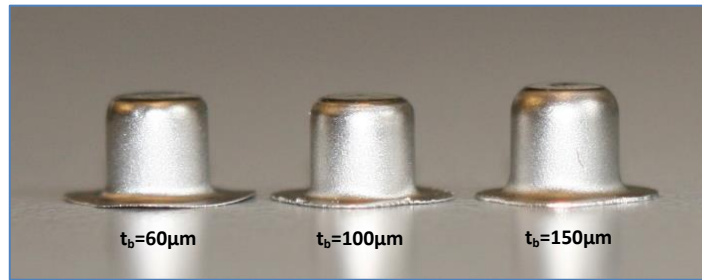


Figure 7-43. Physical cups formed using blanks of different initial thickness ( $t_b$ )

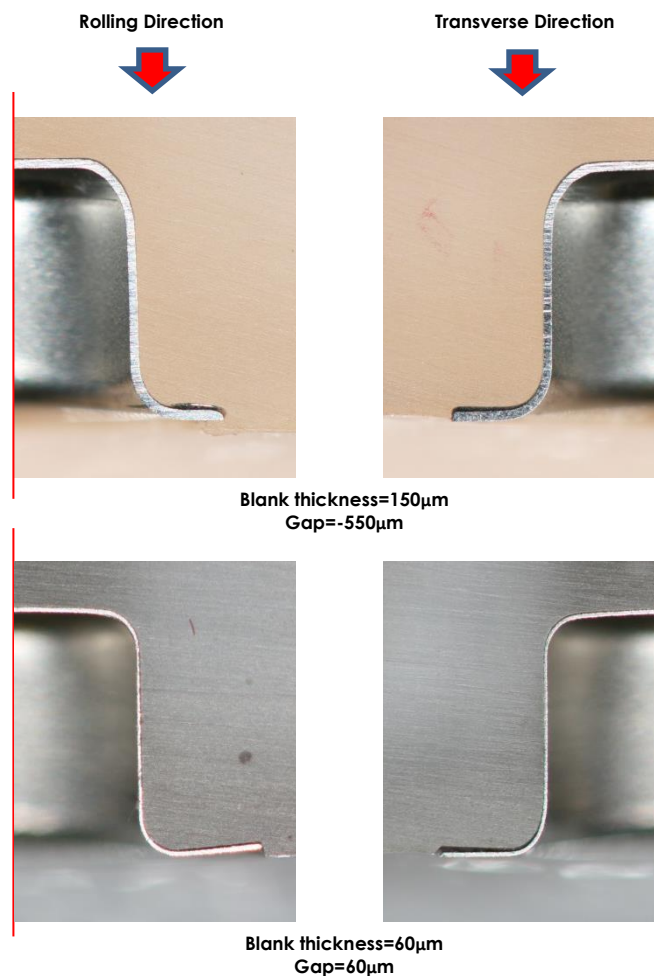


Figure 7-44. Physical cups drawn from blanks of 150  $\mu\text{m}$  and 60  $\mu\text{m}$  in thickness

For this experimental work, blank diameter of 10mm, rubber material of 63A and initial holding force of 300N were employed as well as the process conditions were intended according to the scaling factor  $\lambda=1$ . In addition, the forming tools used in the current experimental investigation were finished with the surface roughness of approximately 1.09  $\mu\text{m}$  for the blank holder and 2.97  $\mu\text{m}$  for the rigid punch.

Figure 7-43 shows physical cups formed through micro deep drawing experiments utilizing blanks of different thicknesses. Likewise in the numerical models, initial gaps of  $60\mu\text{m}$ ,  $-100\mu\text{m}$  and  $-550\mu\text{m}$  were employed for the experiments achieved with blank thicknesses of  $60\mu\text{m}$ ,  $100\mu\text{m}$  and  $150\mu\text{m}$ , respectively. In order to compare the experimental results with the numerical predictions, the formed cups were cut along the rolling and transverse directions as illustrated in Figure 7-44. Figure 7-45 to Figure 7-47 report the thickness distributions along the directions aforementioned, which obtained from the experiments and the simulations for micro cups formed from ss 304 sheet of different initial thicknesses.

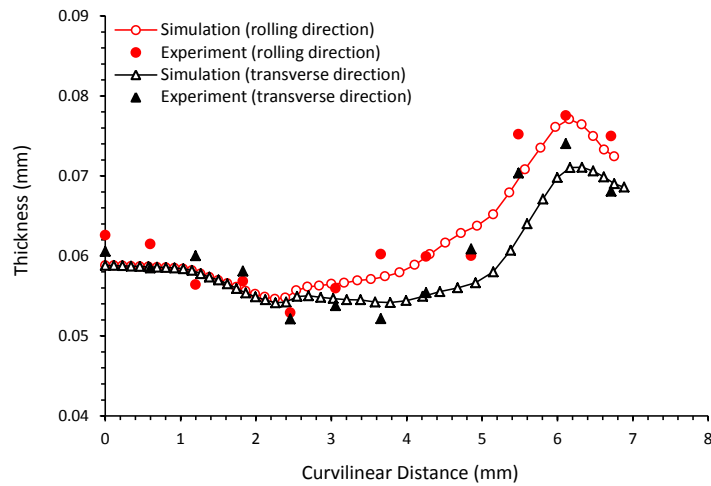


Figure 7-45. Experimental and numerical thickness distributions obtained using a blank of  $60\mu\text{m}$  in thick

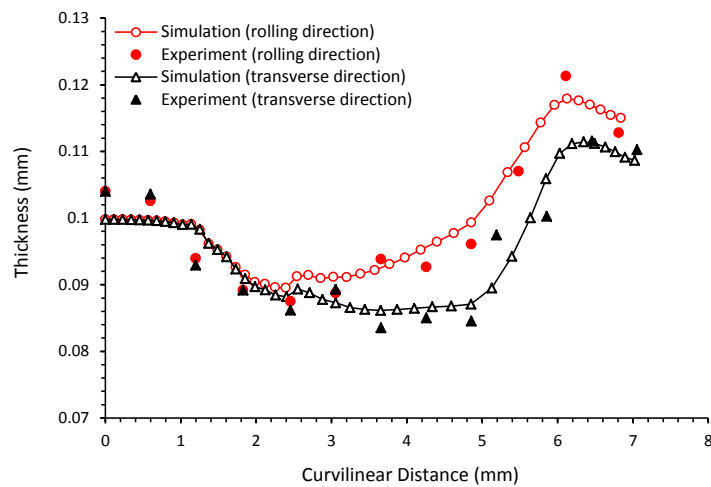


Figure 7-46. Experimental and numerical thickness distributions obtained using a blank of  $100\mu\text{m}$  in thick

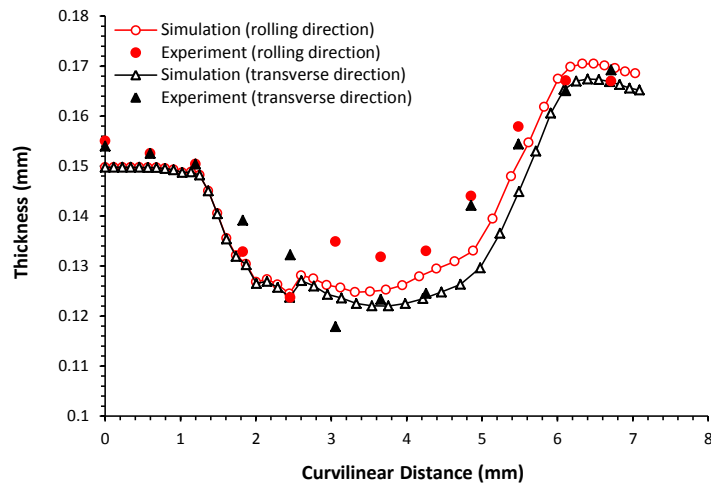


Figure 7-47. Experimental and numerical thickness distributions obtained using a blank of 150µm in thick

One can noticed that the experimental curves expose well correlation with that obtained from the numerical predictions in regard of the increments and decrements of thickness values. It can be indicated that no significant difference between the two simulation curves at the rolling and transverse direction for the cups of 60µm and 150µm initial thickness. That is also dented by the thickness measurements taken from the physical products as seen in **Figure 7-45** and **Figure 7-47**. However, a remarkable deviation can be recognised obviously at the side wall between the curves obtained for the cup of 100µm thickness whether those represent the numerical or experimental results. Nevertheless, the thickness distribution of the physical cup well match with the simulation results (see **Figure 7-46**).

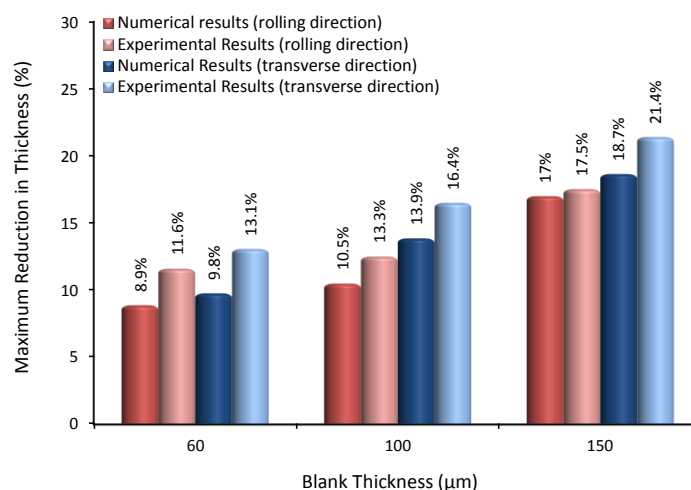


Figure 7-48. Maximum reductions in thickness with different blank thicknesses

**Figure 7-48** demonstrates a comparison between the corresponding maximum reductions in thickness occurred for the products obtained from the experiments and simulations. It can

be noticed that the highest deviations in the maximum thickness reductions between the two considered directions are obtained for the case of 60 $\mu\text{m}$  blank thickness. On the other side, the smallest deviations are measured for the cups drawn with 150 $\mu\text{m}$  initial blank thickness. These actions were exactly revealed by the FE simulations, which refers to a good correlation between the experimental and numerical results. Although that, it is important to mentioned here that the greatest error percentage is 4.1% which acquired for the blank of 60 $\mu\text{m}$  in thickness at the rolling direction, and however the lowest error percentage is 0.6% for the blank thickness of 150 $\mu\text{m}$  at the rolling direction as well.

#### 7.7.4.2 PUNCH LOAD-TRAVEL RELATIONSHIPS

The punch load-travel relationships obtained from experiments and simulations for the parts produced with blank thicknesses of 60 $\mu\text{m}$ , 100 $\mu\text{m}$  and 150 $\mu\text{m}$  are declared in **Figure 7-49**. It can be indicated that each corresponding pair of the experimental and numerical curves presented in this figure have similar key features. In other words, the curves acquired from the experiments well match with that taken from the FE models in terms of the distribution mode of wall thicknesses. However, it is clear that the experimental curves are slightly higher than the numerical predictions. In addition, **Figure 7-50** detects the maximum values of the punch load experienced by the cups that were produced through the drawing operations and the numerical simulations considered in the current investigation.

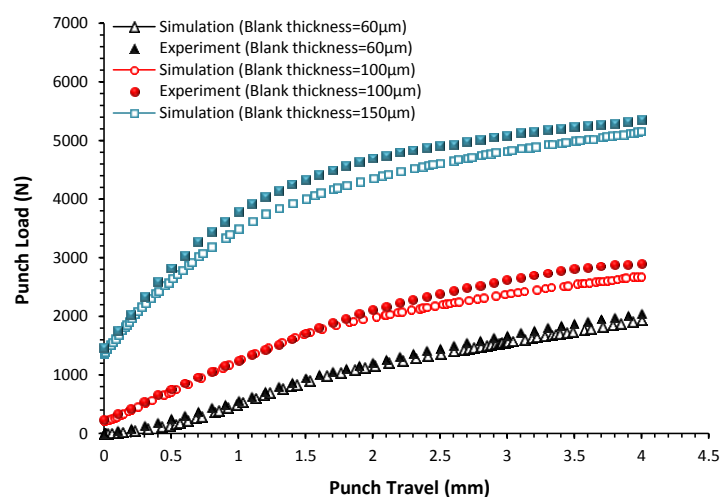


**Figure 7-49.** Comparison between punch load-travel relationships obtained using different blank thicknesses

The results show that the maximum loads taken from the working machine increase as the initial blank thicknesses increase, and this action was previously reported by the

corresponding simulations. Also, it can be deduced that experimental maximum load values well correlate with those predicted by the numerical models. The results revealed that the percentage errors in the maximum punch load that are calculated for the forming operations of 60 $\mu\text{m}$ , 100 $\mu\text{m}$  and 150 $\mu\text{m}$  blank thicknesses are 6%, 8.1% and 3.8% respectively. In fact, the deviations between the experimental and simulation results in regard of punch loads comparatively depend on the accuracy of manufacturing the various components that compose the experimental set up. Also, the additional friction forces between these different components, which were not considered in the numerical models, such as the friction activity between the guide posts and their slots could affect the punch force required for a particular drawing process. Moreover, the difficulty of establishing accurate friction coefficients at blank/tool contact interfaces so that be exactly equal those adopted in the numerical models may also results in the obtained percentage errors.

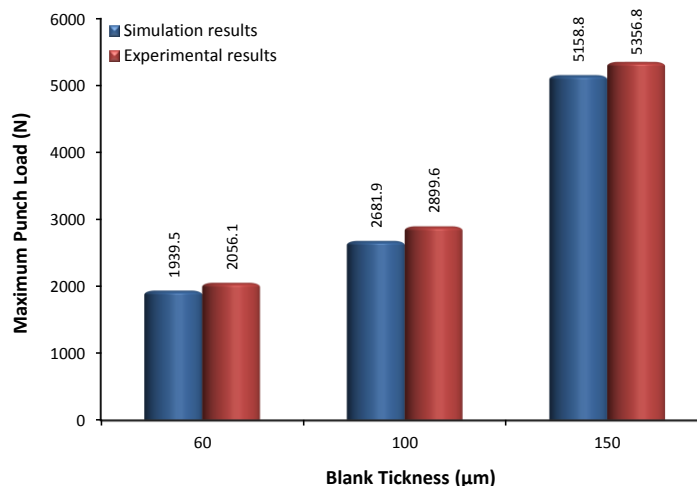


Figure 7-50. Comparison between maximum punch loads obtained with using different blank thicknesses

## 7.7.5 PUNCH TRAVEL

### 7.7.5.1 THICKNESS DISTRIBUTION

In micro deep drawing technology, the aspect ratio (cup height to punch diameter ratio) is regarded on of the essential measures for assessing the success of drawing processes. In other words, providing micro cups with relatively high aspect ratio; that is higher than unity according to Jenn-Terng et al. [130], implies that the forming technique utilized is efficient foe such applications. In order to prove that the micro drawing technique proposed in the current work can be employed experimentally to produce micro cups of different aspect ratios and

high forming quality, micro deep drawing experiments were conducted. Owing to establish a reasonably comparison with the corresponding numerical models, the same aspect ratios of 0.75, 1 and 1.25; i.e. 3mm, 4mm and 5mm in cup depth in accordance with the scaling factor  $\lambda=1$ , were targeted in the experimental work. For this purpose, the processes conditions adopted in the FE simulations were utilized in this experimental investigation, such as blank diameter of 10mm, blank thickness of 100 $\mu\text{m}$ , rubber 63A hardness and initial holding force of 300N. Also, the surface roughness of 1.41 $\mu\text{m}$  for the blank holder and 2.97 $\mu\text{m}$  for the rigid punch were employed at all drawing operations.

**Figure 7-51** reveals a comparison of the cups produced by experiments with those obtained from the FE models in regard of geometrical profiles. It can be obviously observed the similarity between each pair of the corresponding products. The influence of the sheet anisotropic behaviour particularly at the flange portion can be recognised to increase with increasing the depth of the final cups.

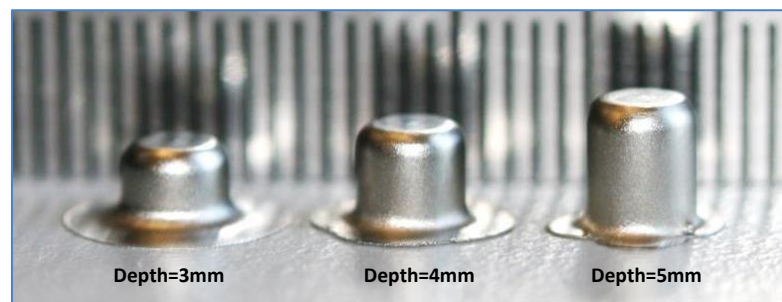


**Figure 7-51. Comparison between the numerical and experimental cups with different depths**

**Figure 7-52** to **Figure 7-54** present thickness distributions along the rolling and transverse directions of the parts formed via experiments and simulations with aspect ratios of 0.75, 1 and 1.25 respectively. The key features of the numerical curves in terms of thickening and thinning regions are well validated by the experimental results. It can obviously indicate that the sheet anisotropy dictates on the thickness distributions remarkably at the side wall and however less slightly at the cup flanges. In addition, it is clear that the curves that represent thickness distribution at the rolling direction are in general the higher whether those taken from experiments or from the simulations. This action implies that the maximum thinning occurred at the transverse direction for all cases of different aspect ratios.



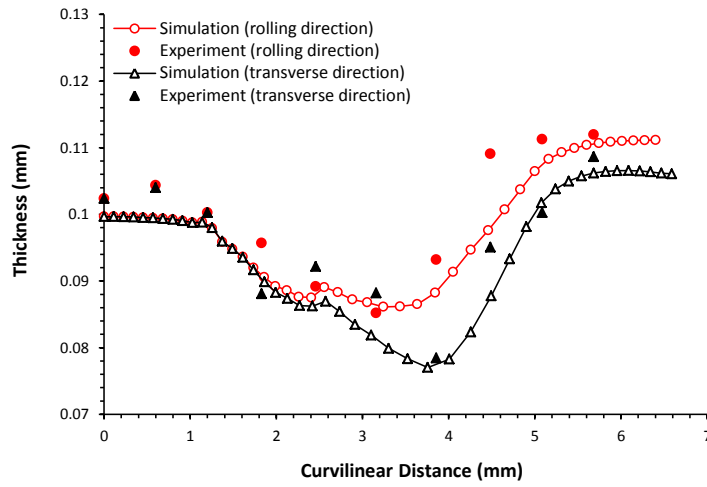


Figure 7-52. Experimental and numerical thickness distributions obtained for aspect ratio of 0.75

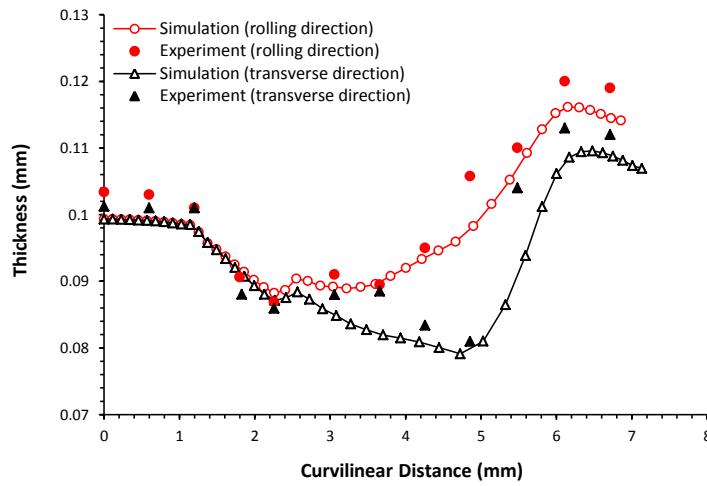


Figure 7-53. Experimental and numerical thickness distributions obtained for aspect ratio of 1

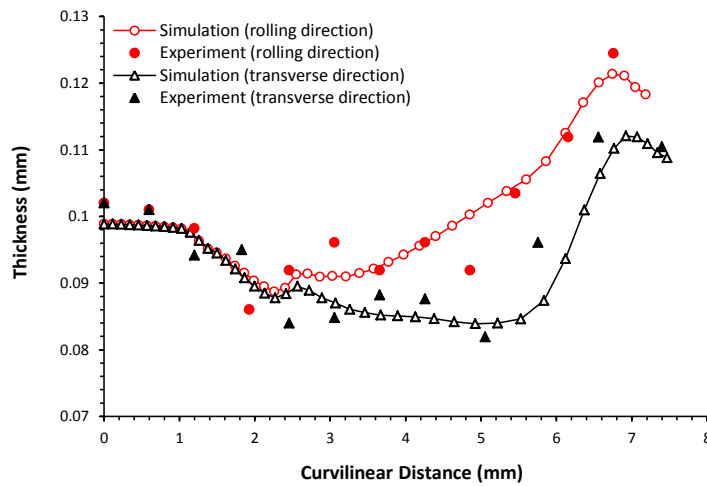


Figure 7-54. Experimental and numerical thickness distributions obtained for aspect ratio of 1.25

Figure 7-55 show the maximum reductions in thickness of the products drawn to the aforementioned aspect ratios. The interesting observation in this figure is that both the experimental and numerical results are agreed that the maximum reduction in thickness decreases as the aspect ratio (the final depth of the formed cups) increases. This action is exactly in contrast to what happen in the conventional deep drawing processes, where a deeper product means a higher thinning. However, this finding can be properly realized if one remembers that the initial gaps -100 $\mu$ m, -50 $\mu$ m and 0 were adopted for 0.75, 1 and 1.25 aspect ratios. Thus, it can be deduced that the maximum reductions in thickness resultant in this investigation mainly depend on the initial gaps although the depth of the obtained cups were increased in the range of 3mm to 5mm. The figure reports clearly that the maximum thinning values along the transverse direction are significantly higher than that along the rolling directions. Furthermore, the highest percentage error in thickness is 3.1% which can be indicated at the rolling direction for the case of aspect ratio 1.25.

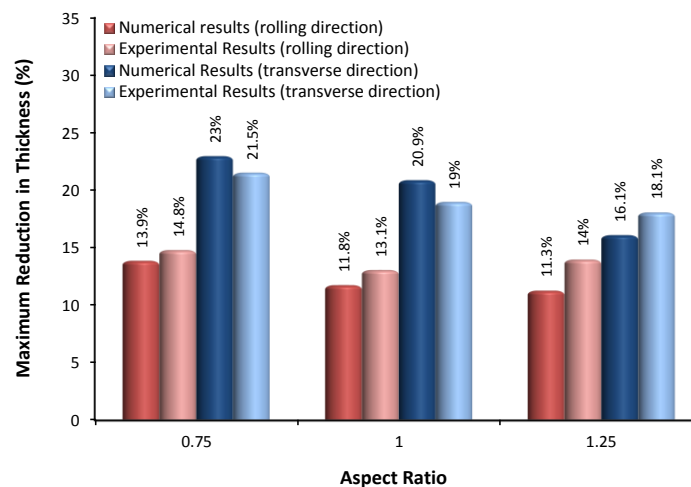


Figure 7-55. Maximum reductions in thickness with different aspect ratios

The deviations between the experimental results and the predictions obtained from the FE simulations in terms of thickness distributions and magnitudes can be attributed to various reasons. First of all, the accuracy of manufacturing the different components of the experimental set up as some features have to be precisely coincide with each other, for example the holes in the upper and lower plates as well as the guide posts and their slots. Secondly, the difficulty of producing surface roughness for the effective forming tools, which were required to provide friction coefficients in the experiments equivalent exactly to those adopted in the numerical models. The third activity is the accuracy of the cutting operations that were conducted on formed cups. It was difficult to keep the cutting paths exactly on the

planes along the considered directions (rolling and transverse directions). In addition, using the microscope employed in this work to measure wall thicknesses of the obtained products might not be very accurate strategy in comparison with other facilities such as laser scanning systems for such applications considered in this work. The procedure followed for this purpose was to identify tow points; one at each edge of the cup wall; at the position where the thickness is required to be measured. Thereafter, a straight line was drawn between these points and then the length of this line was calculated by the software operated with the employed microscope.

### 7.7.5.2 PUNCH LOAD-TRAVEL RELATIONSHIPS

In regard of drawing loads, **Figure 7-56** presents a comparison between the punch load-travel relationships acquired from the experiments and the simulations for different aspect ratios-drawing processes. It can indicate a well matching between the two groups of the curves presented in this figure. Although that. It is clear that the experimental curves are in general slightly higher than the predictions provided by the FE models. Both the experimental and numerical results reveal that the punch load required at a particular drawing stroke is higher for the lower aspect ratio case. For example, at punch travel of 1mm the forming load required for the drawing process of aspect ratio 0.75 is greater than that when the aspect ratio is 1.25.

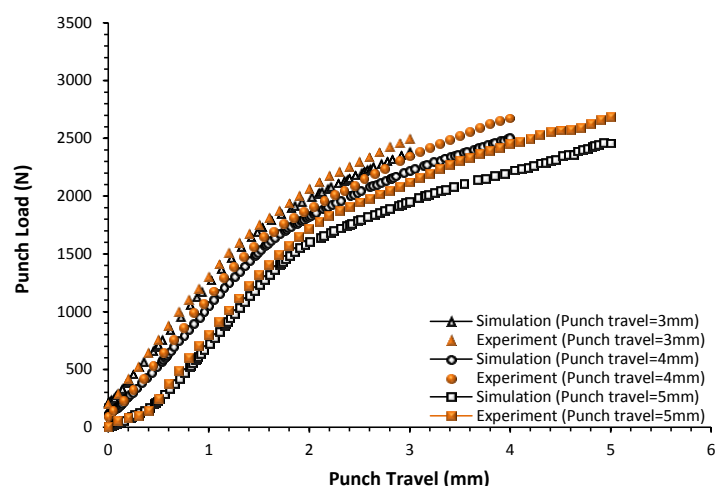


**Figure 7-56.** Comparison between punch load-travel relationships obtained for different aspect ratios

**Figure 7-57** exposes the maximum punch load values that were needed in the experiments and the simulations to complete forming the cups with depths of 3mm, 4mm and

5mm (aspect ratios 0.75, 1 and 1.5). It can detect the influence of the initial gaps employed for these cases, where though the noticeable increase in the aspect ratio but the difference between the maximum punch loads are slightly small.

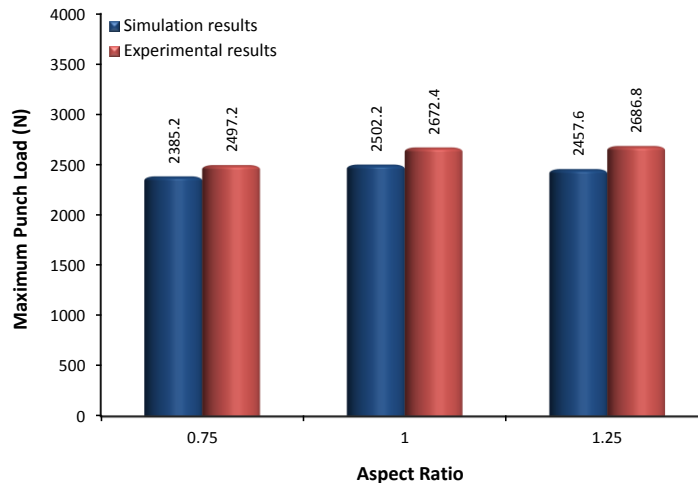
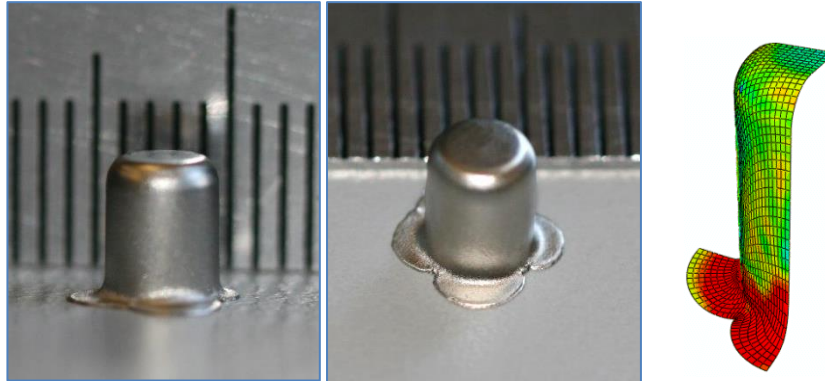


Figure 7-57. Comparison between maximum punch loads obtained with different aspect ratios

The trend of the punch loads predicted by the numerical models was accurately validated by the experimental values. Moreover, it can be indicated that the highest percentage error of 9.3% is detected for the case of aspect ratio 1.25, while the smallest percentage error is 4.7% with aspect ratio of 0.75.

The multi-strokes-micro deep drawing technique proposed in chapter four was employed successfully via FE numerical models. The acquired results reveal comparatively good quality for the final products where the minimum wall thickness was 0.0739mm; i.e. maximum thinning of 26.3%. In order to produce physical cups by utilizing this technique, several micro deep drawing experiments were conducted for this purpose. Experimentally, the same forming conditions adopted for the FE simulations were used such as blank diameter of 11mm, blank thickness of 100 $\mu$ m, rubber material 63A and initial holding force of 300N. The other process dimensions were intended in accordance with the scaling factor  $\lambda=1$ . The depth targeted for the cups in this investigation was 5.9mm to be equal to that obtained from the simulations. **Figure 7-58** presents a comparison of the physical cups with that produced through the numerical models in terms of the geometrical profiles. It can denote that there is a remarkable matching between the two parts. The features observed on the flange region predicted by the simulations due to the anisotropic nature of the ss394 sheet metal are obviously declared on the formed cups. The final depth of the cups obtained from the

experiments was 5.72 which imply an aspect ratio of 1.43. As a result, it can be indicated that the percentage error for the maximum depth is 3.1%



**Figure 7-58. Comparison between the physical and simulated cups using the multi sub-strokes-drawing technique**

On the other side, three size-scaled micro deep drawing systems were fabricated according to the scaling factors  $\lambda=0.25$ ,  $\lambda=0.5$  and  $\lambda=1$  in regard of the process dimensions. In order for a reasonable comparison with the corresponding numerical models, the same forming conditions were utilized in the experiments achieved using these systems. The diameters of the working blanks used for this investigation were 2.75mm at  $\lambda=0.25$ , 5.5mm at  $\lambda=0.5$  and 11mm at  $\lambda=1$ . First of all, the beginning was with  $\lambda=0.5$  and  $\lambda=1$  for aspect ratio of unity, and **Figure 7-59** illustrates physical cups drawn under these conditions. It can denote the similarity in the geometrical profiles of the final products formed at the two different size scales, and this action was rightly predicted by the numerical models.

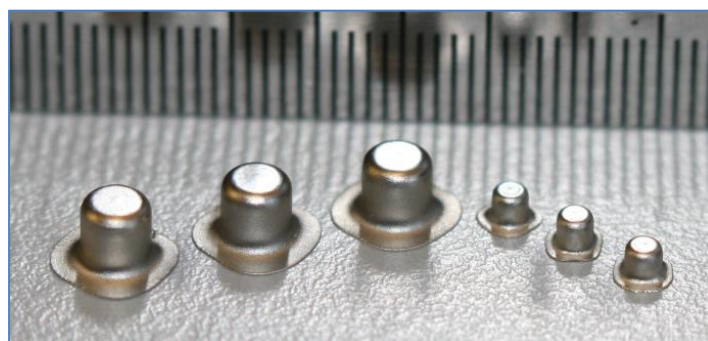


**Figure 7-59. Physical cups drawn at the scaling factors  $\lambda=0.5$  and  $\lambda=1$**

Jenn-Terng et al. [130] report that it cannot produce micro ss 304 cups at room temperature with high cup height to outer diameter (CH/OD) ratio by using a single stage deep drawing die. They indicated in this work that high CH/OD refers to a ratio greater than unity. They used ss 304 sheet with initial thickness of 200 $\mu$ m and rigid punch of 2mm in diameter

with three drawing dies of 2.44mm, 2.22mm and 2.11mm in diameter. A number of drawing experiments were conducted to prove that the micro deep drawing technique presented in the current study using a flexible forming die is more efficient than that of Jenn-Terng for producing micro cups even at smaller size scaling levels. For this purpose, a stainless steel 304 sheet of 100 $\mu$ m in thickness was utilized as well as the same surface roughness for the forming tools were intended at the three different scaling factors aforementioned. **Figure 7-60** shows two groups of physical micro cups that were formed at  $\lambda=0.25$ ,  $\lambda=0.5$  and  $\lambda=1$ . The parts in the first group were drawn to aspect ratio of 1, while in the second group the aspect ratios were in fact various in dependence on how the sheet material enough to produce useful and successful cups at each scaling factor case. In addition to the results regarding  $\lambda=1$ , it was detected that for  $\lambda=0.25$  and  $\lambda=0.5$  the depths of the final cups were 1.5mm and 2.98mm which means aspect ratios of 1.5 and 1.49 respectively.

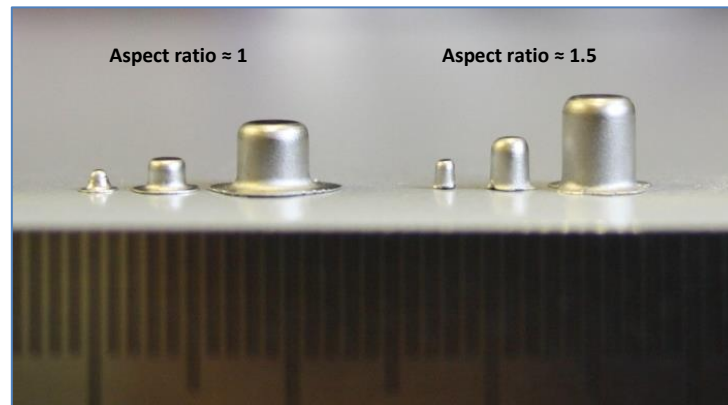


**Figure 7-60.** Physical cups drawn at different scaling factors for different aspect ratios

## **CHAPTER EIGHT**

# **CONCLUSION AND FUTURE WORK**

\*\*\*\*\*

## 8.1 CONCLUSION

Due to the growing demands on miniaturized devices utilized for various applications, the need of providing compatible components at micro scale; particularly those made of sheet metals, is increasing at a tremendous rate. For this purpose, developing competitive and innovative micro manufacturing techniques is imperatively required to produce miniature parts with high quality and relatively low production cost. A novel and comprehensive technique is proposed in this research study for deep drawing processes at micro scale by utilizing a flexible forming die. In this technique, an initial gap is set; positive or negative in accordance with the case conditions considered, between the blank holder and the ring fixture used in the adopted drawing system. Through varying the value of this initial gap in dependence on the requirements of particular drawing conditions, micro cups with similar key geometrical features can be produced. This activity is intended in order to establish reasonable comparisons between the obtained products at different drawing cases.

Stainless steel 304 sheets, which are widely used in microforming industries, were employed in the current work to supply the required workpieces. The characterizations of the deformation behaviour of the SS 30 materials were defined via the well-known tensile test. In order to obtain testing results with high standard of accuracy, a non-contacting advanced video extensometer was used for measuring strains during the tensile tests. Polyurethane rubber materials were employed for the flexible forming die involved in the micro deep drawing technique presented here. The deformation response of the rubber materials were determined via uniaxial and volumetric compression tests.

Finite element simulations were performed using the commercial code Abaqus/Standard to model the micro forming systems established in accordance with the proposed technique. In the numerical models, both the workpieces and the rubber dies were defined as deformable parts, whereas the other components in the considered systems were defined as rigid parts. Owing to validate the results acquired from the numerical simulations, a special microforming set up was designed and fabricated for conducting micro deep drawing experiments. Three size-scaled micro drawing systems were simulated and manufactured with various scaling factors of  $\lambda=1$ ,  $\lambda=0.5$  and  $\lambda=0.25$ . This activity was intended to investigate the capability of the presented technique to be employed at various dimension levels. In



accordance with these scaling levels, micro cups were formed of 4mm, 2mm and 1mm in diameter, respectively with aspect ratios of approximately 1 and 1.5.

Of the process parameters that their influences were investigated via the FE simulations and experiments were initial gap, rubber types, rubber properties, blank diameter, blank thickness, friction coefficients at the contact interfaces and process dimensions. For this purpose, stainless steel 304 sheets of different initial thicknesses of 60 $\mu$ m, 100 $\mu$ m and 150 $\mu$ m were utilized for drawing blanks. Also, the rubber dies employed for the current forming technique were intended with different hardness of 40, 63 and 75 Shore A. the aim of this action is to reveal the effect of this parameter on the drawing quality and to identify the optimum rubber material for a given forming conditions. Moreover, in order to investigate how the initial blank diameter contributes in the micro drawing window, circular ss 304 blanks were cut with 9mm, 10mm, 11mm and 12mm in diameter from the same sheet thickness of 100 $\mu$ m. furthermore, the influence of friction coefficients was revealed for the deep drawing systems considered in this study at blank/blank holder, blank/rigid punch and blank/rubber die contact interfaces. The friction coefficients were adopted with the values of 0, 0.05, 0.1, 0.15, 0.2 and 0.25 for each of the mentioned cases.

Since the initial gap is the key process parameter by which micro cups with similar geometrical aspects can be produced, thus it is of high importance to detect hoe the initial gap dictates on the other drawing process parameters. For this activity, initial gaps of -100, -50, 0, 50 and 100 $\mu$ m were adopted for various deep drawing cases. In addition, the interactions between the main forming parameters were analysed in this study owing to identify the optimum conditions for producing a part with parameter requirements. The results obtained from the numerical models and the experiments can be summarized as following:

- » For the range of initial gaps declared in this study, it was deduced that adopting smaller gaps caused the maximum reductions in thickness to significantly increase. Also, this activity resulted in an increase in in the maximum punch load required for implementing a particular drawing operation completely. In fact, this action can be rationalized that as the initial gap was reduced the pressure excited inside the rubber material was higher at the same particular drawing stroke. That in turn resulted in high holding force on the flange portion of the blank being formed and in the same time necessitated a higher punch load to resist rubber pressure.

- » An interesting observation relating to rubber material types is that the forming quality of the final products in terms of geometrical features depended on the deformation behaviour of the rubber material. In other words, the mechanical properties of the rubber material utilised for a certain drawing process identify the shape features of the formed cups. The results showed that it is of high importance to compromise between the rubber material properties and the initial gap owing to produce a cup with as much as possible close to the geometrical featured required. For example, although the rubber 63A material is harder and however less incompressible than the rubber 40A, but they resulted in cups of precisely similar geometry features with no initial gap. Nevertheless, the rubber 75A material under these conditions caused the cup formed shallow at its shoulder corner. Therefore, smaller initial gap was adopted to obtain parts like those produced with the former rubber materials.
  
- » It was revealed that the quality of the drawn cups in terms of wall thickness distribution can be remarkably improved through reducing the initial blank diameter utilized for a given drawing conditions. This action is because smaller blank diameter implies smaller flange area which results in a reduction in the friction forces at this region as well as lower holding pressure applied by the rubber die according to the current technique.
  
- » The results stated that the micro deep drawing technique presented in this study can be successfully employed to produce cups with high forming quality from different sheet thicknesses. It was reported also that in order to obtain cups with similar final profiles, a smaller initial gap was required for the thicker sheets.
  
- » An important indication was acquired from the current work is that the friction status at blank/rubber contact interface had no noticeable effects whether on the thickness distribution or the thickness reduction of the formed cup wall. While, increasing the friction coefficient at the blank/punch interface improved thickness reductions at the bottom region of the produced part and had no effect on the wall thickness of the other regions. However, the friction conditions between the blank

and the blank holder surfaces significantly affected the thickness distribution and also the maximum reduction of thickness at the side wall. The increase of the friction coefficient at this region caused the thickness distribution to be more nonuniform and increased the maximum thickness reduction. In general, the friction status at the three contact interfaces aforementioned had no noticeable influence on the punch load-travel relationships and also on the maximum punch load required for a complete drawing operation.

- » The proposed drawing technique was efficiently utilised for producing micro cups with reasonably high quality at the different scaling levels considered in this work. It was observed that for a given blank thickness, the initial gap was required to be reduced with minimizing the size scaling level to produce cups of relatively same profile aspects.
  
- » Due to the limited drawing ratio (LDR) of stainless steel 304 sheet in deep drawing processes at micro scale, it cannot produce micro cups with high cup height/diameter ratio (CH/OD) by using a single stage deep drawing die. For this purpose, Gau et al. [130] used three micro drawing systems with three different sets of punches and dies to formed cups of 200  $\mu\text{m}$  initial thickness with maximum CH/OD ratio of 1.37. However, it is proved that the new technique proposed in the current study can be utilized to produce micro cups of even thinner sheets, i.e. 100  $\mu\text{m}$ , with higher CH/OD of 1.41 through just a single micro deep drawing stage using. Moreover, that same CH/OD ratio is achieved by adopting the proposed technique even when the process is size scaled down in accordance with scale factor of 0.5 where the rigid punch diameter is 1mm and final cup height is 1.6mm, which means smaller than Jenn's process about 50%. These activities confirm that the proposed technique is obviously more efficient than the conventional deep drawing for forming micro stainless steel 304 cups.

**8.2 RECOMMENDATIONS FOR FUTURE WORK**

- » Employment of laser cutting technology for sheet metals:

The cutting procedures utilized for both tensile test samples and drawing blanks in this study demonstrated remarkable difficulties and drawbacks to cutting operations of the thin ss 304 sheets used. Thus, in order to save time and cost of cutting processes as well as to obtain accurate dimensions with clean and smooth cutting edges simultaneously for the required pieces, it is recommended to use laser cutting technology for sheet metals.

- » Upgrading the accuracy of rubber die dimensions:

Since the dimensions of the rubber forming dies played a significant role in optimization of process conditions, it is essential to obtain them with a high accuracy standard. In order for avoiding the need for many number of rubber pieces and then choosing the best one, it is advised to adopt casting technology for the rubber materials using dies fabricated with reasonably high dimension quality.

- » Modification of the experimental set up used for micro deep drawing processes:

The existing micro drawing set up showed drawbacks in measuring the initial gap that is allocated in accordance with the proposed technique between the blank holder and the ring fixture. Therefore, to overcome this difficulty it will be feasible to utilize a displacement measuring device, such as digital dial gauge or non-contacting measurement facilities, somehow for this purpose.

- » Employment of laser thickness scanner for micro deep drawn products:

In fact, the measuring procedure of the product-wall thicknesses followed in this work is reasonable and convincingly accurate. However, for applications in which product thickness value is crucial and substantial key parameter, it can utilize laser scanning technology or even ultrasonic technology to attain high accuracy standard. Also, such techniques would be more robust and consistent for the products formed at relatively at small size scaling levels.

### **8.3 FUTURE WORK**

- » Investigation of micro deep drawing technique using a floated metallic ring positioned between the blank and the rubber die is in progress. A number of FE simulations have been accomplished to predict the optimum forming conditions for particular cases. After experimental validation of the numerical simulations, the results could be applied as design guidelines for identifying thickness, inner diameter, outer diameter and shoulder corner radius of the floated ring for any given drawing conditions. Also, of the process parameters planned to be studied are punch-ring clearance, rubber material types, blank/ring friction coefficient and forming velocity.
  
- » Incorporating the micro drawing technique proposed in the current work on a wide variety of alloys commonly used in the microforming industry such as brass, aluminium, copper and even plastic materials.
  
- » Upgrading the capabilities of the existing experimental set up appropriately to be used with applying ultrasonic vibration on the rigid punch. The main object of utilizing the ultrasonic vibration technology is to study its influence on the friction status at blank/tool contact interfaces and on the deformation behaviour of both the rubber die material and the sheet metal used.
  
- » Improving the multi sub-strokes-micro deep drawing technique presented here. The FE numerical models built for this purpose would be adopted to predict the convenient forming conditions for a wide range of initial diameter and thickness of blanks at different scaling factors. This technique would be employed to produce micro cups with aspect ratio higher than 1.5.

## References

---

- [1] **John A. Schey**, "*Introduction to Manufacturing Processes*", Third Edition ed.: McGraw-Hill, 2000.
- [2] **Serope Kalpakjian and Steven R. Schmid**, "*Manufacturing Processes for Engineering Materials*", Fourth Edition ed.: Prentice Hall, London, 2003.
- [3] **Mikell P. Groover**, "*Fundamentals of Modern Manufacturing: Materials, Processes, and Systems*", Third Edition ed.: John Wiley & Sons, Inc., 2007.
- [4] **Karl-Heinrich Grote and Erik K. Antonsson**, "*Springer Handbook on Mechanical Engineering*": Springer Science and Business Media, LLC New York, 2008.
- [5] **Roy A. Lindberg**, "*Processes and Materials of Manufacture*", Third Edition ed.: Allyn and Bacon, Inc., 1983.
- [6] **Boron extrication**, (2012), "<http://boronextrication.com/tag/list-of-vehicles-with-boron-and-uhss/>".
- [7] **Z. Marciniak, J.L. Duncan and S.J. Hu**, "*Mechanics of Sheet Metal Forming*", Second Edition ed.: Butterworth-Heinemann, 2002.
- [8] **R. Padmanabhan, M. C. Oliveiram, J. L. Alves and L. F. Menezes**, "*Influence of process parameters on the deep drawing of stainless steel*", *Finite Elements in Analysis and Design*, vol. 43, pp. 1062-1067, 2007.
- [9] **S. J. Allen and S. M. Mahdavian**, "*The effect of lubrication on die expansion during the deep drawing of axisymmetrical steel cups*", *Journal of Materials Processing Technology*, vol. 199, pp. 102-107, 2008.
- [10] **G. Palumbo, D. Sorgente, L. Tricarico, S.H. Zhang and W.T. Zheng**, "*Numerical and experimental analysis of the Warm Deep Drawing process for Mg alloys*", *Journal of Achievements in Materials and Manufacturing Engineering*, vol. 14, pp. 111-118, 2006.
- [11] **Swadesh Kumar Singh and D. Ravi Kumar**, "*Effect of process parameters on product surface finish and thickness variation in hydro-mechanical deep drawing*", *Journal of Materials Processing Technology*, vol. 204, pp. 169-178, 2008.
- [12] **Custompart.Net**, "<http://www.custompartnet.com/wu/sheet-metal-forming>".
- [13] **Anwar Kandil**, "*An experimental study of hydroforming deep drawing*", *Journal of Materials Processing Technology*, vol. 134, pp. 70-80, 2003.
- [14] **S. Thiruvardchelvan**, "*The potential role of flexible tools in metal forming*", *Journal of Materials Processing Technology*, vol. 122, pp. 293-300, 2002.
- [15] **S. Thiruvardchelvan**, "*Elastomers in metal forming: A review*", *Journal of Materials Processing Technology*, vol. 39, pp. 55-82, 1993.
- [16] **Edward M. Mielen**, "*Metalworking Science and Engineering*", First Edition ed.: McGraw-Hill, Inc., 1991.
- [17] **Aichi Quality**, (2012), "<http://www.aichi-brand.jp/corporate/type/fabricated/noguchi-seisakusho-e.html>".
- [18] **V. Chiles S. C. Black, A. J. Lissaman and S. J. Martin**, "*Principles of engineering manufacture*", Third edition ed.: London : Arnold ; New York : Halsted Press, 1996.
- [19] **H. J. Kleemola and J. O. Kumpulainen**, "*Factors Influencing the Forming Limit Diagram: Part 1-The Experimental Determination of the Forming Limits of Sheet Steel*", *Journal of Mechanical Working Technology*, vol. 3, pp. 289-302, 1980.
- [20] **Serope Kalpakjian and Steven Schmid**, "*Manufacturing Processes for Engineering Materials*", Fifth edition ed.: Prentice Hall, 2007.
- [21] **William F. And Robert M.**, "*Metal Forming, Mechanics and Metallurgy*", Third Edition ed.: Cambridge University Press, 2007.
- [22] **R. Hill**, "*A theory of the yield and plastic flow of anisotropic metals*", *Proceedings of the Royal Society of London, Series A*, vol. 193, pp. 281-297, 1948.
- [23] **Badawy A.**, "*Cup deep drawing, an optimization problem*", *process Modeling Tools*, *Proceeding of ASM Materials and Processes Congress*, p. 75, 1980.
- [24] **S. K. Singh and D. Ravi Kumar**, "*Effect of process parameters on product surface finish and thickness variation in hydro-mechanical deep drawing*", *Journal of Materials Processing Technology*, vol. 204, pp. 169-178, 2008.

## References

---

- [25] **A. Wifi and A. Mosallam**, "Some aspects of blank-holder force schemes in deep drawing process", *Journal of Achievements in Materials and Manufacturing Engineering*, vol. 24, pp. 315-323, **2007**.
- [26] **Vedat Savas and Omer Secgin**, "A new type of deep drawing die design and experimental results", *Materials & Design*, vol. 28, pp. 1330-1333, **2007**.
- [27] **H. Nezami-Esfahlan, S. Abbasnejad-Dizaji and F. Djavanroodi**, "Experimental and numerical analysis for hydroforming of Ti6Al4V alloy used in aerospace, assisted by floating disk", *Journal of Applied Sciences*, vol. 9, pp. 2925-2932, **2009**.
- [28] **Cebeli Özek and Muhammet Bal**, "The effect of die/blank holder and punch radiuses on limit drawing ratio in angular deep-drawing dies", *Int J Adv Manuf Technol*, vol. 40, pp. 1077-1083, **2009**.
- [29] **Wisetool**, "<http://www.wisetool.com/deepdraw.htm>", **2012**.
- [30] **Alumatter**, (2012), "[www.aluminium.matter.org.uk/content/html/eng/default.asp?catid=199&pageid=2144416949](http://www.aluminium.matter.org.uk/content/html/eng/default.asp?catid=199&pageid=2144416949)".
- [31] **Nagpal V.**, "Analysis of Thickness Reduction in Deep Drawing with Simultaneous Ironing", 6th NAMRC, SME Dearborn, Michigan, pp. 158-165, **1978**.
- [32] **Yi Qin**, "Micro-manufacturing engineering and technology", First Edition ed.: Elsevier Inc., **2010**.
- [33] **Nasr Abdelrahman Shuaib**, "An Investigation of Size Effect on Thin Sheet Formability for Microforming Applications", University of Kentucky, Lexington, Kentucky, USA, **2008**.
- [34] **Interactive Architecture.Org**, (2012), "<http://www.interactivearchitecture.org/category/devices>".
- [35] **Maxon Motor**, (2012), "<http://www.maxonmotor.com/maxon/view/content/products>".
- [36] **T. Shimizu K. Manabe, H. Koyama, M. Yang and K. Ito**, "Validation of FE simulation based on surface roughness model in micro-deep drawing", *Journal of Materials Processing Technology*, vol. 204, pp. 89-93, **2008**.
- [37] **Sasawat Mahabunphachai and Muammer Koç**, "Investigation of size effects on material behavior of thin sheet metals using hydraulic bulge testing at micro/meso-scales", *International Journal of Machine Tools and Manufacture*, vol. 48, pp. 1014-1029, **2008**.
- [38] **Mendell**, (2012), "[http://www.mendell.com/cardiovascular\\_and\\_endovascular.php](http://www.mendell.com/cardiovascular_and_endovascular.php)".
- [39] **Hyun Bo Shim**, "Improving Formability to Develop Miniature Stamping Technologies", *International Journal of Precision Engineering and Manufacturing*, vol. 10, pp. 117-125, **2009**.
- [40] **M. Geiger, M. Kleiner, R. Eckstein, N. Tiesler and U. Engel**, "Microforming", *CIRP Annals - Manufacturing Technology*, vol. 20, pp. 445-462, **2001**.
- [41] **SchottGlass Manufacturers**, (2012), "<http://www.us.schott.com/defense/english/ep/index.html>".
- [42] **U. Engel and R. Eckstein**, "Microforming-from basic research to its realization", *Journal of Materials Processing Technology*, vol. 125-126, pp. 35-44, **2002**.
- [43] **Frank Vollertsen, Zhenyu Hu, Hendrik Niehoff, H. Schulze and Carmen Theiler**, "State of the art in micro forming and investigations into micro deep drawing", *Journal of Materials Processing Technology*, vol. 151, pp. 70-79, **2004**.
- [44] **Halil Ibrahim Demirci, Cemal Esner and Mustafa Yasar**, "Effect of the blank holder force on drawing of aluminum alloy square cup: Theoretical and experimental investigation", *Journal of Materials Processing Technology*, vol. 206, pp. 152-160, **2008**.
- [45] **A.S. Wifi H. Gharib, M. Younan, and A. Nassef**, "Optimization of the blank holder force in cup drawing", *Journal of Achievements in Materials and Manufacturing Engineering*, vol. 18, p. 4, **2006**.
- [46] **H. Gharib, A.S. Wifi, M. Younan and A. Nassef**, "An analytical incremental model for the analysis of the cup drawing", *Proceedings of the 14th International Scientific Conference on Achievements in Mechanical and Materials Engineering AMME2006*, Wisla, **2006**.
- [47] **M.J. Saran, E. Schedin, A. Samuelsson, A. Melander and C. Gustafsson**, "Numerical and experimental investigations of deep drawing of metal sheets", *Journal of Engineering for Industry, Transactions of the ASME*, vol. 112, pp. 272-277, **1990**.
- [48] **Shoichiro Yoshihara, Ken-Ichi Manabe and Hisashi Nishimura**, "Effect of blank holder force control in deep-drawing process of magnesium alloy sheet", *Journal of Materials Processing Technology*, vol. 170, pp. 579-585, **2005**.

- [49] **M. A. Hassan, R. Suenaga, N. Takakura and K. Yamaguchi**, "A novel process on friction aided deep drawing using tapered blank holder divided into four segments", *Journal of Materials Processing Technology*, vol. 159, pp. 418-425, **2005**.
- [50] **K. Mori, S. Nishijima and C. J. Tan**, "Two-stage cold stamping of magnesium alloy cups having small corner radius", *International Journal of Machine Tools and Manufacture*, vol. 49, pp. 767-772, **2009**.
- [51] **Jaromir Audy and Emil Evin**, "Exploring Efficiency of Tool Coating via Deep Drawing of Cylindrical Cups", *M M Science Journal*, pp. 20-23, **2008**.
- [52] **G. Ambrogio, L. Filice, G. Palumbo and S. Pinto**, "Prediction of formability extension in deep drawing when superimposing a thermal gradient", *Journal of Materials Processing Technology*, vol. 162-163, pp. 454-460, **2005**.
- [53] **D. V. Hai, S. Itoh, T. Sakai, S. Kamado and Y. Kojima**, "Experimentally and Numerical Study on Deep Drawing Process for Magnesium Alloy Sheet at Elevated Temperatures ", *Materials Transactions*, vol. 49, pp. 1101-1106, **2008**.
- [54] **J. Lin, S. D. Zhao, Z. Y. Zhang and Z. W. Wang**, "Deep drawing using a novel hydromechanical tooling", *International Journal of Machine Tools and Manufacture*, vol. 49, pp. 73-80, **2009**.
- [55] **S. Thiruvarudchelvan and M. J. Tan**, "A note on fluid-pressure-assisted deep drawing processes", *Journal of Materials Processing Technology*, vol. 172, pp. 174-181, **2006**.
- [56] **A. Kocanda and H. Sadlowska**, "Automotive Component Development by Means of Hydroforming", *Archives of Civil and Mechanical Engineering*, Warsaw University of Technology, Poland, vol. VIII, pp. 55-72, **2008**.
- [57] **Wei Liu, Yi-Zhe Chen, Gang Liu and Xiao-Lei Cui**, "Welded double sheet hydroforming of complex hollow component", *Transactions of Nonferrous Metals Society of China*, vol. 22, Supplement 2, pp. s309-s314, **2012**.
- [58] **Joachim Danckert and Karl Brian Nielsen**, "Hydromechanical Deep Drawing with Uniform Pressure on the Flange", *CIRP Annals - Manufacturing Technology*, vol. 49, pp. 217-220, **2000**.
- [59] **Yi Qin and Raj Balendra**, "Design considerations for hydromechanical deep drawing of sheet components with concave features", *Journal of Materials Processing Technology*, vol. 145, pp. 163-170, **2004**.
- [60] **Lihui Lang, Joachim Danckert and Karl Brian Nielsen**, "Investigation into the effect of pre-bulging during hydromechanical deep drawing with uniform pressure onto the blank", *International Journal of Machine Tools and Manufacture*, vol. 44, pp. 649-657, **2004**.
- [61] **Gerrit Kurz**, "Heated Hydro -Mechanical Deep Drawing of Magnesium Sheet Metal", *Magnesium Technology Symp.*, vol. TMS Annual Meeting, pp. 67-71, **2004**.
- [62] **T. Khandeparkar and M. Liewald**, "Hydromechanical deep drawing of cups with stepped geometries", *Journal of Materials Processing Technology*, vol. 202, pp. 246-254, **2008**.
- [63] **Amirt Dixit and D. Ravi Kumar Swadesh K. Singh**, "Optimization of the design parameters of Modified Die in Hydro-mechanical Deep Drawing Using LS-DYNA", *International Journal of Advanced Manufacturing Technology*, vol. 38, pp. 32-37, **2008**.
- [64] **Lihui Lang, Joachim Danckert and Karl Brian Nielsen**, "Study on hydromechanical deep drawing with uniform pressure onto the blank", *International Journal of Machine Tools and Manufacture*, vol. 44, pp. 495-502, **2004**.
- [65] **S. Thiruvarudchelvan and F. W. Travis**, "Hydraulic-pressure-enhanced cup-drawing processes--an appraisal", *Journal of Materials Processing Technology*, vol. 140, pp. 70-75, **2003**.
- [66] **Ho Choi, Muammer Koç and Jun Ni**, "Determination of optimal loading profiles in warm hydroforming of lightweight materials", *Journal of Materials Processing Technology*, vol. 190, pp. 230-242, **2007**.
- [67] **F. Vollertsen, R. Breede and K. Lange**, "A Method for Deep Drawing with Multiple Elastomer Membranes", *CIRP Annals - Manufacturing Technology*, vol. 48, pp. 221-226, **1999**.
- [68] **M. H. Parsa and P. Darbandi**, "Experimental and numerical analyses of sheet hydroforming process for production of an automobile body part", *Journal of Materials Processing Technology*, vol. 198, pp. 381-390, **2008**.
- [69] **Lihui Lang, Joachim Danckert and Karl Brian Nielsen**, "Investigation into hydrodynamic deep drawing assisted by radial pressure: Part I. Experimental observations of the forming



- process of aluminum alloy*", Journal of Materials Processing Technology, vol. 148, pp. 119-131, **2004**.
- [70] **Lihui Lang, Joachim Danckert and Karl Brian Nielsen**, "Investigation into hydrodynamic deep drawing assisted by radial pressure: Part II. Numerical analysis of the drawing mechanism and the process parameters", Journal of Materials Processing Technology, vol. 166, pp. 150-161, **2005**.
- [71] **Nader Abedrabbo, Michael A. Zampaloni and Farhang Pourboghra**, "Wrinkling control in aluminum sheet hydroforming", International Journal of Mechanical Sciences, vol. 47, pp. 333-358, **2005**.
- [72] **Lin Gao and Minghe Chen Huiting Wanga**, "Hydrodynamic Deep Drawing Process Assisted by Radial Pressure with Inward Flowing Liquid", International Journal of Mechanical Sciences, vol. 53, pp. 793-799, **2011**.
- [73] **S. Thiruvarudchelvan and H. B. Wang**, "Pressure generated in the hydraulic-pressure augmented deep-drawing process", Journal of Materials Processing Technology, vol. 74, pp. 286-291, **1998**.
- [74] **S. Thiruvarudchelvan and H. Wang**, "Investigations into the hydraulic-pressure augmented deep drawing process", Journal of Materials Processing Technology, vol. 105, pp. 161-175, **2000**.
- [75] **S. Thiruvarudchelvan and H. Wang**, "Erratum to "Investigations into the hydraulic-pressure augmented deep drawing process" [*J. Mater. Proc. Technol.* 105 (1/2) (2000) 161-175]", Journal of Materials Processing Technology, vol. 110, pp. 112-126, **2001**.
- [76] **Muamar Benisa, Bojan Babic, Aleksandar Grbovic and Zoran Stefanovic**, "Computer-Aided Modeling of the Rubber-Pad Forming Process", Materials and technology, vol. 46, pp. 503-510, **2012**.
- [77] **Maziar Ramezani, Zaidi Mohd Ripin and Roslan Ahmad**, "Computer aided modelling of friction in rubber-pad forming process", Journal of Materials Processing Technology, vol. 209, pp. 4925-4934, **2009**.
- [78] **Antonio Del Prete, Gabriele Papadia and Babara Manisi**, "Computer Aided Modelling of Rubber Pad Forming Process", Key Engineering Materials, vol. 473, pp. 637-644, **2011**.
- [79] **M. Ramezani, Z. M. Ripin and R. Ahmad**, "Numerical Simulation of Sheet Stamp Process Using Flexible Punch", Journal of Engineering Manufacture, vol. 223, pp. 829-840, **2009**.
- [80] **Zhong-Jin Wang, Xin-Yun Wang and Zhong-Ren Wang**, "Viscous pressure forming (VPF) of corrugated thin-walled sheet part with small radius", Journal of Materials Processing Technology, vol. 145, pp. 345-351, **2004**.
- [81] **M. Husnu Dirikolu and Esra Akdemir**, "Computer aided modelling of flexible forming process", Journal of Materials Processing Technology, vol. 148, pp. 376-381, **2004**.
- [82] **Junhua Liu, Bert Westhoff, Mustafa A. Ahmetoglu and Taylan Altan**, "Application of viscous pressure forming (VPF) to low volume stamping of difficult-to-form alloys --results of preliminary FEM simulations", Journal of Materials Processing Technology, vol. 59, pp. 49-58, **1996**.
- [83] **Wang Zhong-Jin, Li Yi, Liu Jian-Guang and Zhang Yi-He**, "Evaluation of Forming Limit in Viscous Pressure Forming of Automotive Aluminum Alloy 6k21-T4 Sheet", Transactions of Nonferrous Metals Society of China, vol. 17, pp. 1169-1174, **2007**.
- [84] **J. Liu, M. Ahmetoglu and T. Altan**, "Evaluation of sheet metal formability, viscous pressure forming (VPF) dome test", Journal of Materials Processing Technology, vol. 98, pp. 1-6, **2000**.
- [85] **Leonid B. Shulkin, Ronald A. Posteraro, Mustafa A. Ahmetoglu, Gary L. Kinzel and Taylan Altan**, "Blank holder force (BHF) control in viscous pressure forming (VPF) of sheet metal", Journal of Materials Processing Technology, vol. 98, pp. 7-16, **2000**.
- [86] **David J. Browne and Emil Battikha**, "Optimisation of aluminium sheet forming using a flexible die", Journal of Materials Processing Technology, vol. 55, pp. 218-223, **1995**.
- [87] **Giuseppe Sala**, "A numerical and experimental approach to optimise sheet stamping technologies: part II — aluminium alloys rubber-forming", Materials & Design, vol. 22, pp. 299-315, **2001**.
- [88] **Nasr Abdelrahman Shuaib**, "An Investigation of Size Effects on Thin Sheet Formability for Microforming Applications", Doctor of Philosophy, College of Engineering, University of Kentucky, **2008**.

- [89] **U. Engel and E. Egerer**, "Basic research on cold and warm forging of microparts", Key Engineering Material, vol. 233-236, pp. 449-456, **2003**.
- [90] **J.F. Michel and P. Picart**, "Size effects on the constitutive behaviour for brass in sheet metal forming", Journal of Materials Processing Technology, vol. 141, pp. 439-446, **2003**.
- [91] **S. Miyazaki, H. Fujita and H. Hiraoka**, "Effect of specimen size on the flow stress of rod specimens of polycrystalline Cu-Al alloy", Scripta Metallurgica, vol. 13, pp. 447-449, **1979**.
- [92] **Linfa Peng, Fang Liu, Jun Ni and Xinmin Lai**, "Size effects in thin sheet metal forming and its elastic-plastic constitutive model", Materials & Design, vol. 28, pp. 1731-1736, **2007**.
- [93] **C H. Chen, R. S. Lee and J. T. Gau**, "Size effect and forming-limit strain prediction for microscale sheet metal forming of stainless steel 304", Journal of Starin Analysis, vol. 45, pp. 283-299, **2010**.
- [94] **K. F. Zhang and L. Kun**, "Classification of size effects and similarity evaluating method in micro forming", Journal of Materials Processing Technology, vol. 209, pp. 4949-4953, **2009**.
- [95] **M. Geiger, F. Vollertsen and R. Kals**, "Fundamentals on the Manufacturing of Sheet Metal Microparts", CIRP Annals - Manufacturing Technology, vol. 45, pp. 277-282, **1996**.
- [96] **M. Geiger, A. Mebner and U. Engel**, "Production of microparts-size effects in bulk metal forming, similarity theory", Production Engineering, vol. 4, pp. 55-58, **1997**.
- [97] **T. A. Kals and Ralf Eckstein**, "Miniaturization in sheet metal working", Journal of Materials Processing Technology, vol. 103, pp. 95-101, **2000**.
- [98] **Sasawat Mahabunphachai**, "A Hybrid Hydroforming and Mechanical Bonding Process for Fuel Cell Bipolar Plates", Doctor of Philosophy, Mechanical Engineering, The University of Michigan, **2008**.
- [99] **E. O. Hall**, "Deformation and Ageing of Mild Steel", Physical Society-Proceeding, vol. 64, pp. 747-753, **1951**.
- [100] **F. Vollertsen**, "Categories of Size Effects", Production Engineering Research and Development, vol. 2, pp. 377-383, **2008**.
- [101] **M. Geiger, U. Engel, F. Vollertsen, R. Kals and A. Messner**, "Metal forming of microparts for electronics", Production Engineering, vol. 2, pp. 15-18, **1994**.
- [102] **L. V Raulea, L. E. Govaert and F. P. T. Baaijens**, "Grain and Specimen Size Effects in Processing Metal Sheets", Advanced Technology of Plasticity, Proceedings of the sixth international conference on technology of plasticity nuremberg, Springer, Berlin., vol. II, pp. 939-944, **1999**.
- [103] **L.V. Raulea, A.M Goijaerts, L.E. Govaert and F.P.T. Baaijens**, "Size effects in the processing of thin metal sheets", Journal of Materials Processing Technology, vol. 115, pp. 44-48, **2001**.
- [104] **Jenn-Terng Gau, Chris Principe and Jyhwen Wang**, "An experimental study on size effects on flow stress and formability of aluminum and brass for microforming", Journal of Materials Processing Technology, vol. 184, pp. 42-46, **2007**.
- [105] **Frank Vollertsen and Zhenyu Hu**, "Analysis of punch velocity dependent process window in micro deep drawing", Production Engineering, vol. 4, pp. 553-559, 2010/12/01 **2010**.
- [106] **Yasunori Saotome, Kaname Yasuda and Hiroshi Kaga**, "Microdeep drawability of very thin sheet steels", Journal of Materials Processing Technology, vol. 113, pp. 641-647, **2001**.
- [107] **Y. Marumo, H. Saiki and L Ruan**, "Effect of sheet thickness on deep drawing of metal foils", of Achievements in Materials and Manufacturing Engineering, vol. 20, pp. 479-482, **2007**.
- [108] **Chi-Han Chen, Jenn-Terng Gau and Rong-Shean Lee**, "An Experimental and Analytical Study on the Limit Drawing Ratio of Stainless Steel 304 Foils for Microsheet Forming", Materials and Manufacturing Processes, vol. 24, pp. 1256-1265, 2009/12/21 **2009**.
- [109] **G. Hirt, H. Justinger and N. Witulski**, "Analysis of size effects in micro sheet forming", 1<sup>st</sup> Colloquium Processscaling, Bremen **2003**.
- [110] **Wang Chun-Ju, Guo Bin and Shan De-Bin**, "Effect of die cavity dimension on micro U deep drawing behaviour with T2 foil", Transactions of Nanoferrous Metals Society of Chone, vol. 19, pp. 790-794, **2009**.
- [111] **Y. Marumo, H. Saiki and A. Onoue**, "Effect of lap-sheets on deep drawing of metallic foil cups", Journal of Materials Processing Technology, vol. 119, pp. 48-51, **2001**.
- [112] **Z. Hu and F. Vollertsen**, "Investigation on the optimisation of the blank shape for micro deep drawing of rectangular parts", Steel Research International, vol. 82, pp. 974-978, **2011**.

## References

---

- [113] **Zhenyu Hu and Frank Vollertsen**, "Optimisation of the blank shape for micro deep drawing of rectangular parts", Proceeding of Esafform 2011, Blafast, UK, **2011**.
- [114] **M. W. Fu, B. Yang and W. L. Chan**, "Experimental and simulation studies of micro blanking and deep drawing compound process using copper sheet", Journal of Materials Processing Technology, vol. 213, pp. 101-110, **2013**.
- [115] **Zhenyu Hu**, "Realisation and application of size dependent FEM-simulation for deep drawing of rectangular work piece", CIRP Journal of Manufacturing Science and Technology, vol. 4, pp. 90-95, **2011**.
- [116] **F. Vollertsen**, "Effects on the deep drawing diagram in micro forming", Production Engineering, vol. 6, pp. 11-18, 2012/02/01 **2012**.
- [117] **K. Manabe, T. Shimizu and H. Koyama**, "Evaluation of milli-scale cylindrical cup in two-stage deep drawing process", Journal of Materials Processing Technology, vol. 187-188, pp. 245-249, **2007**.
- [118] **Feng Gong, Bin Guo, Chunju Wang and Debin Shan**, "Effects of lubrication conditions on micro deep drawing", Microsystem Technologies, vol. 16, pp. 1741-1747, 2010/10/01 **2010**.
- [119] **Feng Gong, Bin Guo, Chunju Wang and Debin Shan**, "Micro deep drawing of micro cups by using DLC film coated blank holders and dies", Diamond & Related Materials, vol. 20, pp. 196-200, **2011**.
- [120] **Yushiro Murashige Tetsuhide Shimizu, Kuniyoshi Ito and Ken-Ichi Manabe**, "Influence of surface topographical interaction between tool and material in micro-deep drawing", Journal of Solid Mechanics and Materials Engineering, vol. 3, pp. 397-408 **2009**.
- [121] **N. Witulski, H. Justinger and G. Hirt**, "Validation Of FEM-Simulation For Micro Deep Drawing Process Modeling", MATERIALS PROCESSING AND DESIGN: Modeling, Simulation and Applications - NUMIFORM 2004 - Proceedings of the 8th International Conference on Numerical Methods in Industrial Forming Processes, Columbus, Ohio (USA) vol. 712, pp. 952-957, **2004**.
- [122] **Chunju Wang, Bin Guo, Debin Shan and Xinmei Bai**, "Experimental research on micro-deep drawing processes of pure gold thin sheet using DLC-coated female die", The International Journal of Advanced Manufacturing Technology, pp. 1-11, 2012/12/01 **2012**.
- [123] **Zhenyu Hu, Alexej Schubnov and Frank Vollertsen**, "Tribological behaviour of DLC-films and their application in micro deep drawing", Journal of Materials Processing Technology, vol. 212, pp. 647-652, **2012**.
- [124] **Takaaki Horiuchia, Shoichiro Yoshiharaa and Yu Iriyamab**, "Dry deep drawability of A5052 aluminum alloy sheet with DLC-coating", Wear, vol. 286-287, pp. 79-83, **2012**.
- [125] **Fung-Huei Yeh, Ching-Lun Li and Yuung-Hwa Lu**, "Study of thickness and grain size effects on material behavior in micro-forming", Journal of Materials Processing Technology, vol. 201, pp. 237-241, **2008**.
- [126] **X. Ma, R. Lapovok, C. Gu, A. Molotnikov, Y. Estrin, E. V. Pereloma, C. H. J. Davies and P. D. Hodgson**, "Deep drawing behaviour of ultrafine grained copper: modelling and experiment", Journal of Material science, vol. 44, pp. 3807-3812, **2009**.
- [127] **R. Lapovok, I. Timokhina, P. W. J. Mckenzie and R. O'donnell**, "Processing and properties of ultrafine-grain aluminium alloy 6111 sheet", Journal of Materials Processing Technology, vol. 200, pp. 441-450, **2008**.
- [128] **Gerrit Behrens, Julien Kovac, Bernd Köhler, Frank Vollertsen and Heinz-Rolf Stock**, "Drawability of thin magnetron sputtered Al-Zr foils in micro deep drawing", Transactions of Nonferrous Metals Society of China, vol. 22, Supplement 2, pp. s268-s274, **2012**.
- [129] **Frank Vollertsen, Zhenyu Hu, Heinz-Rolf Stock and Bernd Koehler**, "On the limit drawing ratio of magnetron sputtered aluminium-scandium foils within micro deep drawing", Production Engineering, vol. 4, pp. 451-456, 2010/10/01 **2010**.
- [130] **Jenn-Terng Gau, Sujith Teegala, Kun-Min Huang, Tun-Jen Hsiao and Bor-Tsuen Lin**, "Using micro deep drawing with ironing stages to form stainless steel 304 micro cups", <http://www.sciencedirect.com/science/article/pii/S1526612513000236>, **2013**
- [131] **M. Fu, W. Chan and B. Yang**, "Study of size effects on material deformation behaviour in micro-deep drawing of copper sheet Metal", Proceedings of the 10<sup>th</sup> International Conference on Technology of Plasticity ICTP, September 25 – 30, 2011, Aachen, Germany, **2011**.

## References

---

- [132] **Fabrizio Quadrini, Loredana Santo and Erica Anna**, "Flexible forming of thin aluminum alloy sheets", *International Journal of Modern Manufacturing Technologies*, vol. II, pp. 79-84, **2010**.
- [133] **Linfa Peng, Peng Hu, Xinmin Lai, Deqing Mei and Jun Ni**, "Investigation of micro/meso sheet soft punch stamping process – simulation and experiments", *Materials & Design*, vol. 30, pp. 783-790, **2009**.
- [134] **Linfa Peng, Dong'an Liu, Peng Hu, Xinmin Lai and Jun Ni**, "Fabrication of Metallic Bipolar Plates for Proton Exchange Membrane Fuel Cell by Flexible Forming Process-Numerical Simulations and Experiments", *Journal of Fuel Cell Science and Technology* vol. 7, pp. 0310091-9, **2010**.
- [135] **M. A. Maslennokiv**, "Russians develop punchless drawing", *Metaworking Production*, vol. 16, pp. 1417-1420, **1957**.
- [136] **Maziar Ramezani and Zaidimohd Ripin**, "A study on high ratio cup drawing by Maslennikov's process", *The International Journal of Advanced Manufacturing Technology*, vol. 58, pp. 503-520, 2012/01/01 **2012**.
- [137] **M. A. Hassan, N. Takakura and K. Yamaguchi**, "Friction aided deep drawing of sheet metals using polyurethane ring and auxiliary metal punch. Part 1: experimental observations on the deep drawing of aluminium thin sheets and foils", *International Journal of Machine Tools and Manufacture*, vol. 42, pp. 625-631, **2002**.
- [138] **M. A. Hassan, K. Hino, N. Takakura and K. Yamaguchi**, "Friction aided deep drawing of sheet metals using polyurethane ring and auxiliary metal punch. Part 2: analysis of the drawing mechanism and process parameters", *International Journal of Machine Tools and Manufacture*, vol. 42, pp. 633-642, **2002**.
- [139] **Yanxiong Liu, Lin Hua, Jian Lan and Xi Wei**, "Studies of the deformation styles of the rubber-pad forming process used for manufacturing metallic bipolar plates", *Journal of Power Sources*, vol. 195, pp. 8177-8184, **2010**.
- [140] **Sasawat Mahabunphachai and Muammer Koç**, "Fabrication of micro-channel arrays on thin metallic sheet using internal fluid pressure: Investigations on size effects and development of design guidelines", *Journal of Power Sources*, vol. 175, pp. 363-371, **2008**.
- [141] **Trans-Matic: A Metal Stamping Company**, (2013), "<http://transmatic.com/DeepDrawnStampings/deep-drawing-process>".
- [142] **Wikipedia**, (2013), "[http://en.wikipedia.org/wiki/Deep\\_drawing#cite\\_ref-1](http://en.wikipedia.org/wiki/Deep_drawing#cite_ref-1)".
- [143] **Stainless Sales Corporation**, (2013), "<http://www.stainlesssales.com/304-stainless-steel-rolled-coil.html>".
- [144] **Phani Kumari Paritala**, "Drawing Stainless Steel 304 Micro Cups Through Multi-Stage Draw", Master of Science, Mechanical Engineering, Northern Illinois University, **2009**.
- [145] **American Society for Testing and Materials (Astm)**, "E8 Standard Test Methods of Tension Testing of Metallic Materials", *Annual ASTM Standards*, vol. 99, **2007**.
- [146] **A. Le Port, F. Toussaint and R. Arrieux**, "Finite element study and sensitive analysis of the deep drawing formability of commercially pure titanium", *International Journal of Material Forming*, vol. 2, pp. 121-129, **2009**.
- [147] **Abaqus 6.9 Analysis User's Manual**, (2013), "<http://abaqus.civil.uwa.edu.au:2080/v6.9/books/usb/default.htm?startat=pt05ch19s02abm21.html#usb-mat-canisoyield>".
- [148] **Daeyong Kim, Myoung-Gyu Lee, Chongmin Kim, Michael Wenner, Roberth Wagoner, Frederic Barlat, Kwansoo Chung, Jaeryoun Youn and Taejin Kang**, "Measurements of anisotropic yielding, bausinger and transient behavior of automotive dual-phase steel sheets", *Metals and Materials International*, vol. 9, pp. 561-570, 2003/12/01 **2003**.
- [149] **J. Danckert and K. B. Nielsen**, "Determination of the plastic anisotropy  $r$  in sheet metal using automatic tensile test equipment", *Journal of Material Processing Technology*, vol. 73, pp. 276-280, **1998**.
- [150] **Srbislav Aleksandrović, Milentije Stefanović, Dragan Adamović and Vukić Lazić**, "Variation of Normal Anisotropy Ratio " $r$ " during Plastic Forming", *Journal of Mechanical Engineering*, vol. 55, pp. 392-399, **2009**.
- [151] **Custom Molded Urethane C.U. E. Inc.**, (2013), "<http://www.cue-inc.com/urethane-benefits.html>".
- [152] **Eriks**, (2013), "<http://rubbertechnology.info/en/products/overview-rubberqualities/different-compounds/polyurethane-rubber-au-eu/>".

## References

---

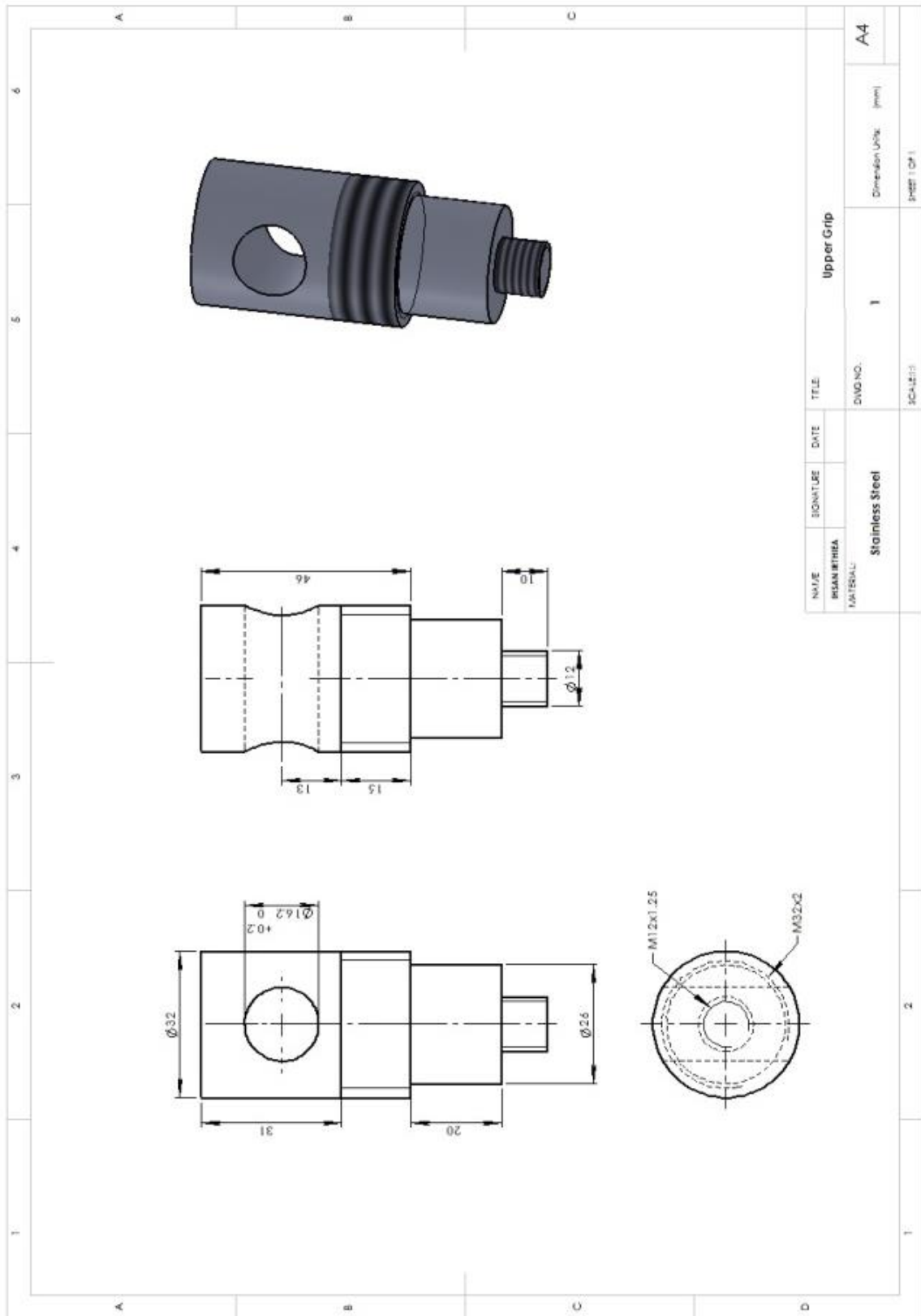
- [153] **Allan F. Bower (2009)**, "Applied Mechanics of Solids", Chapter three: Constitutive Models Relations between Stress and Strain, [http://solidmechanics.org/text/Chapter3\\_5/Chapter3\\_5.htm](http://solidmechanics.org/text/Chapter3_5/Chapter3_5.htm)
- [154] **American Society for Testing and Materials (Astm)**, "D 575 Standard test methods for rubber properties in compression", Annual Book of ASTM Standards vol. 91, **2007**.
- [155] **Gregory L. Bradley, Peter C. Chang and Andrew W. Taylor**, "Determination of ultimate capacity of elastomeric bearings under axial loading", Report to United State Department of Commerce, National Institute of Standards and Technology (NIST) **1998**.
- [156] **B. C. Duncan, A. S. Maxwell, L. E. Crocker and R. Hunt**, "Verification of hyperelastic test methods", NPL Report CMMT(A)226, PAJ1 Report No 17, **1999**.
- [157] **Evgeny Barkanov**, "Introduction to the Finite Element Method", Institute of Materials and Structures, Faculty of Civil Engineering, Riga Technical University, **2001**.
- [158] **G.P.Nikishkov**, "Introduction to the Finite Element Method", Lecture Notes, UCLA, [www.nliebeaux.free.fr/ressources/introfem.pdf](http://www.nliebeaux.free.fr/ressources/introfem.pdf), **2001**.
- [159] **J. N. Reddy**, "An Introduction to the Finite Element Method", 2nd ed.: McGraw-Hill series in mechanical engineering, **1993**.
- [160] **Çaglar Sonmez**, "Investigation of the Deep drawability of Steel and Aluminum Sheets by Finite Element Simulation", Thesis of Master Degree of science, Middle East Technical University, **2005**.
- [161] **Colin Caprani**, "Structural Analysis IV-Matrix Stiffness Method", [www.colincaprani.com/files/4%20-%20Matrix%20Stiffness%20Method](http://www.colincaprani.com/files/4%20-%20Matrix%20Stiffness%20Method), **2013**
- [162] **S.S. Bhavikatti**, "Finite Element Analysis": New Age International (P) Limited, **2005**.
- [163] **Abaqus 6.9 Documentation**, "Getting started with Abaqus: Interactive Edition", <http://abaqusdoc.ucalgary.ca/v6.9/books/gsa/default.htm>, **2013**
- [164] **Strategic Simulation and Analysis (Ssa)**, (2013), "<http://www.ssanalysis.co.uk/Abaqus-standard.htm>".
- [165] **A. H. Van Den Boogaard, T. Meinders and J. Huetink**, "Efficient implicit finite element analysis of sheet forming processes", International Journal for Numerical Methods in Engineering, vol. 56, pp. 1083-1107, **2003**.
- [166] **Xincun Zhuang, Zhen Zhao, Hongye Li and Hua Xiang**, "Experimental Methodology for Obtaining the Flow Curve of Sheet Materials in a Wide Range of Strains", steel research international, vol. 84, pp. 146-154, **2013**.
- [167] **Ulf Engel**, "Tribology in microforming", Wear, vol. 260, pp. 265-273, **2006**.
- [168] **Azonetwork Uk Ltd**, (2013), "<http://www.azom.com/article.aspx?ArticleID=6641>".
- [169] **Thomasnet News (Tnn)**. (2013), "<http://news.thomasnet.com/fullstory/Test-Connectors-accommodate-thin-medical-device-tubing-537872>".
- [170] **Re-Owned.Com Llc**, (2013), "<http://www.re-owned.com/itemcode-k98628727-c1>".
- [171] **Mindsets (Uk) Ltd**, (2013), "[http://www.mindsetsonline.co.uk/advanced\\_search\\_result.php?keywords=gearbox](http://www.mindsetsonline.co.uk/advanced_search_result.php?keywords=gearbox)".
- [172] **Inc. Unipunch Products**, (2013), "<http://www.unipunch.com/Home.aspx>".

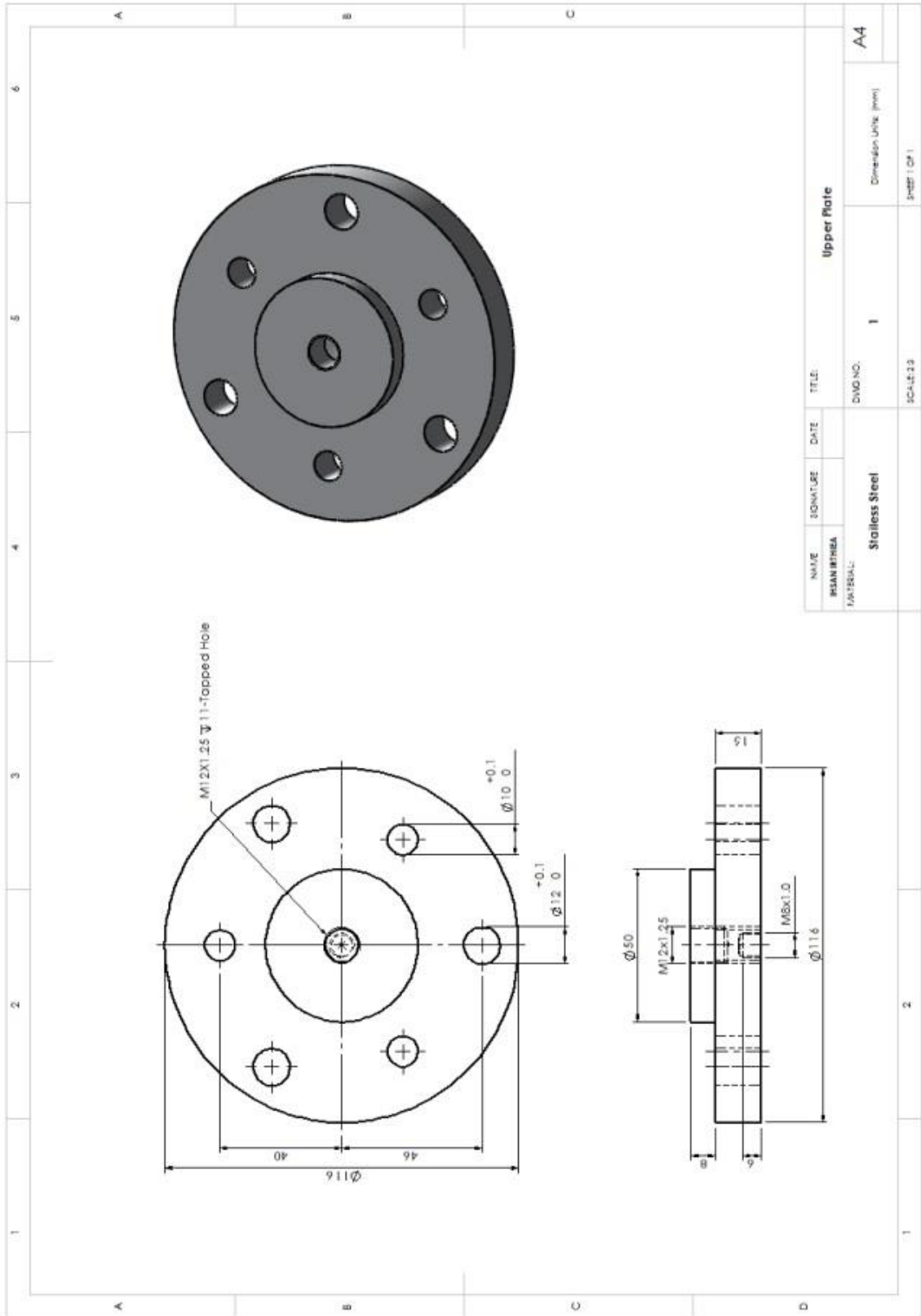
## **Appendix A**

---

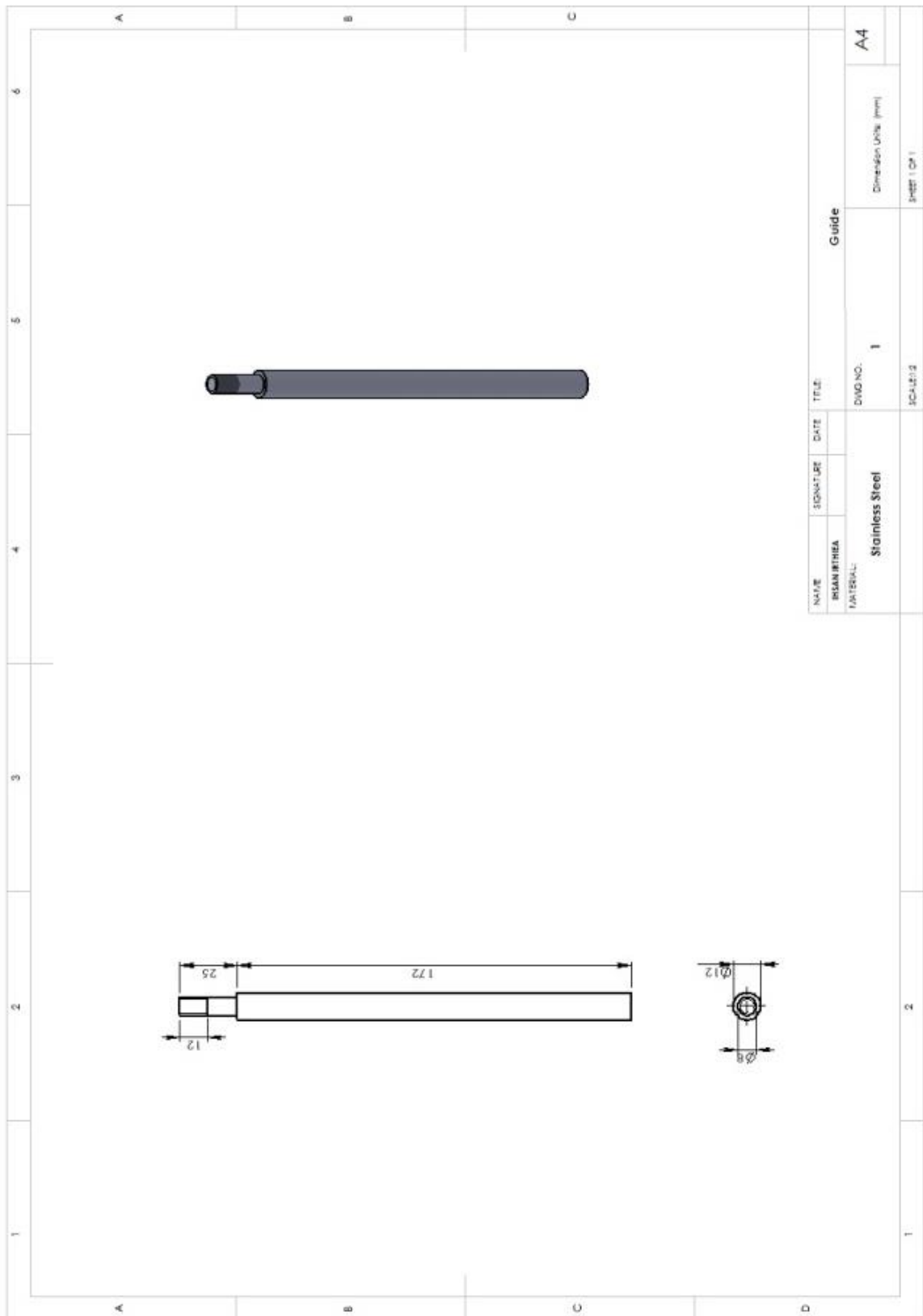
# **DRAWINGS OF THE DIFFERENT PARTS OF THE EXPERIMENTAL SET UP EMPLOYED OF THE CURRENT WORK**

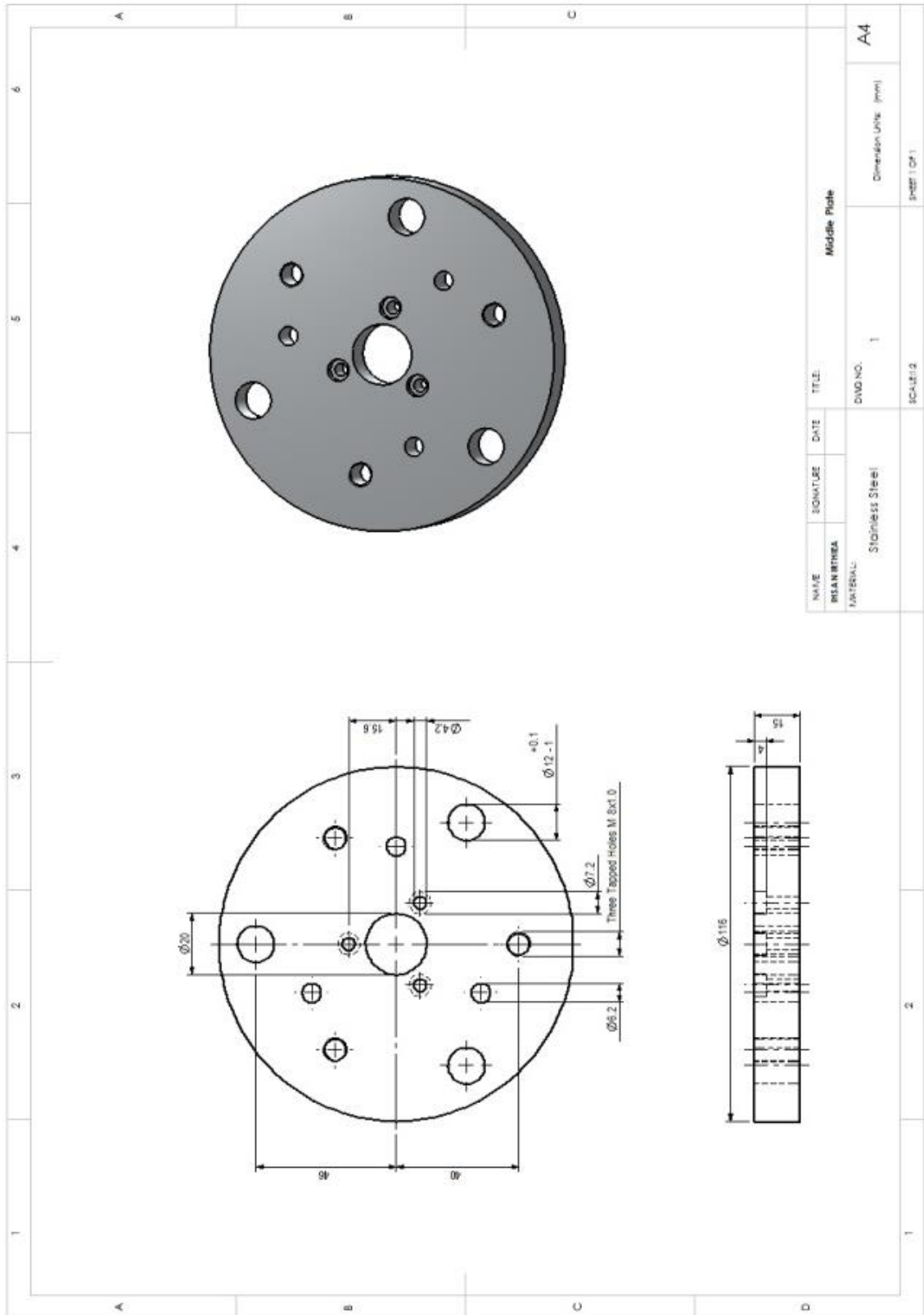
\*\*\*\*\*

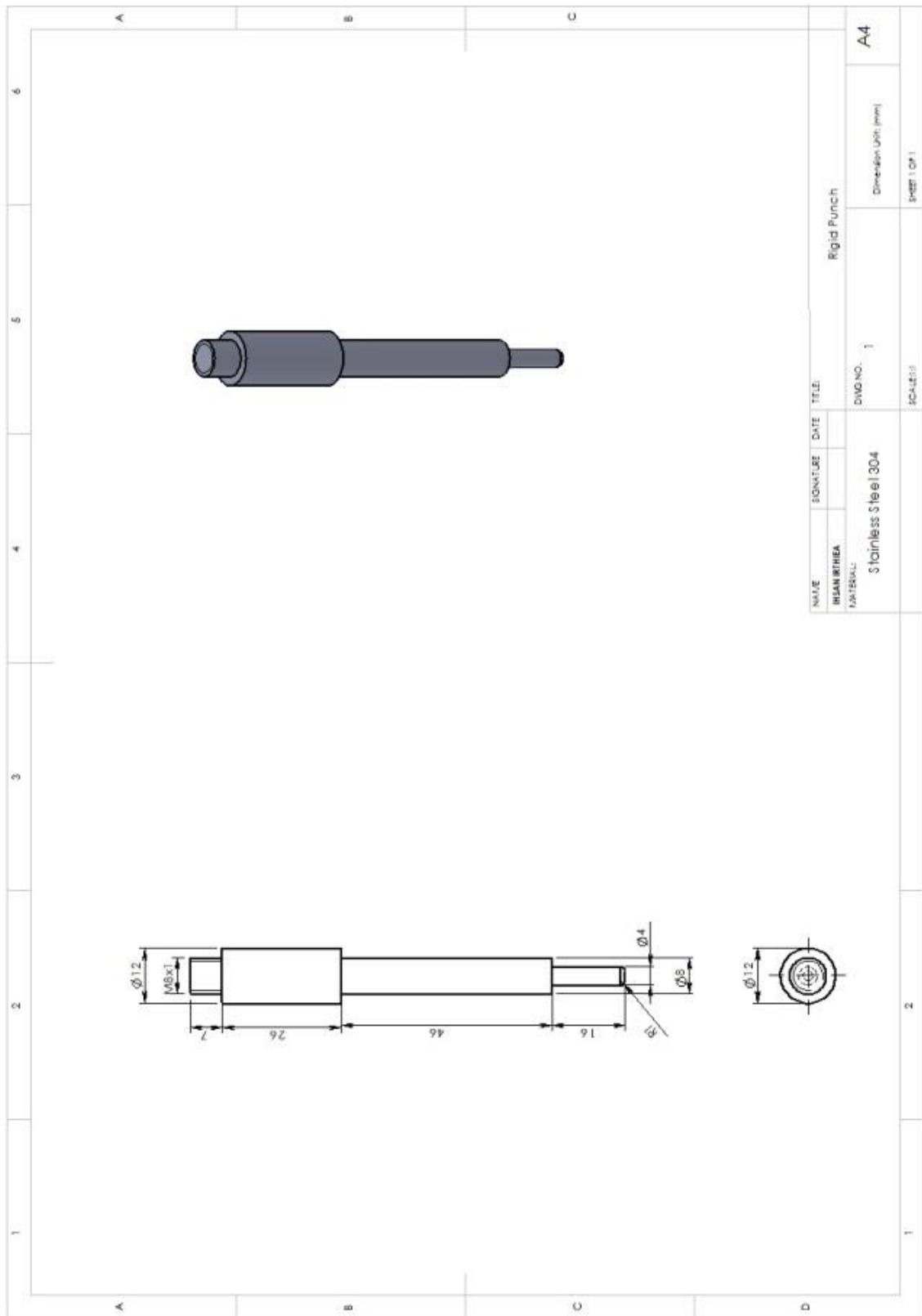


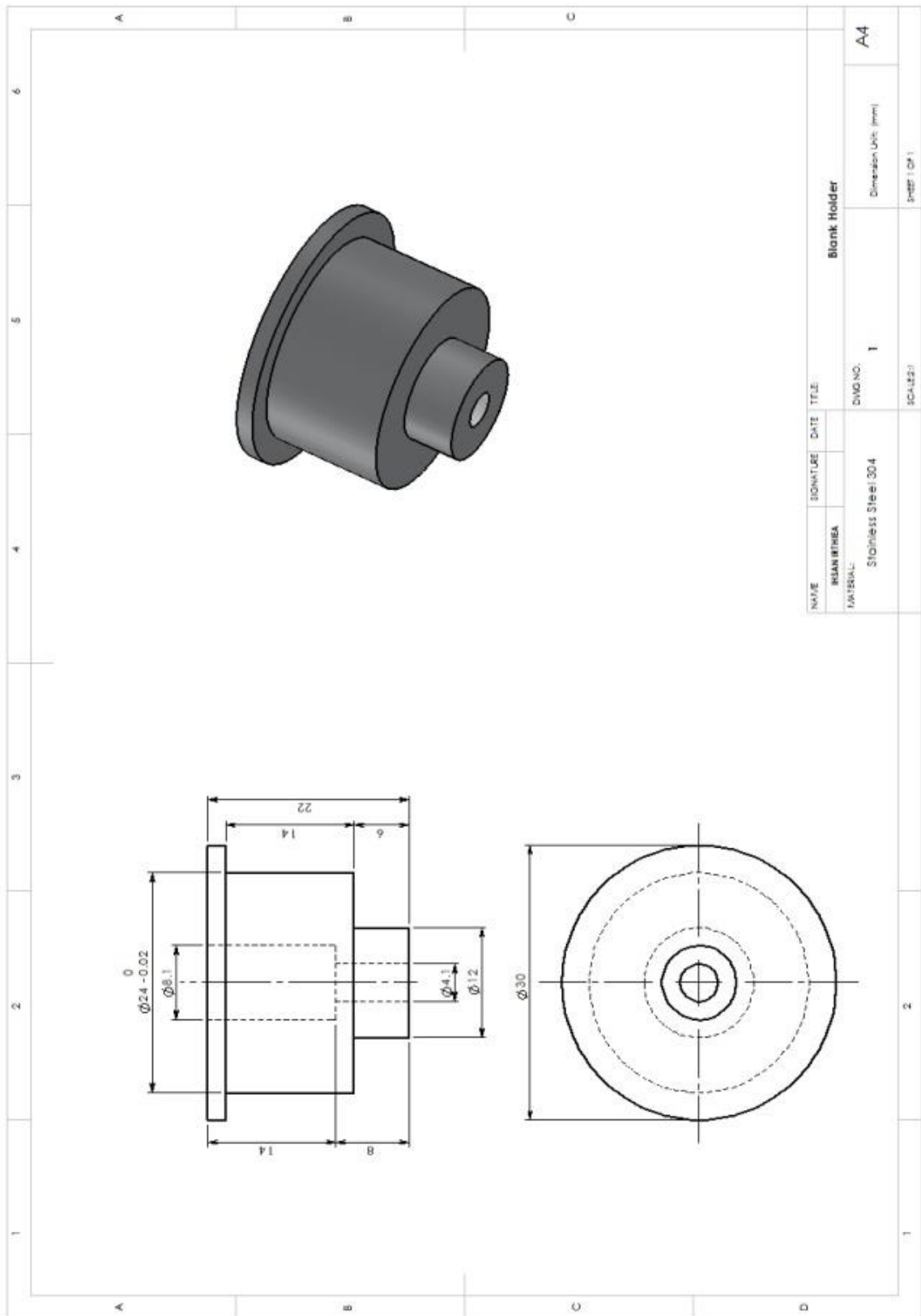


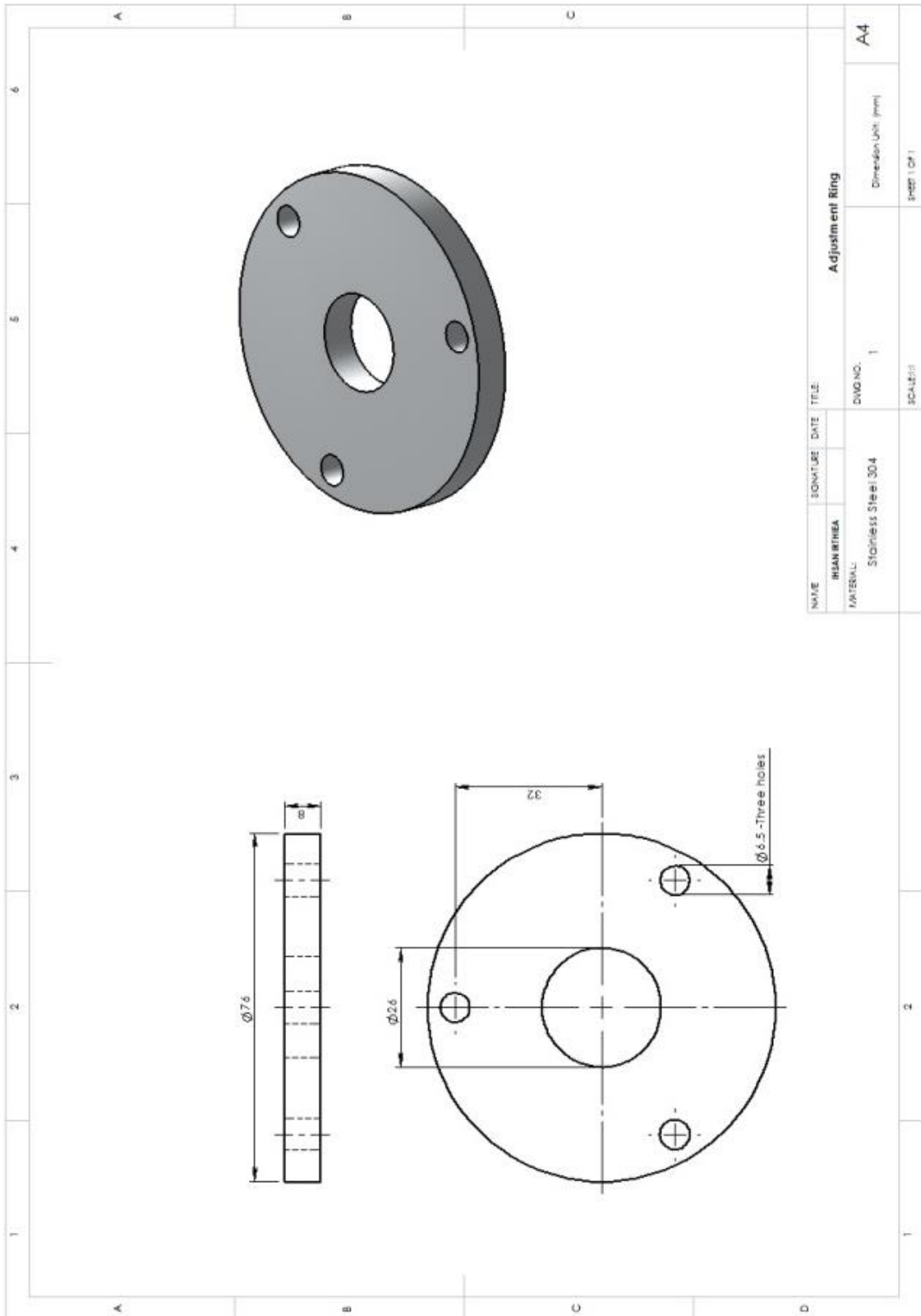




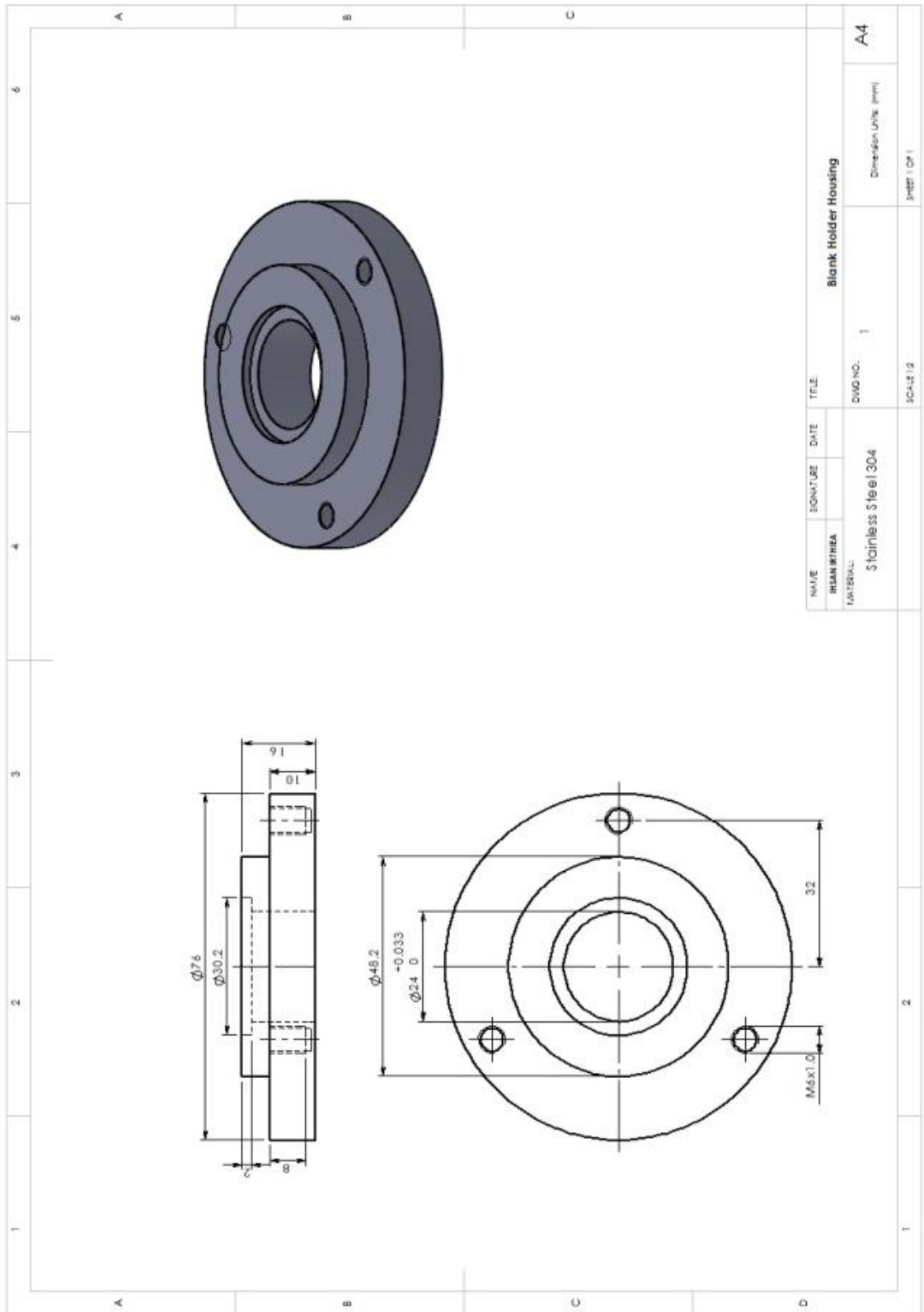


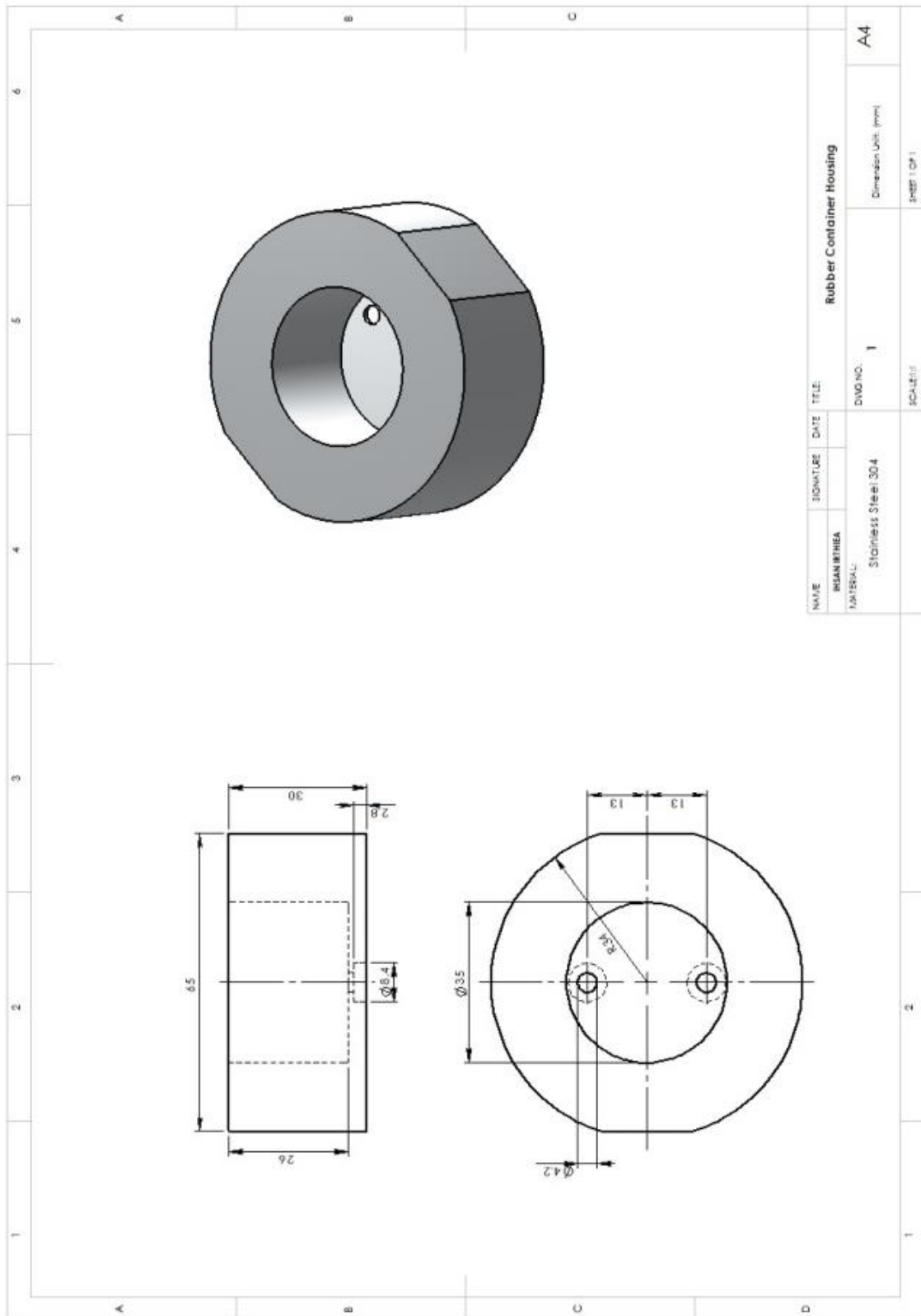


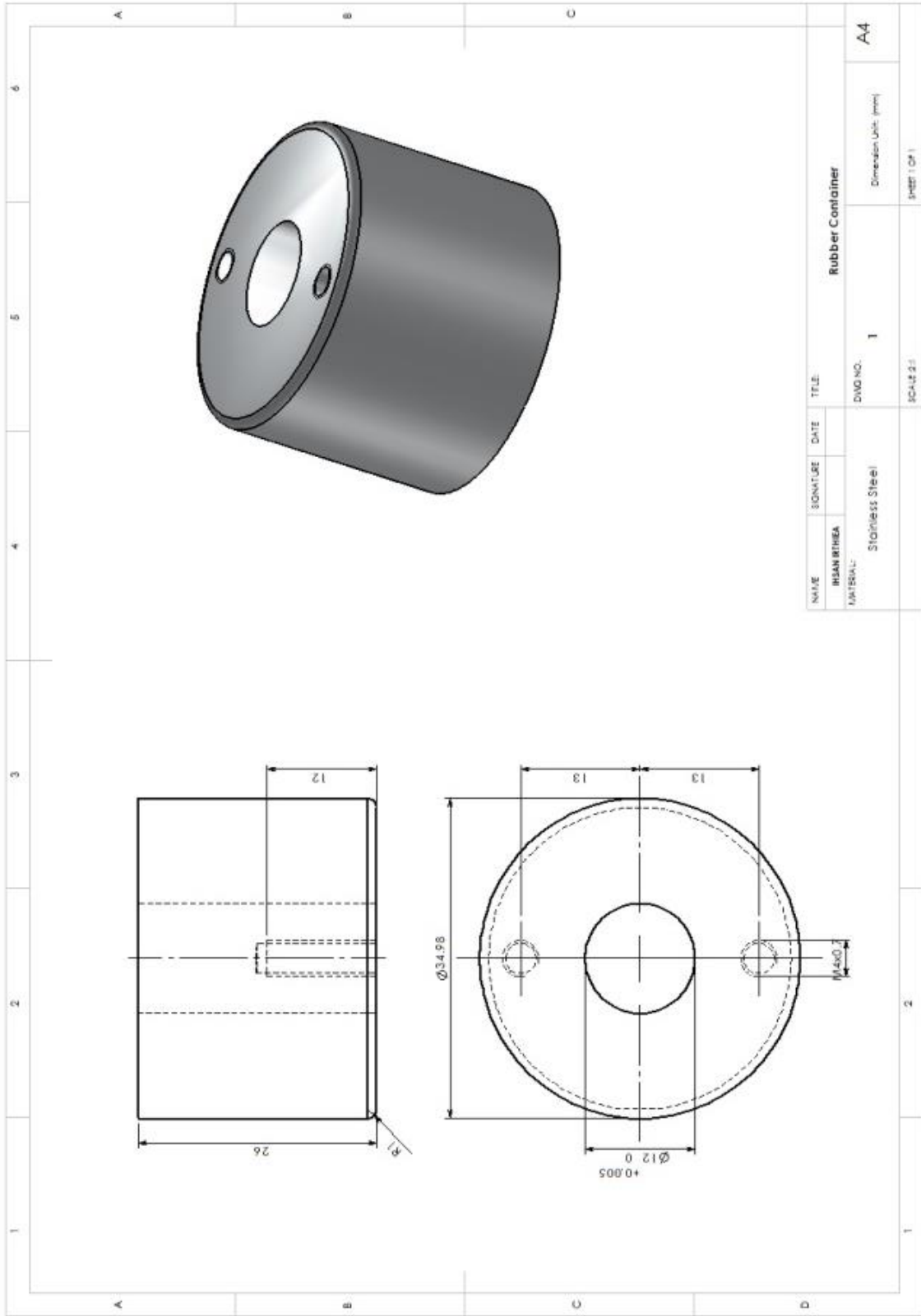




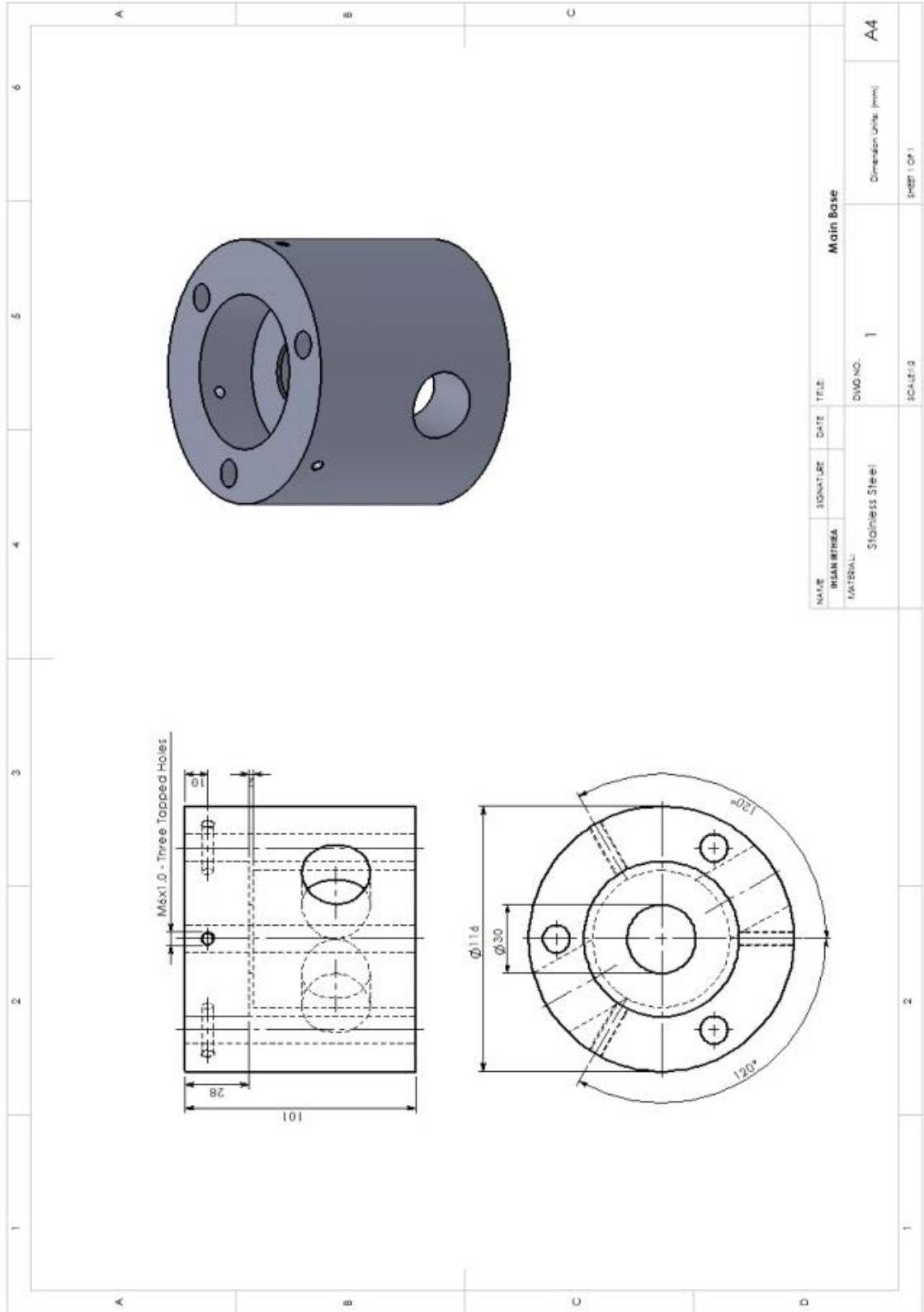
NAME	SIGNATURE	DATE	TITLE
HISAN RIHBA			Adjustment Ring
MATERIAL:	Stainless Steel 304	DWG NO. 1	Dimension Unit: (mm)
		SCALE: 1:1	SHEET 1 OF 1











## **Publications**

---

### **Conference Paper**

1. Ihsan Irthiea, Graham Green and Safa Hashim, " Investigation of Micro/Milli Flexible Deep Drawing Process", 14<sup>th</sup> International Conference on Advances in Materials and Processing Technologies (AMPT 2011), Istanbul/Turkey.

### **Journal Papers**

1. Ihsan Irthiea, Graham Green and Safa Hashim, " Investigation of Micro/Milli Flexible Deep Drawing Process", Advanced Materials Research Vol. 445 (2012) pp 241-246.
2. Ihsan Irthiea, Graham green, Safa Hashim and Abdulbast Kriama, "Experimental and numerical investigation on micro deep drawing process of stainless steel 304 foil using flexible tools", International Journal of Machine Tools & Manufacture Vol. 76 (2014) pp 21-33.